Dissertation zur Erlangung des Doktorgrades

der Fakultät für Chemie und Pharmazie

der Ludwig-Maximilians-Universität München

Cationic and anionic phosphatidyldiglycerol-based thermosensitive liposomes for the targeted delivery of chemotherapeutics and immunoadjuvants

Matteo Petrini

aus

San Benedetto del Tronto, Italien

2019

Table of Contents

1 Introduction

In Europe, cancer caused ~1.3 million deaths in 2014, whereas estimated prediction for 2019 suggested a further increase of 4.8 % in mortality [1]. Considering 3.7 million new cases each year, cancer represents the second cause of death and morbidity in our country as well as on a global scale [2].

Nowadays, cancer treatment in standard clinical practice mainly relies on chemotherapy, radiotherapy and surgery. These conventional methods are often unsuccessful, and some types of cancer are still associated with dismal prognosis, remission and resistance [3-5]. Solid efforts are currently concentrated on broadening cancer treatment approaches. Targeted therapy, hormone therapy, stem cell transplantation and precision medicine are presently being implemented in clinical practice [6, 7]. Besides these novel treatments, immunotherapy approaches and recent advance in biomaterial technologies showed high potential to enhance therapeutic efficacy [8-11]. The use of nanocarriers has been extensively developed for different applications, such as theranostic agents, imaging tools and drug delivery systems (DDS) for targeted therapy [12]. In the latter case, advantages in using DDS in comparison to conventional chemotherapy are mainly related to potentially improved tumor targeting, less off-target exposure, minimized risk of resistance and overall enhanced therapy outcome [13]. Among all DDS, stimuli-responsive nanocarriers engineered to trigger release of encapsulated drugs under specific conditions (e.g., pH change, light exposure, heat, mechanical stress) have proven to further broaden the potential applications of DDS [14]. On the other side, immuno-oncology focuses on artificial stimulation of the patient´s immune system towards cancer cell recognition and killing and has shown remarkable effectivity in some types of cancer [15, 16]. Interestingly, it has been demonstrated that tumors with high mutational burden (e.g., melanoma, lymphomas) are more susceptible to immuno-therapy approaches [17, 18]. Novel treatments such as checkpoint inhibitors are currently being used as first-line treatment for such tumors whereas chimeric antigen receptor T-cells (CAR T) are successfully used for some hematologic malignancies with well-defined tumor antigens [19, 20]. Additionally, cancer vaccine approaches have shown unique advantages in the generation of anticancer immunity, and hold great promises also for non-immunogenic tumors [21, 22].

Although remarkable progress has been obtained in cancer therapy over the last decades, there is still a need to improve conventional treatments for several cancer types. The use of nanomedicine as a targeted delivery system for chemotherapeutics or novel immunoadjuvants should therefore be further investigated in such context.

2 Background

2.1 Conventional solid tumor therapy

Cancer rises from a genomic instability of few cells which lose control over replication and thus are characterized by unlimited growth and if malign, also with potential dissemination/invasion into other parts of the body [23]. Potentially, every tissue in the human body could undergo mutations and raise malignant neoplasms. Hence, tumor features rise uniquely from the specific type of cell, thereby underlying significant differences in cancer type, properties of infiltration and aggressiveness. [24]. Cancer mortality is mainly due to dissemination of small tumor fragments (metastases), which detach from primary tumors and invade surrounding and distant tissue via blood and lymphatic circulation [25]. As anticipated above, conventional strategies for reliable tumor treatment focus on surgery, radiotherapy and chemotherapy. In case of non-metastasized tumors, first-line treatment is usually surgical resection. Tumor mass with part of healthy tissue in the nearby surrounding is removed, whereas radiotherapy might be applied afterwards to minimize the risk of recurrence and spreading [26, 27]. While surgery and radiation may promote local control of primary tumors, a weak or negligible effect is expected in disseminated metastases. Furthermore, tumor resection is not always feasible, especially in case of organ, vessel or nerve infiltration. Hence, to reduce tumor mass and attack already present metastases, neoadjuvant systemic chemotherapy is often preferred in these high-risk patients. The treatment regime is wisely chosen in relation to cancer type, stage and patients characteristics. Shortcomings of systemic chemotherapy are usually caused by systemic side effects driven by the lack of selectivity and a limited efficacy due to the development of resistance.

Doxorubicin is currently one of the most often used chemotherapeutic drugs for different types of cancer. This anthracycline agent was first isolated from *Streptomyces peucites*, a variety of bacteria collected in soil samples near Castel del Monte (Italy), which were already well-known to produce a red anthracycline metabolite, known as daunorubicin [28]. By modifying bacteria with N-nitroso-N-methyl urethane, a derivation of *S. peucites* was found among surviving colonies. The modified bacteria were found to produce a 14-hydroxyl derivate of daunorubicin, termed doxorubicin (DOX) and traded as Adriamycin® [29]. Clinically, DOX is used as a first-line treatment for acute leukemia, neuroblastoma, ovarian cancer, small cell lung cancer, lymphoma, breast cancer, bladder cancer and sarcomas. Its main mechanism is based on cellular inhibition of macromolecular biosynthesis by intercalating base pairs of DNA/RNA, whereas its selectivity is exclusively driven by the cell proliferation rate [30]. As for all systemic chemotherapeutics, potential side effects are expected on tissues with a rapid replication pattern, such as red blood cells, hair follicles, epithelium of

gastrointestinal tract and bone marrow cells. Furthermore, cardiotoxicity due to acute oxidative stress in cardiomyocytes is also often associated among cancer patients undergoing DOX chemotherapy [31]. Hence, further solutions for improving target specific actions of chemotherapeutics and thereby limiting off-target toxicity should be developed.

2.2 Liposomes as drug delivery system

2.2.1 Liposomes

In recent years tangible improvements were achieved in pharmaceutical technologies and biomaterials, broadening drug delivery strategies. Novel DDS focus on improving local targeted delivery by reducing off-target toxicity of different active pharmaceutical ingredients (APIs). Among these systems, self-forming lipid-based vesicles called liposomes are the most exploited and well characterized. Liposomes were first observed in 1965 by Bangham et al., who described the spontaneous assembling of phospholipids to vesicles when in contact with an aqueous solution [32]. Already in 1973, liposomes were investigated as potential DDS for antibiotics, such as penicillin [33]. Consequently, these nanocarriers rapidly became one of the most extensively studied systems used for delivery of chemotherapeutics, genetic material and vaccine adjuvants [34].
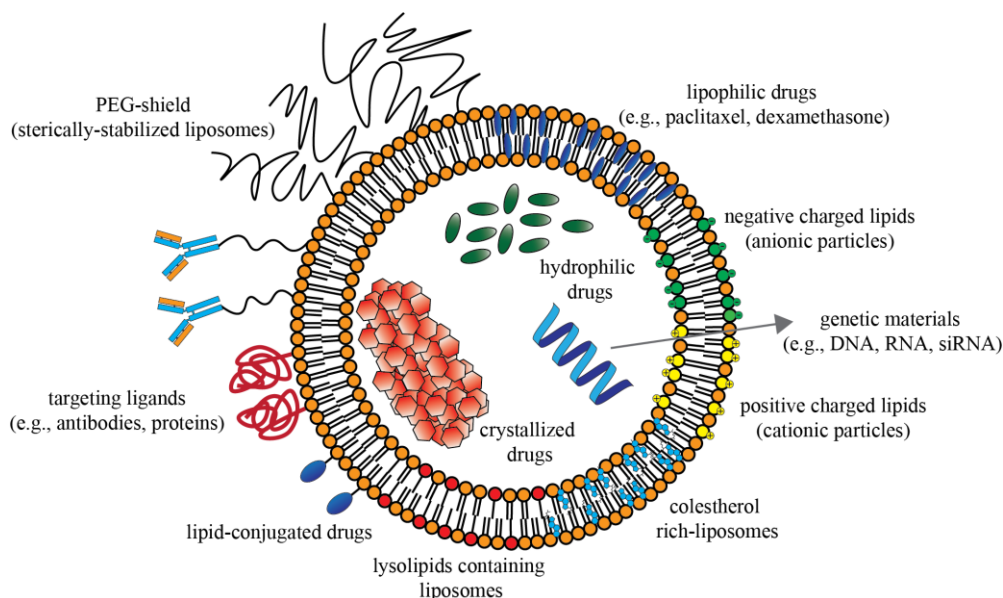
Figure 1 Schematic structure of liposome and potential functionalization.
Liposomes are conventionally made of phospholipids and different strategies for liposomes functionalization are possible by acting on the liposomal bilayer. The presence of positive or negative charged lipids, polyethylene glycol (PEG), antibodies, proteins or small molecules crafted for targeting purposes will confer specific characteristics to these vesicles. The aqueous internal environment and the hydrophobic bilayer section created by the phospholipid acyl chains can encapsulate hydrophilic and lipophilic drugs, respectively.

Biophysical and biochemical properties of liposomes are strictly related to their bilayer composition, preparation method and potential functionalization. Fundamental properties as bilayer rigidity, charge (ζ-potential), phase transition temperature (T_m), surface tension and vesicle size can be finely tuned in accordance to the main goals of application. Additionally, liposomes are usually formed by natural phospholipids, thus, they are biologically inert with high biocompatibility and biodegradability [35]. As shown in Figure 1, the co-presence of both, an aqueous core and a hydrophobic bilayer, in the liposome structure makes them ideal for encapsulating a wide range of drugs with different physicochemical properties [36]. Different strategies for drug loading in liposomes are currently available and they are strictly dependent on the type of molecule to be

encapsulated. The active loading strategy was found to be highly efficient for amphipathic molecules by exploiting membrane gradients driven by pH or ammonium salts [37, 38].

Early formulations were relatively simple but a high interaction with opsonins, usually encountered after systemic administration, led to a relatively fast clearance via the mononuclear phagocytic system (MPS) [39, 40]. In the late 70`s, the addition of cholesterol was found to be beneficial to improve circulation time by increasing the order of membrane packing at fluid state [41]. This effect was maximally exploited whenever cholesterol was mixed to sphingomyelin or ganglioside (e.g., GM1) in the liposomes bilayer [42]. An essential modification was further achieved with the addition of polymers such as PEG grafted onto the liposomes surface to improve circulation [43]. By the addition of flexible PEG, the steric hindrance was increased and thereby a repulsion of serum proteins was achieved. This resulted in particle shielding against macrophage uptake and, thus, a significantly prolonged circulation time was achieved [44]. Furthermore, liposomes can be functionalized with a targeting moiety (e.g., antibodies, sugars, proteins) present on theirs surface and, hence, enhancing the specificity for cancer cells (Figure 1).

2.2.2 Conventional liposomes tumor targeting

Solid tumors have substantially different characteristics in comparison to healthy tissue, such as a possibility of a necrotic core, high interstitial pressure due to absence of lymphatic drainage and immature vessels leaving gaps (*fenestrae*) in the endothelium [45, 46]. The latter is a microenvironmental factor usually associated with fast-developing tumors and thus pronounced angiogenesis [47]. A fenestrated endothelium allows macromolecules and other materials distributed via blood vessels to extravasate into the tumor interstitial space and to be retained in situ [48]. This process is known as "enhanced permeability and retention" (EPR) effect and it is the fundament for a broad class of formulations targeting solid tumors [49]. Nowadays, several liposomal formulations approved for clinical practice rely on the EPR effect to passively accumulate in the tumor (passive targeting strategy, Figure 2) [50]. The first liposomes encapsulating chemotherapy were designed to improve poor biodistribution properties of DOX for systemic chemotherapy of cancer patients. This formulation was initially approved for the treatment of AIDS-related Kaposi sarcoma and obtained FDA-approval in 1995 (Doxil®), later extended also to treatment of multiple myeloma and refractory ovarian cancer [51]. Consisting of long-circulating liposomes, Doxil® relies on an enhanced EPR effect to passively accumulate in solid tumors [52, 53]. When tested in patients, DOX formulated via Doxil® greatly enhanced half-life in comparison to non-liposomal DOX, with an improved biodistribution profile, a higher DOX-tumor enrichment and less off-target toxicity [54-56]. However, the anti-tumor effectiveness of Doxil® in clinical practice seems to be connected to tumor features, highlighting potential challenges for a broad application of this liposomal formulation. In

fact, whilst in several clinical studies a higher accumulation of DOX was observed in tumors, therapeutic response was somewhat comparable to non-liposomal DOX application. Hence, major advantages in using Doxil® are mainly related to the improved toxicity profile [57, 58]. Similar outcome was achieved during clinical trials for other FDA-approved conventional formulations, such as liposomal vincristine (Marqibo®) and liposomal irinotecan (CPT-11, Onivyde®) [59, 60].
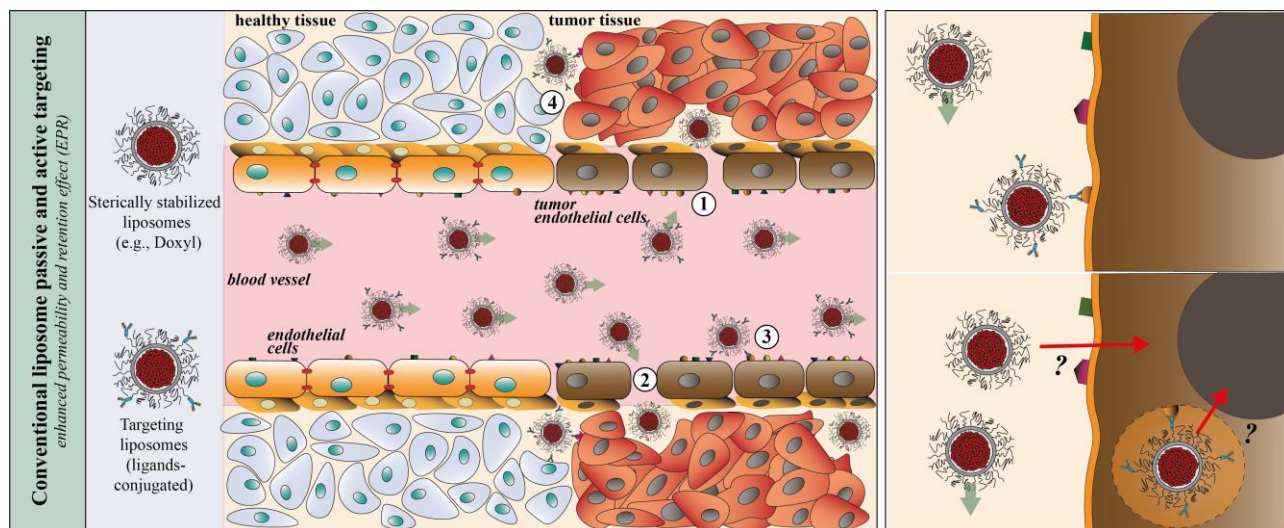
Figure 2 Different strategies for liposomal solid tumor targeting.
Passive liposomal tumor targeting via EPR effect with conventional sterically stabilized liposomes (e.g., Doxil®) and active liposomal targeting with ligands-conjugated liposomes. Sterically stabilized liposomes circulate freely in the body and exploit the EPR effect for tumor targeting (1). Gaps among endothelial cells ease the extravasation process and lead to a better accumulation in the tumor interstitium (2). Ligand-conjugated liposomes use specific ligand-targeted interactions to improve particle accumulation. Targets might be present either at vascular level (3) or on the surface of tumor cells (4). Potential limitations of stable liposomes in releasing bioavailable drug are shown in the panels on the right.

In an attempt to improve the overall therapeutic outcome for EPR-based delivery systems, antibodies or other ligands can be attached to PEG chains or specific linkers which are connected to the liposomal bilayer [61, 62]. The functionalization of liposomes is addressed to target distinct structural differences observed in cancer cells, such as overexpressed membrane proteins. Chosen targets should have a high-density distribution in the tumor microenvironment (TME), but limited or no expression in other areas [63, 64]. Liposome's active targeting approach mainly focuses on two different strategies: i) vascular targeting and ii) tumor cell targeting. In case of vascular targeting, liposomes interact with tumor endothelial cells (TECs) by exploiting overexpressed negatively charged proteins, such as integrins, growth factors or adhesion molecules [65]. Liposome binding of specific targets on TECs membrane will allow further uptake and internalization of the nanocarriers and, thus, potential vascular damage [66, 67]. These specific targets can be recognized on cancer cell surfaces promoting specific liposome-cell interactions whereas the second approach relies mainly on particle extravasation via EPR and passive accumulation in tumor interstitium [68].

Overall, passive and active liposomal tumor targeting achieved controversial results with different studies promoting either apparent efficacy or no improvements [69-71]. The complexity of

tumor phenotypes might be the reason of this fluctuating efficacy [72]. In fact, high heterogeneity among cancer patients is associated with a large variability of the EPR-effect placing substantial challenges in its potential [73-75]. Not all tumors possess an ideal pathophysiology suitable for EPR-based approach, and in the majority of the cases an efficient particle accumulation is hampered by high interstitial pressure, dense cellular matrix and poor penetration of nanoparticles [74, 76]. By screening several pre-clinical studies, Wilhelm et al. showed that only a minor percentage of total injected dose (ID) reached the tumor site via EPR effect, averagely equal to 0.7 % [77]. Furthermore, the lack of a release mechanism and a typically high stability of EPR-based nanocarriers are additional reasons for the underlying limitations in the amount of bioavailable drug in the active site [78, 79].

2.2.3 Thermosensitive liposomes

Localized triggered drug delivery from stimuli-responsive nanocarriers holds great promises in increasing the concentration of a bioavailable drug in specific regions. Specifically investigated stimuli-responsive release mechanisms focus either on microenvironmental factors (e.g., pH change, enzymatic degradation in TME) or external factors (e.g., light, ultrasound, temperature) [14, 80]. In the latter scenario, the increase of temperature exclusively in the tumor area via external devices has been widely recognized to affect TME in multiple ways [81]. By exploiting this local tumor temperature increase, thermosensitive materials can undergo conformational changes and, thus, release loaded drugs in a targeted fashion. In case of thermosensitive liposomes (TSL), the designing of these particles should focus on the selection of appropriate lipids to ensure heat-triggered release at the desired temperature [82]. Lipid membranes of vesicles engineered for this set up physically change their state from solid-gel to liquid crystalline phase while approaching their melting phase transition temperature (T_m). In liposome vesicles, phospholipids acyl chains are fully extended and organized and form a well-packed bilayer, whereas the hydrophilic polar headgroups are exposed to the internal and external aqueous environment (Figure 3). In the solid gel phase ($T < T_m$), membrane permeability is lowest and a loaded drug is well retained in the liposomal aqueous core (Figure 3A). By increasing the temperature, energy in the form of heat is absorbed by phospholipids acyl chains which thereby undergo trans-gauche isomerization [83]. Such a thermotropic transition affects the bilayer physical state, which will shift from a gel to a liquid crystalline phase.
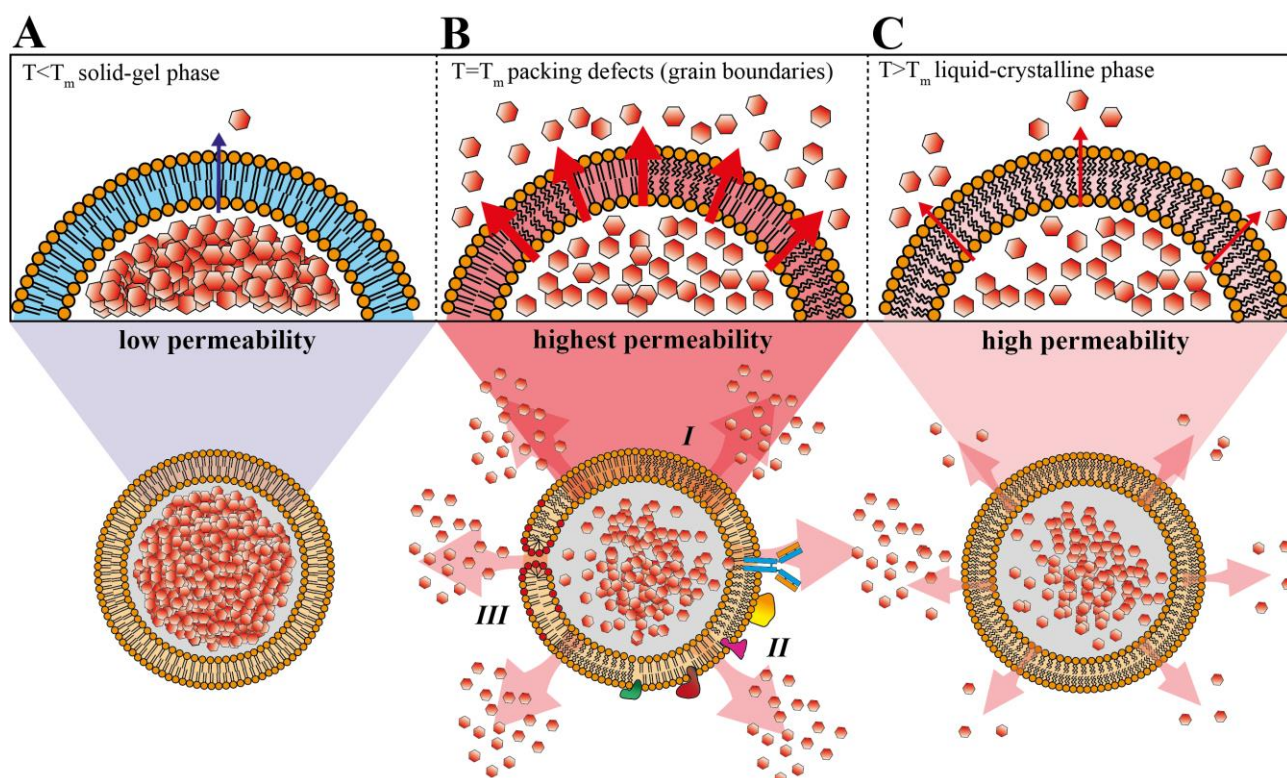
Figure 3 Schematic representation of temperature-dependent phase transition and factors affecting drug release.
When T < T$_m$, bilayer is in gel-phase with low permeability and thus negligible drug escape (A). At T$_m$, grain boundaries between lipid rafts undergo phase transition inducing membrane defects and thereby increasing bilayer permeability at its highest, allowing rapid release of encapsulated drugs (depending on lipid composition) (B). Mechanisms of drug escape are related to different factors: drug diffusion driven by concentration gradient (***I***), proteins/blood components intercalating with membrane bilayer (***II***), specific lipid components affecting bilayer packing (e.g., lysolipid and pore formation) (***III***). At T > T$_m$, all phospholipids underwent phase transition and membrane bilayer is in liquid crystalline phase, characterized with disordered fluid state and high permeability, however not as high as in the latter phase (C). Adapted and modified with permission form the reference [324].

By approaching T$_m$, a pre-transition might be visible in specific lipid bilayers strongly depending on the type of headgroups, identified as ripple phase [84]. At this moment, a further increase in temperature promotes grain boundaries formation among lipid bilayer rafts with some undergoing phase transition and others still in pre-transition (T = T$_m$, Figure 3B) [85]. Hence, membrane packing defects induced by mismatch of liquid and solid chains, further increase bilayer permeability, thus, facilitating the escape of encapsulated drugs from the aqueous core [86]. At a temperature higher than T$_m$, the structural framework of the lipid matrix will result in a disordered fluid state due to increased mobility of phospholipids in such a conformation [87]. However, the lack of grain boundaries leads to a more homogenous liquid crystalline state with lower permeability in comparison to the previous phase (Figure 3C) [88]. The temperature-dependent transition is dependent on the nature and homogeneity of the hydrocarbon chains and can be easily observed via a variety of techniques such as differential scanning calorimetry (DSC) or x-ray diffraction.

Yatvin and coworkers reported a first TSL formulation exploiting a heat-triggered release concept in 1978. In this study, neomycin and carboxyfluorescein (CF) release were investigated in liposomes formed by mixture of 1,2-dipalmitoyl-sn-glycero-3-phosphocholine (DPPC) and 1,2-distearoyl-sn-glycero-3-phosphocholine (DSPC) in combination with mild-hyperthermia (HT, 41-43

°C) [89]. The *in vitro* heat-triggered release was successful between 42-45 °C using TSL formed by DPPC ($T_m = 41$ °C) and DSPC ($T_m = 55$ °C) in the ratio of 3:1. Poor circulation time and suboptimal release kinetics though strongly limited a potential *in vivo* application. The introduction of PEG into the liposomal bilayer drastically improved circulation time by avoiding fast clearance by the reticuloendothelial system (RES) (e.g., Doxil®). Later on, a PEGylated TSL formulation designed to increase circulation time and heat-triggered release of its content *in vivo* was developed [90, 91]. This traditional TSL was similar to the Yatvin formulation, but with PEG grafted onto the bilayer via the inclusion of 1,2-distearoyl-sn-glycero-3-phosphoethanolamine-N-(amino(polyethylene glycol)-2000 (DSPE-PEG$_{2000}$) and cholesterol to increase membrane stability. Needham and Dewhirst further improved release kinetic by decreasing overall liposomal T_m in order to increase burst release at tumor sites, which holds the fundament for a new generation of TSL. This new PEGylated TSL is characterized by a low membrane rigidity since DSPC and cholesterol were removed while a certain amount of lysolipids were added to the formulation [92, 93]. The inclusion of lysolipids (e.g., 1-stearoyl-sn-glycero-3-phosphocholine) in a DPPC bilayer results in a lower T_m and a faster formation of grain boundaries. Additionally, lysolipids are hypothesized to circulate freely in the bilayer and to form pores on the membrane surface around T_m, promoting a fast escape of encapsulated drugs (Figure 3C, III) [94]. This low-temperature sensitive liposome (LTSL) can fully release its content in the HT range within few seconds, resulting in a considerable improvement of tumor DOX exposure when compared to traditional TSL *in vivo* [95, 96]. Celsion Corporation currently owns the LTSL formulation under the trade name ThermoDOX®, which is presently facing clinical trials for different types of cancer [97-99]. However, a recently completed phase III study of ThermoDOX® in combination with radiofrequency ablation (RFA) did not show improvement in comparison to RFA treatment alone, implicating further optimization is required for an enhanced therapeutic outcome [100]. Limitations of lysolipid containing TSLs are related to an overall sub-optimal stability observed at normothermia (37 °C, NT). Recent findings have shown that lysolipids can be extracted during circulation time from LTSL particle, inducing bilayer instability with a subsequent potential loss of encapsulated drug [101]. This translates into a constant rate of leakage *in vivo*, with a significant shorter circulation time compared to more stable TSL formulations [101, 102].

Nowadays, other examples of TSLs are trying to find an optimal balance between ultra-fast drug release and optimal stability at physiological conditions. For instance, PEG-based TSL without lysolipid or cholesterol showed promising results when applied in co-administration with mild-HT [103, 104]. Other examples concern the usage of detergents (e.g., Brij78) as alternatives of lysolipid in so-called HaT (**H**eat-**a**ctivated cyto**T**oxic) TSL formulation [105]. More recently, novel TSL based on the key lipid component 1,2-dipalmitoyl-sn-gylcero-3-phospho-di-glycerol (DPPG$_2$, $T_m = 39.7$ °C) were investigated in terms of heat-triggered release and *in vivo* application. An ultra-fast drug release

was observed from DPPG$_2$-based TSL (PG$_2$-TSL) formed by DPPC/DSPC/DPPG$_2$ 50:20:30 (mol:mol), whereas an improved stability was observed *in vitro* when compared to LTSL [106]. The incorporation of a certain percentage of DPPG$_2$ in a DPPC/DSPC bilayer was found to be effective and to successfully prolong the circulation time of particles similarly to PEG polymers [107]. Furthermore, blood components (e.g., serum proteins) and their interaction with membrane bilayer were found to play a crucial role in enabling heat-triggered release from PG$_2$-TSL at HT condition (Figure 3B, II) [108]. Gemcitabine (dFdC)-loaded PG$_2$-TSL in combination with mild-HT were able to successfully improve therapeutic outcome in tumor-bearing rats when compared to naked-dFdC or NT control [109]. In a similar study, DOX-loaded PG$_2$-TSLs were compared to Doxil®, LTSL and non liposomal DOX unveiling improvements in the overall DOX tumor enrichment [110]. Remarkably, PG$_2$-TSL-DOX showed excellent compatibility and positive therapeutic outcome in cats with spontaneous locally advanced soft tissue sarcoma [111].

2.2.4 Hyperthermia and TSL as drug delivery strategy

Besides being the underlying trigger mechanism of thermosensitive liposomes, local mild HT induces essential changes in TME. Several studies showed a significant enhancement in therapeutic outcome whenever chemotherapy is administrated in combination with regional HT. Heat-induced effects in the tumor area can be divided into two primary levels: microscopic and macroscopic. At macroscopic level, an increase in temperature is usually associated with enhanced blood flow and oxygenation, vasodilation and a more permeable endothelium [112, 113]. Hence, uptake of materials such as small molecules, macromolecules and liposomes circulating in the bloodstream and their extravasation in tumor interstitium is facilitated whenever HT is applied [114-116]. At microscopic level, HT induces several changes in cell membrane and intracellular pathways, with an increase in cell membrane permeability, inhibition of DNA repair mechanism, release of heat-shock proteins (HSP), expression of surface molecules as major histocompatibility complex (MHC) class I, direct activation of dendritic cells (DC) and T-cell population cross-talking [117, 118]. Due to the vast spectrum of HT-induced effects in the tumor area, potential synergistic effects in combination with chemotherapeutics are to be expected. In pre-clinical settings, DOX co-administrated in combination with regional heat enhanced antitumor response [119]. Issels and Lindner brought significant contributions to the field due to their study with neoadjuvant chemotherapy and local HT in sarcoma patients [120]. Patients treated with chemotherapy in the form of etoposide, ifosfamide and DOX in combination with HT showed improved response rate (28.8 vs. 12.7 %) in comparison with chemotherapy alone. More recently, long term outcomes of chemotherapy plus HT treatment were assessed in a follow-up study with a duration of more than 11 years showing the improved response

is associated with higher survival, when compared to chemotherapy alone (52.6 % vs. 42.7 %, respectively) [121].
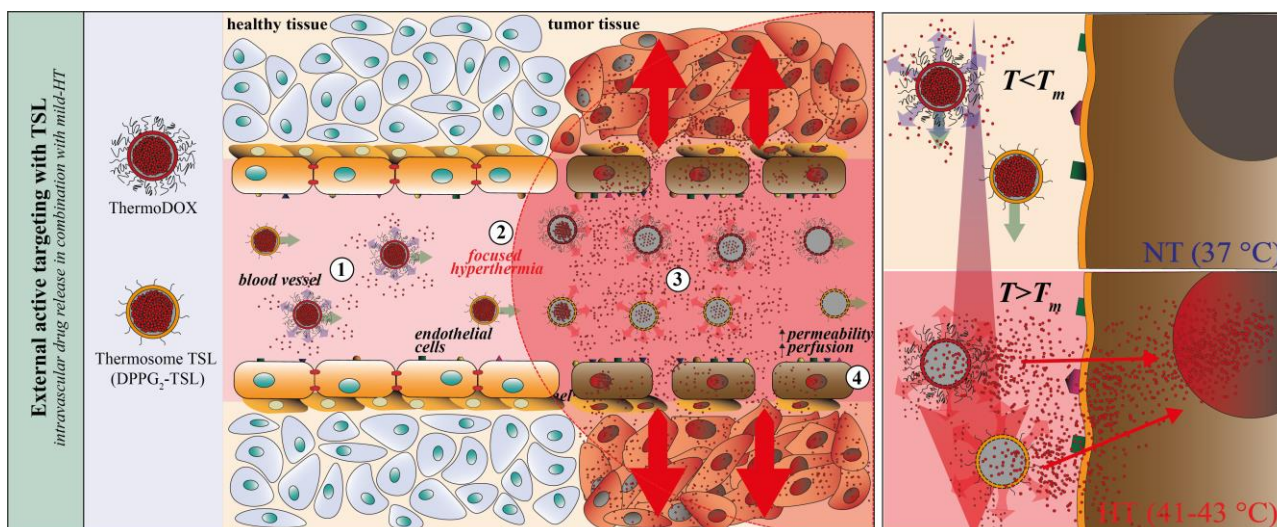
Figure 4 Schematic representation of tumor-targeting approach by thermosensitive liposomes in combination with HT.
TSLs freely circulate in the bloodstream after intravenous administration, with potential leakage of encapsulated core in relation to formulation stability (1). Vesicles reach tumor vessels, which are brought to mild-HT temperature via an external device (41-43 °C) (2). Intravascular heat-triggered drug release (3) with a high concentration peak in tumor vessels. Drug extravasation and tumor tissue penetration driven by concentration gradient (4). Focus on TSL stability at physiological condition and intravascular heat-triggered release is shown in the panels on the right.

In the case of TSL chemotherapy, adjuvant HT triggers liposomal solid gel-liquid crystalline phase transition, while above mentioned additional effects provide further benefit in terms of drug biodistribution. Figure 4 shows an overview of tumor-targeting concept utilizing TSL in combination with mild-HT. TSLs distributing in the body via the bloodstream will reach tumor vessels where HT triggers targeted release leading to a high peak concentration of bioavailable drugs at vasculature level (intravascular drug release). Released drugs extravasate towards the tumor interstitium driven by concentration gradient and are immediately available to be taken up by cancer cells [122] (Figure 4). Transport of drugs via TSL and heat-triggered release upon HT significantly improved a homogeneous distribution of the drug in the tumor volume and increased penetration depth from vessels when compared to free drug [123]. Different methods are currently well established in clinical practice to induce HT in patients, such as radiofrequency (RF) applicators and recirculation systems [124-127]. Next-generation devices such as magnetic-resonance guided high intensity focused ultrasound (MR-HIFU) are presently emerging to improve potential shortcomings such as limited penetration depth as well as spatial accuracy [128].

2.3 Dual tumor-targeting approach

2.3.1 Cationic TSL

Exploiting affinity of targets highly expressed in cancer cells or in tumor vasculature with specific ligands is a valid strategy to increase potential targeting of functionalized materials. Tumor endothelial cells (TECs) are shown to regulate important aspects of tumor progression such as metastases, oxygen and nutrients supply, angiogenesis, vascularization, T-cell adhesion and recruitment, co-inflammatory and immunosuppressive cytokine production [129-131]. Thus, tumor vasculature targeting with functionalized material should be pursued as a potential strategy to overcome biological barriers and improve anti-cancer therapy [132, 133]. As mentioned above, liposomes can be functionalized with moieties to increase the specificity of liposomal binding to tumor vasculature and interstitium. Anti-angiogenetic therapy mediated via antibody-connected immuno-liposomes achieved promising results in vasculature targeting [134-136]. The same strategy can be further broadened to TSL, promoting a new attractive concept termed dual targeting. In recent years, TSLs were developed also for binding selectively epidermal growth factor receptors such as EGFR, HER2, CD13 and folate receptors showing promising results *in vitro* and *in vivo* [137-140]. It is important to notice that particles engineered for vascular targeting do not rely on the EPR effect, hence, do not need to extravasate for an efficient accumulation in the tumor, increasing their potential impact in tumors where EPR is poorly observed [141].
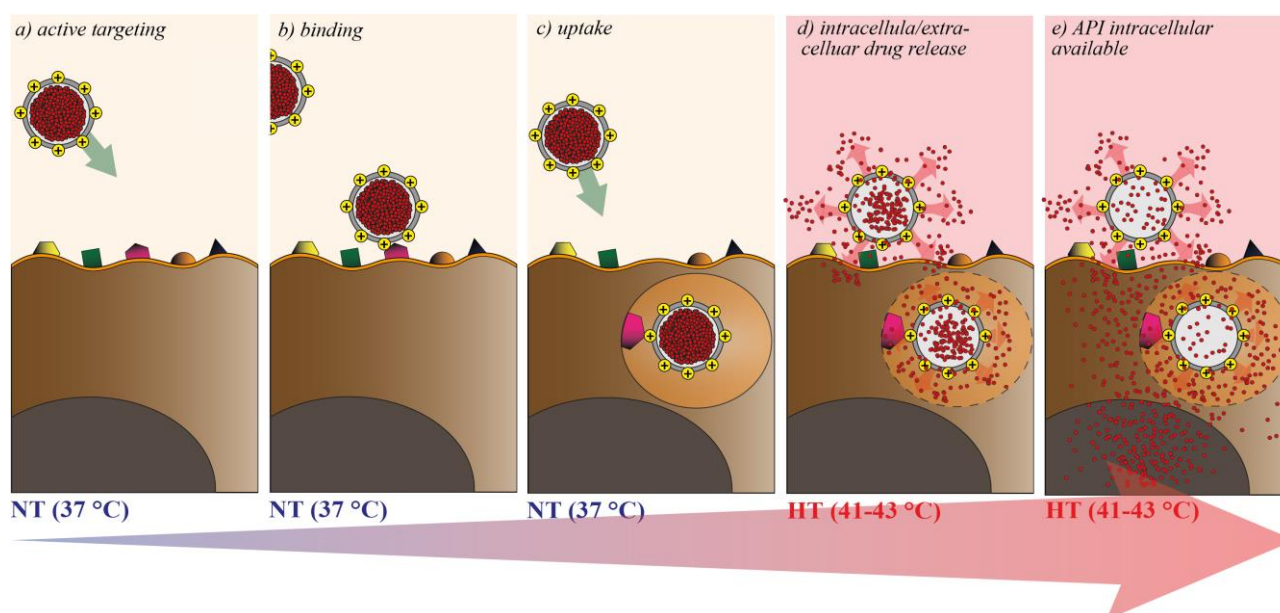
Figure 5 Schematic representation of CTSL tumor-targeting approach in combination with focused HT.
Cationic TSLs circulate in the bloodstream and accumulate in tumor vasculature by means of electrostatic interaction with over-expressed negatively charged membrane proteins (a, b). After binding, nanoparticles are usually internalized in tumor endothelial cells (c). Regional HT focused on tumor area triggers drug-release from endothelium associated CTSL, inducing a high concentration of drug at intracellular level (dual targeting approach) (d, e).

Positively charged nanoparticles also showed to target inflammatory sites and angiogenic vessels after systemic administration [142, 143]. The main underlying mechanism for cationic particle accumulation in tumor vessels seems to be related to an atypical phenotype expressed by TECs and cancer cells such as an aberrant number of negatively charged membrane proteins, creating an ideal platform for cationic nanoparticle interactions [144, 145]. Several cationic liposome formulations were tested in pre-clinical settings, showing promising results in inhibiting tumor vascular growth [146-150]. In the current project, a novel concept of dual tumor targeting was investigated by combining the targeting potential of cationic liposomes in combination with the heat-triggered release capability of the TSL delivery platform. By using cationic thermosensitive liposomes (CTSL), the heat-triggered release effect in conjunction with the active targeting approach driven by cationic nanoparticles was investigated to potentially release a higher amount of payload directly to TECs (Figure 5).

2.3.2 Potential disadvantages of sterically stabilized liposomes in targeting approach

Polymers as PEG are responsible for increasing steric hindrance on particles and creating a mechanical repulsion, with therefore less interaction with opsonins and other serum proteins responsible for particle clearance via the MPS [151-153]. However, several shortcomings were recently reported about PEG polymers, underlying potential limitations of its broad applications. Firstly, PEG-coated nanoparticles or macromolecules have shown to produce anti-PEG antibodies (Abs) after repetitive injections [154]. These Abs were found to belong mainly to the IgM class and, once present, sharply reduced circulation properties of PEGylated materials by increasing elimination, in a process termed accelerated blood clearance [155]. More critically, throughout the last decades, an increasing trend of pre-existing PEG Abs was reported in healthy blood donors, from a 0.2 % incidence rate in 1984 to 42 % in 2015 [156, 157]. Besides promoting specific IgM Abs, PEG was also correlated to other immunological responses such as complement activation-related pseudo-allergy, which may further broaden potential concern for clinical use of PEGylated-based therapeutics [158]. Secondly, repulsion of serum proteins and lipoproteins is the underlying mechanism of prolonged circulation of PEG-containing particles. However, this might create issues on the targeting approach due to high steric hindrance of the polymer chains, reducing the chance for a successful liposome-cell interaction. In fact, if on the one side PEG can successfully enhance circulation time, on the other side it might hinder targeting efficiency, in case the formulation is designed for such an aim [159, 160]. Recent findings reported incorporation of DSPE-PEG$_{2000}$ (chemical structure in Figure 6) in different kind of functionalized liposomes to decrease potential liposome-cell interactions and, thus, hamper deliver efficiency of encapsulated compounds [161-163]. Thirdly, PEG-containing

liposomes were observed to hinder endosomal escape after particle uptake, a key step in order to release bioavailable drug. These interferences are caused by inhibition of endosomes membrane fusion together with endocytosed particles due to PEG shielding [164, 165].

In conclusion, these effects are raising awareness for potential limitations of PEG in clinical practice, generally addressed in different reviews as the "PEG dilemma" [166]. Hence, liposomal targeting might benefit from the development of other type of TSLs, where the primary mechanism for prolonged circulation relies on a different mean. Due to the absence of PEG grafted ontp liposome´s surface, PG_2-based TSLs ($DPPG_2$ chemical structure shown in Figure 6) might provide a new and exciting alternative for a dual targeting approach in combination with mild-HT.
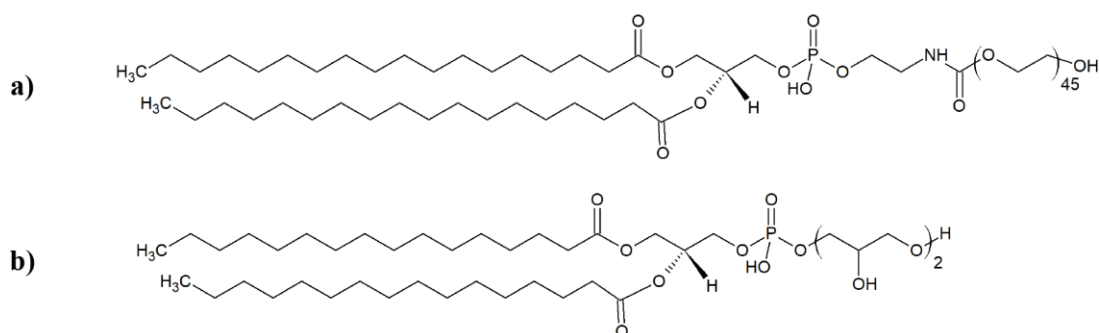
Figure 6 Chemical structure of DSPE-PEG$_{2000}$ (a) and DPPG$_2$ (b).
The main difference between the two phospholipids is related to the headgroup size, which is significantly smaller in case of DPPG$_2$ (148 vs. 2000 Da). Therefore, DPPG$_2$ is more capable of forming lamellar structure and can be incorporated up to 70 mol% in liposomes bilayer, whereas DSPE-PEG is limited to a maximal amount of 10 mol% due to its critical micelle concentration (0.5-1.0 μM) [107, 167].

2.4 Cancer immunotherapy

2.4.1 Fundamentals of cancer immunotherapy

Cancer immunotherapy has recently gained a central role in the treatment of different kinds of malignancies [168]. Substantial contributions to this therapy approach were brought from a broad range of compounds and recent studies, focusing on the generation of a robust and durable immune response towards cancer cells. Several types of strategies are currently used in clinical practice, as i) monoclonal antibodies, ii) non-specific immunotherapies, iii) oncolytic viruses, iv) T-cell therapy, and v) cancer vaccines [169]. Non-specific immunotherapies consist of administration of cytokines as interferons (IFN) or interleukins (IL) for the treatment of different diseases. Currently, IFN-γ (Actimmune®) and IL-2 (Aldesleukin®) are approved for the treatment of chronic granulomatous disease and metastatic melanoma, respectively [170, 171]. However, severe immune-related adverse effects (irAE) are observed during administration, especially in case of the acute regime of IL-2, which is usually associated with capillarity leak syndrome, flu-like symptoms, tachycardia, and extreme fatigue [172].

Pioneers Allison and Honjo significantly contributed to the field in parallel but independent works, laying the foundation of modern cancer immunotherapy and awarding a Nobel prize in medicine for their efforts [173]. Their research focused on the possibility to block checkpoint signaling mediated by cytotoxic T-cell lymphocyte-associate protein 4 (CTLA-4) and programmed cell death 1 (PD-1) on cancer cells with specific Abs resulting in improved T-cell-mediated immune-response [174, 175]. Subsequently, several monoclonal Abs were designed as ipilimumab (Yervoy®), pembrolizumab (Keytruda®) and nivolumab (Opdivo®), which are currently approved for different cancer treatments [176-178]. A fascinating novel approach is based on *in vitro* functionalization of patients T-cells with chimeric antigen receptors (CAR) able to recognize specific tumor-associated antigens. Engineered CAR-T-cells are then administrated in the patients via infusion [179]. A first CAR-T received FDA-approval in 2017 (Yescarta™) for non-Hodgkin lymphoma, quickly followed by a second (Kymriah™) in the same year [180]. However, serval clinical trials are undergoing which might increase the portfolio of available CAR-T therapies in the near future [181-183].

2.4.2 Cancer vaccine & immunoadjuvants

Besides various checkpoint inhibitors and CAR-T therapies already used in clinical practice, cancer "vaccines" hold great promises. This new breakthrough immunotherapy strategies exploit direct administration of potent immune-response modifiers (IRMs) in the TME, in an attempt to modulate immune-tolerance towards an active immune-response [184]. It has been demonstrated that cancer vaccines loaded with tumor-associated antigens (TAAs) are able to induce antigen-specific

immunities against tumors, rather than non-specific immunological responses triggered by other methods such as the checkpoint-blockade therapy [16]. However, although the administration of tumor-specific peptides or proteins has been reported to induce an immunogenic response towards TAA, the large heterogeneity of patients strongly hampered their clinical applications [185]. On the other side, whole cancer vaccines made by tumor lysates showed limitations in terms of process scalability and insufficient therapeutic response [186]. IRMs approach consists in activating DCs by specific cytokines, with capability of the latter to be antigen-presenting cells, migrate in close-reach tumor-draining lymph nodes and trigger maturation of cytotoxic T lymphocytes and memory T cells. These drugs act mainly on the innate immunity by activating specific intracellular pathways such as IRF3, STAT3, STING, NFκB, and NLRP3 inducing pro-inflammatory signals [187-190]. Due to their main effect, these compounds are generally referred to as immunoadjuvants (IAVs). IRMs specifically bind pathogen recognition receptors (PRRs), a large family of receptors which function is to recognize pathogen-associated molecular patterns (PAMPs), a crucial step for the activation of the innate immunity [191]. PAMPs represent a host´s first line of defense against infections by association with bacteria and virus material, such as lipopolysaccharides (LPS), endotoxins and nucleic acid variants. Additionally, damages-associated molecular patterns (DAMPs) as cytosolic self-DNA released from apoptotic cells is also recognizable via these means, generating an immune response against a potential insult [192]. PAMPs recognition by PRRs triggers above mentioned intracellular pathways, with a fast and robust response mediated via cytokine production of IFNs and different ILs [193].

Nowadays, different PRRs like retinoic acid-inducible gene receptors, cyclic guanosine monophosphate-adenosine monophosphate synthase, and nucleotide-binding oligomerization domain-containing protein 1 receptors are known and their functions are fully characterized [194]. Among these, toll-like receptors (TLRs) were shown to play a crucial role in enhancing the immune-response towards bacteria, viruses or tumor cells. TLRs are a large family of proteins mainly expressed by immune cells from innate immunity [195]. So far, 13 members of the TLRs superfamily have been characterized, even though TLR-11, 12 and 13 were found only in rodents and not in humans [196]. TLRs are type I transmembrane glycoproteins formed by an ectodomain with leucine-rich repeats (LRR), a transmembrane domain and a cytoplasmatic region equipped with a Toll/interleukin-1 receptor (TIR) domain [197]. Generally, localization of each TLRs, as well as structures and functions, are highly conserved among mammalians with comparable effects observed upon activation [198]. TLR-4 was the first TLR to be characterized in mammals and later used as a main comparison to identify other TLRs by similarity in structure and function [199]. TLR-4 and TLR-2 are present on cell membranes and recognize LPS and microbial lipopeptides, respectively. TLR-1 and TLR-6 are conjugated with TLR-2 forming heterophilic dimers and helping to

discriminate between diacyl or triacyl lipopeptides. TLR-7, TLR-8 and TLR-9 are present at endosomal level and are essential for the detection of non-viral ssRNA (TLR-7,8) and CpG DNA (TLR-9), whereas in the same location TLR-3 binds viral dsRNA [200]. Upon PAMPs or DAMPs binding at LRRs region, TRLs undergo conformational changes making cytoplasmatic domain TIR available for adapter proteins such as MyD88, TRIF, TIRAP/Mal, TRAM [201]. The generation of these signalosomes promote kinase signaling cascades with common downstream activation of transcription factors like NF-κB, IRF and AP-1. The complex signaling cascade is strongly regulated by tyrosine kinases, ubiquitination and glycosylation process which hamper or hinder activation of the pathways mentioned above [202].

In cancer therapy, TRLs are usually described to have pleiotropic dynamic effects leading to either tumorigenic or anti-tumor outcomes in relation to different contest, and thereby they have been referred as a "double-edged sword" [203]. In fact, for some tumor types, TLR-4, TLR-2 and TLR-3 signaling were associated with chemoresistance, increased angiogenesis, and proliferation. Overexpression of specific TLRs was also associated with clinicopathological features of tumors [204, 205]. On the other side, several pre-clinical and clinical studies confirmed the apparent effectiveness of TLR-4, TLR-7, TLR-8, and TLR-9 stimulation, with a strong anti-tumor effect mainly mediated by DCs and γδ T-cells activation [206, 207]. Cancer type, route of administration (e.g., local vs. systemic therapy), kind of TLRs involved as well as potential cooperative stimulation are essential factors to be evaluated to forecast the outcome of TLRs activation [208, 209].

2.4.3 Imidazoquinolines as TLR agonists

Currently, several agonists for TLR-7, TLR-8, and TLR-9 are now either approved for cancer treatments or undergoing clinical investigations [210]. In the 1980´s, synthetic novel imidazoquinolines compounds were found to have high specificity for TLR7 and TLR-8 [211]. Imiquimod (R837, chemical structure in Figure 7), a TLR-7 agonist, was the first FDA-approved IAV (Aldara®) for topical treatment of genital warts, superficial basal cell carcinoma (BCC) and actinic keratosis [212]. In a phase III study, topical application of Aldara® resulted in a significant histological clearance rate of 82 % in patients affected by BCC [213]. Remarkably, R837s positive response was also observed in other types of skin cancers such as breast cancer skin metastases and cutaneous T-cell lymphoma (CTCL), whereas a liquid formulation (Vesimune™) is currently tested in a phase II study for non-invasive bladder cancer [214, 215]. The primary mechanism of R837 activity is related to the recruitment of tumor-infiltrating T-helper cells mediated by activation of plasmacytoid DCs (pDCs) and macrophages via cytokine production (IFN-α, IL-6 and tumor necrosis factor (TNF) α) [216].

Resiquimod (R848), is an R837 analog with a 2-hydroxy-2-methylpropyl at N1 instead of 2-methylpropyl and an extra ethoxy-methyl chain connected at C-2 (Figure 7). R848 shows some advantages in comparison to R837, leading to a 40 % higher potency when compared to the latter [217, 218]. Administration of TLR-7,8 agonists have been investigated in animal models and humans using different dosages and administration routes. In all cases activation and proliferation of DCs, monocytes ad macrophages were demonstrated, accompanied by the production of cytokines and chemokines such as TNF-α, IL-1, IL-6, IFN-γ and IL-12 [217, 219]. Additionally, TLR-7,8 have been described to activate B-cell memory activation, creating a platform for long-lasting immunological protection, a valid help against tumor relapse [220, 221]. When applied topically, R848 induces secretion of various interleukins, interferons, and TNFα by monocytes, macrophages, and peripheral blood mononuclear cells present in the treated area. This treatment has led to significant therapeutic effects in patients affected by various superficial cancers (squamous and basal cell carcinomas) [222, 223]. Remarkably, R848 was recently described to remodel tumor and host responses to promote survival in pancreatic cancer in pre-clinical settings [224]. Furthermore, in a recent phase I study, topical R848 was found to be effective in patients affected by CTCL [225]. However, systemic administration therapies resulted in a lower efficiency and were more prone to fail, due to TLR tolerance after multiple injections [226, 227]. Besides, a fast clearance is usually observed after systemic administration, with transient and reversible side effects such as neutropenia and flu-like symptoms [228, 229]. Nowadays, several novel TLR agonists are facing clinical trials for solid tumor cancer therapy, either as single therapy or in combination with immune-check point blockade [230, 231]. In these clinical investigations, these compounds are generally intratumorally (i.t.) administrated, with potential limitations related to inhomogeneous tumor biodistribution, deep-seated tumors and patient compliance.

IAVs application might benefit from delivery with specific carriers to circumvent tolerance induction, improve toxicity profile and possibly increase tumor targeting. Recent studies already confirmed the usefulness to formulate TLR-7,8 in nanoparticles or liposomes. In a 2013 survey, liposomal R848 was found to be effective against *Leishmania donovani* in a murine model, confirming the effectiveness of TLR agonists systemic therapy against parasites [232]. More recently, R848 formulated in nanoparticles (NPs) was used to target lymph nodes in mice in order to stimulate dendritic cells and macrophages. The study was a proof of concept for R848 to help and improve an antitumor immune response [233]. Remarkably, Chen and coworkers designed a novel approach by combining nanoparticles containing TLR-7 in combination with photothermal therapy and immune checkpoint inhibitors for the treatment of different types of cancers [234]. The combinational treatment promoted an "in situ" cancer vaccine with the generation of a strong immune response not only effective against primary tumors but also on artificial metastases and re-challenges. Similar

therapeutic response was observed when NPs formed by β-cyclodextrins encapsulating R848 were tested in a murine model of colorectal adenocarcinoma [235].
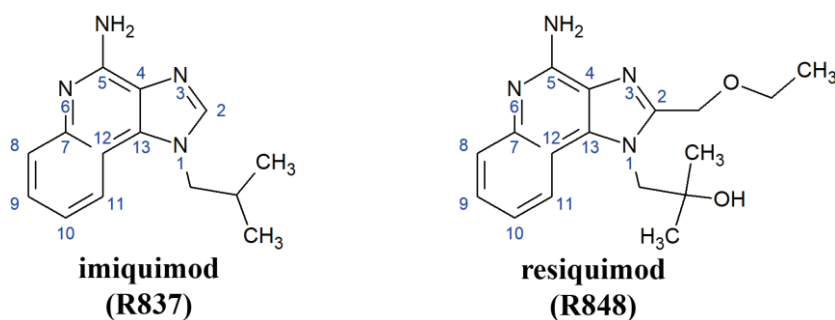

Figure 7 Chemical structure of imiquimod (R837) and resiquimod (R848).
Imidazoquinoline compounds with higher potency were found to contain a short alkyl chain at the C-2 position and a short hydroxyalkyl chain at N-1 (192). R848 modification at N-1 and C-2 increased potency in PBMC when compared to R837 and considerably changed physicochemical properties of the molecule. The addition of hydroxy groups provides an improved hydrophilicity in comparison to R837 (the latter non-water soluble) and, thus, a higher compatibility with the liposomal delivery system.

2.4.4 Cold & hot tumors

Cancer immunotherapy is currently the first line of treatment for renal cell carcinoma, melanoma, lung cancer and triple-negative breast cancer [236]. Clear advantage in using immune therapeutics is the possibility to generate an immune response which acts not only against primary tumors but also against metastases (abscopal effect) and recurrence (long-lasting immune memory) [237, 238]. However, not all cancer types respond to immuno-therapy approaches, and in such cases, more conventional methods should be considered. Recent findings reported a correlation between tumor mutational burden (TMB) and immunotherapy effectiveness, unveiling a better outcome for cancer with higher TMB [239]. Nowadays, the TMB as well as the number of infiltrating immune cells (immunoscore, IS) are important tools for patient screening and, thus, improve therapy response [240]. The IS score is a standardized and validated system to define the amount of CD3$^+$ and CD8$^+$ cells at the tumor center and margin. IS ranges from I0 (low density of immune cells in both locations) to I14 (high density of immune cells in both areas) and defines other essential parameters such as tumor stage and basal inflammation [241]. Tumors characterized by a low IS are defined as "cold" tumors and low response is expected with checkpoint blockade, whereas a better response is usually observed in case of inflamed "hot" tumors with high IS [242]. Hence, "cold" tumors are currently a therapeutic challenge for immunotherapy approaches [243].

Mild-HT application modulates TME and induces activation of immune cells in the heated areas by improving tumor cell recognition and killing. The effects are mainly driven by extra-cellular release of HSP-70 or exosomes, overexpression of MHC-I class on DC cells, modulation of T-cells trafficking, potential cancer cell apoptosis depending on the magnitude of applied heat dose [117, 244]. Combinational treatment together with IAVs is expected to further enhance immune response, even though little information is currently available in literature. Also, improved IAVs tumor

targeting via specific delivery systems as TSLs, which rely on heat for triggered release, would further broaden the potential synergistic effect in combination with mild-HT to stimulate immune response. Hence, a synergistic 3-factor system consisting of mild-HT, heat-triggered, local release and IAVs might define a possible strategy to improve tumor T-cell infiltration and basal inflammation, overcoming current limitations in cold tumors immunotherapy.

2.5 Objective of the thesis

The main focus of the thesis is the design, investigation, and characterization of novel heat-triggered liposomal nanosystems based on DPPG$_2$ phospholipid, for local targeted release of chemotherapeutics and IAVs. The thesis is formed by two main parts. In the first part, the optimal drug delivery system is identified among screening of different TSL formulations and targeting strategies (e.g., dual targeting vs. intravascular drug release). In the second part, the most promising delivery strategy was selected to assess feasibility for IAV delivery, laying the foundation for immuno-cancer therapy approach with TSL technology.

1. Here, the feasibility of heat-triggered release in combination with the active targeting approach driven by cationic nanoparticles was investigated to potentially release a higher amount of payload directly to tumor vasculature. A novel DPPG$_2$-based cationic TSL formulation (PG$_2$-CTSL) was designed and tested in comparison to PEG-based cationic TSLs to highlight possible advantages in using DPPG$_2$ against PEG in terms of cell binding and DOX delivery efficiency. To unveil whether dual targeting mediated via cationic TSL in combination with regional HT improves overall DOX delivery efficiency in comparison to conventional TSL strategy, previously reported DPPG$_2$-/ and PEG-based anionic TSLs were also enrolled in the study. For all (C)TSLs, stability at physiological temperature and DOX-release rate at HT was assessed *in vitro* by fluorometry. Cancer cell targeting capability and effect of protein adsorption was evaluated looking at liposome-cell interactions via fluorescence microscopy. DOX pharmacokinetic (PK) profiles were assessed *in vivo* after intravenous injection (i.v.) in rats. (C)TSL-DOX biodistribution (BD) was evaluated in tumor-bearing animals in combination with regional HT to assess DOX enrichment in tumors and exposure to related organs.

2. Motivated by promising recent findings in cancer immunotherapy, the aim of this study was the design of a novel DPPG$_2$-based TSL for heat-triggered release of IAVs. In clinical trials, immunotherapies with novel and potent IAVs is usually performed via intratumoral injection, with potential limitations due to inhomogeneous API distribution and poor patient compliance. Additionally, systemic administration of IAVs such as R848 showed different side effects and it is usually associated with poor therapeutic efficacy. Hence, our goal was to define a strategy to stably encapsulate R848 in DPPG$_2$-TSL and control the release exclusively via mild HT. Active and passive loading were tested for R848 loading into TSLs. Additionally, it has already been proven that HT can modulate TME and immune cell activation. Thereby, synergistic effects between R848 and HT in stimulating immune cells to target and kill cancer cells were investigated. Different cancer cell lines were screened (BN175, SKOV-3) and their

immunogenicity tested *in vitro* in presence of human peripheral blood mononuclear cells (PBMCs) activated with R848 with or without mild HT. Finally, the recently developed DPPG$_2$-TSL-R848 formulation was tested *in vivo* and PK profile compared to non-liposomal R848 to assessed improvements in circulation property.

3 Materials & Methods

3.1 Chemicals and kits

DPPG$_2$ was provided by Thermosome GmbH (Planegg, Germany). DPPC and DSPC were purchased from Corden Pharma Switzerland LLC (Liestal, Switzerland). DSPE-PEG$_{2000}$, phosphatidyl-ethanolamine-dioleoyl-sulforhodamine B (Rho-PE) and 1,2-dipalmitoyl-*sn*-glycero-3-phospho-ethanolamine-N-(7-nitro-2-1,3 benzoxadiazol-4-yl (NBD-PE) were obtained from Avanti Polar Lipids (Alabaster, Alabama, USA). Cationic lipids as 1,2-dimyristoyl-3-trimethylammonium-propane (DMTAP), 1,2-dipalmitoyl-3-trimethylammonium-propane (DPTAP), 1,2-stearoyl-3-trimethylammonium-propane (DSTAP) and 3ß-[N-(N',N'-dimethylaminoethane)-carbamoyl]-cholesterol (DC-Chol) were also acquired from Avanti Polar Lipids. DOX was acquired from Puren Pharma GmbH & Co. KG (München, Germany). R848 and R837 in powder form were purchased from Enzo Life Sciences (Lörrach, Germany) and TCI chemical Deutschland (Eschborn, Germany). Fetal calf serum (FCS) and Collagen G were provided by Biochrom AG (Berlin, Germany). Cell tracker green CMFDA, Lysotracker Red 99, and Hoechst 33342 were purchased from Thermofisher Scientific (Waltham, Massachusetts, USA). ELISA kit for SC5b-9 and certified human serum for complement activation were acquired from TecoMedical (Sissach, Switzerland). ELISA kit for human cytokine analysis (hTNF-α and hIL-6) were obtained from ThermoFisher, whereas ELISA for rat cytokine analysis (rTNF-α and rIL-6) were acquired from Sigma Aldrich GmbH (München, Germany). Protein quantification kit DC^{TM} protein assay was obtained from Bio-Rad (Hercules, California, USA). Density gradient medium (Lymphoprep^{TM}) for isolation of mononuclear cells was from Stemcell Technologies (Vancouver, Canada). Activated caspase 3 and secondary Alexa Fluor ^{TM} 594 antibodies were acquired from Bio-Techne GmbH (Wiesbaden, Germany) and ThermoFisher, respectively. TACS$^{®}$ 2 TdT in situ apoptosis detection kit was from Trevigen (Gaithersburg, Maryland, USA). All other chemicals used were obtained either from Sigma Aldrich GmbH (München, Germany) or Carl Roth GmbH (Karlsruhe, Germany). All buffers and solutions used in the study were prepared with deionized and purified water from the ultrapure water system (Milli Q Advantage, Merck Millipore, Darmstadt, Germany).

3.2 Liposome preparation

3.2.1 Lipid film hydration and extrusion

Liposomes were prepared by lipid film hydration and extrusion method [107]. Briefly, lipids were weighted and dissolved in CHCl₃/MeOH solution (9:1, v/v). Organic solvent was removed under vacuum using a rotary evaporator (Laborota 4001, Heidolph Instruments GmbH, Schwabach, Germany), allowing lipids to form a homogenous dry lipid film. The lipid film was hydrated with appropriate buffer or solutions in relation to specific purposes (refer to section 3.3 for API loading) for 10 min at 60 °C. Obtained multilamellar vesicles (MLVs) were extruded though polycarbonate membranes (Whatman® Nucleopore Tracked-Etched Membrane, Sigma Aldrich GmbH, München) using a high-pressure extruder (Lipex™ Thermobarrel Extruder, Northern Lipids Inc., Burnaby, Canada) also set at 60 °C. High pressure extrusion of MLV resulted in small unilamellar vesicles (SUV), which were stored at 2-8 °C until further steps (e.g., API active loading). All liposomes used to assess vascular targeting (refer to section 4.1) were extruded 5 times through 200 nm and 5 times through 100 nm polycarbonate filters. Additionally, exclusively for cationic TSL, pre-extrusion through 600 nm and 400 nm was performed before downsizing liposomes through 200 and 100 nm filters. Liposomes used for R848 loading (refer to 4.2) were extruded 10 times though 200 nm membrane filters.

3.2.2 Incorporation of fluorescent-labeled lipid

For targeting investigation *in vitro*, fluorescently-labeled cationic and anionic liposomes were used. Hence, a certain percentage of either Rho-PE (0.1 mol%) or NBD-PE (0.3 mol%) in chloroform solution was spiked in the lipid mixture. Lipid film was hydrated with HEPES-buffered saline (HBS) pH 7.4 using the same above reported condition for hydration (10-15 min at 60 °C). After extrusion, liposomes were stored in the fridge at 2-8 °C until use.

3.3 APIs loading and fluorophore incorporation in TSLs bilayer

3.3.1 Passive loading

R848 stock solution was formed by solubilizing the powder with acetate buffer 40 mM pH 5.2 with 5 % ethanol at a final concentration of 3.19 mM (1 mg/ml). Gentle mixing at 37 °C for 20-30 min was required to induce full API solubilization. R848 solution was aliquoted in test tubes (1 ml each) and at - 20 °C until use. For passive loading, a lipid film was hydrated with 3.19 mM R848 solution in the medium mentioned above for 10-15 min at 60 °C. Unencapsulated R848 was separated by size exclusion chromatography (PD-10 columns, GE Healthcare, München, Germany) against HEPES-buffered saline (HBS) pH 7.4. General settings of passive loading experiments are shown in Table 1.

Table 1. R848 passive loading method conditions.

Hydration volume (ml)	R848 (mM)	Lipid concentration (mM)	Condition hydration	R848/lipid (mol:mol)
2	3.19	32	10-15 min 60 °C	0.1

3.3.2 Active (remote) API loading

Remote loading of DOX and R848 in pre-formed liposomes was performed via gradient method already published with minor modifications [37, 245]. Transmembrane proton (H^+) or ammonium (NH_4^+) gradients were established by buffer exchange via PD-10 column equilibrated in specific extra-liposomal buffer, as described in Table 2.

Table 2 DOX and R848 active loading conditions.

API	Intra-liposomal medium	Extra-liposomal medium	Loading condition	Drug/lipid (mol:mol)
DOX	240 mM $(NH4)_2SO_4$ pH 5.4	HBS pH 7.8	37 °C/1 h (38 °C/1 h)[*]	0.05
R848	300 mM $(NH4)_2SO_4$ pH 5.4	HBS pH 5.2 / HBS pH 6.4	37 °C/1 h 30 °C/8 h	0.1 /0.2
	300 mM $(NH4)_2HPO_4$ pH 7.4	HBS pH 5.2 / HBS pH 6.4	30 °C/8 h	0.1 /0.2
	300 mM Citrate pH 4	HBS pH 6.4	37 °C/1 h	0.2

[*]These conditions were used exclusively for the active loading of DOX in cationic TSLs.

In all loading experiments, lipid concentration was adjusted at a final lipid concentration of 3 mM, whereas DOX and R848 amount were adjusted accordingly to the desired drug/lipid ratio. Encapsulation was performed for the desired time and temperatures as described in loading conditions (Table 2) in a thermoshaker (Eppendorf GmbH, Hamburg, Germany). For fluorescent drugs, loading in liposomes decreases overall fluorescence intensity due to self-quenching, in a fashion highly dependent on concentration and physical properties of the fluorophore. The encapsulation was monitored by assessing fluorescence intensity of samples over time (DOX: Ex/Em 470/555 nm; R848: Ex/Em 260/270 nm) via fluorometer (Cary Eclipse, Varian Inc., Palo Alto, California, USA). Batches were cooled at 2-8 °C for 10-15 min and liposomes concentrated via centrifugation (Avanti-J26XP, Beckman Coulter, Krefeld, Germany) at 75,600 x g for 60 min at 10 °C. Supernatant was discarded and liposomal pellet resuspended in specific buffer (DOX: HBS pH 7.4; R848: HBS pH 7.4 or cryoprotectant-containing buffer as described in section 4.2.2.7). For cationic non-PEG containing liposomes, filter centrifugation via Amicon Filter 10K (Merck-Millipore, Darmstadt, Germany) was preferred to remove unentrapped DOX and concentrate liposomes after DOX active loading (4,000 x g for 20 min at 10 °C, repeated 3 to 5 times until desired concentration was obtained). Finally, for all CTSLs, a gel chromatography was performed to remove potential remaining non-liposomal DOX.

3.4 Liposome characterization

3.4.1 Dynamic light scattering

Hydrodynamic diameter (Z-average), PDI and ζ-potential (ζ-POT) were measured by dynamic light scattering (DLS) using Zeta Sizer Nano ZS (Malvern Instruments, Worcestershire, UK). Size and PDI were measured after diluting (C)TSLs in saline (NaCl 0.9 %, 1:50 dilution v/v) at room temperature (RT). ζ-POT of (C)TSLs was measured either in saline or 20 mM HEPES buffer without saline (HEPES pH 7.4).

3.4.2 Lipid determination

Lipid quantification was assessed via phosphorus content adapted from a published method [246]. A 1 g/L phosphate solution (phosphate standard, Merck, Darmstadt, Germany) was used to create a calibration standards in the range of 0.2 to 0.9 mM for linear regression. Liposomes were diluted in NaCl 0.9 % in specific concentration range accordingly to calibration range. Standards and samples were transferred to glass test tubes (Duran®, Mainz, Germany) and oxidation of the organic lipids was carried out by the addition of sulfuric acid and perchloric acid at 300 °C for 2 h, in order to generate inorganic phosphate. The addition of ammonium heptamolybdate formed a complex detectable at 660 nm via spectrophotometry (Beckmann DU 640, Beckman Coulter GmbH, Krefeld, Germany).

Lipids were also analyzed qualitatively and quantitatively via high-performance liquid chromatography (HPLC), the method used is reported in section 3.8.4.

3.4.3 Fatty acids and lyso-lipid determination

Lipid composition in TSL formulations and generation of lipid-degradation products during storage were assessed via HPLC-CAD or thin-layer chromatography (TLC). In the latter case, a previously described method was used [106]. Briefly, 1,500 nmol of lipids in the form of TSLs were disrupted with 1 ml of NaCl 0.9 % and 2 ml of $CHCl_3$/MeOH 1:1 (v/v). Mixture was vortexed and phase separation achieved via centrifugation (3,100 x g, 10 min, RT). The underneath organic phase was transferred to fresh tubes and fully dried under nitrogen stream at 40 °C. Residue was re-dissolved in 100 µL $CHCl_3$/MeOH 9/1 (v/v) and 1.2 µl of such solution spotted onto a TLC-plate (Silica 60, Merck, Darmstadt, Germany). Plates were placed in TLC-chamber equilibrated with $CHCl_3$/MeOH/CH_3COOH/H_2O 100:60:10:5 (molar ratio) allowing lipids/lyso-lipids separation during the run. So-performed chromatography was able to separate lysolipids, phosphocholines (PC; DPPC & DSPC), $DPPG_2$ and DSPE-PEG$_{2000}$. A standard was always used to check chromatography efficiency. At the end of the run, plates were dried and stained with molybdenum spray, as reported

elsewhere [247]. Since molybdenum spray reacts with phosphate groups, only phospholipids can be detected by this mean. Cationic lipids do not present a phosphate headgroups, hence an alternative staining was used for cationic-based TSLs. In this case, plates were stained with a solution of 10 % $CuSO_4$ (wt:wt) in 8 % H_3PO_4 [248]. After drying, heat was required to induce chemical reaction and thus generate dark spots on the chromatogram in relation to lipids retentions. However, due to artifacts generated during heating on the chromatogram area this method was exclusively used to qualitatively detect cationic lipid presence and not to perform densitometric analysis.

Lipid degradation products as fatty acids were also quantified via HPLC-CAD method as reported in 3.8.4.

3.4.4 Osmolality

To assess the osmolality of hydration solutions, buffers and final TSLs, a vapor pressure osmometer (Vapro 5600, Wescor Inc., Logan, Utah, USA) was used. Standard solutions with different osmolalities (100 mmol/kg, 290 mmol/kg and 1,000 mmol/kg) were used to calibrate the device prior usage. After the calibration, 10 µl of sample was pipetted on a specific filter unit and osmolality assessed.

3.4.5 Differential Scanning calorimetry

Differential scanning calorimetry (DSC) was performed with freshly prepared batches after API loading to assess T_m of different TSL formulations. All tested liposomal samples were concentrated via spin columns (Amicon filters 30K, Merck-Millipore, Darmstadt, Germany). Concentrated liposome suspension (20 µl, lipid range 40-55 mM) was transferred into aluminium pans and measured on a Mettler Toledo DSC 821e (Mettler Toledo, Giessen, Germany). All samples were scanned with 1 °C/min heating rate from 20 to 60 °C.

3.4.6 Cryo-TEM

Cryo-transmission electron microscopy (Cryo-TEM) was performed (Mrs. Sabine Barnert, Pharmaceutical Technology and Biopharmaceutics, Albert-Ludwigs-University Freiburg, Germany) using a method reported elsewhere [249]. TSLs were diluted in HBS pH 7.4 to final lipid concentration of 10 mM. About 3 µl of liposomes suspension was placed on 400 x 100 mesh Quantifoil® S7/2 holey carbon film on copper grids. The paper was snap-frozen into liquid ethane (Kryogen, 90K) and transferred into the TEM (120 keV). Images were taken with an amplified camera at magnifications from 6,300x-12,500x.

3.4.7 Short-term storage stability study

3.4.7.1 DOX loaded TSL at 2-8 °C

Cationic and anionic liposomes subjected of DOX loading were subsequently stored at 2-8 °C and vesicle size & size distribution , DOX leakage and lipid degradation products assessed weekly in a 30 days investigation. Size, PDI & ζ-POT were assessed as described in section 3.4.1. DOX leakage was investigated via fluorescence spectroscopy and lipid hydrolysis via TLC method.

3.4.7.2 R848-loaded TSL at 2-8 °C and -20 °C

Similar to above reported investigation for DOX-loaded TSL, DPPG$_2$-TSL-R848 storage stability was also performed in a 30 days investigation. In this case, storage at fridge condition (2-8 °C) or frozen condition (- 20 °C) where both assessed and compared. TSL physical properties were monitored weekly via DSL analysis (section 3.4.1), R848 leakage and lipid degradation products were both assessed via HPLC analysis (method reported in section 3.8.3).

3.5 API determination and encapsulation efficiency

3.5.1 DOX

DOX quantification in TSLs was assessed via either fluorescence spectroscopy or HPLC. In the case of fluorometry, calibration standards of DOX in H_2O were used (calibration range: 0-1.13 µM). DOX-loaded TSLs were diluted in HBS pH 7.4 to the calibration range, Doxil® liposomes were also used in the assay to control method quality. All samples and standards were further diluted in Triton X-100 10 % (1:11, v/v) and placed in a thermoshaker at 45 °C for 15 min in order to ensure full liposome disruption. Thereafter, DOX fluorescence intensity was assessed in samples after diluting them 1:151 (v/v) in HBS pH 7.4 (DOX Ex/Em 470/555 nm) (Cary Eclipse, Varian Inc.). For DOX HPLC method, refer to section 3.8.1.

3.5.2 R848

R848 was detected via the HPLC method described in section 3.8.3.

3.5.3 Encapsulation efficiency

Final encapsulation efficiency (EE) is expressed as a percentage and it is calculated by using the following formula:

$$EE\ (\%) = (D/L)_{final}\ /\ (D/L)_{initial} * 100 \hspace{2cm} \text{Equation 1}$$

where D/L_{final} is the drug/lipid molar ratio after the loading and separation process whereas $D/L_{initial}$ is the initial drug/lipid molar ratio at the beginning of the loading process.

3.6 Temperature-dependent drug release

3.6.1 DOX-loaded TSLs

For temperature-dependent DOX release profiles, loaded TSLs were diluted in HBS pH 7.4 (1:4, v/v) and further diluted in fetal calf serum (FCS) 1:10 (v/v). 20 µl of the liposome suspension was placed in a pre-heated thermoshaker set at different temperatures ranging from 37 °C to 45 °C, to reach target temperature in few seconds. Incubation was carried out either for 5 min (37-45 °C) or for 1 h (37 °C and 42 °C) with mild-shaking (750 rpm). After incubation, release was stopped by adding 1 ml of ice-cold HBS pH 7.4. DOX release was measured by fluorescence spectroscopy (Ex/Em 470/555 nm). Fluorescence intensity for 100 % release (I_∞) was obtained after incubation of a sample with 10 % Triton X-100 (1:2, v/v) for 15 min at 45 °C. Percentage of DOX released was calculated as follows:

$$DOX\ (\%) = (I_{T\,°C} - I_{RT})/(I_\infty - I_{RT}) * 100 \hspace{2cm} \text{Equation 2}$$

where $I_{T\,°C}$ is the fluorescence intensity after incubation for the time at a specific temperature and I_{RT} is the fluorescence baseline when the sample is incubated at RT for 5 min.

3.6.2 R848-loaded TSLs

Heat-triggered release of R848 from DPPG$_2$-based TSL was assessed by adapting a previously published method used for dFdC [109]. Briefly, R848-loaded TSLs were diluted in either FCS or HBS pH 7.4 1:12 (v/v) with a final volume of 120 µl. TSLs were incubated either for 5 min (37-45 °C) or 1 h (37 and 42 °C) in a thermoshaker under mild-shaking (750 rpm). To assess 100 % content (I_∞), TSL were diluted 1:2 in either FCS or HBS pH 7.4 (according to what matrix was used in the investigation), and 20 µl of so-diluted liposomes were mixed 1:2 (v/v) with 10 % Triton X-100 (45 °C, 15 min). The incubation was immediately stopped by placing the samples in an ice-water mixture and by adding 200 µl of ice-cold HBS pH 5.2 buffer (280 µl for Triton samples). Samples were stored in the fridge at 2-8°C until released-R848 fractions were separated from liposomal-R848 using centrifugal filter units (Amicon Filter 30K, Merck Millipore, Darmstadt, Germany). All filter units were previously passivated with 5 % Triton X-100 overnight. The whole sample volume (300 µl) was loaded into the filter unit and centrifuged at 14,000 x g for 10 min at 10 °C. The filtrates were collected and stored at - 20 °C until HPLC measurement (section 3.8.3). Percentage of release was calculated using Equation 2.

3.7 Time-dependent drug release

3.7.1 DOX-loaded TSLs

Kinetics of release were assessed for DOX-loaded liposomes using an already published method [106]. TSLs were diluted 1:4 (v/v) in HBS pH 7.4, 20 µl of the liposomes suspension was then transferred in pre-heated and stirred FCS (1:151, v/v) at desired temperature in a range between 37 and 42 °C. Release kinetics were investigated by measuring change in fluorescence intensity over 60 min time span with 2 to 4 min assessment rate. To evaluate 100 %-release, TSLs were diluted in Triton X-100 (1:2, v/v) and liposomes disruption conducted for 15 min at 45 °C in a thermoshaker. The reaction was stopped by addition of HBS pH 7.3 (1:2, v/v). 20 µl of this solution was added in parallel to each probe samples to assess maximum fluorescence intensity at the specific temperature range. DOX release was assessed over time by using the above reported formula (Equation 2). Release rate at 41 and 42 °C was fit through an exponential one-phase association and rate constant (K) assessed for the first 300 s.

3.7.2 R848-loaded TSLs

Release kinetics of R848 from TSL was assessed using the same method as described above for the temperature-dependent release profile (section 3.6). In this case, release kinetics were assessed at 37 and 42 °C for specific time intervals (5, 10, 20, 30, 40 and 60 min), either in FCS or HBS. At mentioned time points, samples were removed from the thermoshaker and immediately cooled on water-ice mixture. All samples were run through passivated centrifugal filters (Amicon filters 30K) to separate the released fraction of R848 from the liposomal one. Filtrates were collected and stored at – 20 °C until HPLC measurement (refer to section 3.8.3). R848 release rate at 37 and 42 °C was fit through an exponential one-phase association and rate constant (K) assessed for 60 min of R848 release.

3.8 High-performance liquid chromatography (HPLC)

3.8.1 HPLC DOX determination in aqueous, plasma and cell lysate matrices

DOX HPLC analysis was carried out via a Waters HPLC system equipped with 510 HPLC pumps, 717plus autosampler and a 470 fluorescence detector. DOX and internal standard (DAU) were eluted using a Kinetex® C18 (250 x 4.6 mm, 5 µm, 125 Å) equipped with C18 pre-column (Phenomenex Ltd., Torrance, California, USA), whit Ex/Em at 480 and 560 nm, respectively. HPLC analysis was performed with a mobile phase A formed of 120 mM KH_2PO_4 pH 5.5 and acetonitrile (ACN) 74:26 (v/v), and a mobile phase B consisting of 70 % ACN in H_2O. DOX and DAU were separated via isocratic elution with 100 % mobile phase A, whereas a gradient towards 100 % B was rapidly applied around min 7 to flush the column. The flow rate was set at 0.4 ml/min whereas column oven was raised up to 30 °C, total time run was 25 min. A representative chromatogram obtained with above described condition is shown in Figure 8.
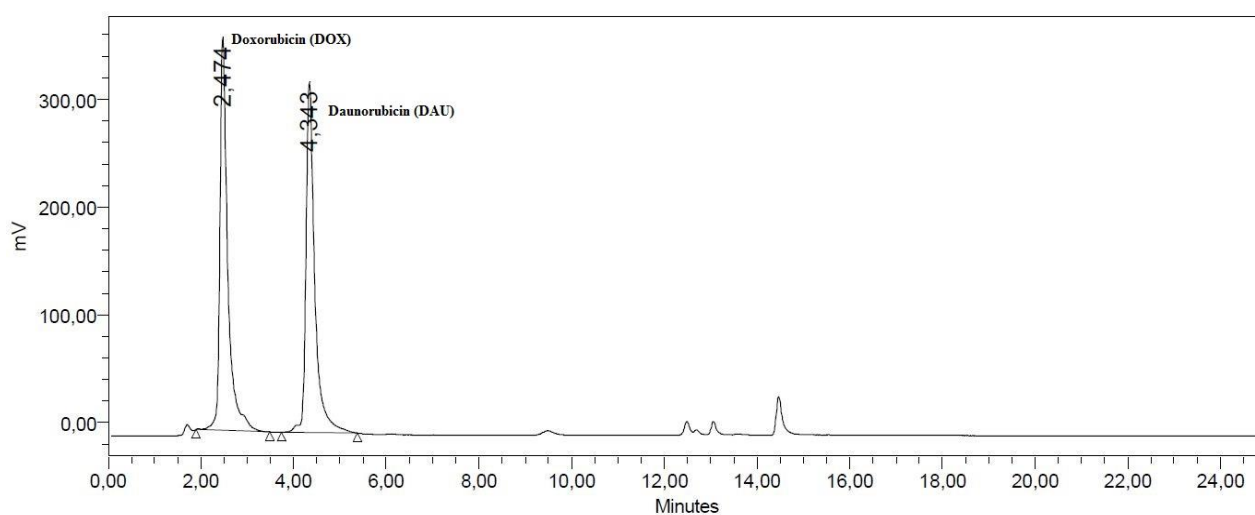

Figure 8 Representative chromatogram obtained after injection of DOX and DAU in mobile phase.
DOX elution peak was assessed at ~ 2.4 min (relative retention time, RRT: 1.00) whereas internal standard DAU elutes ~ 4.3 min (RRT: 1.79)..

For buffer, plasma and cell-culture samples an organic solvent extraction via ACN precipitation was performed, respectively. Liposomes were diluted in HBS pH 7.4 1:50 and 1:100 (v/v), whereas samples from cell culture were pre-treated in order to ensure cell disruption and thus ease DOX extraction (refer to section 3.10.5 for full protocol description). Calibration standards were created with DOX in H_2O ranging from 2.5 to 10 µg/ml. Samples and standards were placed in fresh tubes (50 µl) and a DAU was added as internal standard (50 µl of a 10 µg/ml solution). Organic solvent extraction was performed by adding 600 µl of ACN and mixing all samples vigorously in a thermoshaker (1,000 rpm) for 10 min at RT. Thereafter, samples were centrifuged (20,000 x g, 10 min, RT), supernatant collected and dried under nitrogen stream at 40 °C. Residues were resolved

with 1 ml of mobile phase (120 mM K_2HPO_4/ ACN 74/26, v/v) and injected in the HPLC system (100 µl injection volume).

3.8.2 HPLC DOX determination in tissue

For DOX analysis in e.g., full blood, organs and tumors a solid-phase extraction (SPE) sample preparation method was applied.

For DOX detection in rat full blood, DAU was added to 100 µl of sample and mixed with MeOH (1:11, v/v). Full liposomes disruption was conducted for 10 min in a thermoshaker set at 1,000 rpm and RT. Samples were diluted in H_2O and centrifuged (14,000 x g, 16 min, RT) Thereafter, STRATA-X columns (Phenomenex Ltd., Torrance, California, USA) were mounted in a 24-position vacuum manifold (Phenomenex Ltd., Torrance, California, USA) and conditioned with 2 ml of MeOH and subsequent 2 ml of H_2O (SPE setup shown in Figure 9). Supernatants collected after centrifugation were added to the columns and interactions with SPE cartridge was allowed. Columns were washed with separate water/MeOH solutions at increased MeOH concentrations (10, 20 and 30 %). Next, DOX was eluted with 2 % formic acid in MeOH. Vacuum was applied to completely elute the entrapped DOX. Organic solvent was removed under nitrogen flushing at 40 °C and the dry pellet was resuspended in mobile phase prior to HPLC analysis.

For tissue, samples were cut in small pieces (~ 100 mg) and placed in 2 ml Eppendorf tubes. Internal standard (100 µl DAU, 5 µg/ml), 500 µl of H_2O and 1,100 ml of MeOH were added. Tissue was homogenized in a TissueLyser (30 Hz, 4 x 4 min) (Qiagen GmbH, Hilden, Germany), thereafter 200 µl of 33 % $AgNO_3$ (wt/wt) was added to the mixture and samples immediately cooled on ice for 10 min. At the end of the incubation time, samples were centrifuged at 20,000 x g for 16 min at RT, supernatant collected and used for SPE extraction as reported above. Depending on the matrix, calibration standards were created by spiking DOX either in blood or liver tissue covering a range between 2.5 to 33.3 µg/ml and 0.5 to 10 µg/ml, respectively.

Figure 9 SPE manifold setup.
The manifold allows the position of 24 SPE columns, vacuum is generated via a pump connected to the glass chamber.

3.8.3 HPLC R848 in aqueous and plasma samples

R848 HPLC analysis was carried out on a Scientific Ultimate 3000 HPLC system equipped with a diode-array detector (DAD) (ThermoFisher, Dionex[TM]), a Kinetex® C18 column (250 x 4.6 mm, 5 µm, 125 Å) equipped with a C18 pre-column (Phenomenex Ltd., Torrance, California, USA) and a detection wavelength of 242 nm. Elution of both R848 and R837 was performed using a mobile phase A of 100 mM ammonium acetate buffer pH 4 and ACN 85:15 (v/v), and a mobile phase B consisting of 30 % ACN in H_2O. A gradient elution was established starting with A at 85 % and decreasing gradually to 50 % in the initial 3 min after sample injection. Flow rate was adjusted at 0.5 ml/min whereas column oven was set at 35 °C, total run was 12 min. Typical chromatogram obtained with above described condition is shown in Figure 10.
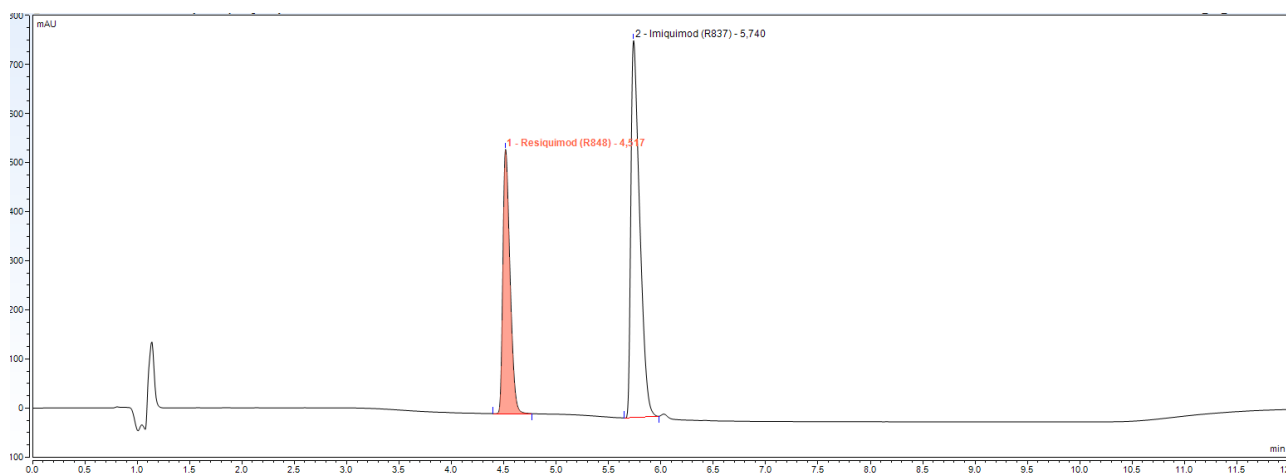

Figure 10 Representative chromatogram obtained after injection of R848 and R837 in mobile phase.
R848 elution peak is ~ 4.5 min (relative retention time, RRT: 1.00) whereas internal standard R837 elutes ~ 5.7 min (RRT 1.27).

An extraction process based on ACN precipitation was developed, similar to the method used for DOX extraction from aqueous matrices (refer to section 3.8.1). Briefly, 50 µl of probe was

transferred in a fresh test tube and 10 µl of R837 (263 µg/ml) was added as internal standard. For R848 quantification in liposomal suspension, a pre-dilution of TSL in HBS pH 7.4 (1:30 and 1:60, v/v) was performed. Extraction was carried out by the addition of 560 µl of ACN to the solution and samples vigorously agitated in a thermoshaker at 1,000 rpm for 10 min at RT. Samples were centrifuged (2,000 x g, 10 min, RT) and supernatant transferred in fresh test tubes. Drying step was performed under nitrogen flow at 40 °C, residues were resuspended in 450 µl of mobile phase (acetate buffer pH 4/ACN 85/15, v/v). Samples were injected in the HPLC system via automated sampler with 50 µl injection volume. According to the type of matrix, calibration samples were created by spiking R848 in either HBS pH 5.2, FCS or rat plasma covering a range between 5 to 100 µg/ml.

3.8.4 Lipid & fatty acid quantification via HPLC-CAD

Lipids were also analyzed qualitatively and quantitatively via high-performance liquid chromatography (HPLC, Scientific Dionex^{TM} Ultimate, 3000) equipped with a charged aerosol detector (CAD Corona Veo) (ThermoFisher, Waltham, Massachusetts, USA). Chromatographic separation was carried out with an Xbridge$^{®}$ Phenyl column (150 mm x 2.1 mm, 3.5 µm, 130 Å) and a Xbridge$^{®}$ BEH Phenyl V-Gd as pre-column (Waters, Milford, Massachusetts). Lipids solubilized in MeOH were used as standard, creating a quadratic calibration curve for DPPC, DSPC and DPPG$_2$ ranging from 116 to 513 µM. Liposomes were diluted in water in accordance to the calibration range and directly injected (5 µl injection volume). Phospholipids separation was achieved via a mobile phase A formed by 100 mM ammonium acetate pH 6 and 100 % MeOH as mobile phase B. Isocratic elution was performed with an initial 90 % of mobile phase A, whereas at 10 min after injection a rapid gradient up to 100 % A was applied to flush the column after elution of the analytes. Flow rate was adjusted at 0.4 ml/min whereas column oven was set at 35 °C, total run required 25 min. A representative chromatogram of phospholipids separation obtained with above described condition is shown in Figure 11.

HPLC-CAD was also used to assess lyso-lipid and fatty acid content potentially generated after loading procedures and during prolonged storage. Calibration standards were created by spiking different concentrations of palmitic and stearic acids in MeOH (96-1,000 µM range). Liposomal samples were diluted in H$_2$O 1.20 (v/v) and injected in the HPLC with 5 µl injection volume. Same mobile phases A and B above reported for phospholipids elution were also used in this method. However, the gradient applied was slightly different, with an initial 65% A and a gradual increase to 100 % A in 22 min. Flow rate was set at 0.4 ml/min whereas column oven was 35 °C, total run required 33 min.

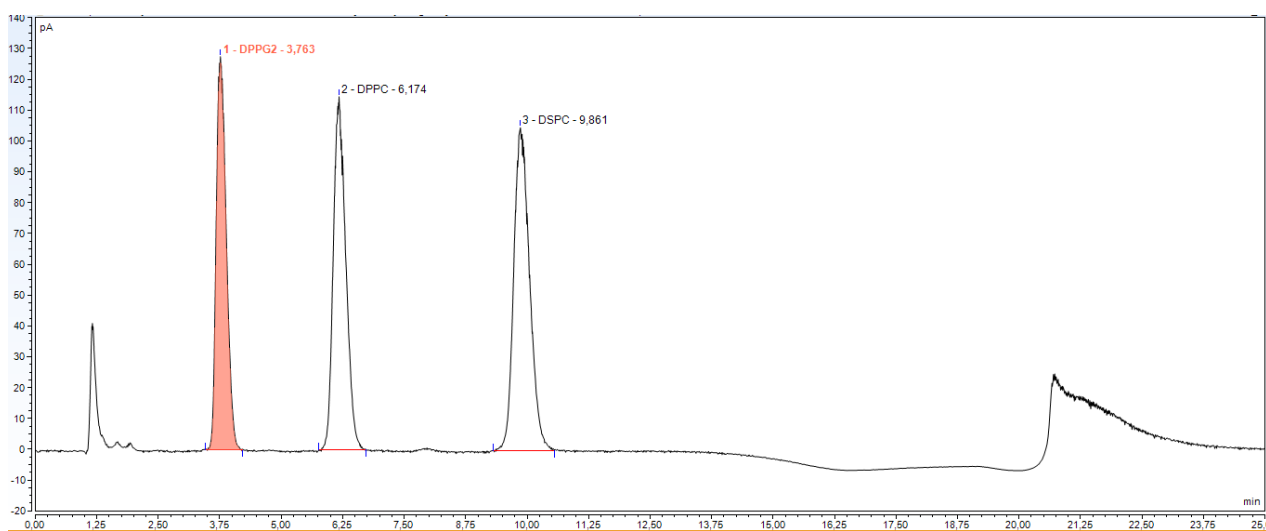**Figure 11 Representative chromatogram obtained after injection DPPG$_2$, DSPC and DPPC.**
Phospholipids in MeOH. Elution peaks of DPPG$_2$, DPPC and DSPC were detected at ~ 3.7, ~ 6.2 and ~ 10 min retention time, respectively.

3.9 Protein corona

3.9.1 Protein corona liposomes

Protein adsorption of liposomes was assessed by adapting a method described in Palchetti et al [250]. Briefly, 25 mM of (C)TSLs were incubated in pre-centrifuged FCS (75,600 x g, 10 °C, 1 h) for 1 h at 37 °C in a thermoshaker with mild shaking (450 rpm). Liposomes with respective protein corona (P-(C)TSL) were separated from serum pool via centrifugation for 1 h at 75,600 x g. Supernatant was discarded and liposome pellet washed with HBS pH 7.4 three times. Finally, pellet was resuspended in HBS pH 7.4 buffer and P-(C)TSLs physicochemical properties assessed (e.g., DLS, ζ-POT).

3.9.2 Protein quantification

Protein amount was assessed via DC^{TM} protein quantification kit using manufacturer instruction and bovine serum albumin (BSA) as standard. Protein corona liposomes were diluted 1:5 or 1:10 in NaCl 0.9 %, whereas full FCS tested as positive control was usually diluted 1:80 and 1:100 (v/v) to meet calibration range. Liposomes w/o protein corona and buffer systems were also tested to assess potential background signals generated from the assay.

3.9.3 Gel electrophoresis

About ~ 20 nmol of protein corona TSLs obtained after purification via centrifugation was subjected to gel electrophoresis and silver staining. In brief, a 10 % acrylamide sodium dodecyl sulfate (SDS) gel was run and fixed for 20 min in 50:5:45 (v/v/v) MeOH/CH$_3$COOH/H$_2$O, followed by sensitization in 200 mg/ml sodium thiosulfate for 1 min. Next, the gel was incubated for 20 min in a 1 mg/ml AgNO$_3$ solution in 0.03 % formalin. Finally, the color was developed in 20 mg/ml NaHCO$_3$ in 0.04 % paraformaldehyde (PFA) and the reaction was stopped by 5 % CH$_3$COOH.

3.10 *In vitro* cell work packages

3.10.1 Cell culture

Rat soft tissue sarcoma cell line (BN175) syngeneic to Brown Norway rats was provided by Timo ten Hagen, Erasmus MC, Rotterdam. Human umbilical vein endothelial cells (HUVECs) were generated from pooled donors and they were kindly provided by the Department of Pharmaceutical Biology, Faculty of Chemistry and Pharmacy, Ludwig-Maximilians Universität (LMU), München (originally acquired from PromoCell GmbH, Heidelberg, Germany). Human ovarian serous cystadenocarcinoma (SKOV-3) were purchased from ATCC (Manassas, Virginia, USA). Peripheral blood mononuclear cells (PBMCs) were separated in-house via Lymphoprep^{TM} (Stemcell Technologies, Vancouver, Canada) gradient from healthy donors (refer to section 3.10.9). Specific culturing conditions for each cell line are shown in Table 3.

Table 3 Cell culturing conditions.

Cell line	Medium	Supplement	FCS heat inactivated	Trypsin/EDTA (concentration)	Coating
BN175	RPMI 1640 medium, NaHCO$_3$ buffered, with L-glutamine (Biochrom AG, Berlin, Germany)	10 % FCS 1 % pen/strep	No	0.05 %	No
HUVEC	Easy Cellovation Medium (Pelo Biotech, Martinsried, Germany)	Supplement mix included in medium kit	No	0.25 %	Yes / 50 µg/ml Collagen G in PBS
SKOV-3	McCoy 5A medium, with NaHCO$_3$ and L-glutamine (Sigma Aldrich)	10 % FCS 1 % pen/strep	No	0.05 %	No
PBMC	RPMI 1640 medium. NaHCO$_3$ buffered, with stable glutamine (Biochrom AG, Berlin, Germany)	10 % FCS 1 % pen/strep	Yes (30 min at 57 °C in water bath)	/	No

pen/strep = penicillin & streptomycin. FCS = fetal calf serum

All cell lines were cultured at 37 °C in a humidified atmosphere at 5 % CO$_2$. Adherent cells were passaged when 80-90 % confluency was reached. Fast replicating cells as BN175 and HEK-293 were subcultured with a 1:10 ratio and usually passaged every third day, whereas HUVEC and SKOV-3 were usually divided every 4 to 5 days with a 1:4 or 1:6 ratio. For hyperthermic experiments,

cells were sealed in plastic wrap and placed on 41 °C (HT) water bath for 1 h. Water temperature was constantly checked via temperature probe in the nearby of plate position. Corresponding normothermic treatment (NT, 37 °C) was performed in the same condition by setting the water temperature to 37 °C. During HT or NT treatments, cell culture medium was replaced with a HEPES-based buffer system medium (RPMI 1640 HEPES-buffered), when possible. Depending on the type of experiment, either full supplemented medium or non-FCS containing medium was used.

3.10.2 Fluorescence microscopy on fixed cells

3.10.2.1 Cationic TSL targeting

Cells were seeded in chamber slides (Nunc™ Lab-Tek™ II, 1-well/slide, ThermoFisher) at a final concentration of 5 x 10^5 cells/well and incubated for 24 h to adhere. Cells were incubated with CMFDA 10 µM in serum-free media for 30 min, thereafter cells were washed and incubated with 1.1 mM Rho-labeled (C)TSLs (corresponding to the amount of lipids required to deliver roughly 50 µM of DOX in liposomal form) in serum-free media. Liposomes were let to interact with cells for 1 h, then unbound fractions were removed and cells washed three times with serum-free media. Hoechst 5 µg/ml was applied on cells prior to fixation with PFA 4 % for a total time of 10 min. Chambers were removed and slides covered with mounting medium and coverslips. Slides were stored at 2-8 °C until fluorescence imaging performed using a Zeiss laser scanning confocal microscope (LSM 510, Zeiss, Germany). Rho-PE fluorescence was detected by 488 nm Argon laser and CMFDA was monitored by a 543 nm Helium-Neon laser, whereas a Neon laser at 364 nm was used to evaluate Hoechst fluorescence. Images (1,808 x 1,808 pixels, 63x/1.4 Oil DIC objective) were analyzed using Zeiss LSM image software (Zeiss, Germany).

3.10.2.2 Immunofluorescence microscopy

Cells were seeded in chamber slides (Nunc™ Lab-Tek™ II, 4-well/slide, ThermoFisher) at final concentration of 1 x 10^5 cells/well and incubated for 24 h to adhere. Freshly purified PBMCs were added to each well at final ratio of cancer cell/PBMC 1:10. R848 at final concentration of 10 µM was added to co-cultured cancer cells, whereas control groups received medium. Incubation was performed at 37 °C in the incubator for 72 h. Subsequently, cells were washed with phosphate-buffered saline (PBS) and fixed via PFA 4 %. TUNEL assay was performed via TACS® 2 TdT in situ apoptosis detection kit, following manufacture´s instruction. Next, slides were washed carefully with PBS, a 10 µg/ml solution of anti-caspase 3 antibody (rabbit antihuman) was added to each slides and incubation carried out at 2-8 °C overnight. Slides were rinsed twice with PBS, Alexa Fluor ™ 594 secondary antibody (goat anti-rabbit) at 1 µg/ml was added to each slide for 30 min at RT. Slides were washed three times with PBS and covered with mounting medium and coverslips. Fluorescence

microscopy was performed using a Leica wide-field microscope provided with Optigrid technology. Images (696 x 520 pixels, 60x/1.4 Oil objective) were performed using Leica LAS X image software (Leica, Germany).

3.10.3 Live-settings fluorescence microscopy

3.10.3.1 Cationic TSL targeting

Live-cell fluorescence imaging on BN175 and HUVEC was performed using lysotracker and NBD-labeled (C)TSLs. In a parallel experiment, DOX was also imaged in cell compartments after incubation with unlabeled DOX-loaded (C)TSLs, after NT and HT treatments. In both experiments, cells were seeded in a glass inserted chamber slide (μ-Dish 35 mm, Ibidi, Germany) and let adhere for 24 h. Cells were either incubated with NBD-labeled (C)TSL or DOX-loaded (C)TSLs (1.1 mM final lipid concentration, serum-free media) for 1 h at 37 °C. In case of NBD-labeled liposomes, Lysotracker red 99 was added after the first 30 min at a final concentration of 0.5 μM. At the end of the incubation time, cells were washed three times with serum-free media and incubated with Hoechst (5 μg/ml, 5 min). Cells were washed again, placed in FCS-containing media and fluorescence microscopy was performed (NT time point). Thereafter, chambers were placed in a water bath set at 41 °C and fluorescence imaged again after 1 h (HT time point). Live-cell microscopy was performed using a Leica wide-field microscope provided with Optigrid technology. Images in live settings (696 x 520 pixels, 60x/1.4 Oil objective) were acquired using Leica LAS X image software (Leica, Germany).

3.10.3.2 Live cell imaging on immune and cancer cells

Live cell fluorescence imaging on PBMC and SKOV-3 cancer cell was performed using lysotracker and NBD-labeled $DPPG_2$-TSL (DPPC/DSPC/$DPPG_2$, 50/20/30 mol:mol), with similar settings as above reported (3.10.3.1). Briefly, SKOV-3 and PBMC were seeded at 1 x 10^5 and 5 x 10^5 cells/well, respectively, in glass inserted chamber slide (μ-Dish 35 mm, Ibidi, Germany). After 24 h incubation, NBD-labeled $DPPG_2$-TSL were added at final concentration of 0.5 mM (final lipid concentration, serum free media) for 1 h at 37 °C. Lysotracker red 99 was added after the first 30 min incubation at a final concentration of 0.5 μM. At the end of the incubation, cells were washed three times with PBS and imaged immediately in live settings with Leica wide-field microscope (696 x 520 pixels, 60x/1.4 Oil objective).

In case of live imaging of cancer and immune cells in co-culture, SKOV-3 were seeded at 1 x 10^5 cells/well in glass inserted chamber slide (μ-Dish 35 mm, Ibidi, Germany). The day after, PBMC were added to the same chamber at final ratio of SKOV-3/PBMC 1:10. Cells were imaged in live

settings the next day via bright-field (Leica wide-field microscope, 696 x 520 pixels, 60x/1.4 Oil objective).

3.10.4 Fluorescence-activated cell sorting (FACS)

Binding efficiency of (C)TSLs to cells was measured by FACS analysis and fluorescence imaging using Rho-labeled liposomes. Cells were seeded at 3×10^5 cells/well in 6-well plates and incubated for 24 h. (C)TSLs were added at final lipid concentration of 1.1 mM in serum-free media. After 1 h incubation at 37 °C, cells were washed three times with serum-free media and manually scraped in the presence of 500 µl PBS per well. FACSCalibur III (Beckton Dickinson, New Jersey, USA) was used to sort cells using Iso-PE channel for 10,000 events. 25 mM NBD-labeled (C)TSL liposomes were incubated in full rat blood (1:12 dilution, v/v) collected in Li-heparin microvette and placed in thermoshaker at 37 °C for 1 h at mild shaking (450 rpm). Subsequently, 500 µl of blood were diluted in 1 ml Red Blood Cell Lysing Buffer Hybri-Max^{TM} (Sigma Aldrich) and erythrocytes lysed using manufacturer instruction. Briefly, samples were incubated at RT in a thermoshaker for 10 min with mild-shaking (450 rpm) and centrifuged at 500 x g for 5 min at 10 min. Supernatant was discarded and 1 ml fresh lysis buffer was added, repeating incubation time as previously described. The resulting leukocytes were washed two times with PBS and resuspended in 500 µl PBS. FACS analysis was carried out with FACSCalibur III, monocyte, lymphocyte and granulocyte populations were gated by forward and side scatters and sorted via isoFITC channel for 10,000 events.

3.10.5 Recovery of API after incubation

DOX delivery efficacy by using anionic and cationic TSLs was assessed by evaluating the DOX amount in cells after liposome incubation. Briefly, cells were seeded in 6-well plate at 5×10^5 cells/well. After 24 h, cells were incubated with 50 or 100 µM of free DOX or liposomal DOX. Incubation was carried out for 1 h at 37 °C in serum-free media. After washing cells three times, serum-containing media was added and NT and HT treatments applied for 1 h, as described above. Then, medium was removed and cells trypsinized and pelleted down in 1.5 ml Eppendorf tubes at 2,000 x g for 10 min at RT. Cells were resuspended in lysis buffer (1 % Triton X-100, 0.1 % SDS, 150 mM NaCl, 20 mM TRIS, pH 7.4) and placed on ice for 30 min. Samples were sonicated for 1 min in ice with a probe sonicator, centrifuged (2,000 x g, 10 min, RT) and stored at - 20 °C until DOX HPLC analysis (refer to section 3.8.1).

3.10.6 *In vitro* toxicity of DOX-loaded (C)TSLs

Cells were seeded in 96-well plate at 5×10^3 cells/well in a total volume of 200 µl. Cells were incubated with different concentrations of liposomal DOX ranging from 0.37 µM to 100 µM. After

1 h incubation at 37 °C, cells were washed and fresh serum-containing media was added. Plates were either placed inside the incubator at 37 °C (NT treatment) or in a water bath set at 41 °C (HT treatment), for 1 h and then inside the incubator at 37 °C for 3 days. Toxicity of DOX-loaded (C)TSLs incubation was assessed by performing Sulforhodamine B (SRB), as reported in section 3.10.8.1.

3.10.7 Hemocompatibility

Hemocompatibility was investigated *in vitro* assessing complement activation magnitude in human serum incubated with (C)TSLs. Anionic and cationic liposomes were incubated for 15 min with normal human serum (1:12, v/v) and complement activation assessed via SC5b-9 ELISA test. Zymosan A (10 mg/ml in NaCl 0.9 %) and HEPES buffer pH 7.4 were used in the assay as positive and negative control, respectively.

3.10.8 Cell-viability assay

3.10.8.1 Sulforhodamine B assay (SRB)

Cell viability was measured by SRB assay by assessing total protein amount [251]. Cells were fixed with trichloroacetic acid 1 % and placed in the fridge at least for 1 h. Cell monolayer was washed under gentle water flow and solution of SRB 5 % was added in each well. After 20 min, cells were rinsed carefully with acetic acid solution 1 % to remove unbound dye. Plates were dried at either 60 °C for 3 h or 37 °C over night. 100 μl of 10 mM Tris solution (pH 10.5) was added to each well and plates gently stirred on an orbital shaker for 10 min to solubilize the protein-bound dye. Absorbance was quantified via a microplate reader at 450 nm.

3.10.8.2 WST-1 assay

WST-1 (F. Hoffman-La Roche, Basel, Switzerland) was added to a final 1:10 dilution (v/v) per each well. Plates were placed back in the incubator to allow colorimetric reaction. Absorbance was quantified after 3 h incubation time via a microplate reader at 450 nm.

3.10.9 PBMC purifications

Fresh blood from healthy donors was used to obtain PBMCs by using a method reported elsewhere [252]. In brief, blood was diluted 1:2 (v/v) with PBS and placed carefully on an equal volume of Lymphoprep™ in a 50 ml Falcon tube, paying attention to form two distinct phases. Gradient centrifugation was performed at 800 x g for 20 min at RT. PBMCs at interphase between plasma and the gradient were carefully collected and transferred in fresh Falcon tubes. Cells were

washed twice with PBS 1:20 (v/v) and centrifugation at 450 x g for 10 min at RT. Finally, PBMCs were seeded in either 24-well plates or 96-well plates for experimental procedures.

3.10.10 *In vitro* cytokines detection by enzyme-linked immunosorbent assay (ELISA)

Freshly isolated PBMCs were seeded at final concentration of 1×10^6 cells per well in a 24-well plate or at final concentration of 1×10^5 cells in 96-well plate. Induction of cytokines was carried out via incubation with R848 (naked-R848 or liposomal-R848) at different concentration or with LPS (1 μg/ml, positive control). Stimulation with IAVs was conducted either for 1 h or 24 h, whereas cytokines were always assessed in cell supernatant after 24 h. In case of 1 h incubation, cells were washed via centrifugation at the end of the incubation time (450 x g, 10 min, RT) and placed back in the same well with fresh medium. Hyperthermic or normothermic treatments were performed in accordance as described in section 3.10. Supernatant samples were loaded onto ELISA wells and assay was carried out following the manufacturer's instructions. In parallel experiments, human PBMCs were seeded in 96-well plate at 10×10^5 cells/well in a total volume of 200 μl. Cells were incubated either with R848 or RPMI medium (negative controls). Cell proliferation was assessed via WST-1 assay at different incubation time (24, 48, 72, 120 and 168 h) (refer to section 3.10.8.2).

3.10.11 IAV toxicity & immune-mediated cancer cell killing *in vitro*

Cancer cells (BN175 or SKOV-3) were seeded in 96-well plate at 5×10^3 cell/well density. Cells were let rest for 24 h and R848 was then added at different concentrations ranging from 0.1 to 100 μM. Incubation was prolonged for 24 and 72 h, in both cases hyperthermic or normothermic treatments were performed in accordance as described in section 3.10. At the end of incubation time, cell viability was evaluated via SRB assay as reported in section 3.10.8, 3.10.8.1. To assess immune cell killing of cancer cells, a co-culture method was developed. Briefly, SKOV-3 cells were seeded at 5×10^3 cells/well in a 96-well plate. Cells were let adhere for 24 h, thereafter PBMCs (50×10^3 cells/well) were added to create a 1:10 ratio cancer cells/PBMCs. On the same day, R848 was added at different concentrations ranging from 0.1 to 100 μM, whereas negative controls were treated with simple medium. Hyperthermia or normothermia was applied immediately after IAVs incubation for 1 h (refer to section 3.10). Plates were placed back in the incubator at 37 °C and cell viability assessed via SRB assay after 72 h (refer to section 3.10.8.1).

3.11 *In vivo* work packages

Animal experiments were performed according to protocols approved by the responsible authority (Regierung of Oberbayern, Az. ROB. 55.2-2532.Vet_02-17-208 and Az. ROB. 55.2-

2532.Vet_02-18-61). Brown Norway rats were acquired from Charles River GmbH (Sulzfeld, Germany) and housed with max 4 animals per cage with free access to autoclaved chow (Ssniff Spezialdiäten GmbH, Soest, Germany) and water. Day/night cycle was set at 12 h rate with RT monitored at 21 °C. A sitting-in of at least 7 days was permitted after animal arrivals before starting the experiments. For *in vivo* experiments, animals were placed under anaesthesia (5 % isoflurane for induction and 2 % for maintenance) (Forene®, Abbott GmbH & Co. KG, Wiesbaden, Germany) and 1.5-2.0 l/min of O_2. Physiological body temperature was preserved via a heat-mattress set at 37.5 °C, warm gloves and a blanket if required. Rats were medicated with metamizole (Vetaglin®, Intervet Deutschland GmbH, Unterschleißheim, Germany) and meloxicam (Metacam®, Boehringer Ingelheim Pharma GmbH & Co. KG, Ingelheim am Rhein, Germany) at 100 mg/kg s.c. and 0.05 mg/kg s.c., respectively. For BD studies, buprenorphine at a final dosage of 0.05 mg/kg was also administrated before starting the experiment. Animal euthanasia was performed via intracardiac administration of 300 mg/kg pentobarbital (Release®, WDT GmbH, Garbsen, Germany).

3.11.1 Pharmacokinetic studies

Brown Norway rats were kept under appropriate conditions as reported above until experimental procedures. Drugs in solution or formulated in TSLs were injected via a catheter implanted in the tail vein, after injection catheter was flushed with 200 μl of physiological saline. Blood or plasma samples were generated at 0, 2, 10, 30, 60 and 120 min via incision of the tail with a scalpel and collected in Li-heparin microvette (Sarstedt, Nümbrecht, Germany). To assess DOX circulation half-life, full blood was transferred in 1.5 ml Eppendorf tubes from the microvette system and then frozen at - 20 °C until HPLC analysis (refer to section 3.8.2). For R848, blood was immediately centrifuged (4,000 x g, 10 min, RT) and plasma collected and stored at - 20 °C until HPLC analysis (refer to section 3.8.3). The blood or plasma concentration of DOX or R848, respectively, were fitted using a mono-exponential function (Equation 3) or bi-phasic exponential function (Equation 4):

$$c(t) = c(0) * e^{-k*t} \qquad \text{Equation 3}$$

$$c(t) = c(0) * e^{-k1*t} + c(0) * e^{-k2*t} \qquad \text{Equation 4}$$

where c(t) is drug concentration in the blood/plasma at time *t* (min) after i.v. administration and *k* is the constant rate of elimination. The area under the curve (AUC) was calculated by integrating the exponential fit from 0 to 120 min while half-life (t_α) was assessed with the following formula:

$$t_\alpha = \ln (0.5)/k \qquad \text{Equation 5}$$

3.11.2 Biodistribution

DOX organs/tumor distribution was assessed in tumor-bearing rats in combination with regional mild-HT. BN175 cells were cultured as described and 1.5×10^6 total cells were inoculated in the left and right hind flanks. Tumor growth was monitored each second day and volume assessed using the ellipsoid volume formula (Equation 5):

$$V = a * b * c * (\pi/6) \hspace{4cm} \text{Equation 6}$$

where a, b and c are length, width and height, respectively. When tumors reached a 0.5 cm^3 volume, they were excised and cut in small pieces, creating tumor fragments. The latter were inserted subcutaneously in both right and left hind legs in rats. Tumor growth was monitored each second day and rats were enrolled in the study when tumor volume reaches a threshold size of 0.5 cm^3 (8-11 days after implantation). One of the tumors received HT (41 °C, 1 h) via cold-light lamp (Photonic PI2000, Photonic Optics, Vienna, Austria), whereas the second tumor on the opposite side was kept at physiologic temperature. HT-tumor temperature was measured invasively using an internal probe, whereas body temperature was monitored via rectal probe. (C)TSL-DOX i.v. injection via tail vein catheter was performed as soon as HT-tumor temperature of 41 °C was reached. Liposomes were let circulate for 1 h while HT-tumor temperature was kept between 41 and 42 °C. At the end of HT application, rats were medicated with 30 mg/kg pentobarbital intracardial to ensure deep state anaesthesia while isoflurane was increase to 5 %. Whole-body perfusion was performed by opening the thorax and exposing the heart. The right atrium was cut while saline was continuously flushed via the left ventricle in the body (~ 60 ml). Organs and tumors were excised and stored at - 20 °C until DOX assessment via HPLC analysis.

3.12 Software and statistical analysis

The data are expressed as mean ± standard deviation (SD) of at least three independent experiments, unless otherwise specified. Red and green fluorescence intensity (Iso-PE and IsoFITC channel, respectively) assessed via FACS was analyzed via FlowJo software (version 10.5.0). All images obtained via fluorescence microscopy were analyzed via ImageJ free-software to calibrate contrast, intensity and brightness. Analysis of peak intensity of TLC chromatograms was performed via Gimp and ImageJ software. Pharmacokinetic curves and corresponding parameters were assessed via Origin software (version 8.5). Statistical analysis was performed via GraphPad Prism software (version 7.05). Figures were subjected to either two-tailed T-test or one-way ANOVA Bonferroni test with significance indicated when $p > 0.05$.

4 Results

4.1 Dual tumor targeting with cationic TSL
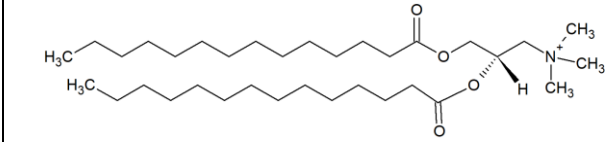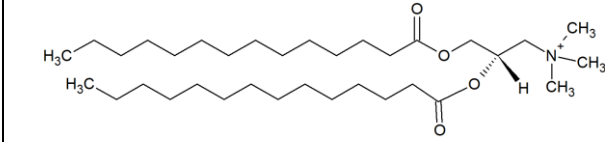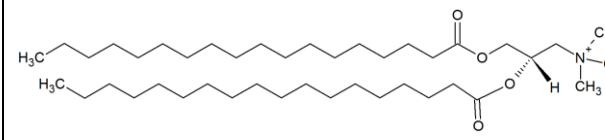
The objective of the study was to investigate if a dual targeting approach with cationic-based liposomes is able to improve traditional TSL delivery. In order to do so, a novel DPPG$_2$-based cationic TSL formulation for potential tumor targeting was designed and tested in the following study. Additionally, the investigation aimed to unveil limitations of PEG in similar settings and to analyze potentially synergistic effects of cationic active targeting and mild-HT for DOX-tumor enrichment. Targeting capability and DOX delivery efficiency were assessed in cancer and endothelial cells both for anionic and cationic TSLs. PK and BD were assessed *in vivo* in combination with mild-HT to investigated potential advantages of dual targeting for tumor cancer therapy.

4.1.1 Formulation design
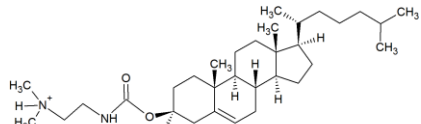
4.1.1.1 Incorporation of cationic lipids in DPPG$_2$-based liposomes

DPPG$_2$ phospholipid is highly compatible in a DPPC/DSPC bilayer and can be included up to 70 mol% in liposomes [107]. According to DPPG$_2$-content, liposomes' surface charge will increase towards a more negative ζ-POT driven by anionic phosphate charge present on phospholipid headgroup. Hence, a DPPG$_2$-based cationic formulation should contain a balanced amount of DPPG$_2$ and specific cationic lipid, with a slight excess of the latter. Furthermore, cationic lipid physical compatibility in the liposomal bilayer needs to be assessed accordingly. In this investigations, different cationic lipids formed by a tri-methyl-ammonium-propane headgroup esterified with different fatty acids were tested (Table 4). Additionally, potential improvement in bi-layer packing driven by the inclusion of cholesterol was also assessed by addition of positively charged DC-Chol.

Table 4 Cationic lipid encapsulated in DPPG$_2$-based TSL and respective T$_m$.

Cationic lipid	Chemical structure	Acyl chain length (carbons)	T$_m$ (°C)
DMTAP		14	39.1 °C[*]
DPTAP		16	52.8 °C[*]
DSTAP		18	62.9 °C[*]

DC-Cholesterol		/	/

All tested liposomes were composed of DPPC/DSPC/DPPG$_2$/cationic lipid at 62.5/25/5/7.5 molar ratio (mol:mol). Cationic TSL were extruded at final 100 nm membrane filters and active loading of DOX performed as reported in section 3.3.2. After separation of unloaded DOX fraction, physicochemical properties of obtained cationic liposomes were assessed (Table 5).

Table 5 Characterization of cationic DPPG$_2$-CTSL with different cationic lipids.
Values are expressed as mean value ± SD for at least three independent batches.

Formulation	Lipid composition	Lipid ratio (mol:mol)	Z-average (nm)	PDI	ζ-POT (mV)
DMTAP	DPPC/DSPC/DPPG$_2$/DMTAP	60/25/5/10	111.7 ± 2.6	0.18 ± 0.01	6.5 ± 1.3
DPTAP	DPPC/DSPC/DPPG$_2$/DPTAP	60/25/5/10	127.5 ± 4.1	0.21 ± 0.05	9.8 ± 2.1
DSTAP	DPPC/DSPC/DPPG$_2$/DSTAP	60/25/5/10	> 200	> 0.5	6.9 ± 1.5
DC-Cholesterol	DPPC/DSPC/DPPG$_2$/DC-Chol	60/25/5/10	128.7 ± 4.5	0.09 ± 0.03	-3.52 ± 3.0

PDI = polydispersity index. ζ-POT = in NaCl 0.9 %.

All liposomes showed comparable and positive ζ-POT when measured in NaCl 0.9 %, besides DC-Chol-CTSL, where a negative surface charge was detected under the same condition. Size and PDI were affected by the type of cationic lipid used in liposome production. DMTAP and DPTAP cationic TSLs showed similar size and a PDI ~ 0.2, with a small second peak appearing during intensity distribution analysis (< 10 % total intensity). Liposomes with DSTAP did not produce a stable suspension, and intensity-based size distribution resulted in several peaks with PDI > 0.5 and average size > 200 nm. When DC-Chol was used in liposome preparation, positive charge was not detected and resulting ζ-POT was slightly negative (Table 5). Surprisingly, DLS analysis on DC-Chol-based CTSL showed a homogeneous size distribution with small PDI and no extra peak visible. All produced cationic TSLs were assessed in terms of heat-triggered DOX release (Figure 12). Among all formulations tested, cationic TSL with DPTAP showed the most promising temperature-release profile, although not optimal yet. In fact, immediate leakage at 37 °C/5 min of around < 20 % was observed, whereas peaks of ~ 80 % DOX were released at 43 °C/5 min (Figure 12). When particles were stressed for 1 h at 37 °C, leakage increased up to ~ 25 %, while incubation at 42 °C/1 h promoted heat-triggered release of 70 % of overall content (Figure 12B). In case of DMTAP, similar behavior was assessed with leakage of ~ 25 % immediately visible after 5 min of incubation at 37 °C, whereas after 1 h at the same temperature increased up to ~ 30 % (Figure 12A, B). Nevertheless,

DMTAP-based CTSL showed suboptimal DOX heat-triggered release at HT condition, with only 65 % of DOX released at 42 °C/1 h (Figure12B). When DSTAP was used in liposomes, an even more modest heat triggered release was observed, potentially caused by aggregation as assessed during DLS analysis (Figure 12A). Remarkably, the inclusion of DC-Chol did not provide TSL with triggerable-DOX release function, since drastic leakage was observed at each temperature range with minimal effect driven by HT. Although at suboptimal stage, heat-triggered DOX release from DPTAP-based cationic TSL showed added benefit when compared to other CTSLs formed by different building blocks. Hence, the DPTAP-based CTSL, from this moment on generally referred to as PG$_2$-CTSL, was used in the next investigation focused on potential optimization.
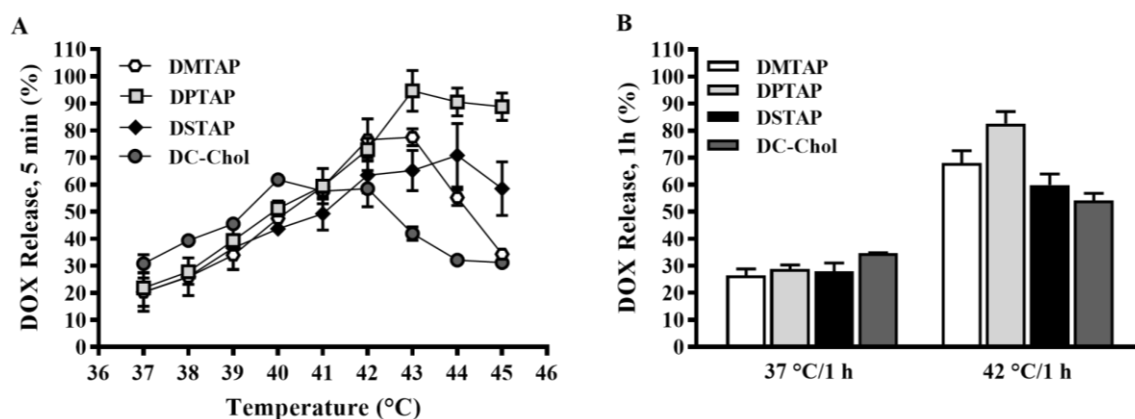
Figure 12 Temperature-dependent DOX release profiles of PG$_2$-CTSL with different cationic lipids.
Cationic TSLs were diluted in FCS and exposed to different temperatures. Released fraction of DOX was measured using fluorescence spectroscopy. Percentage of DOX released after 5 min of exposure to different temperatures ranging from 37 °C to 45 °C (A), and values after 1 h of treatment at 37 °C and 42 °C (B). Values are expressed as mean value ± SD for three independent batches.

4.1.1.2 Formulation optimization

Lipid composition of PG$_2$-CTSL was adjusted in order to improve DOX-retention at physiological condition (e.g., 37 °C) while keeping the observed heat-triggered release patterns at HT. Thereby, PG$_2$-CTSL formulations were produced with different phospholipid molar ratio and tested in a temperature-dependent release assay. Specific lipid composition and physicochemical properties of tested cationic TSL are shown in Table 6.

Table 6 Characterization of cationic DPPG$_2$-TSL with different lipid composition.
Values are expressed as mean value ± SD for at least three independent batches.

Formulation	Lipid composition	Lipid ratio (mol:mol)	Z-average (nm)	PDI	ζ-POT (mV)
PG$_2$-CTSL[1]	DPPC/DSPC/DPPG$_2$/DPTAP	60/25/5/10	127.5 ± 4.1	0.21 ± 0.05	9.8 ± 2.1
PG$_2$-CTSL[2]	DPPC/DSPC/DPPG$_2$/DPTAP	62.5/25/5/7.5	137.3 ± 5.1	0.29 ± 0.03	5.4 ± 2.3
PG$_2$-CTSL[3]	DPPC/DSPC/DPPG$_2$/DPTAP	67.5/20/5/7.5	131.5 ± 2.1	0.26 ± 0.05	4.9 ± 3.5

PDI = polydispersity index. ζ-POT = in NaCl 0.9 %.

The decrease of cationic DPTAP, from an initial 10 mol% in PG$_2$-CTSL^1, to 7.5 mol% in PG$_2$-CTSL^2 improved formulation stability while preserving similar physical properties and a positive ζ-POT (Table 6). PG$_2$-CTSL^1 showed minimal DOX leakage of ~ 10 % after 5 min incubation at 37 °C, and heat-triggered release with DOX peak of ~ 80 % at 43 °C/5 min (Figure 13A). DOX retention assessed by stressing particles for 1 h at 37 °C improved from an initial ~ 70 % in case of PG$_2$-CTSL^1 to ~ 85 % for PG$_2$-CTSL^1, whereas comparable DOX release was observed at 42 °C/1 h (Figure 13B). In an attempt to further increase reactivity at HT condition and speed DOX-heat triggered release, DSPC content was lowered by 5 mol% in favour of DPPC (Table 6). Resulting PG$_2$-CTSL^3 showed improved DOX depletion after 42 °C/1 h. However, stability at lower temperatures was also affected with leakage of ~ 20 % after 5 min at 37 °C (Figure 13B).
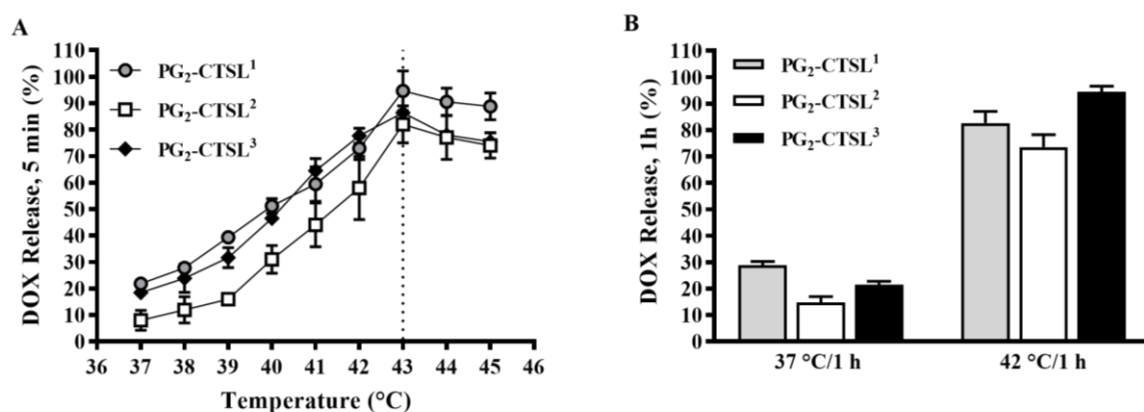
Figure 13 Temperature-dependent DOX release profiles of optimized PG$_2$-CTSL
PG$_2$-TSLs were diluted in FCS and exposed to different temperatures. Released fraction of DOX was measured using fluorescence spectroscopy. Percentage of DOX released after 5 min of exposure to different temperatures ranging from 37 °C to 45 °C (A), values after 1 h of treatment at 37 °C and 42 °C (B). Dashed black lines in panel A indicates temperature where the highest DOX release fractions were observed. Values are expressed as mean value ± SD for three independent batches.

Overall, PG$_2$-CTSL^2 showed a good balance between serum stability at physiological condition and heat-triggered release capability, making a good candidate for the next investigations. In the next steps, the heat-triggered release profiles of optimized PG$_2$-CTSL^2 (from this moment on referred to simply as PG$_2$-CTSL) to PEG-based cationic TSL were compared, the latter formulation was already reported elsewhere [254]. Additionally, to thoroughly identify release mechanism from anionic and cationic TSL, also previously reported anionic PG$_2$-TSL and PEG-TSL were enrolled in the study [103, 106].

4.1.1.3 Anionic and cationic liposome characterization

Next, a comparison between PG$_2$-CTSl and PEG-based CTSL was performed. As reported above (refer to section 4.1.1.2), liposome PG$_2$-CTSLs were composed of DPPC/DSPC/DPPG$_2$/DPTAP 62.5/25/5/7.5 (mol:mol), whereas PEG-CTSLs were formed by DPPC/DSPC/DSPE-PEG$_{2000}$/DPTAP with 62.5/25/5/7.5 molar ratio. Bare CTSLs with neither DPPG$_2$ nor PEG were characterized by DPPC/DSPC/DPTAP with 67.5/25/7.5 (mol:mol) ratio.

Anionic DPPG$_2$- and PEG-based TSLs were used as control and tested with different lipid composition. PG$_2$-TSL^5 and PG$_2$-TSL^{30} were formed by DPPC/DSPC/DPPG$_2$ in molar ratio of 70/25/5 and 50/20/30, respectively. PEG-TSL^{70} and PEG-TSL^{80} were characterized by the same amount of DSPE-PEG$_{2000}$ (5 mol%) and different amounts of DPPC, with a final composition of 70/25/5 and 80/15/5 of DPPC/DSPC/DSPE-PEG$_{2000}$, respectively. All tested formulations were actively loaded with DOX as reported in section 3.3.2, the characterization in terms of physicochemical properties is shown in Table 7.

Table 7 Characterization of anionic and cationic TSLs encapsulating DOX.
Results are shown as mean value ± SD for at least three independent batches.

Liposomes	Lipid composition (mol:mol)	Z-average (nm)	PDI	ζ-POT (a) (mV)	Z-POT(b) (mV)	DOX/lipid (mol:mol)
PG$_2$-TSL^{30}	DPPC/DSPC/DPPG$_2$ (50/20/30)	121.7 ± 5.42	0.06 ± 0.01	- 28.9 ± 5.4	- 54.1 ± 5.3	0.056 ± 0.021
PG$_2$-TSL^5	DPPC/DSPC/DPPG$_2$ (75/25/5)	116.2 ± 3.3	0.07 ± 0.05	- 8.8 ± 2.4	- 30.1 ± 1.1	0.049 ± 0.031
PEG-TSL^{80}	DPPC/DSPC/DSPE-PEG$_{2000}$ (80/15/5)	111.1 ± 0.9	0.05 ± 0.02	- 4.7 ± 3.5	- 17.5 ± 1.6	0.048 ± 0.016
PEG-TSL^{70}	DPPC/DSPC/DSPE-PEG$_{2000}$ (70/25/5)	107.6 ± 0.8	0.06 ± 0.01	-6.29 ± 3.0	- 15.7 ± 2.1	0.049 ± 0.021
CTSL	DPPC/DSPC/DPTAP (67.5/25/7.5)	125.5 ± 5.4	0.19 ± 0.06	11.3 ± 3.6	39.5 ± 4.5	0.048 ± 0.015
PG$_2$-CTSL	DPPC/DSPC/DPTAP/ DPPG$_2$ (62.5/25/7.5/5)	137.3 ± 5.1	0.29 ± 0.03	5.4 ± 2.3	12.9 ± 1.7	0.046 ± 0.006
PEG-CTSL	DPPC/DSPC/DPTAP/ DSPE-PEG$_{2000}$ (62.5/25/7.5/5)	110.9 ± 4.1	0.09 ± 0.07	- 0.2 ± 0.8	5.8 ± 1.7	0.047 ± 0.007

PDI = polydispersity index. ζ-POT (a) = in NaCl 0.9 %. ζ-POT (b) = 20 mM HEPES buffer pH 7.4

Both PG$_2$-CTSL and PEG-CTSL contain a mixture of anionic (5 mol%, DPPG$_2$ or DPE-PEG$_{2000}$) and cationic (7.5 mol%, DPTAP) lipids in the bilayer membrane. ζ-POT analysis in physiological saline showed a higher positive charge for PG$_2$-CTSL (5.4 ± 1.3 mV) than PEG-CTSL (- 0.2 ± 0.8 mV) (Table 7). Analysis in non-saline containing medium (HEPES buffer) showed a positive surface charge for PG$_2$-CTSL 2-fold higher in comparison to PEG-CTSL (~ 13 mV vs. ~ 6 mV). Anionic TSLs were formed exclusively by anionic or neutral lipids and a negative ζ-POT was assessed in both media. For PG$_2$-based anionic liposomes, surface charge decreased from - 8.8 ± 2.4 mV in case of PG$_2$-TSL^5 to - 28.9 ± 5.4 mV for PG$_2$-TSL^{30}, in good accordance with different percentage of negative-charged DPPG$_2$ included in membrane bilayer. On the other side, PEG-TSL^{70} and PEG-TSL^{80} differed only in DPPC/DSPC amount, thus with no detectable differences in overall surface charge. Anionic PG$_2$-based and PEG-based TSL were comparable in vesicle size and showed

a small and homogenous size-distribution (PDI < 0.15). In case of CTSL and PG$_2$-CTSL size and PDI after DOX loading were slightly higher in comparison to all other formulation tested (small second peak was visible during intensity-based DLS analysis, with areas between 5-10 %). Steric stabilization via PEG in cationic TSLs promoted a homogeneous dispersity with small PDI and size comparable to anionic TSLs (size ~ 110 nm, PDI < 0.1) (Table 7). DOX active loading was successfully completed via ammonium gradient in all tested (C)TSLs (> 95 % EE), without observed differences among cationic and anionic TSLs. Osmolality of different (C)TSL-DOX formulations and solutions used for DOX loading are shown in Table 8, with all (C)TSL showing similar osmotic concentration. This results support that the difference in the release profile is not caused by osmotic effects.

Table 8 Osmolalities of cationic and anionic TSL-DOX and solutions used for DOX loading.
Data are presented as mean values ± SD for at least three independent batches.

Liposomes/ solutions	composition (concentration mM)	Osmolalities (mmol/kg)
Ammonium sulfate	(NH$_4$)$_2$SO$_4$ (240 mM)	533 ± 17
HBS pH 7.8	HEPES (20 mM); NaCl (150 mM)	317 ± 10
HBS pH 7.4	HEPES (20 mM); NaCl (150 mM)	313 ±8
PG$_2$-TSL^{30}	/	303 ± 10
PG$_2$-TSL^5	/	299 ± 7
PEG-TSL^{80}	/	298 ± 4
PEG-TSL^{70}	/	300 ± 9
CTSL	/	303 ± 2
PG$_2$-CTSL	/	303 ± 5
PEG-CTSL	/	308 ± 9

4.1.1.4 Differential Scanning Calorimetry

Heat-triggered release profile of drugs from TSL is mostly affected by lipid composition and corresponding T_m of liposomal bilayer. Hence, to investigate how the incorporation of cationic or anionic lipids influences the phase transition and, thus, heat-triggered release profile, DSC measurements were carried out for each tested TSL after DOX loading (Figure 14). According to previous results [106, 108], the inclusion of DPPG$_2$ in a DPPC/DSPC bilayer with final molar ratio of DPPC/DSPC/DPPG$_2$ (50/20/30, mol:mol) results in a T_m of ~ 42 °C (PG$_2$-TSL^{30}, Table 9). With decreasing DPPG$_2$ amount to 5 mol% in favor of DPPC, T_m increased up to 44.5 °C, hence a sub-optimal heat-triggered release efficiency can be expected when using mild-HT range (41-43 °C). The same pattern was observed in PEG-based TSL when DSPC content increased from 15 mol% (PEG-TSL^{80}) to 25 mol% (PEG-TSL^{70}), with a corresponding increase in T_m from ~ 43 °C to ~ 45 °C. All

tested cationic TSLs had a similar lipid composition composed of DPPC, DSPC, and DPTAP, whereas 5 mol% of anionic phospholipids were respectively present in PG_2- and PEG-based cationic TSL. The inclusion of DPTAP in lipid bilayer induced a broader phase transition when compared to non-DPTAP containing liposomes (Figure 14A, B and C). Additionally, two merged peaks were observed in the gel-liquid crystalline phase transition which was overall similar in all cationic TSL, with T_m assessed at around ~ 46 °C.
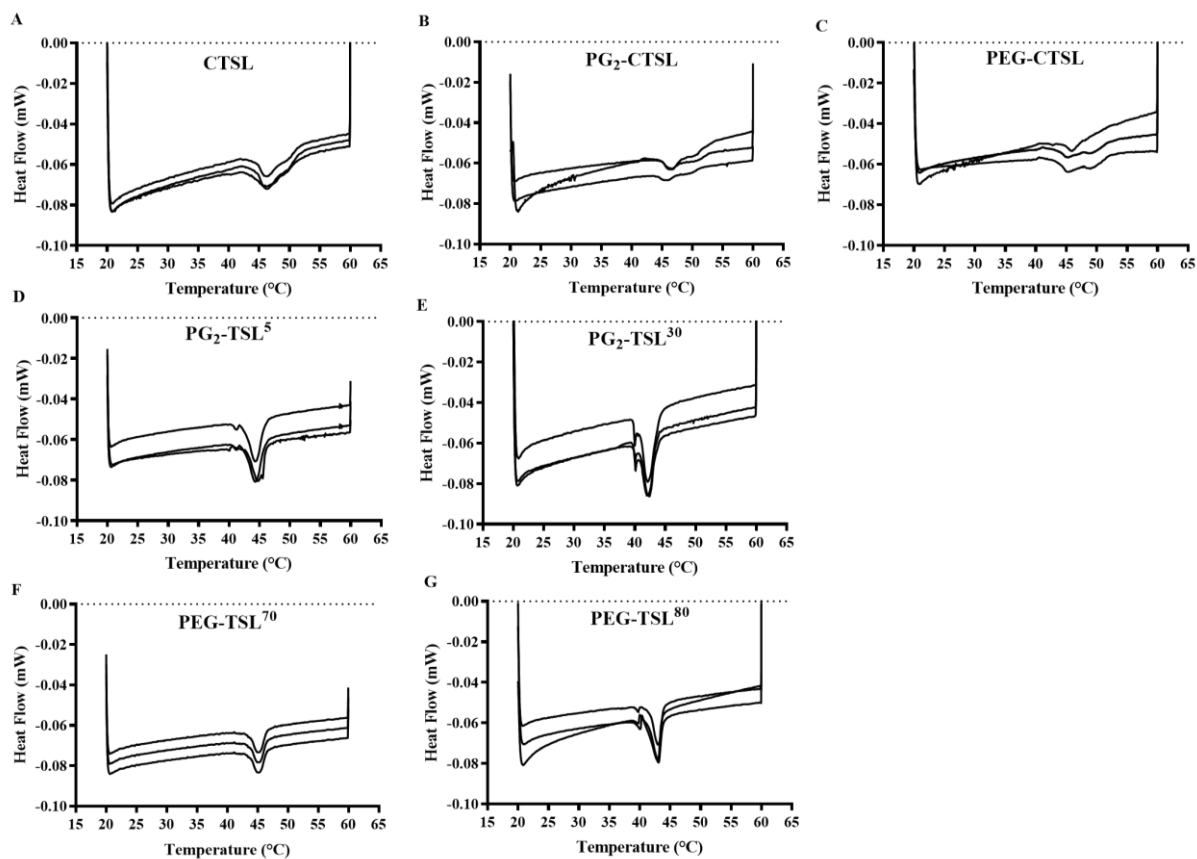

Figure 14 Curves of the heating phase from 20 °C to 60 °C of different anionic and cationic liposomes.
DSC curves were plotted based on heat flux versus time with a heating rate of 1 °C/min. For each liposomal formulation, three different curves are shown corresponding to three independent batches.

Table 9 Overview of T_m for different liposomal formulations.
Values are expressed as mean value ± SD for three independent batches.

Liposomes	Type	T_m (°C)
PG_2-TSL^{30}	Anionic	42.1 ± 0.4
PG_2-TSL^{5}	Anionic	44.5 ± 0.2
PEG-TSL^{80}	Anionic	43.0 ± 0.1
PEG-TSL^{70}	Anionic	45.2 ± 0.2
CTSL	Cationic	46.5 ± 0.2
PG_2-CTSL	Cationic	46.4 ± 0.4
PEG-CTSL	Cationic	46.3 ± 0.2

4.1.1.5 Comparison to cationic and anionic thermosensitive formulations

In case of bare CTSL and PG_2-based cationic TSL, size and PDI were slightly higher in comparison to all to the formulation tested (Table 7). A small extra peak during DLS analysis was usually detected, potentially driven by the formation of bigger aggregates during batch manufacturing (Figure 15). The small second peak was visible only during scatter intensity analysis, with areas between 5-10 %. On the contrary, PEG-CTSL showed a homogenous size distribution with a single peak with comparable shape as assessed for all anionic TSL (Figure 15).
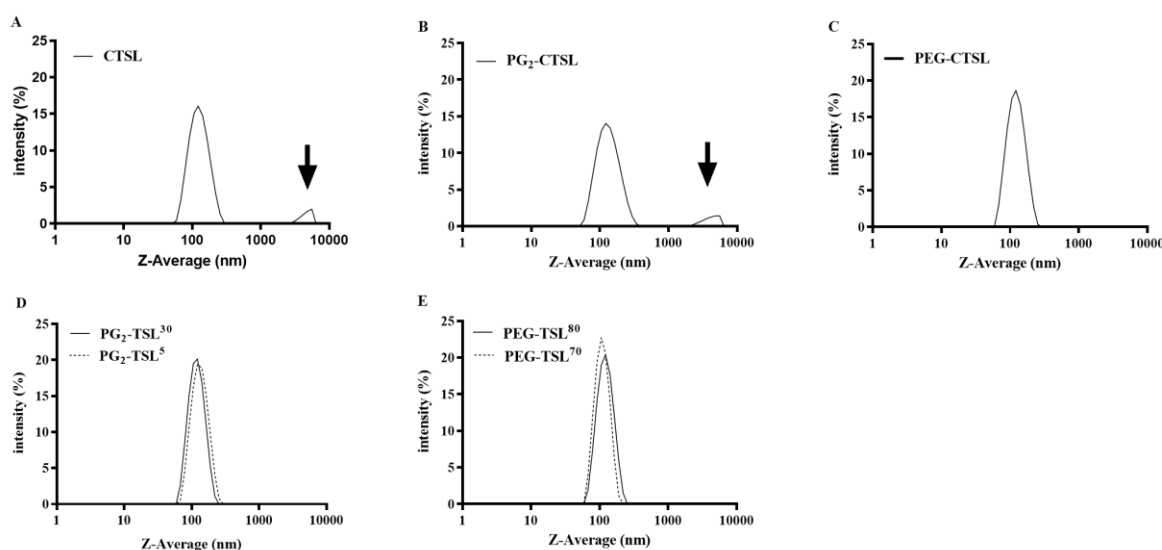
Figure 15 Representative size distribution (intensity) by DSL analysis for all formulation tested.
DOX-loaded liposomes were diluted 1:50 (v/v) in NaCl 0.9 % and size measurement carried out via Zeta Sizer Nano SZ. Black arrows indicate the presence of extra peaks appearing in size measurement with intensity distribution.

4.1.2 Heat-triggered DOX release *in vitro*

4.1.2.1 Temperature-dependent DOX release profile

The previously reported PG_2-CTSL was now compared to other cationic and anionic TSL in terms of heat-triggered DOX release (Figure 16). Cationic TSLs tested in the following investigation showed minimal DOX leakage after dilution in FCS and exposure to 37 °C for 5 min (max 10 % DOX leakage, Figure 16A), whereas peaks of DOX-release fraction were observed at 43 °C/5 min. Bare CTSL showed a sub-optimal profile with a slow and incomplete heat-triggered DOX release. The inclusion of 5 mol% of either $DPPG_2$ or DSPE-PEG_{2000} in CTSL improved DOX-release rate with maximal release of ~ 80 % after 43 °C/5 min. PG_2-CTSL and CTSL showed comparable DOX retention after 37 °C/1 h (~ 15 % DOX leakage). Surprisingly, in case of PEG-CTSL, a significantly lower DOX leakage was measured after stressing particle for 37 °C/1 h when compared to CTSL (Figure 16B). DOX temperature profile for anionic PG_2-TSL formulations was affected by the amount of $DPPG_2$ included in the liposome bilayer. At 30 mol% of $DPPG_2$, PG-TSL[30] showed

optimal drug retention at low temperatures (~ 5 %, 37 °C/5 min) and burst DOX release at HT with peak fraction observed already at 41 °C/5 min (87.7 ± 9.7 %). In accordance to the DOX-release profile shown in Figure 16C, after 42 °C/1 h particles were fully depleted, whereas 90 % of DOX was retained inside liposomes after stressing particle for 37 °C/1 h (Figure 16D). When $DPPG_2$ was reduced to 5 mol%, temperature-dependent DOX-release is nullified and negligible DOX fractions were detected even at HT, as expected from the increased T_m (Table 9). DOX-release profile from PEG-TSLs was also affected by lipid composition and corresponding T_m. PEG-TSL[70] containing 25 mol% of DSPC exhibited sub-optimal heat-triggered profile with ~ 30 % maximal DOX release at 43 °C/5 min, with no substantial changes observed after 42 °C/1 h (~ 30 % DOX release) (Figure 16E). When DSPC content was lowered to 15 mol% in favour of DPPC, resulting PEG-TSL[80] exhibited the highest released DOX-fraction at 42 °C/5 min (~ 50 % DOX), with a 1 °C shift from what was observed for PEG-TSL[70]. Additionally, PEG-TSL[80] stressed for 42 °C/1 h promoted 1.8-fold higher DOX-release fraction when compared to PEG-TSL[70], while comparable and minimal leakage was assessed after 1 h/37 °C (~ 5 %) (Figure 16F). Overall, PG₂-TSL[30] showed the most superior profile of all tested formulation with a sharp change in DOX release kinetics within 1-2 °C.
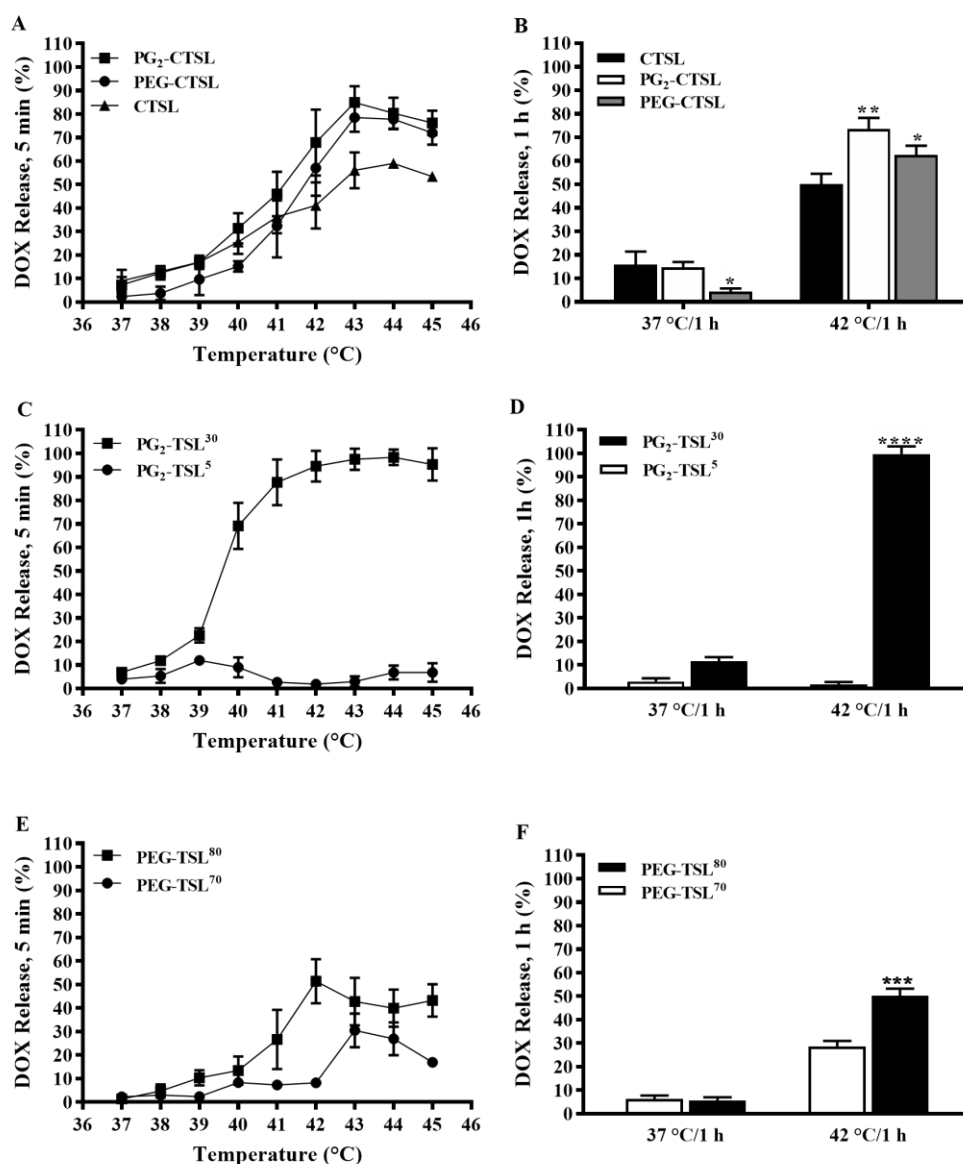
Figure 16 Temperature-dependent DOX release profiles of anionic and cationic TSL.
DOX-(C)TSLs were diluted in FCS and exposed to different temperatures. Figure 16A, C and E show the percentage of DOX released after 5 min exposure to different temperatures ranging from 37 to 45 °C whereas Fig. 16B, D, and F indicate values after 1 h of treatment at 37 °C and 42 °C. Values are expressed as mean value + SD for three independent batches. In Figure A, values were compared to control (bare-CTSL) via one-way ANOVA followed by Bonferroni test, whereas in graphs D & F, data were analyzed via unpaired two-tailed T-test. Asterisks indicate significant difference between groups. **** = $p < 0.0001$, *** = $p < 0.001$, ** = $p < 0.01$, * = $p < 0.05$.

4.1.2.2 Time-dependent DOX release profile

Next, time-dependent release from cationic and anionic TSL was investigated to evaluate release kinetics in more detail. In these experiments, both PG_2- and PEG-based cationic TSL were used, whereas only anionic formulations with more efficiency in DOX-release were tested (PG_2-TSL^{30} and PEG-TSL^{80}). PG_2-CTSL and PEG-CTSL had a comparable DOX-release kinetic at HT condition (~ 70 % at 41 °C/5 min), overall slower when compared to anionic counterparts (Figure 17 & Table 10). The slower release kinetics of CTSLs in comparison to TSLs are in accordance with the higher T_m assessed in cationic liposomal formulation. Within the 20 min kinetic investigation similar

leakage at 37 °C was observed for both CTSL, with 10 to 15 % content loss (Figure 17B, D). PG_2-TSL[30] were fully depleted after a few minutes of incubation either at 41 °C or 42 °C, in good accordance with fast-heat triggered release assessed in section 4.1.2 (Figure 17). PEG-TSL[80] showed a slower DOX release rate at 41 °C when compared to PG_2-TSL, although at 42 °C minimal differences were observed (Figure 17 & Table 10). In both anionic TSLs, optimal drug retention at 37 °C was observed within the investigation range (Figure 17A, C).
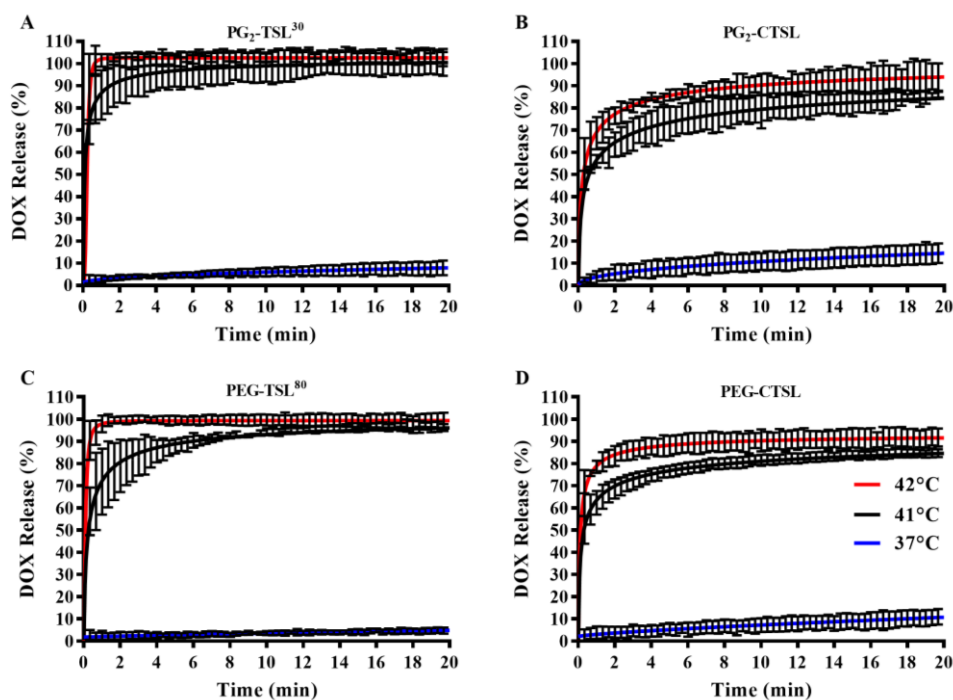
Figure 17 DOX release kinetics from (C)TSL.
Drug retention at 37 °C and kinetics release at mild hyperthermia were evaluated for 20 min in time-dependent release assays. An exponential one-phase association curve was fitted through the 41 °C and 42 °C release sets. Data are shown as mean value ± SD for three independent batches.

Table 10 DOX release rate from (C)TSLs at 41 °C and 42 °C.
K constants and R^2 were calculated from the exponential fit shown in Figure 17, for the first 300 s.

Formulation	K (s-[1]) 41 °C	R^2 (41 °C)	K (s-[1]) 42 °C	R^2 (42 °C)
PG_2-TSL	4.3 ± 0.7	0.9891 ± 0.0021	4.8 ± 1.5	0.9904 ± 0.0054
PG_2-CTSL	2.7 ± 1.7	0.9365 ± 0.0136	2.9 ± 2.0	0.9644 ± 0.0355
PEG-TSL[80]	2.9 ± 1.7	0.9344 ± 0.0782	4.9 ± 1.7	0.0896 ± 0.0424
PEG-CTSL	2.9 ± 1.9	0.9675 ± 0.0199	3.6 ± 1.4	0.9479 ± 0.0057

4.1.3 Targeting cancer and endothelial cells *in vitro*

4.1.3.1 Confocal fluorescence microscopy on fixed cells

Next, the (C)TSL-cell interactions in different conditions were assessed to test cell targeting capability. Positive-charged PG_2- & PEG-based TSL were compared to their anionic counterparts. Targeting was assessed by using cancer cell line BN175 and HUVECs. In both, cancer and endothelial cells, liposomes targeting on BN175 and HUVEC cells was drastically improved when either PG_2-/ or PEG-based CTSLs were used. After 1 h of incubation with cationic TSLs, a large fraction of liposomes was visibly detected intercalating with target cell membranes (Figure 18A, B, C and D, second panels). Confocal Z-sectioning of BN175 confirmed PG_2-based cationic liposomes strongly associated with cell membranes and in minor part at cytoplasm level, whereas minor amounts of anionic liposomes were detected exclusively in cell compartments (Figure 18E). A similar pattern was observed for PEG-based TSL, although to somewhat reduced extent in terms of liposome abundance. Cell fluorescence imaging was coupled to FACS in a parallel experiment to quantify binding efficacy (refer to section 4.1.3.4).
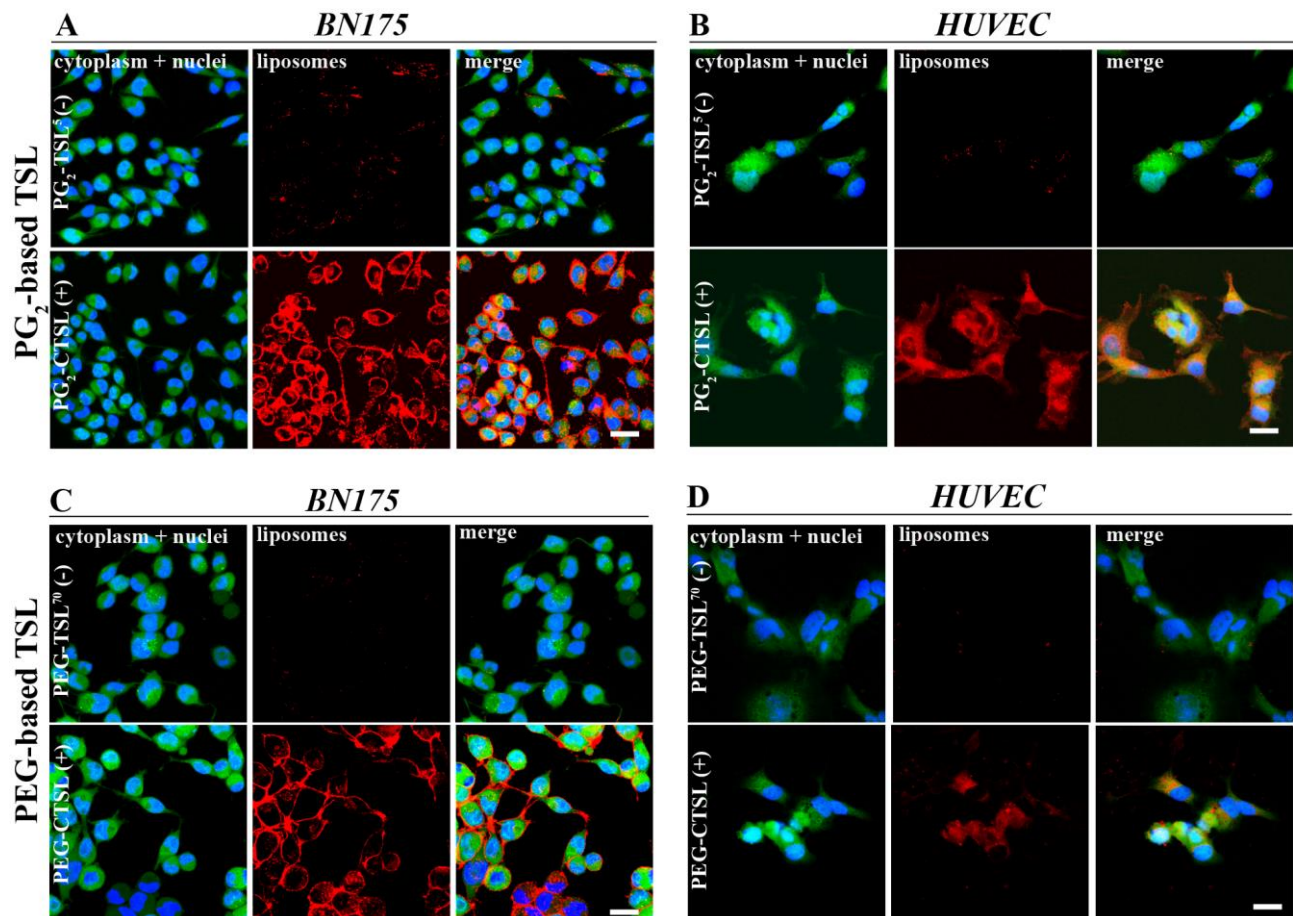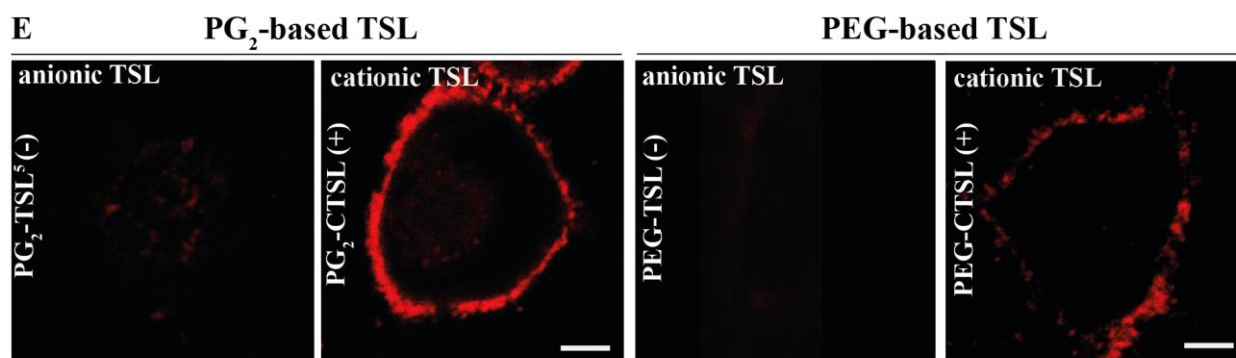
Figure 18 Fluorescence confocal microscopy on cancer and endothelial cells incubated with (C)TSLs
BN175 (A, C) and HUVEC (B, D) cells were exposed to Rho-labeled (C)TSLs (red color) for 1 h at 37 °C. Cell cytoplasms and nuclei are stained with CMFDA (green color) and Hoechst (blue color), respectively. Stack analysis on BN175 was performed by using scaling factor of 0.3 µm (stack size of 10.3 µm) and with 543 nm Argon laser. Pictures showed a representative section imaged at 5.4 µm for anionic and cationic PG2- and PEG-based TSL (E). Scale bar applied to images A-D is 20 µm, scale bar applied to image E is 5 µm. Picture showed a representative section imaged at 5.4 µm for anionic and cationic PG2-based TSL (E).

4.1.3.2 Protein corona liposomes

Previous studies have shown how serum proteins can interact and are being absorbed on particles surface immediately after administration, forming a protein corona [255]. The effect of protein adsorption on the physicochemical properties of cationic and anionic liposomes after incubation in FCS is shown in Figure 19. Protein adsorption significantly reduced positive ζ-POT of PG2-CTSL whereas negligible differences were detected in other (C)TSLs tested (Figure 19A). Additionally, protein corona seemed to destabilize selectively PG2-CTSL since an increase in size and PDI was observed after protein corona formation. On the contrary, all other (C)TSLs tested showed comparable physical properties to non-protein containing liposomes (Figure 19B). Protein amount was evaluated via Bradford assay and protein/lipid ratio (mg/µmol) assessed for tested (C)TSLs (Figure 19C). Surprisingly, no significant differences were observed in relation to overall protein amount in all tested liposomal formulations. Protein corona liposomes were used in an SDS-page with silver staining, to highlight differences in protein-bound fractions. Surprisingly, no significant differences in protein fractions were observed, although positively charged TSL showed darker bands potentially driven by contamination of the cationic lipid (Figure 20).
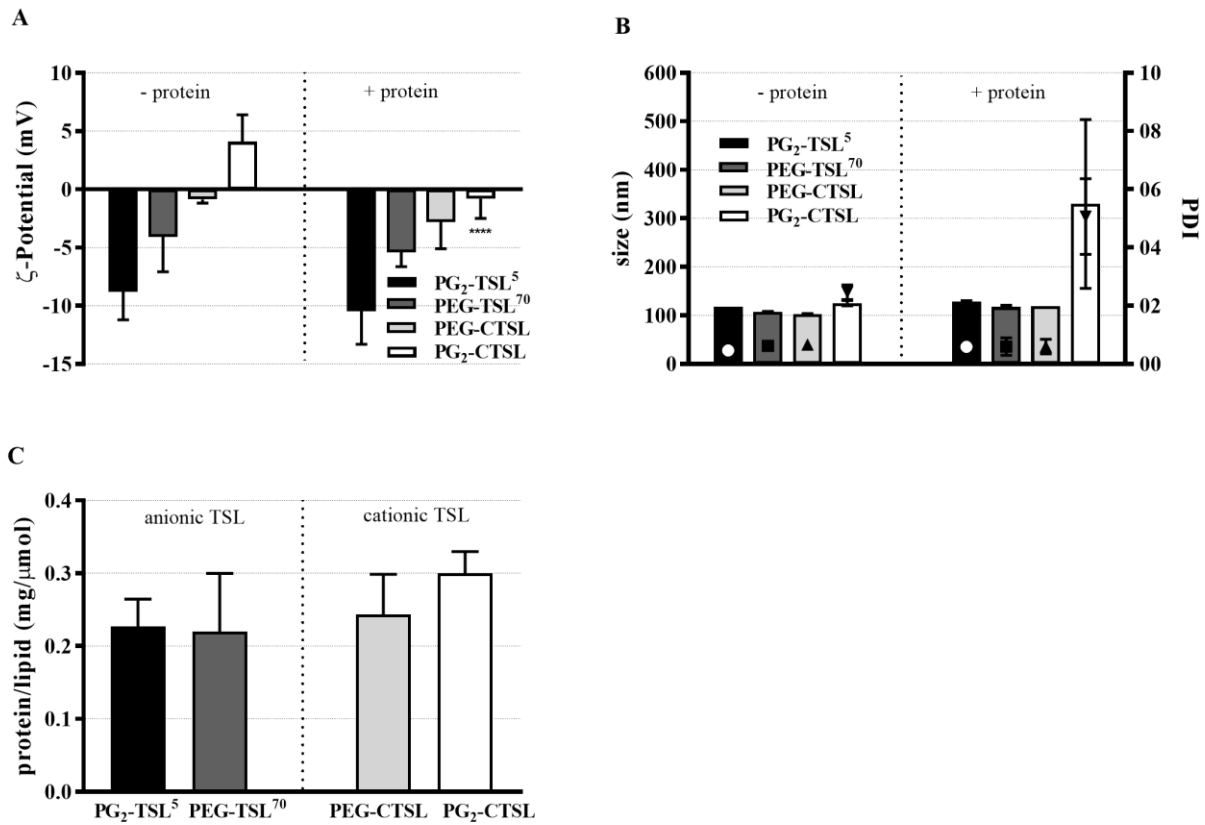
Figure 19 Effects of FCS protein adsorption on physical characteristics of anionic and cationic TSLs.
ζ-POT (A) and size/PDI (B) in relation to (C)TSLs before and after FCS protein adsorption. In figure 19B, bars refer to size (left y-axis) whereas symbols to PDI (right y-axis). Protein:lipid ratio (mg/µmol) per liposome formulation (C). Data are shown as mean value ± SD for three independent measurements. Groups (-protein vs. + protein) were analyzed via a two-tailed T-test and asterisks indicate significant difference between groups.**** = $p < 0.0001$.
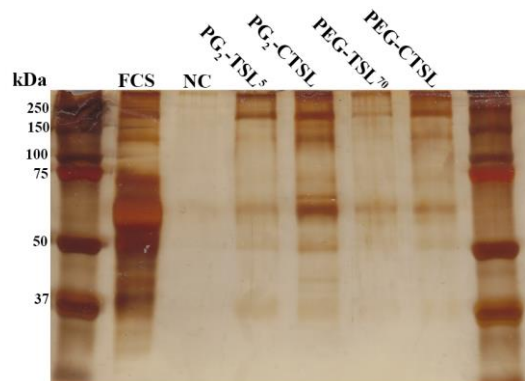
Figure 20 Silver staining of an SDS gel.
Representative SDS-page of protein corona (C)TSLs. FCS without liposomes was used as a negative control (NC) to indicate that the purification procedure totally removed non-liposome associated proteins.

4.1.3.3 Effect of protein corona TSL in targeting approach

To test how bound serum protein might affect targeting effectiveness of (C)TSL, binding was assessed with recovered protein corona liposomes (P-(C)TSLs). Hence, cell fluorescence imaging was repeated using the same conditions as reported above except for CTSLs which were replaced by P-(C)TSLs. As shown in Figure 21, P-PG$_2$-CTSL targeting was still present after protein adsorption

and a larger fraction of liposomes were observed in both cell lines when compared to anionic P-PG$_2$-TSL[5] control (Figure 21A, B, second panels). However, differences in terms of overall binding rate and liposome localization were observed with respect to previously obtained results with PG$_2$-CTSL (Figure 21E). In case of PEG-based TSL, minor differences were observed when cells were incubated with cationic or anionic TSLs, suggesting protein adsorption greatly affected targeting capability (Figure 21C, D).
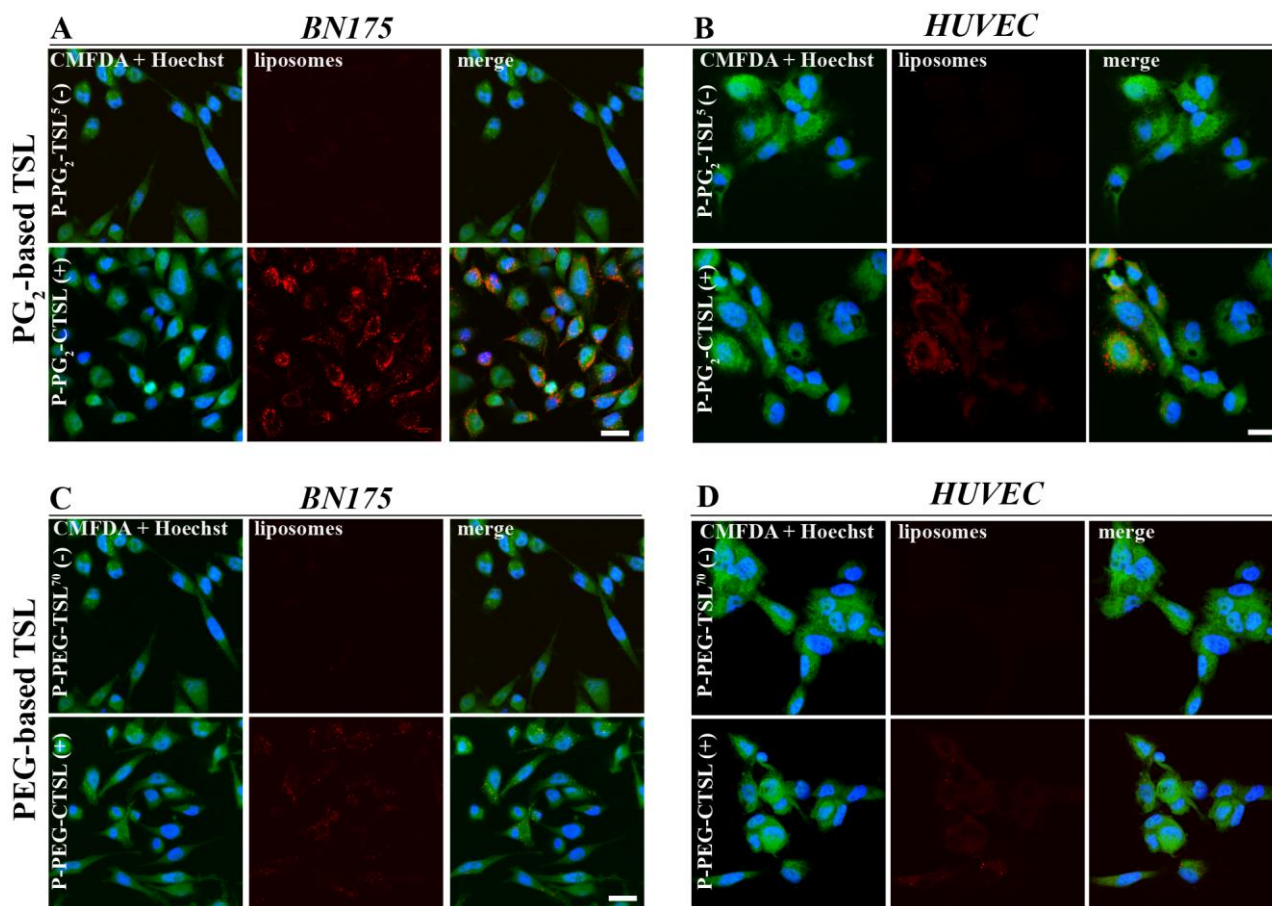

Figure 21 Fluorescence confocal microscopy on cancer and endothelial cells incubated with protein corona (C)TSLs.
BN175 (A, C) and HUVEC (B, D) cells were exposed to (P)-Rho-labeled (C)TSLs (red color) for 1 h at 37 °C. Cell cytoplasm and nucleus are stained via CMFDA (green color) and Hoechst (blue color), respectively. Scale bar applied to all images is 20 µm.

4.1.3.4 Fluorescence-activated cell sorting

Next, the binding of cationic and anionic TSL was quantified via FACS by using the same condition as mentioned above (1 h, 37 °C). The resulting median fluorescence intensity (MFI) from the binding investigation for all cell lines tested is displayed in Figure 22, with Iso-PE shifts shown via histogram graphs (Figure 22A, B). PG$_2$-CTSL significantly improved binding when compared to PEG-CTSL (~ 380 vs. ~ 110 MFI, respectively). The latter, showed an increased binding in comparison to PEG-TSL[70] (10-fold higher in case of BN175), but not as efficient as for PG$_2$-CTSL (12.6-fold when compared to PG$_2$-TSL) (Figure 22C). Additionally, PG$_2$-TSL[5] showed higher cell interactions than PEG-TSL[70] (2-fold) in both cell lines. In a parallel experiment, protein corona TSL were tested in the same settings. The reduction of CTSL binding was confirmed and was found overall

constant for each cell line tested, both for PG_2 and PEG-CTSL of around 1.6-fold loss (Figure 22D). Despite the drastic reduction in binding capability when protein corona is present, a 2-fold higher MFI was retained for P-PG_2-CTSL when compared to P-PEG-CTSLs (Figure 22D).
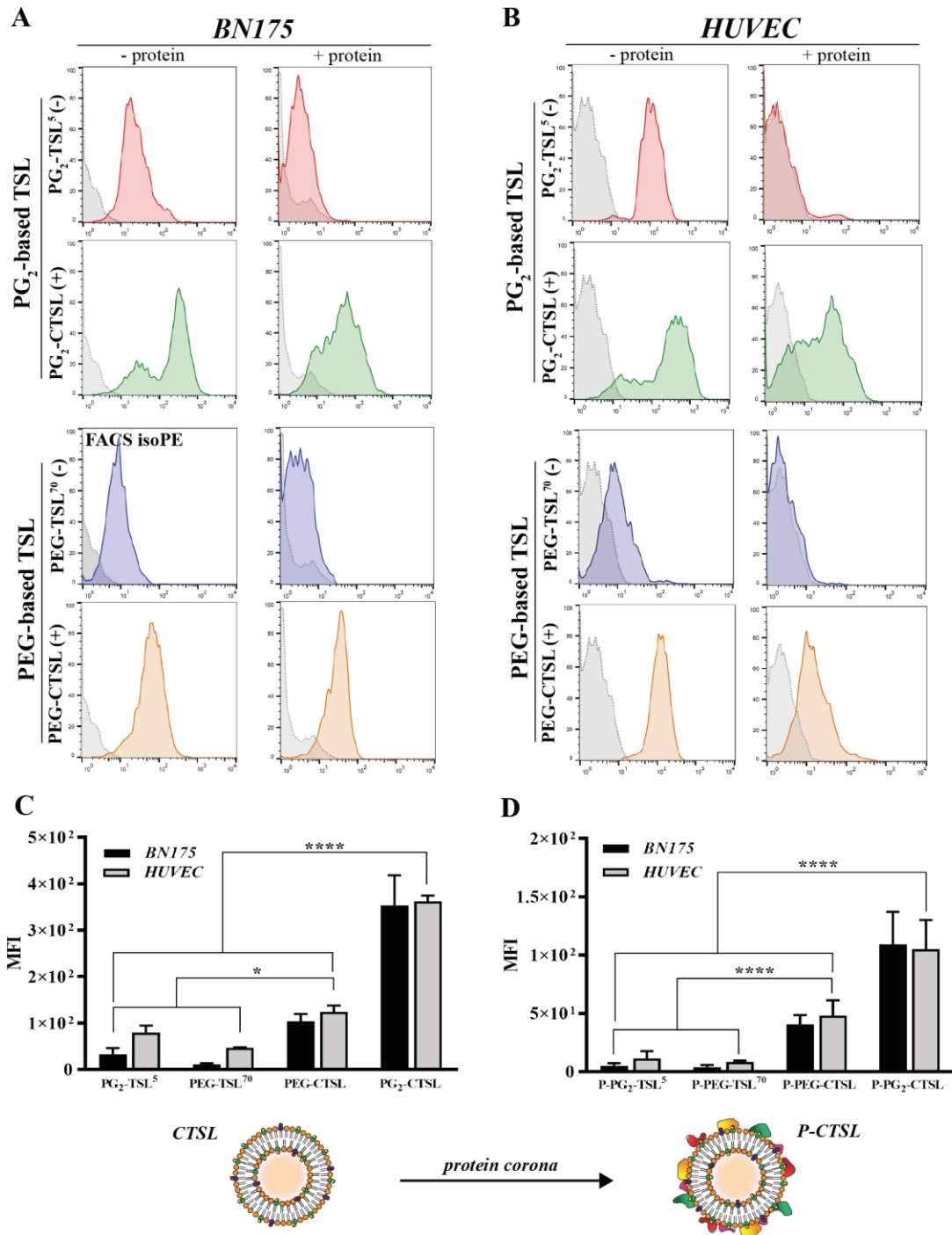

Figure 22 Fluorescence-activated cell sorting of cancer and endothelial cells.
The grey area in the FACS plots represents the background fluorescence, while the colored area is one representative distribution out of three independent measurements (A, B). Background ISO-PE fluorescence (control) was subtracted to each sample and final MFI plotted as mean value ± SD for three independent measurements (C, D). Statistical analysis was conducted via one-way ANOVA followed by Bonferroni test and asterisks indicate significant difference between groups. **** = $p < 0.0001$, * = $p < 0.05$.

4.1.3.5 Targeting on cancer and endothelial cells in live settings

In the next step, the internalization and intracellular fate of liposomes was evaluated as well as DOX-release efficiency after targeting in live settings. After having assessed comparable binding

efficiency of anionic TSL constructed with the different mol% of $DPPG_2$ (PG_2-TSL^5 & PG_2-TSL^{30}) and different DPPC amounts (PEG-TSL^{70} & PEG-TSL^{80}) (data not shown), only the anionic formulations with more efficiency in DOX-release were used in the following experiment (e.g., PG_2-TSL^{30} and PEG-TSL^{80}). Live-cell imaging on cancer and endothelial cells was performed after interactions with NBD-labeled (C)TSL. Liposomes targeting was assessed after a first incubation of 1 h 37 °C (NT) and a second of 1 h 41 °C (HT, water bath), the latter tested exclusively for cationic TSLs since negligible membrane binding was observed for anionic particles.
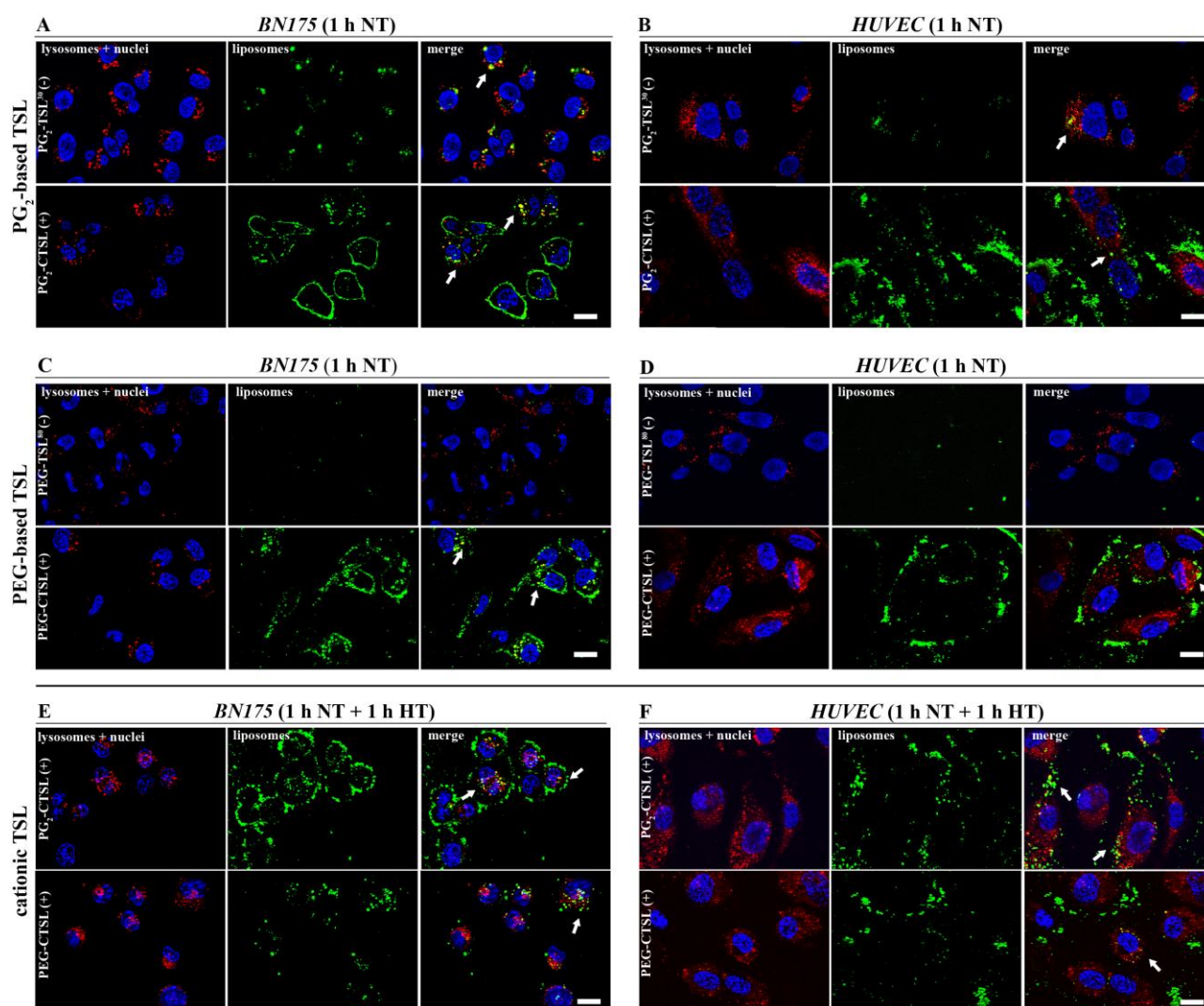
Figure 23 Live-cell fluorescence imaging on cancer and endothelial cells.
BN175 and HUVEC cells were seeded in chamber slides overnight and incubated with different formulation of NBD-labeled (C)TSLs at 1.1 mM. Liposomes were let interact with cells for 1 h at 37 °C, after washing cells were imaged in live settings. NBD-liposome were imaged using GFP filter (green color), lysosomes with DsRed filter (Lysotracker RED, red color) and nuclei with DAPI filter (Hoechst, blue). Arrows indicate colocalization (yellow) of liposomes (green) and lysosomes (red). Images were taken after 1 h 37 °C (A-D) and after 1 h further at 1 h HT (E-F, only CTSL). Bar scale applied to all images is 20 µm.

Buffer loaded NBD-labeled liposomes were used to evaluate binding, whereas lysotracker was used to assess endocytosis. In good accordance with previous results obtained with fixed cells, a larger fraction of liposomes was greatly found intercalated with cell membrane when a positive charge was present (Figure 23A, B, C, and D). Furthermore, co-localization with lysosomes imaged

via Lysotracker Red was present to a certain extent for both PG$_2$-CTSL and PEG-CTSL (white arrows). However, green punctuate patterns in non-acidic lysosomes were also moderately present in both cell lines tested. On the other side, barely any liposomes were visible after incubation with PEG-TSL[80] (Figure 23C, D, first panel), whereas a noticeable fraction of PG$_2$-TSL[30] was well detected in cell cytoplasm in both BN175 and HUVEC cell lines (Figure 23A, B, first panel). To assess kinetics of CTSLs uptake and observe liposome localization after HT treatment, cells were placed in a water bath for 1 h and imaged again thereafter. Differences on PG$_2$-CTSL and PEG-CTSL were detected especially on BN175 cells where PG$_2$-CTSL were still present on cell membrane and co-localized with lysosomes, whereas PEG-CSTL were mostly detected in a punctuate pattern in the cell cytoplasm (Figure 23E, F).

4.1.3.6   Intracellular heat-triggered DOX-release

The improved targeting with CTSLs in comparison to TSLs was further investigated by using (C)-TSL-DOX to assess whether it might translate in better DOX delivery *in vitro*. Hence, DOX delivery efficiency was investigated via fluorescence microscopy using the same settings as described above.
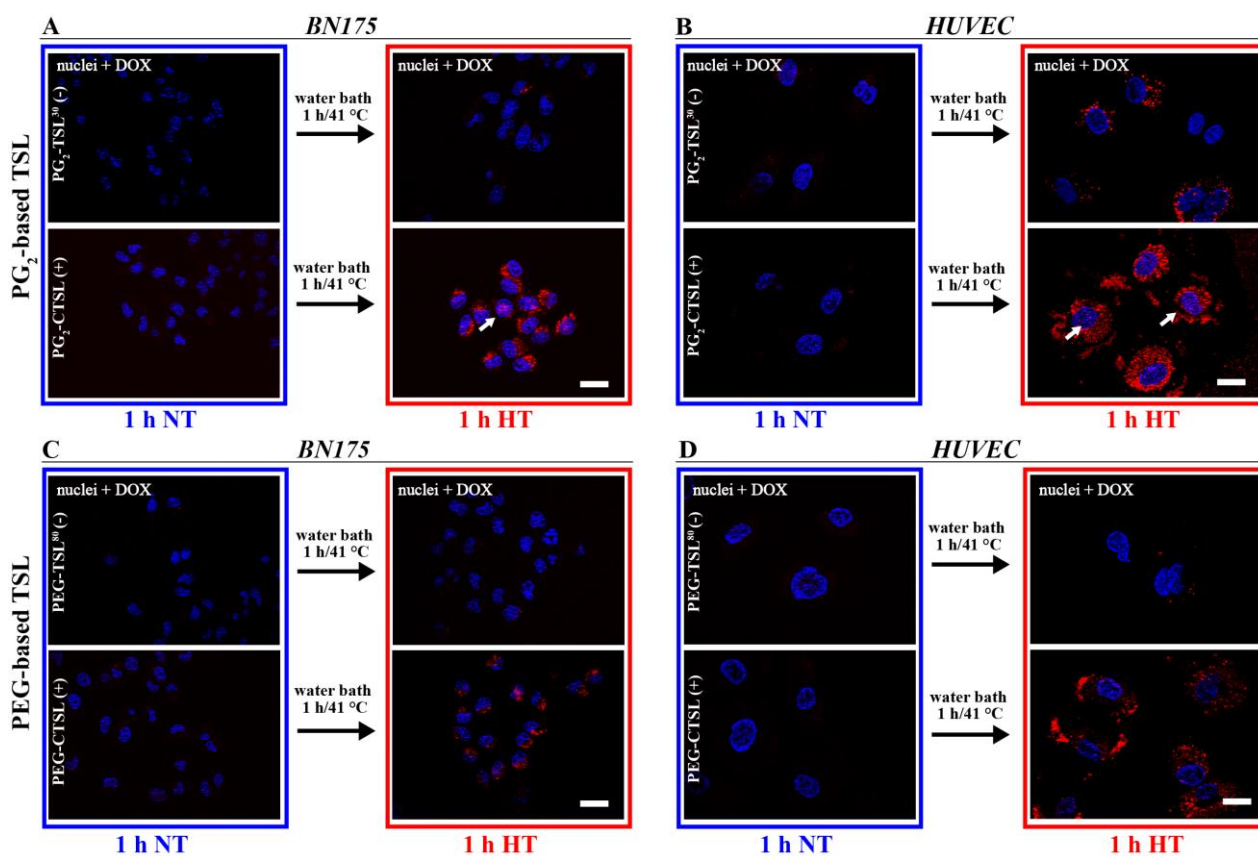

Figure 24 DOX fluorescence imaging on cancer and endothelial cells.
BN175 and HUVEC cells were seeded in chamber slide and treated with 50 µM liposomal DOX using the above described (C)TSLs. Incubation was carried out for 1 h at 37 °C, at the end cells were washed and medium refreshed. Finally, slides were placed in water bath set at 41 °C for HT exposure. Pictures were taken using a wide field microscope using DAPI filter for Hoechst (nuclei, blue) and DsRed filter for DOX visualization (red). Arrows indicate co-localization of DOX and nuclei.

Live fluorescence imaging of BN175 and HUVEC after incubation (1 h NT) with DOX-loaded PG_2-/ and PEG-based (C)TSLs did not show any detectable DOX in cytoplasm or nuclei (Figure 24A, B, C and D). At this stage DOX is well entrapped and self-quenched inside liposomes, confirming good stability of liposomal systems used in the investigation. After the initial incubation, cell chambers were placed in a water bath for 1 h at 41 °C (HT) to trigger DOX intracellular release. Upon HT application, released DOX from PG_2-CTSL was well visible via fluorescence microscopy and detectable inside cells in punctuate pattern (Figure 24A, B, second panel). Although the majority of DOX was assessed inside cell cytoplasms, co-localization of DOX and nuclei was observed to a certain extent and selectively when cells were incubated with PG_2-TSL[30] (Figure 24A, B, white arrows). Cells treated with anionic DOX-loaded PG-TSL[30] also showed detectable DOX in cell cytoplasms, in good accordance with the binding investigations reported above (Figure 24A, B, first panel). In case of PEG-based TSL, higher intracellular DOX was observed after HT-triggered release when incubation was carried out with positively charged liposomes. However, a negligible amount of DOX was observed in case of anionic TSL (Figure 24C, D). By evaluating DOX fluorescence intensity generated in the study PG_2-CTSL was hypothesized to be a better system for DOX delivery efficiency in comparison to PEG-CTSL.

These results were further confirmed when quantifying the total amount of DOX delivered to cells by these means. The same experimental design was used as described above, however after HT application cells were collected and lysed and total amount of DOX quantified via HPLC. Free-DOX was also added to tested formulations to assess maximal efficiency of delivery. As it is shown in Figure 25, total recovered DOX from treated cells with 50 µM in liposomal form was 1.7-folds higher when DOX is applied via PG_2-CTSL in comparison to PEG-TSL (~0.5 and ~0.2 DOX/protein ratio wt/wt for NT treatment, respectively). As expected, no differences between NT and HT groups were observed, confirming that for HT groups either in case of intracellularly or extracellularly released DOX is immediately taken up by cells. For HUVECs, no difference was observed between free-DOX and PG_2-CTSL groups in terms of DOX recovery, whereas PG_2-CTSL significantly improved DOX delivery in comparison to PEG-CTSL (3.2-fold higher, ~1.4 vs. 0.2, respectively). To test possible saturation of binding and thus limiting delivery efficiency above a certain threshold, the investigation was repeated by using a double amount of DOX both as naked and liposomal form. For both BN175 and HUVEC, incubation with 100 µM DOX showed the same pattern observed previously, with PG_2-CTSL significantly increasing DOX delivery efficiency in comparison to PEG-CTSL (2.6-fold higher for BN175 and 3-fold for HUVEC). Recovered DOX in cells treated with 100 µM was in all cases proportionally 2-fold higher in comparison to samples treated with half the amount (Figure 25B, D).
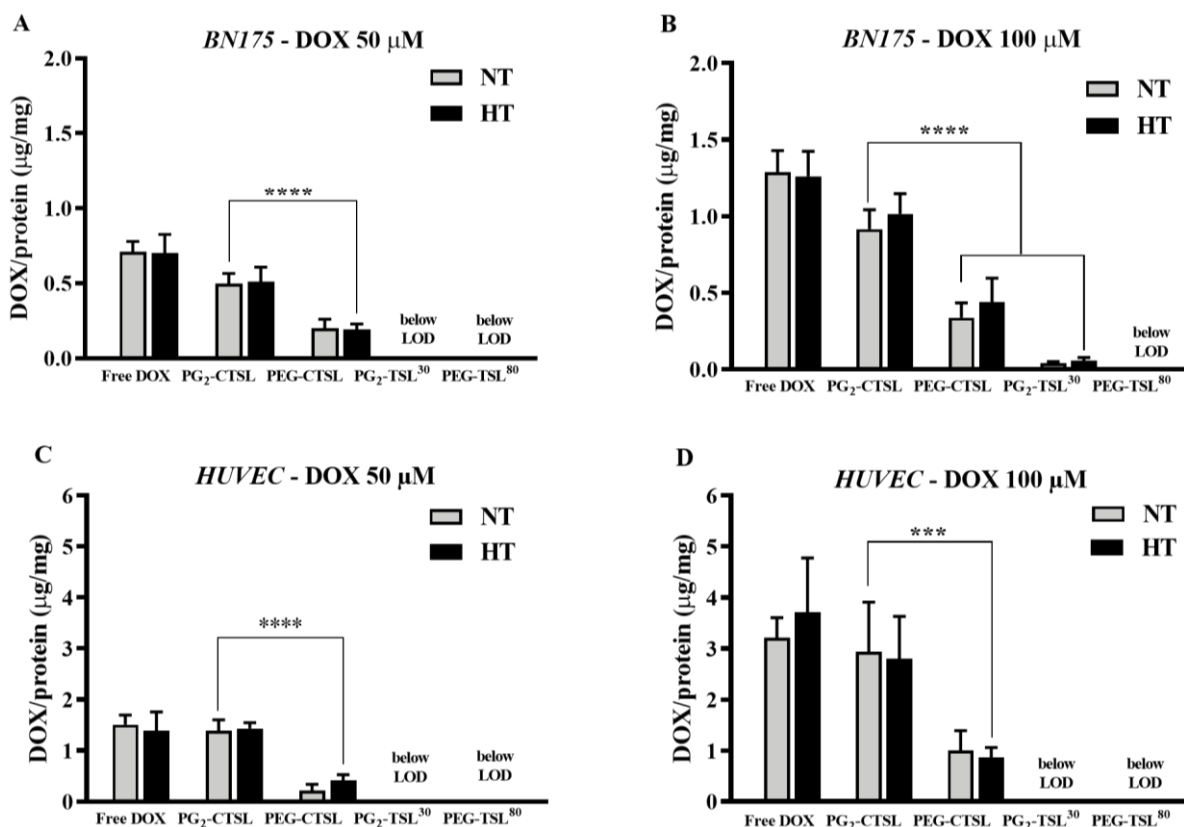
Figure 25 DOX recovery from tumor and endothelial cell lines after (C)TSL-DOX incubation.
BN175 (A, B) and HUVEC (C, D) cells were seeded in 6-well plates and treated with 50 µM liposomal DOX (A, C) or 100 µM liposomal DOX (B, D) using the above described (C)TSLs. Incubation was carried out for 1 h at 37 °C. At the end of the incubation time, cells were washed and medium refreshed. Plates were placed in a water bath set at 41 °C for 1 h. After HT exposure, cells were washed, trypsinized and centrifuged. Cell pellets were collected and resuspended in lysis buffer (150 mM NaCl, 20 mM Tris, 1 % Triton X-100, 0.1 % SDS pH 7.4). Solution was sonicated for 1 min in ice with a probe sonicator and DOX quantified via HPLC. Protein content in cell lysate was assessed via protein assay and results showed as DOX/protein ratio (µg/mg). Data are presented as mean value ± SD for three independent batches. Data were analyzed via one-way ANOVA followed by Bonferroni test and asterisks indicate significant difference between groups. **** = $p < 0.0001$, *** = $p < 0.001$. LOD = limit of detection.

4.1.3.7 *In vitro* cell toxicity investigation with (C)TSL-DOX

To assess whether the higher DOX delivery efficiency obtained via PG2-CTSL might also translate into a potentially higher therapeutic effect, an *in vitro* cell toxicity study on a cancer cell line and endothelial cells was performed. Cells were treated with different concentrations of DOX in liposomal form either with cationic or anionic formulations and HT or NT applied after incubation phase, respectively. The toxicity of different carriers was also evaluated by incubating cells with empty liposomes in combination with HT application. As it is shown in Figure 26, after incubation with liposomal DOX resulting cell viability curves were drastically affected by the type of formulation used in the investigations. In all cases, the inhibitory concentration of DOX killing 50 % of cells (IC50) was lower for positive charge TSL when compared to anionic counterparts (Table 11). PEG-CTSL IC50 in BN175 cell line was 3.5-fold higher when compared to PG2-CTSL, confirming a higher cell killing driven by PG2-CTSL-DOX (IC50 of ~ 5.8 and ~ 1.7 µM in HT condition, respectively). Any significant toxicity was not observed on cells driven by empty carriers in

hyperthermic conditions (Figure 26). No differences between HT and NT groups were detected independently from the (C)TSL used in the investigations (Table 11).
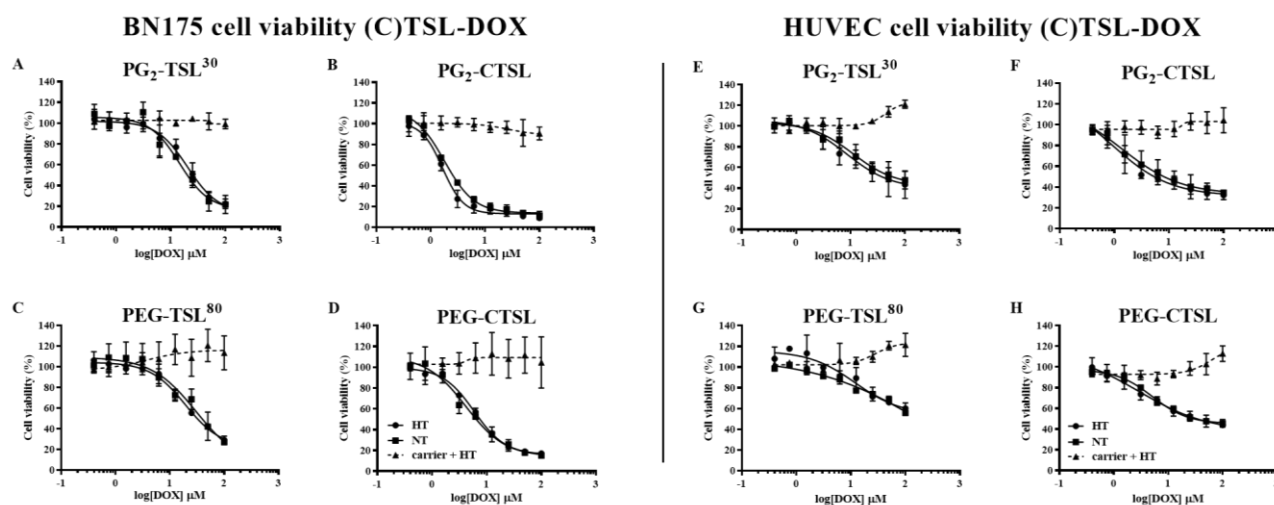

Figure 26 *In vitro* cell toxicity of (C)TSL-DOX on cancer and endothelial cells.
BN175 (A-D) and HUVEC (E-H) cells were treated with different concentration of DOX (log scale). Cell survival is expressed as a percentage of untreated cells (control) in combination with either HT (41 °C/1 h, circles) or NT (37 °C/1 h, squares). Empty liposomes were tested in combination with HT condition (dashed black line). Data are presented as mean value ± SD for three independent analysis. Values were fit by using a non-linear fit. HT and NT groups of each formulation were analyzed via one-way ANOVA followed by Bonferroni test highlighting no significant difference.

Table 11 IC50 of BN175 and HUVEC treated with different liposomal DOX formulation.
IC50 (values in μM) for HT (41 °C, grey rows) and NT (37 °C, white rows) groups. Asterisk indicates statistical significance of PG$_2$-CTSL in comparison to PEG-CTSL by evaluating corresponding IC50 via two-tailed student T-test ($p < 0.001$).

IC50 DOX (μM)	PG$_2$-TSL^{30}	PG$_2$-CTSL	PEG-TSL^{80}	PEG-CTSL
BN175				
IC50 HT	26.1 ± 8.3	1.7 ± 0.2*	29.3 ± 2.1	5.8 ± 0.1
IC50 NT	19.3 ± 9.4	1.8 ± 0.1	30.2 ± 5.9	4.2 ± 2.2
HUVEC				
IC50 HT	9.7 ± 0.4	2.6 ± 1.2	≥ 50	8.5 ± 6.2
IC50 NT	10.1 ± 2.6	2.9 ± 2.2	≥ 50	6.4 ± 3.4

IC50 HT/NT = inhibitory concentration of DOX killing 50 % of cells at HT or NT

4.1.3.8 Hemocompatibility of anionic and cationic liposomes *in vitro*

Hemocompatibility of anionic and cationic TSL was assessed *in vitro* via ELISA test. Complement activation via ELISA test for SC59-b showed the highest signals when human serum was incubated with PG$_2$-CTSL, 10-fold higher compared to control (HBS). PEG-CTSL also significantly triggered complement activation but only 2-fold higher (Figure 27A). Anionic formulation did not show any increased signals in comparison to negative control and thus no complement activation can be assumed for these formulations (PG$_2$-TSL^{30} and PEG-TSL^{80}, Figure 27A). In terms of blood cell interactions, NBD-labeled PG$_2$-CTSL showed the highest magnitude of binding for granulocytes and lymphocytes when compared to all other CTSLs tested (Figure 27B). After 1 h incubation at 37 °C, binding to granulocytes cells was 6-fold higher when compared to anionic PG$_2$-TSL^{30}. PEG-TSL showed the lowest interaction when compared to all other (C)TSLs

tested. For lymphocytes and monocytes, PG$_2$-CTSL showed smaller but still significant binding when compared to control, whereas for other (C)TSLs tested negligible interactions were observed.
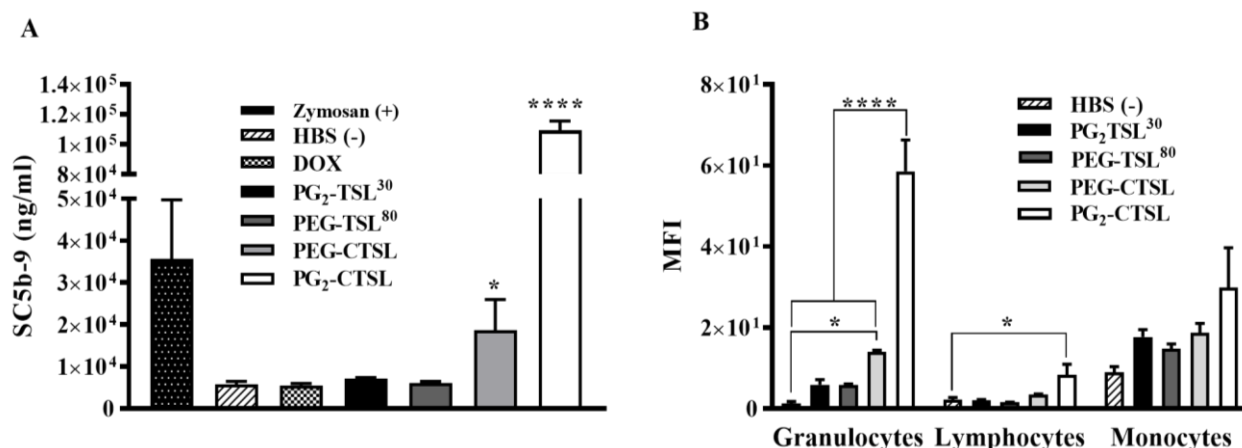

Figure 27 Liposomes-mediated complement activation (A) and liposomes-blood cell interactions (B) *in vitro*.
DOX-loaded (C)TSLs were diluted in certified normal human serum for complement activation analysis (1:12, v/v). Incubation was carried out at 37 °C for 30 min, Zymosan and HBS pH 7.4 were used as positive and negative controls, respectively. ELISA test for SC5b-9 was carried out using the manufacturer´s instructions. To assess liposomes-blood cells interactions, fresh blood was collected from healthy donors and erythrocytes lysed with lysing buffer. NBD-labeled CTSL interactions with blood cells components (granulocytes, lymphocytes, monocytes) shown as MFI, control group is fluorescence background of cells incubated with HBS pH 7.4. Values are expressed as mean value ± SD for three independent measurements. Statistical analysis was performed via one-way ANOVA Bonferroni test and asterisks indicate significant difference between groups. **** = $p < 0.0001$, * = $p < 0.05$.

4.1.4 Short-term storage stability study

4.1.4.1 Size & PDI

Cationic and anionic TSL were stored at 2-8 °C after active DOX loading. Changes in physical property (e.g., size & PDI) were monitored weekly in a 30 days investigational period. All anionic TSL showed remarkable stability with negligible changes in both size and PDI over time (Figure 28A). Cationic PG$_2$-CTSL showed acceptable stability in the first 2 to 3 weeks, whereas a sudden rise in PDI (> 0.5) was assessed when stored more than 3 weeks (Figure 28A). However, no flocculation driven by particle coalescence and precipitation was observed at this time point. PEG-based CTSL showed improved stability over time in comparison to PG$_2$-CTSL, and comparable to anionic TSL. Nevertheless, after 4 weeks storage PEG-CTSL intensity distribution showed appearing of a small second peak with corresponding slight increase in PDI (Figure 28A). All tested liposomes showed no changes in surface charge over time, with comparable ζ-POT to freshly formed vesicles (Figure 28B).
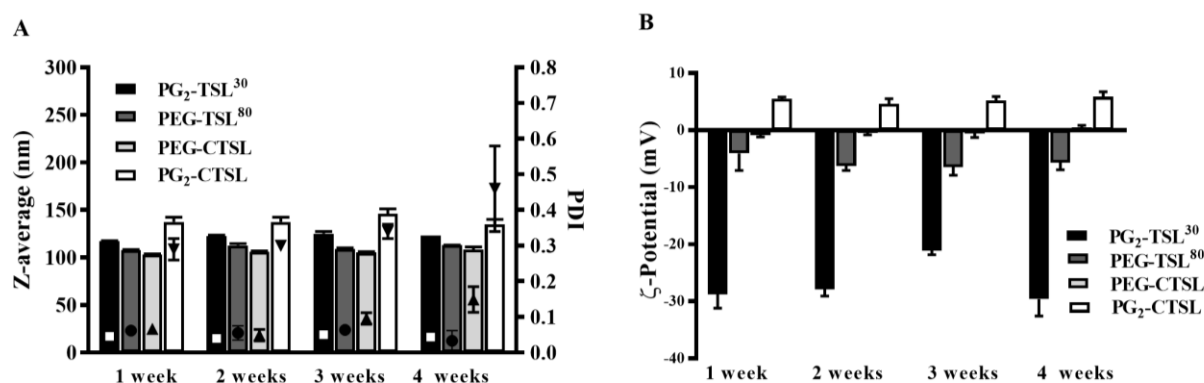
Figure 28 DLS analysis on (C)TSLs during storage at 2-8 °C.
Samples were analyzed weekly by for a total time of 30 days. Values are presented as mean values ± SD of at least three independent batches.

4.1.4.2   DOX leakage and carrier integrity

Besides assessing size & PDI via DLS analysis, DOX leakage was investigated in parallel experiments at same time points. Additionally, lipids and degradation products were analyzed via TLC. A modest trend in DOX leakage was observed in all TSL over 2-8 °C storage, except for PEG-TSL[80] (Figure 29A). Nevertheless, fractions of released DOX did not exceed ~ 7 % of total DOX content, suggesting an acceptable DOX encapsulation stability over time, at least at investigated time points. Lipid composition and generation of lyso-lipids were monitored over time via TLC method. All TSL were run through TLC immediately after DOX loading and after 4 weeks storage 2-8 °C. No lyso-lipids were detected after active loading of DOX, whereas after 4 weeks of storage minimal lipid hydrolysis (1-2 % lysolipid content) was assessed in all formulation tested (Figure 29B). DPTAP is not a phospholipid since it does not have a phosphate group, thereby it cannot be detected via molybdenum spray. Hence, all TLC with cationic TSL samples were done in parallel and stained either via molybdenum spray or copper reagents. Representative chromatograms of TCL either via molybdenum spray or copper reagent staining are shown in Figure 30.
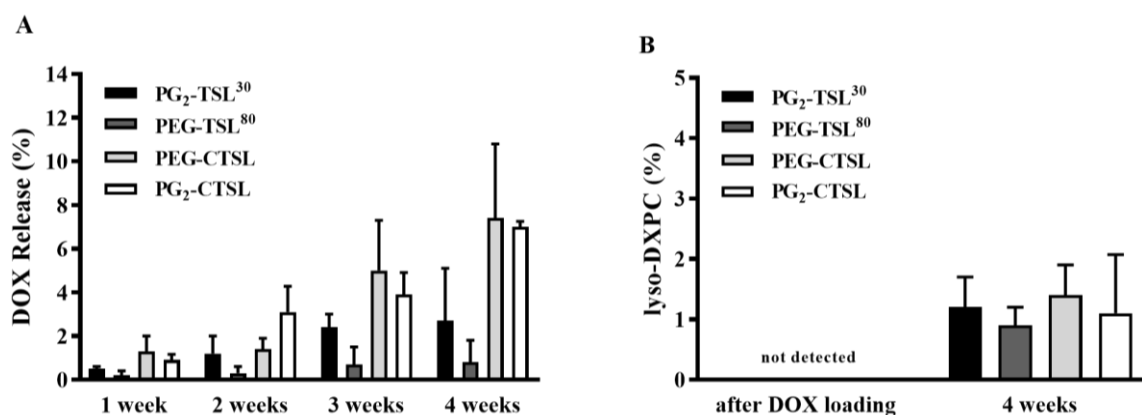

Figure 29 (C)TSL DOX leakage (A) and lyso-lipid content (B) during storage at 2-8 °C.
To assess DOX leakage, freshly loaded (C)TSLs were diluted in HBS pH 7.4 at 1:149 dilution (v/v) and DOX fluorescence detected via fluorometry at Ex/Em 475/555 nm. To assess total DOX content, TSL were destroyed by adding 10 % Triton X-100 (150:1, v/v) and DOX measured as reported above (A). Lyso-lipids were assessed at day 0 and after 4 weeks of storage at 2-8 °C via TLC method (B). Values are presented as mean values ± SD of at least three independent batches.
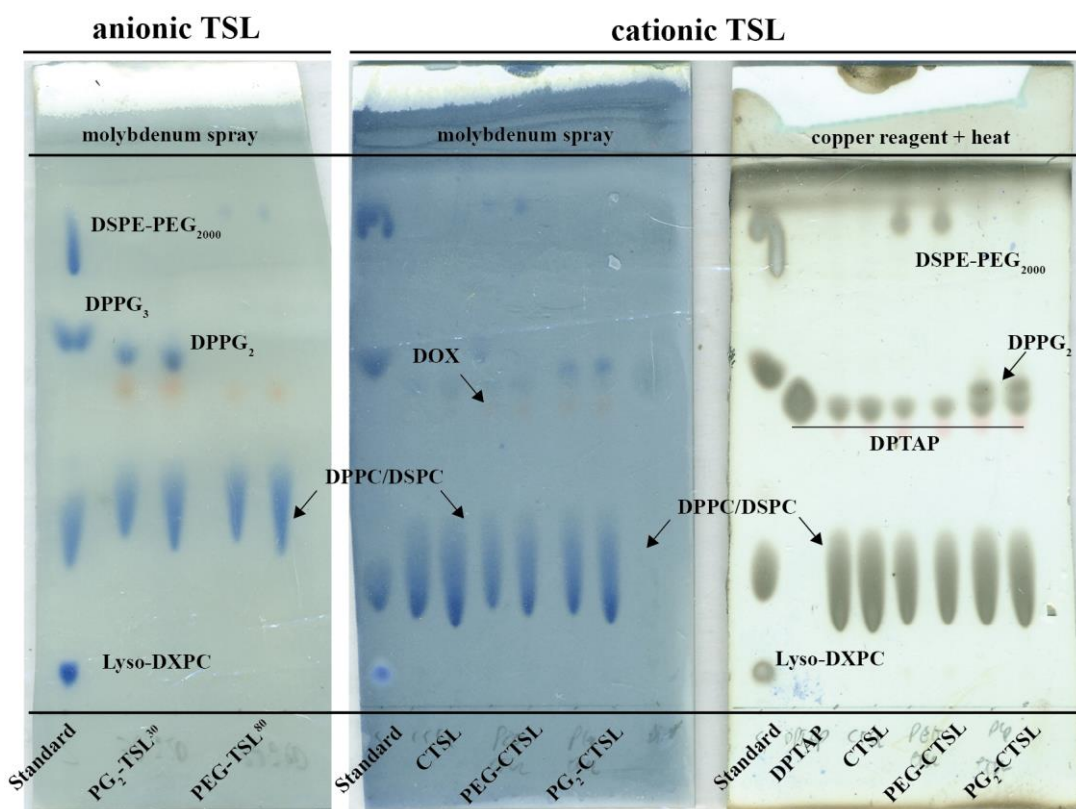
Figure 30 Representative chromatograms obtained via TLC method with anionic and cationic TSL.
Samples were analyzed immediately after DOX loading. Cationic TSL bearing non-phospholipid DPTAP were run in duplo on separate plates and stained either with molybdenum spray or copper reagent.

4.1.5 *In vivo* work package

4.1.5.1 Pharmacokinetic profile

In order to assess if positive charge affects particle circulation and monitor DOX clearance from the bloodstream, PK investigation was carried out in Brown Norway rats. DOX as free drug and in liposomal form was administrated i.v. in Brown Norway rats and PK assessed for 120 min.
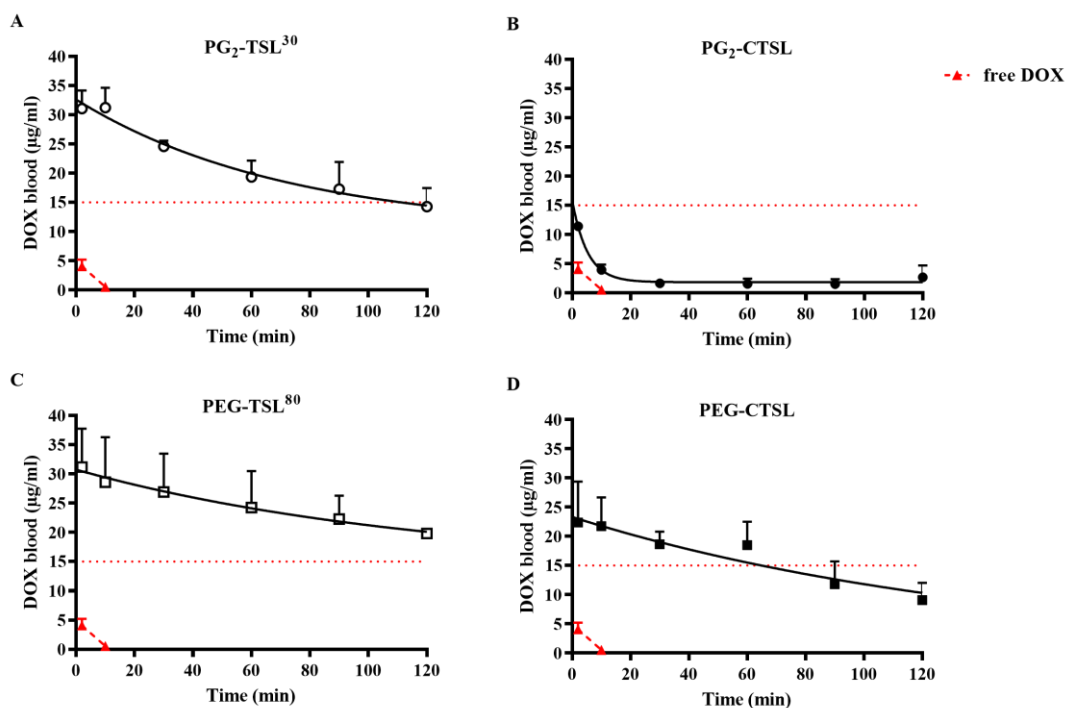
Figure 31 Pharmacokinetic profile of different (C)TSL-DOX formulation in Brown Norway rats.
DOX blood level after administration via PG$_2$-TSL^{30} (A), PG$_2$-CTSL (B), PEG-TSL^{80} (C) and PEG-CTSL (D). In all figures, administration of free-DOX is shown with a dashed red line whereas dotted red line at 15 µg/ml in y-axis highlight threshold of 50 % injected dose. DOX blood concentration values from all TSLs tested were fit using mono-exponential decay formula (Equation 3), besides of PG$_2$-CTSL where a two-phase decay formula was used for the fitting (Equation 4). Data are presented as mean value ± SD, every groups consisted in three animals (n = 3).

After injection of anionic PG$_2$-TSL^{30} and PEG-TSL^{80}, a mono-exponential DOX elimination was observed (Figure 31A, C) with a t_α of 137.6 ± 16.8 min and 305.4 ± 8.5 min, respectively (Table 12). Maximum blood concentration (C$_{max}$) for PG$_2$-TSL^{30} and for PEG-TSL^{80} were similar and comparable to theoretical C$_{max}$, suggesting negligible DOX leakage upon TSL injection (Table 12). In case of cationic TSLs, C$_{max}$ was significantly lower when compared to the anionic counterpart, especially in case of PG$_2$- CTSL (11.4 ± 0.7 µg/ml, 2.7-fold lower in comparison to PG$_2$-TSL). In the latter case, a drop in circulation time was observed immediately upon liposomes injection, with a rapid loss of 65.5 % of total injected dose (ID) (Table 12). DOX blood content after PG$_2$-CTSL administration unveiled a bi-phasic clearance with t_α of 11.5 ± 2.7 min and a slow elimination rate after initial drop, assessing a final DOX blood content at 2 h of 2.7 ± 2.0 µg/ml (Figure 31B,Table 12). According to the fast particle clearance, PG$_2$-CTSL AUC$_{2 h}$ decreased of 70 % when compared to PG$_2$-TSL^{30} (311 vs. 2,261 h*µg/ml, respectively). In case of PEG-CTSL, an initial drop in DOX

blood content was observed but to a lesser extent than for PG_2-CTSL (32.1 % loss ID). Furthermore, a significant 2-fold loss in AUC_{2h} was assessed when compared to the anionic counterpart (Table 12). Nevertheless, DOX clearance rate from PEG-CTSL suggested a slow elimination with monophasic clerance and t_α of 125.4 ± 5.3 min (Figure 31D & Table 12).

Table 12 PK parameters of DOX in (C)TSLs formulation.

Liposomes	Type	t_α (min)	AUC_{2h} (h*µg/ml)	theoretical C_{max} (µg/ml)	C_{2min} (µg/ml)	C_{2h} (µg/ml)	Fit (R^2)
free-DOX	/	/	18	33.1	4.1 ± 1.1	n.d.	/
PG_2-TSL[30]	anionic	137.6 ± 16.8	2,261	33.1	31.1 ± 3.1	14.3 ± 3.2	0.9520
PEG-TSL[80]	anionic	305.4 ± 8.5	2,827	33.1	31.2 ± 6.6	19.8 ± 0.8	0.9714
PEG-CTSL	cationic	125.4 ± 5.3	1,585	33.1	22.4 ± 6.9	9.2 ± 0.9	0.9923
PG_2-CTSL	cationic	11.5 ± 2.7	311	33.1	11.4 ± 0.7	2.7 ± 2.0	0.9871

t_α = half life. AUC=Area under the curve. C = DOX blood concentration.

4.1.5.2 Biodistribution

Targeting of anionic and cationic TSL-DOX formulations was assessed in BD experiments in tumor-bearing rats in combination with lamp mediated HT.
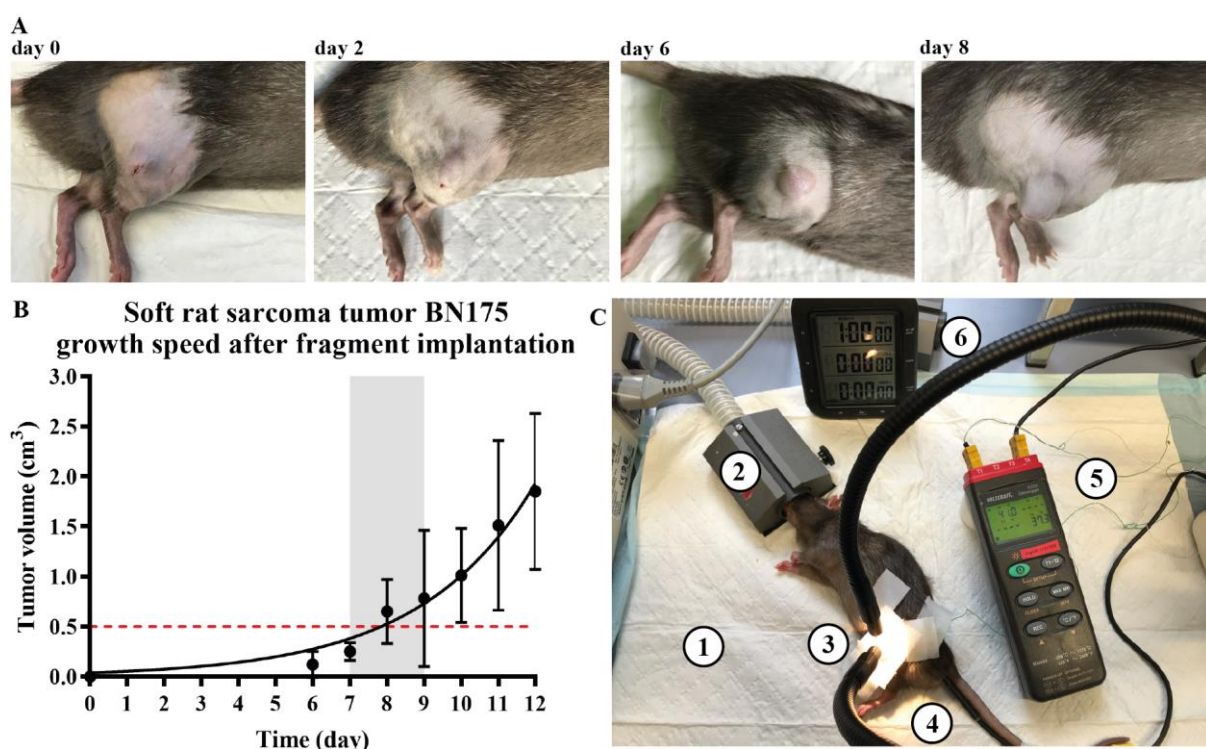
Figure 32 BN175 tumor growth kinetics and setup used for BD investigation.
Representative images of tumor growth kinetics (A) and according tumor volume assessed via caliper measurement (B). Red dotted line on graph B indicates threshold of tumor volume required for the BD study whereas grey area shows usual timing for the tumor to reach desired size (7-9 days). BD setup: heated-mattress pad (1), anesthesia mask (2), lamp mediated HT and tumor invasive temperature probe (3), rectal probe (4), temperature data logger (5), timer (6).

Tumors fragments were installed in both hind legs. Tumor growth was assessed via caliper measurement every other day (Figure 32A, B). Lamp-mediated HT was performed on one of the

tumors (Tumor HT), whereas the tumor located on the opposite hind leg was kept at physiological temperature (setup shown in Figure 32C). In all tested TSL groups, 1 h HT was successful in increasing DOX enrichment in heated tumors, when compared to untreated tumors (Figure 33B). For PG_2-TSL^{30}, a remarkable 14-fold higher DOX concentration was found in heated tumors, when compared to NT tumors. For PEG-based TSL, no differences were observed in terms of DOX enrichment factors between anionic and cationic particles, suggesting positive charge did not affect the external targeting approach mediated by HT. As expected, the fast clearance of PG_2-CTSL observed in PK investigations is mainly due to RES particle removal, as suggested by higher DOX values recovered in liver and spleen (Figure 33A). PG_2-CTSL synergistic targeting in heated tumors led to 3.7-fold higher DOX enrichment in comparison to non-heated tumors. However, no substantial differences in DOX recovery were observed among NT tumors treated with different (C)TSLs, suggesting tumor targeting mediated exclusively by cationic active targeting is negligible at reported time points.
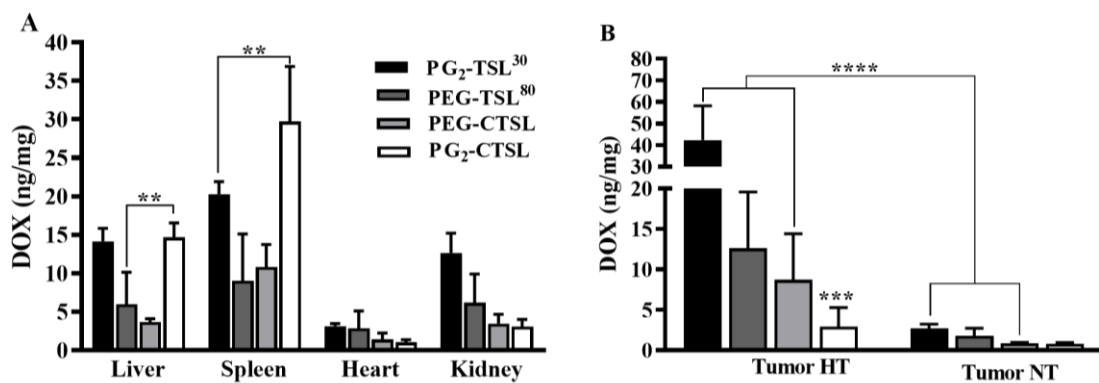
Figure 33 Biodistribution of different (C)TSL-DOX formulation in tumor-bearing Brown Norway rats.
DOX recovered in organs (A) and heated and not-heated tumors (B) after i.v. administration of different (C)TSL-DOX formulations. Data are presented as mean value ± SD, every groups consisted in three animals (n = 3). Data were analyzed via unpaired two-tailed T-test and asterisks indicate significant difference between groups. **** = $p < 0.0001$, *** = $p < 0.001$, ** = $p < 0.005$.

4.2 Immuno-cancer therapy

The objective of the study was the design of a novel DPPG$_2$-based TSL formulation for targeted release of IAVs. The investigation aims to assess feasibility of a TLR-7,8 agonist (R848) encapsulation in TSL and its heat-triggered release upon HT. Besides evaluation of different formulations, the immune-cell activation driven by IAV stimulation and potentially synergistic effect of HT in terms of cytokine production were investigated. Additionally, immunogenicity of R848 and HT in immune-mediated cancer cell killing experiments were assessed. PK parameters after injection of R848 in solution or formulated with DPPG$_2$-TSL were assessed *in vivo* on Brown Norway rats.

4.2.1 R848 properties

4.2.1.1 R848 fluorescence

R848 was dissolved in acetate buffer pH 5.2 at final stock concentration of 1 mg/ml, as described in section 3.3.1. R848 fluorescence spectrum unveiled an excitation peak maximum at 260 nm with an emission peak maximum at 360 nm. R848 fluorescence pattern was assessed at these wavelengths by adjusting the gain (400-1000 V) to investigate linearity between fluorescence and concentration, and potential self-quenching at high concentrations.
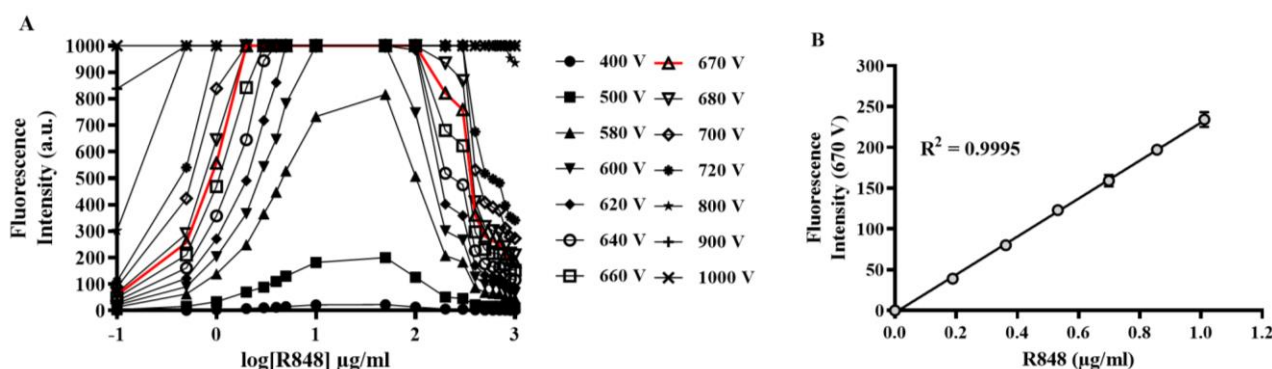
Figure 34 R848 fluorometry analysis.
R848 fluorescence was assessed in a concentration range (0.1-1000 µg/ml) at different voltages (400-1000 V) (A). Red line in graph A higlights R848 fluorescence pattern at 670 V. Focus on R848 fluorescence at 670 V in concentration range between 0.1-1.2 µg/ml (B).

R848 fluorescence showed a concentration-dependency (Figure 34A). From a concentration of 0.1 to 50 µg/ml, fluorescence increased accordingly (Figure 34A). At ~50 µg/ml of R848, fluorescence emission decreased, potential due to a self-quenching effect. At the highest R848 concentration tested (1 mg/ml), partial R848 self-quenching was detected, independently of the voltage used. R848 fluorescence linearity was assessed in a specific concentration range (0.1-1.2 µg/ml), using 670 V (Figure 34B). Due to the self-quenching effect of R848 on the fluorescence intensity, R848 active loading was monitored through fluorescence spectroscopy over time (refer to sections 4.2.2.4 & 4.2.2.5). Nevertheless, due to the incomplete self-quenching of R848, HPLC was always performed to quantify content and loading efficiency.

4.2.1.2   R848 recovery after filter centrifugation

Filter centrifugation via Amicon unit filters 30K is a valid option to separate small hydrophilic molecules from liposomes [109, 256]. Recovery of non-liposomal R848 in the supernatant was evaluated at 3 different concentration (e.g., 1, 5 and 10 µg/ml). Amicon filters without passivation showed a signficant loss of R848 especially at the smallest tested concentation (1 µg/ml, 80 % loss) (Figure 35A). This might be caused by R848 adsoprtion to filter membranes. Filter passivation with 5 % Triton X-100 strongly improved R848 recovery to ~100 % by avoiding material loss.
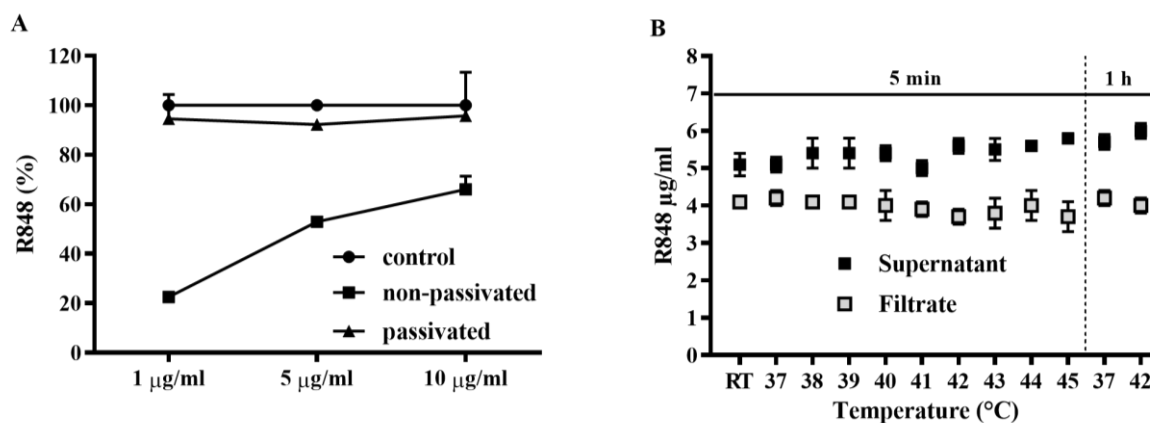
Figure 35 R848 recovery after filter centrifugation (A) and R848 interaction to FCS (B).
In figure 35A, R848 solutions (1, 5 and 10 µg/ml) were filter centrifuged (14000xg, 10 min, 2-8 °C). Filters were either passivated (5 % Triton X-100 overnight) or not passivated. R848 content was assessed in filtrates and compared to initial values assessed in supernatant before centrifugation. In Figure 35B, R848 was spiked in full FCS at 5 µg/ml final concentration. Incubation was carried out at 37-45 °C temperature range for 5 min and at 37 °C and 42 °C for 1 h. Samples were filter centrifuged (14000xg, 10 min, 2-8 °C) using passivated filters. Recovered values are displayed per each incbuation condition. In boths graphs, values are shown as mean values ± SD for three independent measurements.

Next, potential binding of R848 to serum proteins was assessed under different conditions. R848 might be bound to serum proteins [257] and hence not recovered via the above mentioned method. Incubation of R848 in FCS was carried out in similar conditions used as in a temperature-dependent release assay. The recovered R848 was reduced of ~ 20 % in all groups, potentially caused by serum complex formation (Figure 35B). Since serum proteins are not usually filtered, complexed R848 is lost and cannot be recovered. No differences were detected when serum incubation was performed for 5 min or 1 h, independently from incubation temperature (Figure 35B).

4.2.2 Formulation design

4.2.2.1 R848 passive loading in DPPG$_2$-TSL

First, R848 encapsulation was tested via passive loading method. The used conditions are described in Table 1, whereas particle characteristics after R848 passive loading are reported below (Table 13).

Table 13 DPPG$_2$-TSL formulation after R848 passive loading.
Results are shown as mean values ± SD of three independent prepared batches.

Liposomes (mol:mol)	Z-average (nm)	PDI	ζ-POT (mV)	R848 (mM)	R848/lipid (mol:mol)	EE (%)
DPPC/DSPC/DPPG$_2$ (50/20/30)	162.9 ± 3.2	0.118 ± 0.02	-25.9 ± 6.4	0.03 ± 0.06	0.013 ± 0.001	15.3 ± 1.8

PDI = polydispersity index. ζ-POT assessed in NaCl 0.9 %. EE = encapsulation efficacy.

Passive loading of R848 did not affect suspension stability, as size & PDI assessed via DLS data proved a homogenous particles distribution. The negative surface charge detected via ζ-POT analysis was found consistent with previously reported data when 30 mol% of DPPG$_2$ were present in the lipid bilayer (refer to section 4.1.1.3). R848 was encapsulated into DPPG$_2$-TSL with an EE of 15.3 ± 1.8 %. Next, particles were subjected to a temperature-dependent release assay to assess R848 heat-triggered capability (Figure 36). Poor drug retention was observed after 5 min and 1 h at 37 °C, with ~35 % (total content) and ~50 % loss of total R848 content, respectively. At 42 °C, drug release was equal to ~70 % after 5 min and to 85-90 % after 1 h incubation (Figure 36). The high leakage at 37 °C can be explained by the presence of a relevant membrane fraction of R848, subjected to fast removal upon dilution in FCS. This might also explain the higher EE assessed after passive loading, driven by R848 encapsulation both in the aqueous core and in the lipid bilayer.
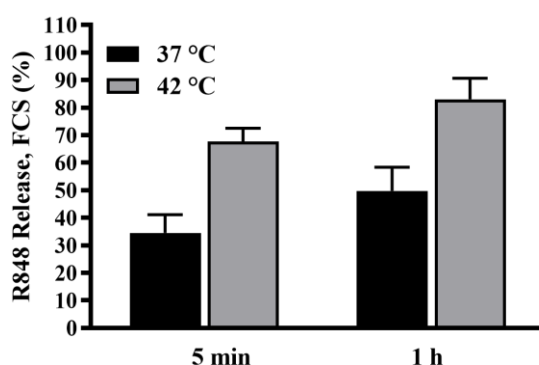

Figure 36 Temperature-dependent R848 release profile of passively loaded DPPG$_2$-TSL-R848.
Release assay was performed in FCS exclusively for 37 °C and 42 °C, both after 5 min and 1 h incubation. Values are given as percentage of total R848 content assessed via incubation of particles with 10% Triton X-100 (1:2, v/v). Release measured after 5 min at RT was used as control. Values are presented as mean values ± SD of at least three independent batches.

4.2.2.2 Investigation of R848 active (remote) loading

R848 active encapsulation in DPPG$_2$-TSL (DPPC/DSPC/DPPG$_2$, 50/20/30 mol:mol) was investigated via a NH$_4^+$ gradient, which is a conventional strategy established for remote loading of weak bases [38]. A method for R848 active loading in non-thermosensitive liposomes was already described in the literature [258]. However, the loading condition consisted in a 4 day incubation at 30 °C with PBS set at pH 5.2 in the extra-liposomal phase and ammonium sulfate (AS) at pH 5.4 as gradient force. Potential degradation of liposomal carriers can be expected by the acidic conditions [259], however the latter point was not assessed by the authors.

To assess whether such prolonged loading is indeed required, fractions of a single liposome batch were loaded for different time points (2, 4, 8, 24, 48 and 72 h), while temperature was set at 30 °C. Active loading was performed with an initial R848/lipid of 0.1 (mol:mol) using AS as intra-liposomal excipient and, HBS at pH 5.2 as extra-liposomal buffer, respectively. Actively loaded TSL-R848 were characterized immediately after loading (Table 14). All liposomes recovered after loading showed comparable size in the range of 156-170 nm and small PDI < 0.1. A dependency between loading time and R848 encapsulation efficiency was observed. Samples loaded for 2 h showed an EE of ~34%, which increased over time up to ~60 % and 80% when loading was protracted for 8 and 24 h, respectively. Loading for 72 h did not improve further R848 encapsulation. As expected, exposure of liposomes at loading condition (30 °C and extra-liposomal phase pH 5.2) significantly increased lipid degradation in a time-dependent fashion (Table 14). Temperature-dependent release assays were performed in all loaded TSL, showing feasibility of DPPG$_2$-TSL for R848 heat-triggered release upon HT (Figure 37). R848-release profile was notably affected by lyso-lipids content and R848/lipid ratio. Batches loaded for 2 and 4 h showed higher R848 leakage at 37-39 °C than TSL loaded for 8 h (~20 % vs. ~5 %). Additionally, a maximum R848 release was detected at 43 °C for TSL loaded for 2 and 4 h, whereas TSL loaded for 8 h showed more rapid release already at 42 °C. The presence of an increasing amount of lipid degradation products shifted R848 release profile towards lower temperatures (Figure 37). Besides, a trend for increasing leakage at NT temperatures was also observed in batches loaded for more time than 8 h.

Table 14 DPPG$_2$-TSL formulation after R848 active loading at different time.
A single experiment was performed per loading condition (n =1).

Loading (h)	Z-average (nm)	PDI	ζ-POT (mV)	R848 (mM)	R848/lipid (mol:mol)	EE (%)	Lyso-lipid day 1 (%)
2	160	0.021	-27.5	0.7	0.02	23.7	n.d.
4	172	0.048	-26.5	1.2	0.048	48.4	0.9
8	168	0.038	-28.7	1.4	0.058	58.7	2.9
24	170	0.041	-25.1	1.6	0.078	78.2	7.2

| 48 | 161 | 0.076 | -28.4 | 1.9 | 0.0893 | 89.3 | 11.3 |
| 72 | 156 | 0.084 | -26.5 | 1.9 | 0.0874 | 87.4 | 13.5 |

PDI = polydispersity index. ζ-POT assessed in NaCl 0.9 %. EE = encapsulation efficacy. Lyso-lipid assessed via TLC method. n.d.= not detected.
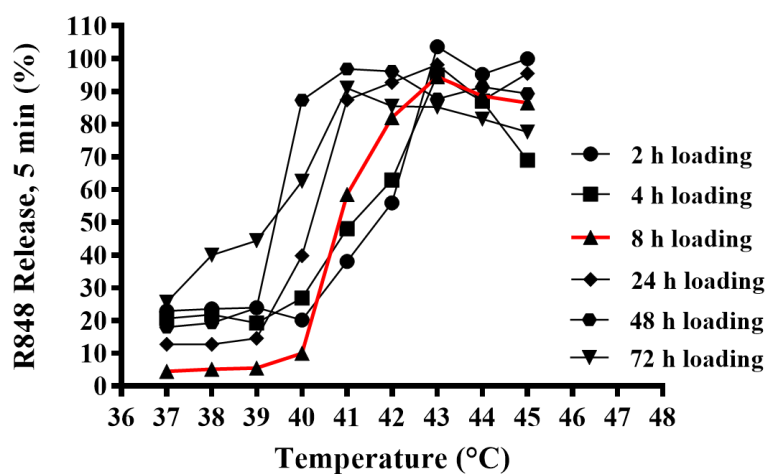

Figure 37 Preliminary temperature-dependent R848 release profile of actively loaded DPPG₂-TSL-R848.
Efficiency of active loading was assessed at different time points (2, 4, 8, 24, 48, 72 h). Temperature dependent release profile was performed with freshly loaded TSL. A single experiment was performed per loading condition (n =1).

Carrier integrity and absence of lipid-degradation products are crucial parameters to control when designing novel liposomal formulations. In this preliminary investigation, prolonged exposure to 30 °C during loading seemed to improve R848 encapsulation but also induced lipid hydrolysis. The batch loaded for 8 h showed potential for further improvements, which were investigated in the next section.

4.2.2.3   R848 active loading optimization – pH & excipients

Optimization of R848 loading into DPPG₂-TSL was investigated by screening different parameters as intra-liposomal excipients and extra-liposomal pH. First, R848 loading via the above reported conditions was replicated, with AS as intra-liposomal excipient (300 mM, pH 5.4) and HBS pH 5.2 in the extra-liposomal phase. Loading was performed for 8 h at 30 °C, with R848/lipid ratio of 0.1 (mol:mol). By increasing the pH to 6.4, R848 protonation was reduced until reaching a 50 % balance between protonated and deprotonated forms (pH 6.4 = pKa). Hence, active loading was also tested with extra-liposomal buffer HBS at pH 6.4, to investigate potential improvements in R848 EE and reduction in lyso-lipid generation (refer to table Table 17 for buffer composition and osmolality measurements). Second, in parallel experiments, DPPG₂-TSL were produced with different intra-liposomal excipients (ammonium phosphate, AP, 300 mM pH 7.4). Also in this case, both extra-liposomal pH conditions (5.2 and 6.4) were tested to unveil the best loading conditions. Physicochemical properties of DPPG₂-TSL after R848 loading are shown in Table 15.

Table 15 DPPG₂-TSL formulation after R848 active loading at 30 °C/8 h.
Results are shown as mean values ± SD of at least three independent batches.

R848-TSL	Intra-vesicle medium	Extra-vesicle medium	Z-average (nm)	PDI	R848/lipid (mol:mol)	EE (%)	Lyso-lipid day 1 (%)	Lyso-lipid day 30(%)
AS-pH 5.2	$(NH_4)_2SO_4$ pH 5.4	HBS pH 5.2	184 ± 5	0.038 ± 0.02	0.062 ± 0.01	62.7 ± 6.9	2.95 ± 0.5	14.5 ± 1.6
AS-pH 6.4	$(NH_4)_2SO_4$ pH 5.4	HBS pH 6.4	187 ± 2	0.054 ± 0.03	0.086 ± 0.04	86.2 ± 3.7	1.1 ± 0.6	7.8 ± 1.2
AP-pH 5.2	$(NH_4)_2HPO_4$ pH 7.4	HBS pH 5.2	187 ± 3	0.044 ± 0.03	0.075 ± 0.02	75.4 ± 2.6	0.6 ± 0.3	5.2 ± 0.3
AP-pH 6.4	$(NH_4)_2HPO_4$ pH 7.4	HBS pH 6.4	175 ± 5	0.078 ± 0.054	0.087 ± 0.03	87.3 ± 3.2	n.d.	8.9 ± 2.3

AS = ammonium sulfate. AP = ammonium phosphate. PDI = polydispersity index. EE = encapsulation efficacy. Lyso-lipid (%) assessed via TLC method. n.d.=not detected

R848 EE significantly increased from ~60 % to ~85 % when the extra-liposomal pH was adjusted to the pKa of R848 (pH 6.4) (Table 15). Furthermore, a consistent decrease in lipid hydrolysis was assessed when compared to TSL loaded at pH 5.2. This is not surprising considering optimal pH for lipid storage should not be lower than 6.5 [259]. When loading was performed via AP, EE of ~75 and ~88 % was assessed when HBS at pH 5.2 and 6.4 were used, respectively. In good accordance with the higher intra-liposomal pH (pH 7.4), lipid hydrolysis was even further reduced (Table 15). All loaded TSL-R848 were tested in terms of heat-triggered R848 release. R848 temperature-curves were overall similar for all loaded TSLs, with a fast and complete drug release at 42-43 °C after 5 min incubation (Figure 38A). Significant leakage at 37 °C was observed after 5 min incubation in all TSL (15 to 25 %), except in TSL loaded with AS-pH 5.2, which showed negligible loss of R848 at this condition. The latter formulation was also observed to have a faster R848 release in comparison to other TSLs (~80 vs. ~50 % R848 release). Payload retention after stressing particles for 1 h at 37 °C showed good stability in case of AS pH 5.2, whereas batches loaded at pH 6.4 via AS gradient showed ~15 % leakage (Figure 38B). Formulations loaded with AP gradient showed higher R848 loss after the same incubation, ~20 and ~24 % for pH 5.2 and 6.4, respectively. In all TSLs tested, prolonged storage at 2-8 °C significantly increased lipid hydrolysis, with higher content for TSL loaded at lower pH (Table 15).
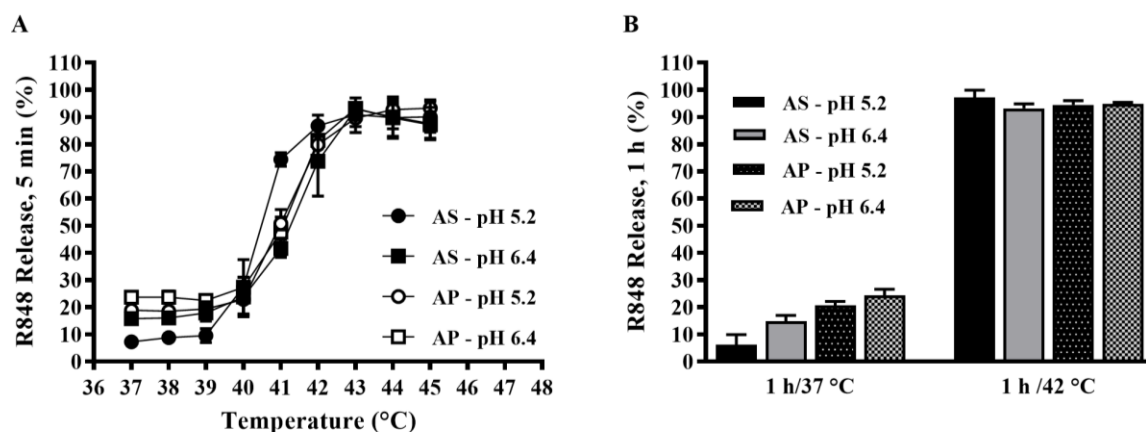
Figure 38 Temperature-dependent R848 release of DPPG$_2$-TSL-R848 with different intra-liposomal excipients.
Temperature dependent release profile for 5 min incubation at 37-45 °C (A) and 1 h at 37 °C and 42 °C (B). Values are presented as mean values ± SD of at least three independent batches.

Due to the above-mentioned results regarding R848 retention at 37 °C, AS was assessed as an optimal excipient for R848 active loading. Particles loaded with extra-liposomal pH 5.2 showed a better performing TDR profile with minimal leakage at 37 °C and a rapid release at 41 °C. However, shortcomings concerning lipid hydrolysis and suboptimal EE were detected. On the other side, batches loaded at pH 6.4 showed almost a complete EE with minimal lipid hydrolysis, while TDR profiles were still considered functional. For the above-mentioned reasons, both formulations were kept in the investigations and used in the next study.

4.2.2.4   R848 active loading optimization – R848/lipid ratio

The significant leakage of R848 immediately after FCS dilution at NT (37-39 °C) temperature might be related to R848 partially incorporated in the membrane bilayer. R848 interactions with lipid bilayer were hypothesized to be a function of total R848 concentration and extra-liposomal pH. Hence by increasing the concentration, a consequent reduction in percentage of membrane bound R848 can be expected. Loading with higher R848/lipid ratio (mol:mol) was tested to highlight potential benefit in terms of encapsulation stability and thus reducing percentage of R848 loss. R848 loading was performed as described above, except for R848/lipid (mol:mol) ratio which was in this case doubled (0.2). TSL showed similar values in terms of size distribution with no differences in PDI and ζ-POT (data not shown). Loading efficiency did not change when 2-fold higher R848 was used in the experiments, with comparable EE values among condition tested. In accordance to higher EE observed for batch loaded at pH 6.4 in comparison to pH 5.2, the same was reported also in this case (Figure 39). Final content formulated via TSL was significantly different, with 2-fold higher R848 content in liposomes loaded at 0.2 R848/lipid ratio, compared to 0.1 ratio (Figure 39).
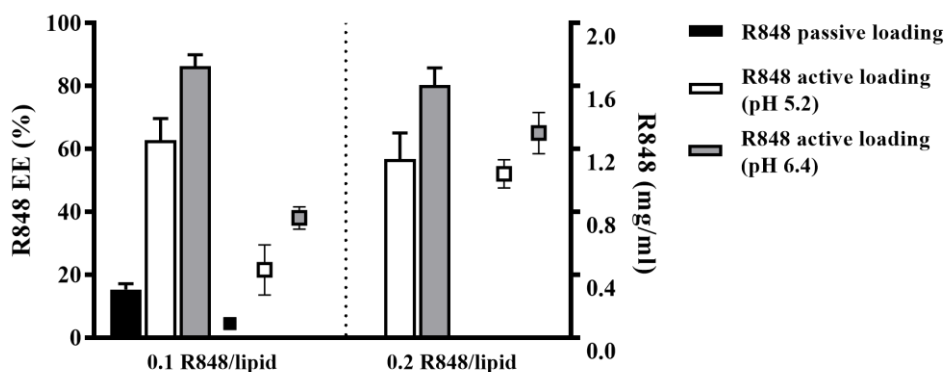
Figure 39 Encapsulation efficacy of R848 via passive and active loading.
Passive (detailed description in section 4.2.2.1) and active loading of R848 with different extra-liposomal pH (5.2 and 6.4) and R848/lipid ratio (0.1 and 0.2, mol:mol). Bars refers to R848 encapsulation efficiency (left y-axis), whereas symbols refer to R848 content (right y-axis). Values are presented as mean values ± SD of at least three independent batches.

The R848 remote loading in DPPG$_2$-TSL was monitored via fluorescence spectroscopy. An investigation on R848 fluorescence property was already assessed in section 4.2.1, showing no complete self-quenching at the highest concentration tested (1 mg/ml). When loading was performed at pH 5.2 for 8 h at 30 °C, the fluorescence decreased in fuction of time but not further than 60 % of initial fluorescence, assessed at 8 h (Figure 40). When extra-liposomal pH 6.4 was tested, fluorescence decreased to 45% of the initial value at 3 h with no further improvements over time. Nevertheless, when loading was performed with a R848/lipid 0.1 (mol:mol), resulting fluorescence measured via the same mean decreased only to a final ~75 % of initial values, for both tested pH. These findings confirm the needs to properly evaluate R848 loading by assessing the final content via HPLC method.
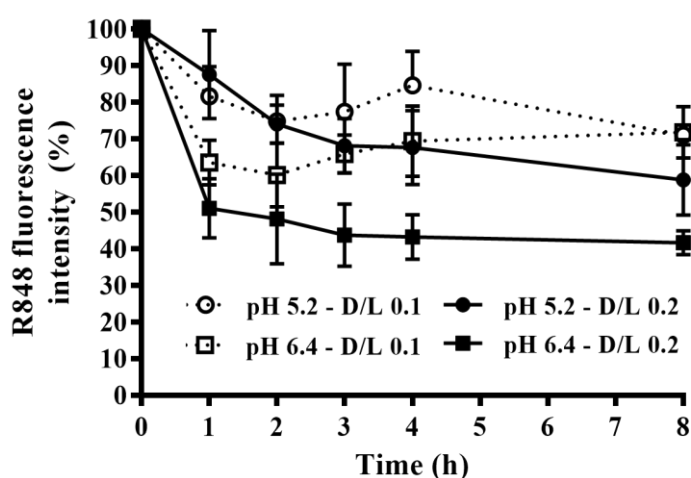
Figure 40 R848 fluorescence spectroscopy during remote loading.
Fluorescence spectroscopy was performed at time 0 and after 1, 2, 3, 4 and 8 h. Values are expressed as percentage of fluorescence intensity found at time 0. Values are presented as mean values ± SD of at least three independent batches.

R848 release profiles on batches loaded with twice the amount of R848 were performed and temperature curves compared to previous obtained results (refer to section 4.2.2.3). Surprisingly, similar pattern in TDR profiles were observed when comparing to TSL loaded at R848/ lipid 0.1 (mol:mol), both for pH 5.2 and 6.4 (Figure 41). In case of loading at pH 5.2, minimal R848 loss were detected between 37-39 °, whereas a rapid burst-like R848 release was observed at 41 °C after 5 min incubation (Figure 41A). As reported above, at pH 6.4 a significant larger R848 loss were observed at 37 °C after 5 min incubation, with negligible further increase in leakage when incubation was prolonged to 1 h. The same was observed when TSL were loaded with two times the amount of R848 using the same condition (Figure 41B, D).
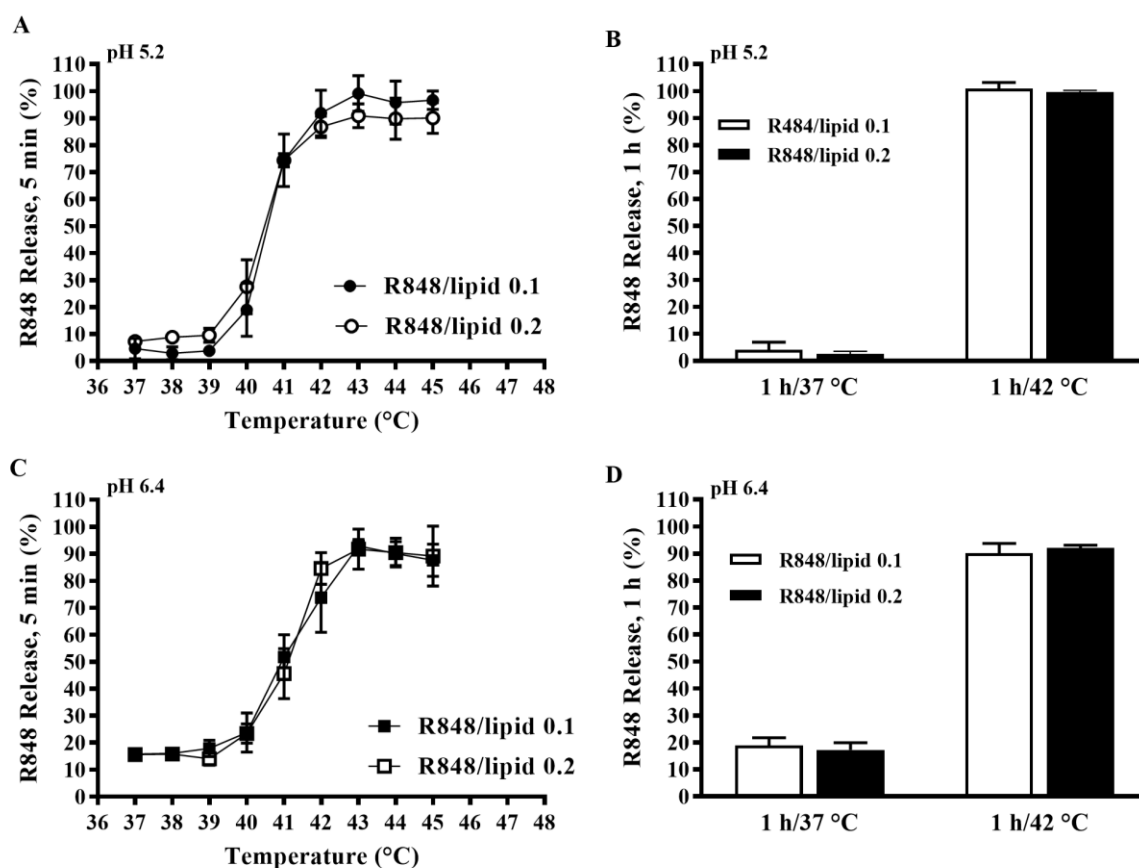
Figure 41 Temperature-dependent R848 release profile of DPPG$_2$-TSL-R848 loaded with different R848/lipid.
Temperature dependent release profile for 5 min incubation at 37-45 °C (A, C) and after 1 h at 37 °C & 42 °C (B, D). Values are presented as mean values ± SD of at least three independent batches.

These results suggested that fraction of R848 lost during incubation in FCS is not affected by the R848/lipid ratio in the range from 0.1 to 0.2 (mol:mol). Nevertheless, particles loaded with double the amount of R848 provided a higher final content formulated via TSL, with potential further benefit for TSL dosage in further *in vivo* studies.

4.2.2.5   R848 active loading optimization –Temperature & Time

In an attempt to ease loading procedures and to reduce lipid hydrolysis, a shorter time for R848 encapsulation loading was investigated. In this case, active loading via NH$_4^+$ gradient was tested at a higher temperature (37 °C) and time was reduced to 1 h. Additionally, the H$^+$ gradient remote loading was also tested in parallel experiments. In the latter case, TSL were hydrated with citrate solution (300 mM, pH 4), whereas the extra liposomal phase was adjusted to pH 6.4 via buffer exchange (PD-10 columns, HBS pH 6.4). Due to the different nature of the gradient, a differences in pH between intra- and extra-liposomal phase is required to drive API encapsulation [38]. Hence, R848 active loading via citrate was only tested with extra-liposomal pH 6.4. R848 active loading was performed at 37 °C for 1 h, both for AS- and citrate-based TSL, with initial R848/lipid of 0.2.

Table 16 DPPG$_2$-TSL formulation after R848 active loading at 37 °C/1 h.
Results are shown as mean values ± SD of at least three independent batches.

R848-TSL	Intra-vesicle medium	Extra-vesicle medium	Z-average (nm)	PDI	R848/lipid (mol:mol)	EE (%)	Lyso-lipid day 1 (%)	Fatty acid day 1 (%)
AS-pH 5.2	(NH$_4$)$_2$SO$_4$ pH 5.4	HBS pH 5.2	174 ± 1.6	0.07 ± 0.01	0.118 ± 0.014	59.6 ± 7.1	1.5 ±0.6	0.13 ± 0.05
AS-pH 6.4	(NH$_4$)$_2$SO$_4$ pH 5.4	HBS pH 6.4	176 ± 2.3	0.07 ± 0.02	0.155 ± 0.003	77.1 ± 2.1	0.6 ± 0.2	0.03 ± 0.01
Citrate	Citrate pH 4	HBS pH 6.4	176.1 ± 5.6	0.05 ± 0.02	0.113 ± 0.023	62.1± 6.5	3.2 ± 0.8	0.35 ± 0.04

AS = ammonium sulfate. Lyso-lipid (%) assessed via TLC method. Fatty acid (%) assessed via HPLC-CAD.

DLS analysis showed homogeneous size distribution (170-180 nm) and small PDI (<0.1) (Table 16). In case of AS-based TSL, a higher EE was observed for batches loaded at pH 6.4, when compared to extra-liposomal pH 5.2 condition. R848 remote loading was also monitored via fluorescence spectroscopy, assessing a fluorescence reduction of 45 and 55 % after 30 min of loading, respectively in case of pH 6.4 and 5.2 (Figure 42). No further decrease was assessed in terms of fluorescence reduction over time. When TSL were loaded with a R848/lipid ratio of 0.1, fluorescence intensity at time 0 resulted half of the one observed in case of 0.2 R848/lipid. In this case, R848 fluorescence at the end of the incubation was reduced not more than 10 to 20% of initial values.
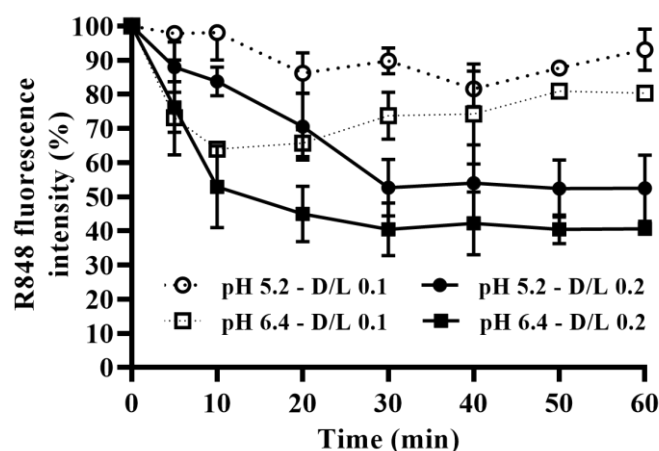

Figure 42 R848 fluorescence spectroscopy during remote loading.
Fluorescence spectroscopy was performed every 10 min for 60 min. Values are expressed as percentage of fluorescence intensity found at time 0. Values are presented as mean values ± SD of at least three independent batches.

R848 temperature-curves of batches loaded via citrate and AS at pH 5.2 showed minimal leakage at 37 °C for 5 min incubation (~10 %) whereas R848 burst release was observed at 41-42 °C, with complete depletion after 5 min. Also in this case, batches loaded at extra-vesicle pH = pKa (pH 6.4), showed a more significant membrane fraction with ~20 % R848 loss immediately upon FCS dilution and incubation at 37 °C for 5 min (Figure 43A). In good accordance with these findings, prolonging the incubation at 37 °C for 1 h did not show increased leakage for AS at pH 6.4 (~20 %),

whereas batches loaded with AS at pH 5.2 and citrate demonstrated a loss of ~15 % (Figure 43B). In all TSLs, full R848 depletion was assessed when particles were stressed for 1 h at 42 °C.
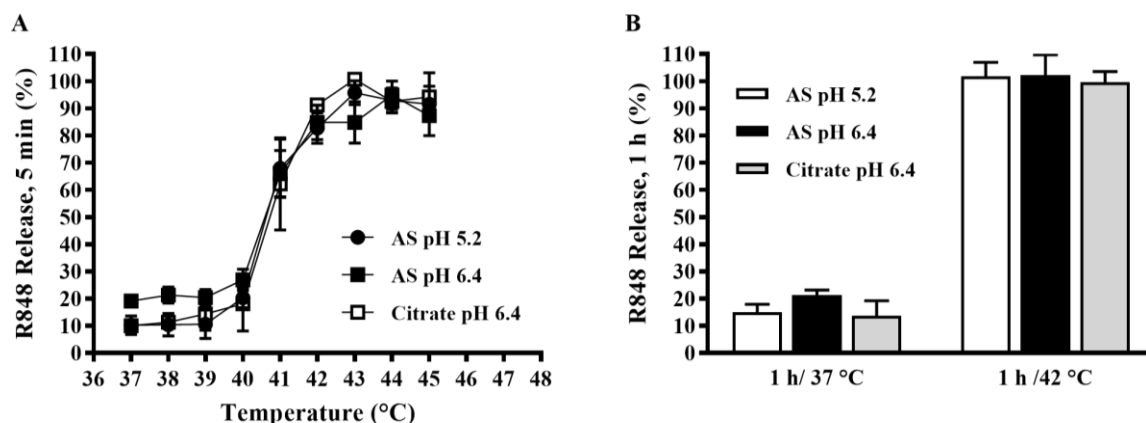

Figure 43 Temperature-dependent R848 release profile of DPPG$_2$-TSL-R848 loaded at 1 h 37 °C.
Temperature dependent release profile for 5 min incubation at 37-45 °C (A) and 1 h at 37 °C & 42 °C (B). Values are presented as mean values ± SD of at least three independent batches.

Citrate loaded TSL did not provide any improvements in terms of encapsulation efficiency or temperature curves, showing a TDR profile comparable to TSL loaded via AS at pH 5.2. Furthermore, the lower intra-liposomal pH induced a 2-fold higher lipid hydrolysis, when compared to AS TSLs (Table 16). Batches loaded with AS at pH 5.2 and 6.4 showed equal results to previously obtained TSLs with same excipients but loaded at 30 °C for 8 h. A direct comparison on temperature curves from these batches is shown in Figure 44. In case of TSLs loaded at pH 5.2, shorter loading at higher temperature affected R848 leakage at lower temperatures, with a loss of 10% (Figure 44A). Similarly rapid R848 release was observed at 41 °C, with peaks of R848 fractions observed at 42-43 °C (90-100 % release). Also for bathes loaded at pH 6.4, the higher incubation temperature during loading promoted a slightly higher R848 loss at lower temperatures (~20 %), whereas a higher R848 release was detected at 41 °C (65 %) in comparison to TSLs loaded at 30 °C for 8 h (45 %) (Figure 44B).
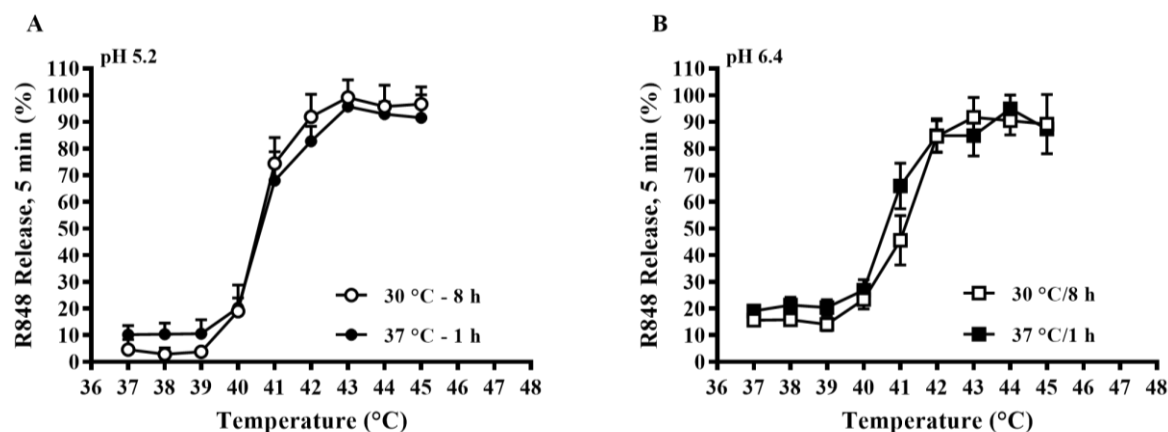

Figure 44 Focus on temperature-dependent R848 release profile of DPPG$_2$-TSL-R848 loaded with different condition.
Temperature dependent release profile for 5 min incubation at 37-45 °C for batches loaded with extra-liposomal pH 5.2 (A) and extra-liposomal pH 6.4 (B). Values are presented as mean values ± SD of at least three independent batches.

Overall, both loading strategies (30 °C/8 h vs. 37 °C/1 h) promoted similar loading efficiency with comparable final R848/lipid ratio (mol:mol). Lipid hydrolysis was also observed, but to a somewhat lower extent than for TSL incubated at 30 °C for 8 h. However, TSLs loaded at higher temperatures induced somewhat more leakage at lower temperatures than batches loaded at lower temperatures over a longer time span. Hence, further investigation *in vitro* and *in vivo* were performed with AS-based DPPG$_2$-TSL-R848 loaded at 30 °C for 8 h.

4.2.2.6 Release kinetics and effect of serum components

To further investigate R848 loss at low temperatures, TSL-R848 loaded either at pH 5.2 and 6.4 (AS, 30 °C/8 h) were tested in a temperature-dependent release assay both in FCS and HBS media. It was reported, that proteins are influential mediators of release of encapsulated compounds from TSL [108]. Hence, temperature-dependent release profiles of R848-loaded TSL were investigated both in FCS and HBS media, to assess potential differences in terms of R848 leakage and heat-triggered release. In addition, the temperature-dependent release profiles were combined with a time-dependent release assay. Batches were produced and release in FCS was measured to allow comparison of results obtained in HBS. The temperature-dependent R848 release profiles in FCS were comparable to the results shown in section 4.2.2.3 (Figure 45A). As expected, a significant lower R848 release rate was observed in buffer, with a peak fraction of 20 % and 40 % for batches loaded at pH 6.4 and 5.2 respectively (Figure 45C). Surprisingly, the 20 % loss of R848 usually observed in TSL loaded at pH 6.4 was not detected, with a R848 leakage of max 10 % at T °C < T$_m$. In time-dependent settings, 5 min incubation at 42 °C in FCS showed similar R848 release fractions to what was previously observed in temperature-depending settings (80-90 %, Figure 45B), with no further changes over time. In HBS, 5 min incubation showed minimal release of 10-30 % release, respectively for batches loaded at pH 5.2 and 6.4. Prolonged incubation at this target temperatures increase release over time, with batches loaded at pH 5.2 showing a faster release (Figure 45D). At 37 °C, both TSLs did not show significant leakage overtime, suggesting optimal liposomal stability in buffer condition.
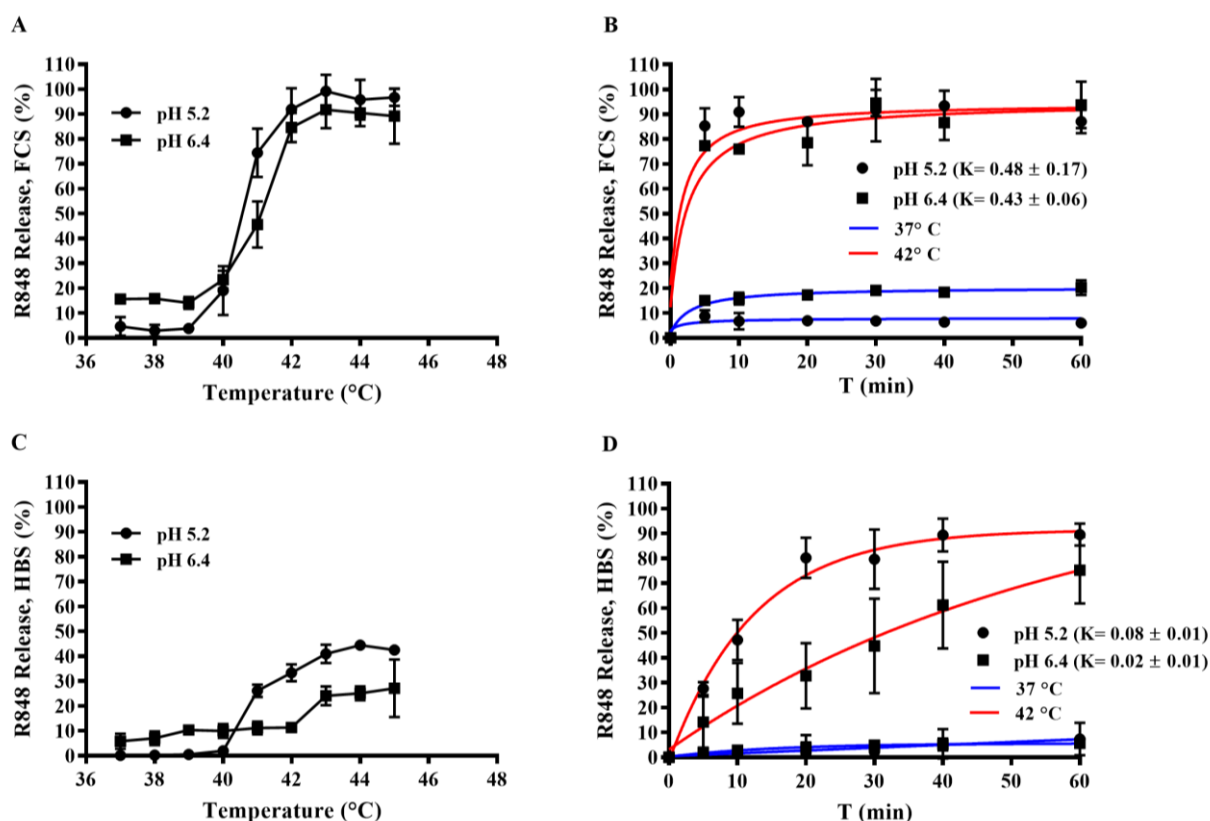
Figure 45 Temperature- and time-dependent release profile of actively loaded DPPG$_2$-TSL-R848.
All TSLs were loaded at 30 °C for 8 h, with R848/lipid ratio of 0.2. Temperature dependent release profile for 5 min incubation at 37-45 °C in FCS (A) and HBS (C). Time-dependent release of 1 h at 37 °C & 42 °C in FCS (B) and HBS (D). An exponential one-phase association curve was fitted through the 37 °C and 42 °C release sets. K constants calculated from the exponential fit at 42 °C for 1 h are shown in graph B & D (expressed as s^{-1}). Data are shown as mean value ± SD for three independent batches.

4.2.2.7 Stability in short-term storage study

DPPG$_2$-TSL-R848 liposomal stability and carrier integrity were tested in a short-term stability study. Since proceeding lipid hydrolysis was assessed within 30 days at 2-8 °C, liposome stability was investigated under frozen condition (-20 °C). Storage at 2-8 °C served as negative control. The study was conducted for 4 weeks. Cryoprotectants are usually added as excipients in liposome formulation undergoing freezing or lyophilisation [260]. Therefore, a buffer consisting of sucrose (300 mM) with HEPES adjusted to pH 7.4 (cryo-buffer) was used for frozen storage in the present study (refer to Table 17 for exact composition and osmolality measurements). TSL stored at 2-8 °C were tested in extra-liposomal buffer HBS pH 7.4 without sucrose to minimize risk of bacterial and or fungal growth due to the sugar content since preparation is done under non-sterile condition. All TSL were actively loaded with R848 (30 °C/8 h) using AS as excipient. After centrifugation, the liposomal pellet was resuspended in cryo-buffer or conventional HBS pH 7.4. DLS analysis showed good liposomal stability over the entire study period, with size between 160 and 175 nm and PDI < 0.1 for all samples (Figure 46A). Liposomes undergoing freezing-thawing (up to 2-cycles) showed comparable size and PDI with freshly formed vesicles (Figure 46A, B). In parallel, TSL were run through HPLC-CAD to assess fatty acid content. As is shown in Figure 46C, lipid integrity was

significantly affected by the loading condition and lipid hydrolysis increased over time, with TSL loaded at pH 6.4 showed ~4 % of fatty acids in lipid bilayer at 30 days of storage at 2-8 °C, whereas 2-fold higher content was assessed for TSL loaded at pH 5.2. In case of storage at -20 °C, the content of lipid decomposition products did not increase over time, with comparable fatty acids content to freshly formed vesicles, when assessed after 30 days storage being (Figure 46C). Leakage of R848 during freezing/thawing was assessed in 2 subsequent cycles. TSL containing cryoprotectant as excipients showed a negligible increase in non-liposomal R848 after 1 cycle when compared to non-frozen TSL, whereas a slight increase was observed after a second cycle (1.5-fold) (Figure 46D). TSL in HBS buffer showed a significant reduction in R848 retention, with 2.5- and 3.5-fold higher amount of non-liposomal R848 respectively after a first and a second cycle (Figure 46D).
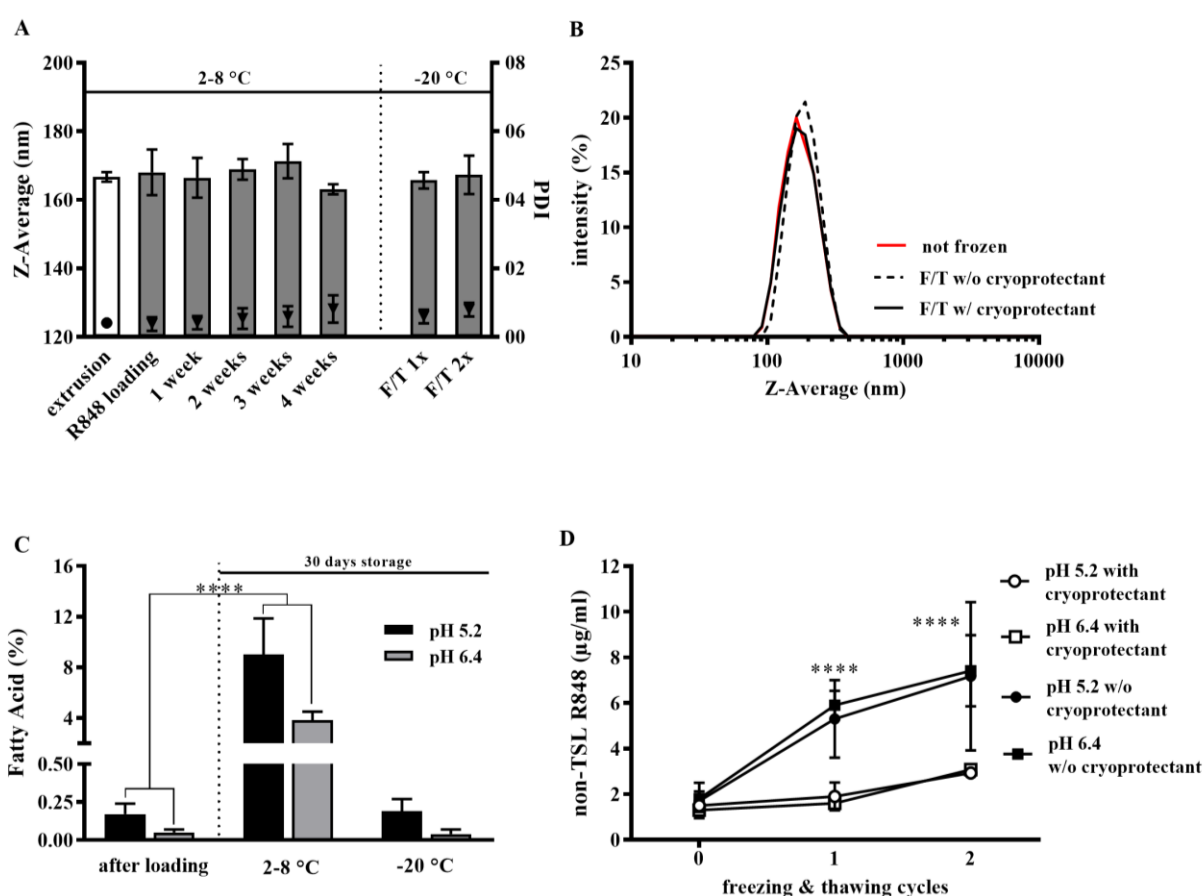
Figure 46 DPPG$_2$-TSL-R848 short-term storage stability study at 2-8 °C and frozen condition.
DLS analysis on (C)TSLs during storage at 2-8 °C for 30 days and after freezing/thawing (A). Representative size distribution via intensity profile of TSL before and after freezing/thawing w- and w/o cryoprotectants (B). Fatty acids content in lipid bilayer was assessed via HPLC-CAD after R848 loading and after 30 days storage at 2-8 °C or at -20 °C (C). Effect of excipients as cryoprotectant during freezing/thawing (D). In graphs A, C and D, data are shown as mean values ± SD of at least three independent batches. Data shown in graphs C and D were analyzed via one-way ANOVA followed by Bonferroni test and asterisks indicate significant difference between groups. **** = $p < 0.0001$, ** = $p < 0.01$.

Besides DLS and lipid degradation analysis, TSLs were tested in terms of R848 heat-triggered release. Temperature-dependent R848 release profiles of freshly formed vesicles were compared to profiles assessed after 30 days of storage at 2-8 °C or at -20 °C and showed a clear effect of the storage condition (Figure 47). When TSL loaded at pH 5.2 were stored for 30 days at 2-8 °C, the

release profile shifted 1 °C towards lower temperatures, with 70 % R848 release assessed already at 40 °C/5 min (Figure 47A). Also for batches loaded at pH 6.4, differences in R848 temperature-curves were observed, with a slight increase in R848 release fraction after 5 min at 41 °C (75% vs. 40%). These results are in accordance with lyso-lipid and fatty acid content assessed during stability study. On the other side, when particles were stored at -20 °C for 30 days, no significant differences were detected when compared to freshly-formed vesicles (Figure 47B).
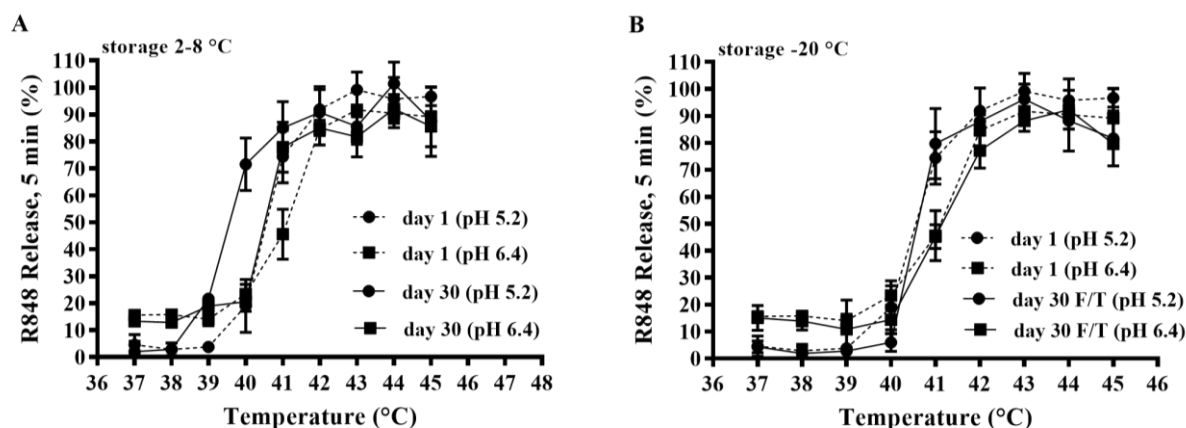
Figure 47 Temperature-dependent release profile of DPPG$_2$-TSL after storage.
Temperature dependent release profile for 5 min incubation at 37-45 °C for 2-8 °C stored TSL (A) and for -20 ° stored TSL (B). Values are presented as mean values ± SD of at least three independent batches.

4.2.2.8 Cryo-TEM, DSC analysis & osmolality

Several studies have already reported the possibility of observing crystal formation of the API in the liposomal aqueous environment after remote loading. For instance, DOX can be easily observed forming circular crystal in contact with inner liposome leaflet [261]. In this investigation, R848-loaded DPPG$_2$-TSL were investigated via cryo-TEM analysis to assess the formation of crystals. As shown in Figure 48A, freshly loaded TSL did not show any detectable differences to control TSLs. The latter were subjected to the same loading procedure and recovery method but without R848. There were no R848-sulfate crystals visible inside the TSL, independently from the loading conditions used (Figure 48A). To evaluate a potential effect of freezing and thawing on the morphology of the TSL, cryo-TEM was conducted again after a single cycle (Figure 48B). A higher number of MLVs were visible in all groups, potentially induced by the freezing/thawing procedure. However, the minimal formation of MLVs did not impact PDI and size distribution, as assessed previously, whereas temperature-curves showed comparable R8748 release profile to freshly prepared TSL that did not undergo freezing and thawing (refer to section 4.2.2.7).
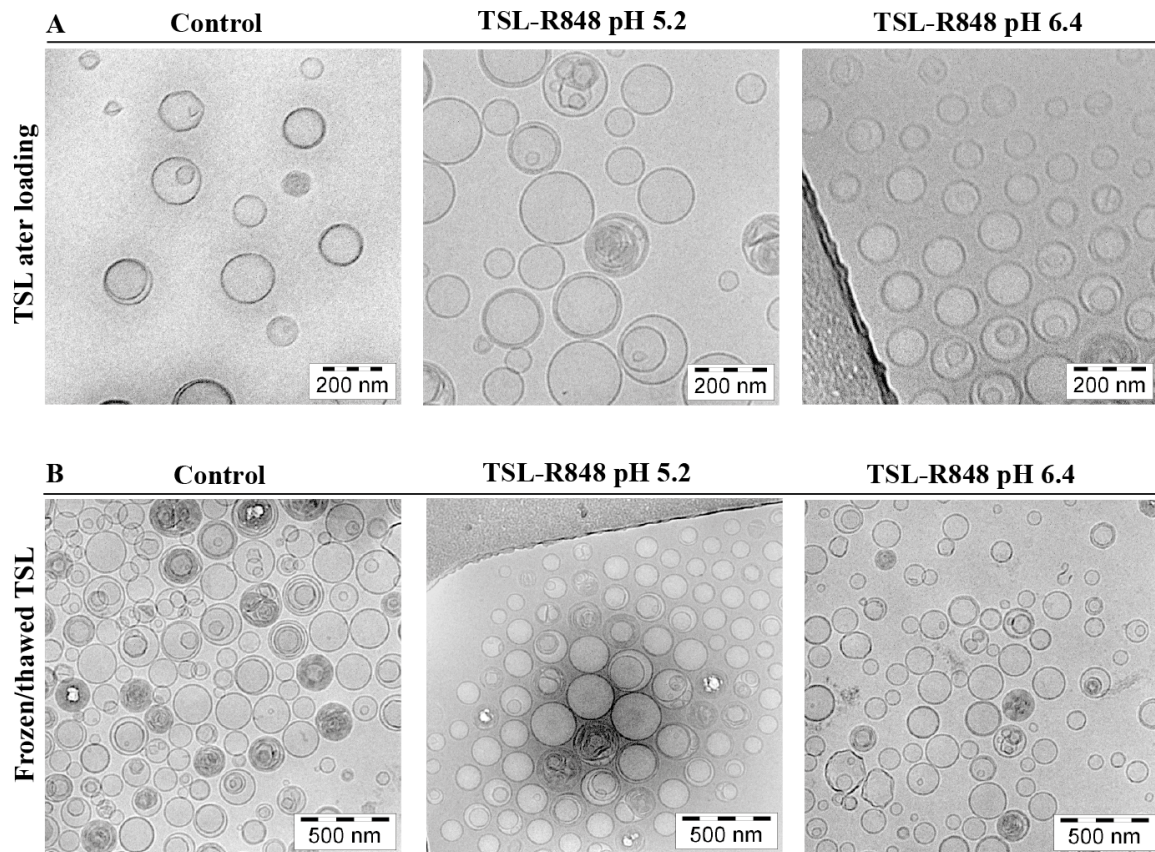
Figure 48 Cryo-TEM of DPPG₂-TSL-R848.
TSLs were imaged after R848 active loading (30 °C/8 h) conducted at extra-liposomal pH 5.2 or 6.4 (A). Control TSL were subjected to loading condition (30 °C/8 h) with extra-liposomal pH 5.2, without R848. DPPG2-TSL-R848 in cryo-buffer were subjected to one cycle freezing and thawing and imaged (B).

Additionally, T_m in freshly formed DPPG₂-TSL-R848 was assessed via DSC. Phase transition temperature was affected by loading condition, with batches loaded at pH 5.2 showing a $T_m = 42.1$ °C, while for TSL loaded at pH 6.4 T_m was 42.7 °C (Figure 49). These data are in good accordance with lyso-lipid generation assessed after loading. No differences were detected between loaded and unloaded TSL in shape of the DSC curves and T_m peak (Figure 49A, B).
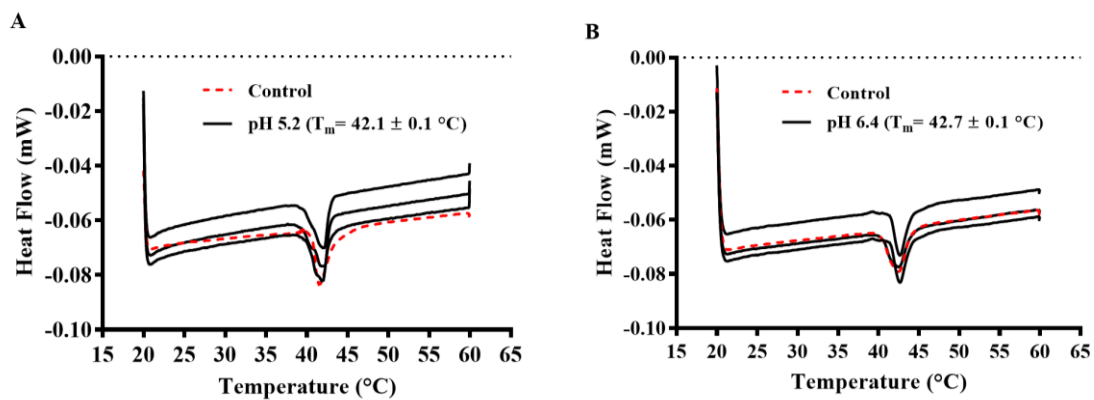
Figure 49 Curves of the heating phase from 20 °C to 60 °C of DPPG₂-TSL-R848.
TSLs were loaded for 37 °C/1 h or 30 °C/8 h, with extra-liposomal pH 5.2 (A) or 6.4 (B). DSC curves were plotted based on heat flux versus time with a heating rate of 1 °C/min. TSLs subjected to similar loading procedure but without R848 were used as controls. For each loading conditions, three different curves are shown corresponding to three independent batches. For controls, a representative curve is shown. T_m is shown as mean value ± SD of the three curves.

Osmolalities of non-formulated R848, DPPG$_2$-TSL and solutions used for active loading are shown in Table 17. No differences were detected in DPPG$_2$-TSL with different intra-liposomal excipients, whereas extra-liposomal buffer significantly affected formulation osmolality.

Table 17 Osmolality of R848-TSL formulation and solutions used for R848 loading.
Data are shown as data $\pm$ SD for at least three independent batches.

Liposomes/ solutions	composition (concentration mM)	Osmolalities (mmol/kg)
R848 (stock)	Ammonium acetate (40 mM); 5 % EtOH (v/v)	46 ± 4
Ammonium sulfate	$(NH_4)_2SO_4$ (300 mM)	633 ± 29
Ammonium phosphate	$(NH_4)_2HPO_4$ (300 mM)	587 ± 10
Citrate	citrate (300 mM)	612 ± 12
HBS pH 5.2	HEPES (20 mM); NaCl (150 mM)	317 ± 10
HBS pH 6.4	HEPES (80 mM); NaCl (120 mM)	313 ± 8
HBS pH 7.4	HEPES (20 mM); NaCl (150 mM)	309 ± 12
Cryo-buffer	Sucrose (300 mM); HEPES (40 mM); NaCl (60 mM)	508 ± 5
R848-TSL (in HBS pH 7.4)	/	312 ± 9
R848-TSL (in Cryo-buffer)	/	486 ± 8

4.2.3 *In vitro* immune-cell activation

4.2.3.1 Generation of PBMCs

All PBMC were generated via gradient separation (Figure 50A) from full blood, as described in detail in section 3.10.9. Purified PBMCs were analyzed via microscopy and FACS, showing a cell population mainly formed by lymphocytes and monocytes, with minor contamination of red blood cells (Figure 50B, C).
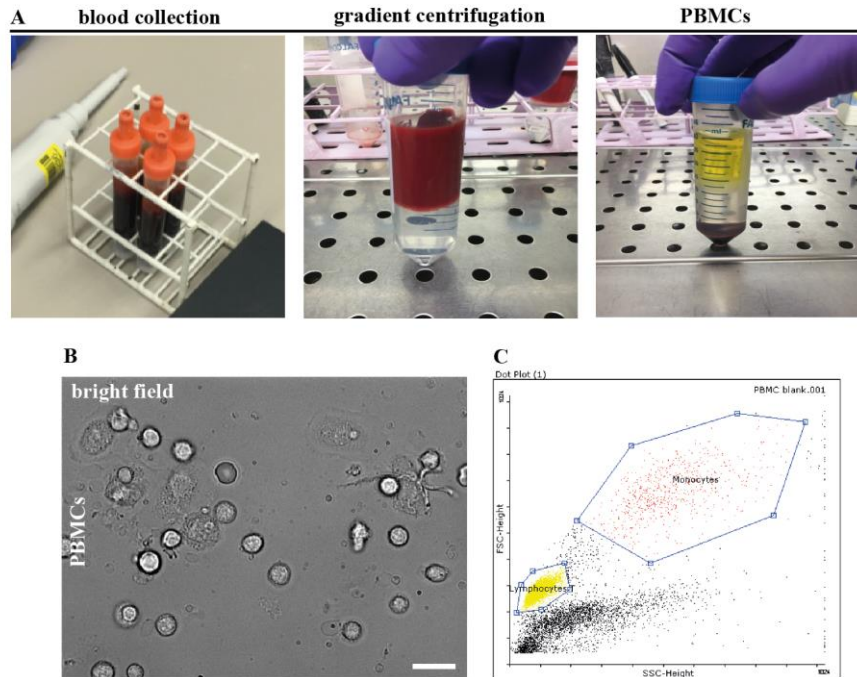

Figure 50 PBMC purification and qualitative analysis.
Fresh blood was collected from healthy donors and used immediately for gradient separation (A). Cells forming a white ring at interphase between plasma and gradient were collected, washed twice with PBS and counted. PBMC were seeded at 1×10^6 cells/ml in µ-slide chamber slides and microscopy performed via bright field analysis in live settings (B). Bar scale applied to image B is 20 µm. In parallel, PBMCs (1×10^6 cells/ml) in PBS were transferred in a FACS tube and analyzed via side and forward scattering. Representative dot plot graph showing distribution of PBMCs and gating used to identify lymphocytes and monocytes (C).

4.2.3.2 Effects of HT and R848 in PBMC cytokine production

PBMCs were incubated with different concentration of R848 in combination with NT or HT to assess potential synergistic effect in terms of PBMC activation and cytokine production. Cytokines production was assessed via ELISA for human IL-6 and TNF-α in the cell culture supernatant. Incubation with R848 significantly increased cytokine production in all tested concentration, when compared to controls (Figure 51A, B). In all cases, R848 induced higher TNF-α production when compared to IL-6 (~2-fold, similar in all tested concentrations). An increasing trend in cytokine production was observed when PBMCs were incubated with increased amount of R848 (1, 5 and 10 µM). However, higher R848 concentration (e.g., 50 µM) did not show further cytokine expression and even resulted in less IL-& and TNF-α detection, when compared to 10 µM samples. In both cases, HT application did not significantly increase cytokine production, both as single treatment (control HT) or in combination with R848 or LPS (Figure 51A, B). Effects on immune cell viability were

assessed via a prolonged stimulation of 168 h. Analysis were carried out via WST-1 assay in independent plates incubated for 24, 48, 72, 120, and 168 h. Group incubated with R848 showed a maximum of 2-fold higher cell viability at 72 h, when compared to control (Figure 51C). Surprisingly, a prolonged exposure (e.g., > 72 h) to R848 promoted a decrease in PBMCs cell viability, with values comparable to control at 120 h and even lower at 168 h (Figure 51C).
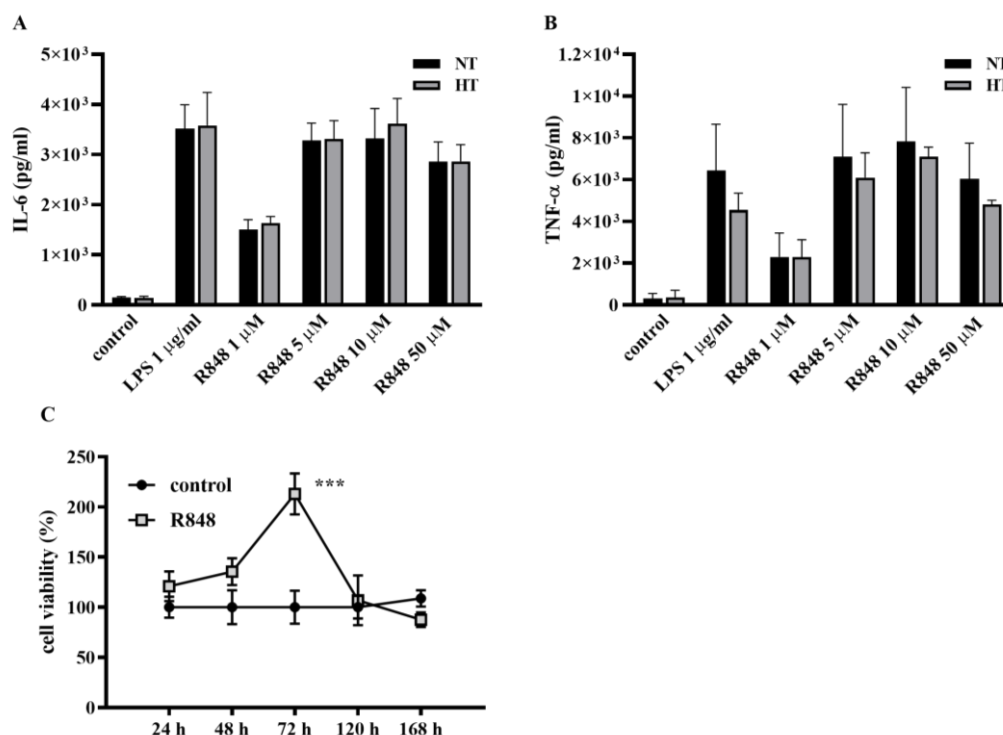

Figure 51 *In vitro* PBMCs activation via R848 stimulation and HT.
Cell culture supernatant was analyzed after 24 h incubation with R848. For NT and HT treatments, cells were placed on a water bath set at corresponding temperature (e.g., 37 °C & 41 °C). Next, plates were transferred back in the incubator for 23 h. ELISA was performed in samples not older than 24 h from the end of incubation time (storage at 2- 8 °C). LPS was always used as positive control, whereas RPMI medium was used as negative control. ELISA was used to assess production of IL-6 (A) and TNF-α (B). Cell viability of R848 stimulated PBMC was assessed in a 168 h investigation windows via WST-1 assay (C). Control groups were incubated with RPMI medium. Data are shown as mean values ± SD of at least three independent experiments. Statistical analysis in graph C was conducted via one-way ANOVA followed by Bonferroni test and asterisks show significant difference between groups. *** = $p<0.001$.

4.2.3.3 *In vitro* cytokine production via TSL-R848

PBMCs activation was tested in parallel experiments with naked-R848 and DPPG$_2$-TSL-R848. In both cases, 1 h HT or NT was applied, in order to heat-trigger R848 release from TSL for the former, and cytokines were detected after 24 h exposure via ELISA. PBMCs stimulated via naked-R848 showed similar results as previously observed, with 2-fold higher TNF-α production when compared to IL-6 (Figure 52). Significant detection of cytokines was assessed in the supernatants of PBMCs incubated with DPPG$_2$-TSL-R848 at NT, whereas a 2-fold increase was observed when HT was applied. Heat-triggered R848 release from DPPG$_2$-TSL in HT groups showed comparable results of naked-R848 in PBMC activation, with 1.5 fold higher TNF-α production in comparison to IL-6 (Figure 52B). Surprisingly, groups treated with DPPG$_2$-TSL-R848 resulted in higher cytokines values than for naked-R848, suggesting a higher potency when formulated in liposomal form. DPPG$_2$-TSL

without R848 (carrier) did not provide any immunogenicity to PBMCs, with cytokine levels comparable to controls (Figure 52).
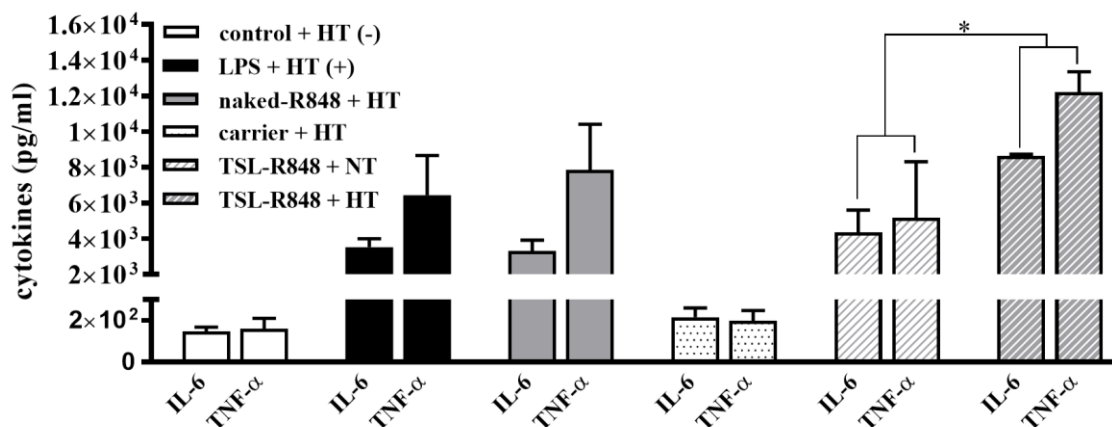

Figure 52 Cytokine assessment in R848-stimulated PBMCs via naked-R848 and DPPG₂-TSL-R848.
Cells were seeded at 1×10^6 cells/well in a 24-well plate. Cells were let rest 24 h, incubation was performed with LPS (1 µg/ml), naked-R848 (10 µM), DPPG₂-TSL-R848 (10 µM) and buffer loaded DPPG₂-TSL (carrier), whereas control received only RPMI medium. In all cases, plates were sealed and placed in a water bath set at 41 °C (HT). Next, cell suspension was centrifuged (10 min 450xg), supernatant was discarded and cells resuspended in fresh medium. Cell suspension was then placed in the same well. For TSL incubated cells, a DPPG₂-TSL-R848 formulation loaded at pH 5.2 (30 °C/8 h) was used, with R848/lipid ratio of 0.12 (mol:mol). In case of empty carrier, cells were incubated with the exact amount of lipid to have a 10 mM R848 incubation. Data are shown as mean values ± SD of at least three independent experiments. NT & HT groups treated with DPPG₂-TSL-R848 were compared to groups treated only with the carrier by one-way ANOVA and Bonferroni test and asterisk indicate significant difference between groups. * = p<0.05.

4.2.3.4 Co-culture method with human cancer cells and PBMCs

In vitro R848 cell toxicity study on cancer cells was performed using the BN175 sarcoma cell and human ovarian cancer cell line (SKOV-3). In both cases, incubation with R848 did not affect cell viability even at highest tested concentration (100 µM) (Figure 53A, B). HT treatment did not induce any further toxicity, neither for BN175 nor SKOV-3. To test immune cell mediated cell killing, SKOV-3 cells were co-cultured with PBMCs and an incubation with R848 was performed. In the latter case, a reduction in cancer cell viability was assessed in accordance to an increasing concentration of R848. Immuno-mediated cancer cell killing induced 40 % loss in cell viability when compared to control at 1 µM, with no further improvement at higher concentration (Figure 53C). Also in this settings, no differences were detected between HT and NT groups. In parallel experiments, R848 was administrated in liposomal form and HT and NT was applied as described above. R848 induced immune-mediated cell toxicity in a similar magnitude as naked-R848, with negligible differences driven by NT or HT application (Figure 53D). IC50 for all groups was around ~0.16 µM, with no significant differences observed between different treatments groups (Table 18). In case of SKOV-3/PBMCs co-culture without R848, no toxicity was observed and resulted cell viability was even higher than controls (SKOV-3 w/o PBMC), potentially due to the fraction of immune cell not washed away during staining (Figure 53E). A representative pictured of co-culture settings with labeled SKOV-3 and PBMCs is shown in (Figure 53F).
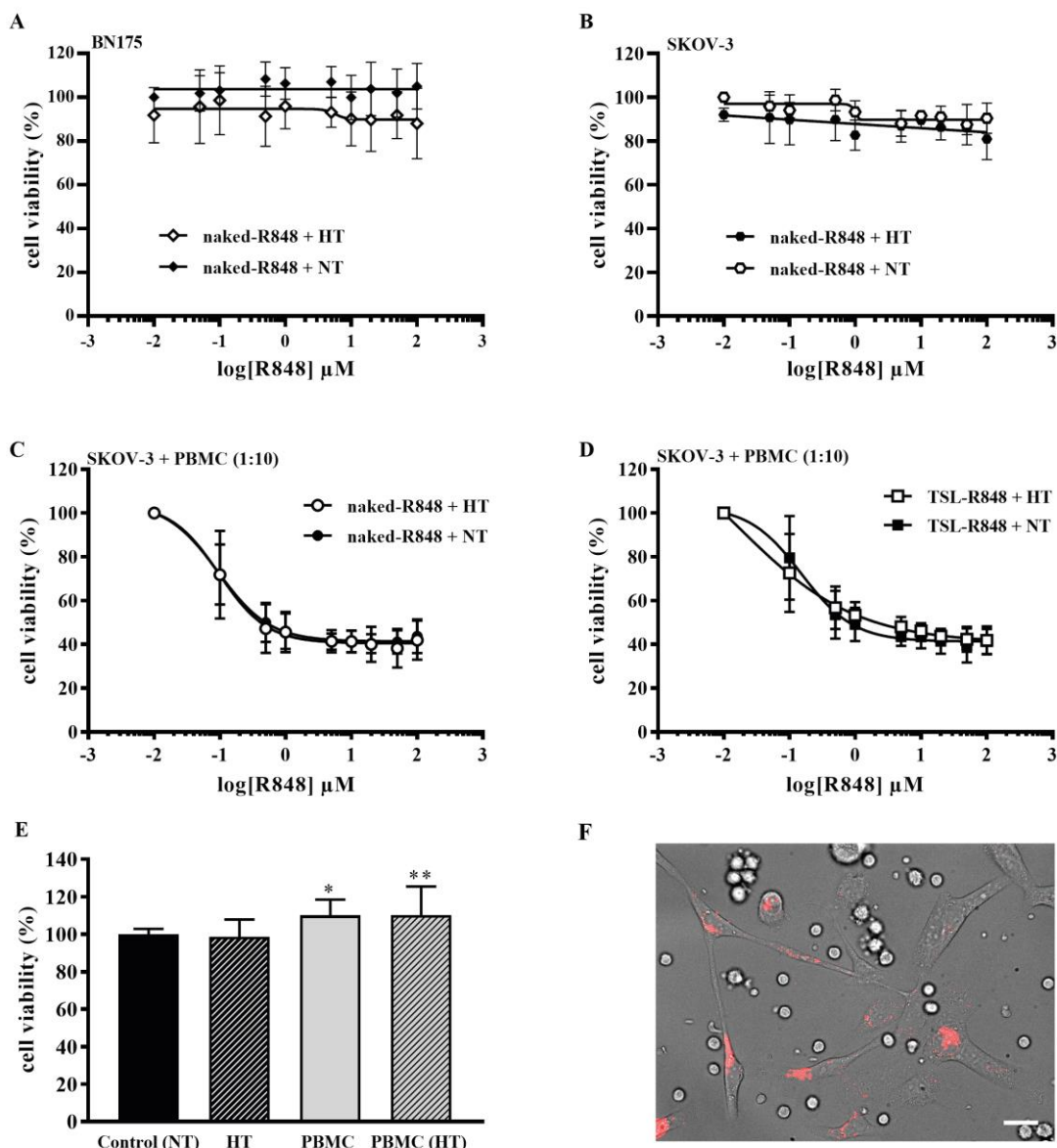
Figure 53 R848-induced toxicity to cancer cells in single culture or co-culture with immune cells.
Cancer cell lines BN175 (A) and SKOV-3 (B) were incubated with different concentrations of R848 (0.1 -100 µM). Plates were placed at 41 °C or 37 °C for 1 h, respectively for HT and NT treatments. Then, plates were transferred in the incubator and cell viability assessed after 71 h (A and B). Co-culture experiments were established at a SKOV-3/PBMC ratio of 1:10. Cells were exposed to different concentrations of R848 in either naked-form (C) or in liposomal form (D). Control groups and effect of HT on cancer cells with and without PBMCs (E). Representative picture of co-culture experiment with SKOV-3 and PBMCs (1:10) at day 1 (F). SKOV-3 cancer cells were labeled via Lysotracker Red 99. Scale bar applied to image F is 20 µM. In graphs A-D, values were fit by using a non-linear fit and data were analyzed via one-way ANOVA followed by Bonferroni test highlighting no significant differences between HT and NT treatments (IC50 of graphs C & D are shown in Table 18). Data shown in graph E were compared to control (NT) via one-way ANOVA followed by Bonferroni test and asterisks indicate significant difference between groups. * = $p < 0.05$. ** = $p < 0.01$.

Table 18 IC50 of immune-mediated cancer cell killing.
IC50 (values in µM) for HT (41 °C) and NT (37 °C) of cell-toxicity curves with co-culture settings showed in Figure 53 (C & D).

SKOV-3 + PBMCs (1:10)	naked-R848 + NT	naked-R848 + HT	TSL-R848 + NT	TSL-R848 + HT
R848 IC50 (µM)	0.15 ± 0.06	0.17 ± 0.12	0.16 ± 0.18	0.14 ± 0.21

IC50 HT/NT = inhibitory concentration of R848 killing 50 % of cells at HT or NT in co-culture setting.

4.2.3.5 Fluorescence microscopy

A significant interaction between cancer cells and DPPG₂-based liposomes was demonstrated by the uptake and particle localization in intracellular compartment (refer to section 4.1.3.5). Hence, the assessment of DPPG₂-TSL endocytosis during incubation time (1 h at 37 °C) should be evaluated further with a cell line used in the investigation. As shown in Figure 54, co-localization of liposomes and lyso-tracker was visible in case of SKOV-3 cancer cells and also for PBMC-derived monocytes.
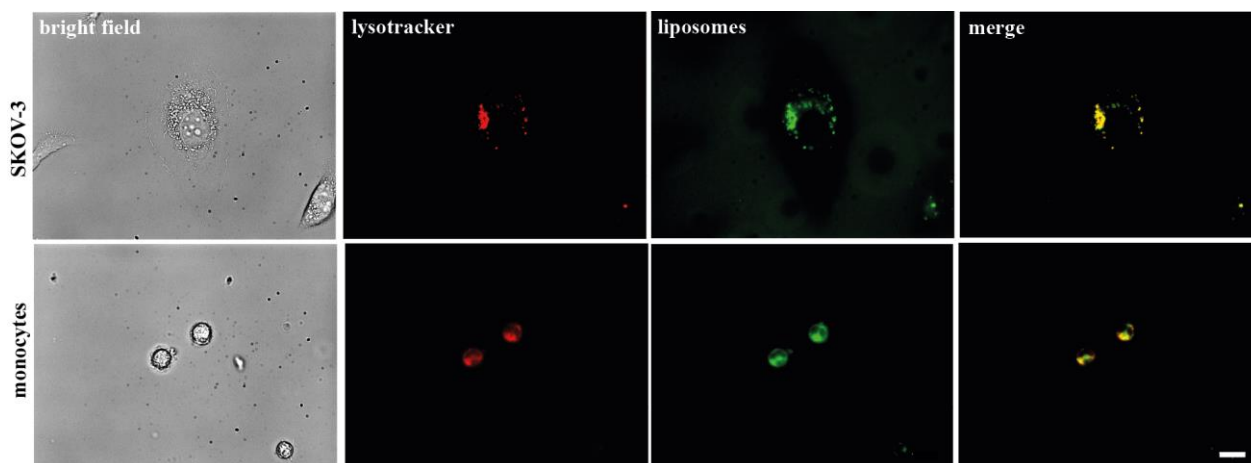
Figure 54 Live cell imaging on PBMCs and SKOV-3 incubated with DPPG₂-TSL.
PBMCs and SKOV-3 cells were seeded in chamber slides overnight and incubated with NBD-labeled DPPG₂-TSLs at 0.5 mM. Liposomes were let interact with cells for 1 h at 37 °C, after washing cells were imaged in live settings. Cells were imaged via bright field, NBD-liposome with GFP filter (green color), lysosomes with DsRed filter (Lysotracker RED, red color). Bar scale applied to all images is 20 µm.

Besides, investigation on the nature of immune-mediate cancer cell killing assessed in co-culture experiments was carried out. In presence of activated PBMCs, cancer cell killing was already reported to be mediated by cytotoxic T-cell (CTL), by induction of the caspase cascade in target cancer cells [262, 263]. The activation of caspases induces cancer cell apoptosis, followed by DNA fragmentation [264]. Immuno-fluorescence microscopy investigation on co-culture experiments assessed higher caspase-3 detection in R848-TSL incubated cells, when compared to controls (Figure 55). TUNEL staining for DNA fragmentation did not detect any significant differences, at the investigated time point (72 h).
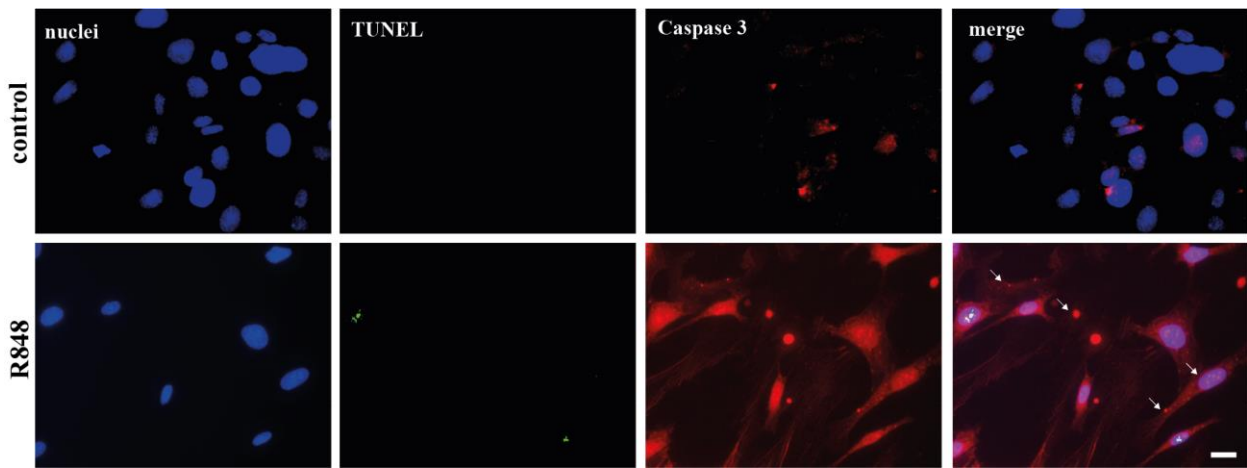
Figure 55 Immuno-fluorescence microscopy on fixed SKOV-3 cells in co-culture with PBMC (1:10).
SKOV-3 and PBMCs cells were seeded in chamber slides overnight and incubated with TSL-R848 (10 µM), whereas control groups received medium. HT treatment was performed via water bath for 1 h. At the end, slides were transfere din the incubator and fluorescence microscopy assesse after 71 h. DsRED filter was used to image Alexa Fluor 495 for Caspase-3, GFP filter for fluorescien of TUNEL staining and Dapi for Hoechst (nuclei). Bar scale applied to all images is 20 µm.

4.2.4 *In vivo* DPPG₂-TSL-R848

4.2.4.1 R848 pharmacokinetics

In order to assess whether encapsulation in DPPG₂-TSL enhance circulation property of R848, a PK study in Brown Norway rats was performed. DPPG₂-TSL loaded either at extra-liposomal pH 5.2 and 6.4 were both tested *in vivo*, to assess potential differences in PK driven by loading condition and R848/lipid ratio. Naked-R848 served as control.
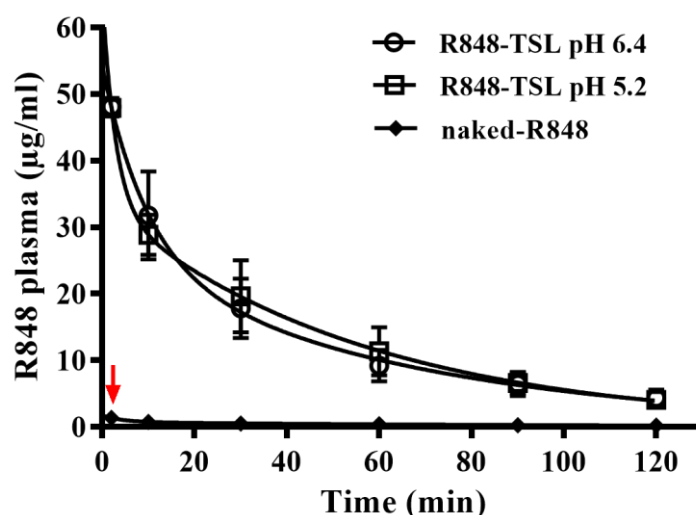
Figure 56 Pharmacokinetic profile of naked-R848 and DPPG₂-TSL-R848.
R848 plasma level after administration via DPPG₂-TSL loaded at pH 5.2 or 6.4, and as free drug. R848 as naked molecule was formulated in HBS pH 7.4 at 0.5 mg/ml concentration. Liposomal R848 was diluted at the same concentration by dilution in NaCl 0.9 %. Red arrow indicates 2 min plasma level after administration of naked-R848. R848 plasma concentration values from all TSLs tested were fit using two-phase exponential decay formula (Equation 4). Data are presented as mean value ± SD, every groups consisted in three animals (n=3).

Formulation of R848 into DPPG₂-TSL significantly improved circulation properties, with 35-fold higher C_{max} (2 min) when compared to naked-R848 (Figure 56, Table 19). Additionally, AUC_{2h} improved from 53.1 h*µg/ml in case of naked-R848 to ~1,600 h*µg/ml in case of DPPG₂-TSL-R848 (30-fold higher) (Table 19). Negligible differences were observed when comparing TSL with different loading conditions and R848/lipid ratio (mol:mol) (Figure 56, Table 19). In both cases, a certain loss of R848 was assessed after liposome administration, equal to ~20% of ID. Nevertheless, t_α was 34.2 ± 7.4 and 39.1 ± 4.25 min, respectively for TSL loaded at pH 5.2 and 6.4.

Table 19 PK parameters of R848 administrated as free drug and in liposomal form.

Formulation	R848/lipid (mol:mol)	t_α (min)	AUC_{2h} (h*µg/ml)	theoretical C_{max} (µg/ml)	C_{2min} (µg/ml)	C_{2h} (µg/ml)	Fit (R^2)
naked-R848	/	/	53.1	62.1	1.36 ± 0.1	0.2 ± 0.1	/
R848-TSL pH 5.2	0.11 ± 0.01	34.2 ± 7.4	1,592	62.1	48.1 ± 1.3	4.4 ± 1.3	0.9989
R848-TSL pH 6.4	0.14 ± 0.01	39.1 ± 4.25	1,627	62.1	47.9 ± 1.3	4.1 ± 0.7	0.9845

t_α = half life. AUC=Area under the curve. C = R848 plasma concentration.

Besides, cytokine (TNF-α and IL-6) induction in rat plasma was also assessed before administration of R848 formulations and at 120 min after i.v. administration. As shown in Figure 57, R848 increased plasma levels of TNF-α when assessed at 120 min, with significantly higher results administrated via DPPG$_2$-TSL liposomes. IL-6 induction was also assessed in the same way but no differences were detected when compared to controls (data not shown).
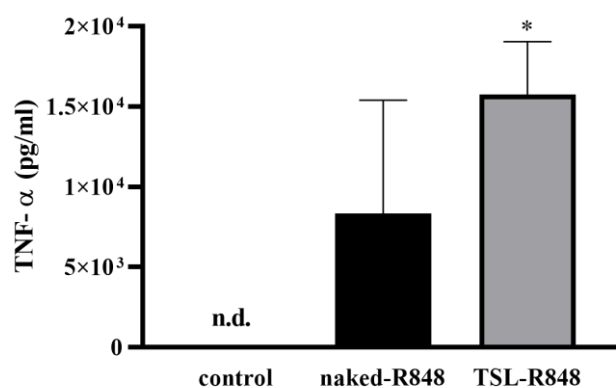
Figure 57 TNF-α in rat plasma after R848 administration.
Cytokines in rat plasma were assessed before R848 injection (control) and at 120 min after injection of naked-R848 and TSL-R848. Data are presented as mean value ± SD, every groups consisted in three animals (n=3). Data were compared via unpaired two-tailed T-test and asterisk indicates significant difference between groups. * = $p < 0.05$

4.2.4.2 Effect of plasma dilution on R848-encapsulation *in vitro*

PK investigation of DPPG$_2$-TSL-R848 unveiled a bi-phasic clearance which may suggest leakage of encapsulated R848 during TSL circulation. Additionally, a ~20 % of content loss was detected immediately after particle i.v. administration. To investigate weather larger dilution may affect payload stability, DPPG$_2$-TSL-R848 was diluted in FCS at two different final concentration and incubated at 37 °C to mimic physiological condition. TSL obtained from different loading procedures (30 °C/8 h vs. 37 °C/1 h) or excipients (AS vs. citrate) were tested to unveil potential differences due to loading conditions. In all groups diluted 1:12 (v/v), a significant R848 loss at RT was observed, with differences in relation extra-liposomal pH of loading conditions (~5 % vs. ~20 %, respectively for pH 5.2 vs. pH 6.4) (Figure 58). Incubation at 37 °C/ 5 min increased R848 leakage exclusively for batches loaded at pH 5.2, with 20% R848 loss, similar to initial loss found for TSL loaded at pH 6.4 for RT. In the latter case, no differences were detected between RT and 37 °C/5 min groups. Higher liposome dilution (1:30, v/v) showed similar R848 loss at RT, whereas incubation at 37 °C/5 min induced further leakage up 30-40 % of total content, depending to on loading conditions and excipients used (Figure 58). These data suggest potential instability of encapsulated compound as a function of dilution and temperature, explaining also the similar pattern observed for both DPPG$_2$-TSL-R848 loaded either at pH 5.2 or 6.4.
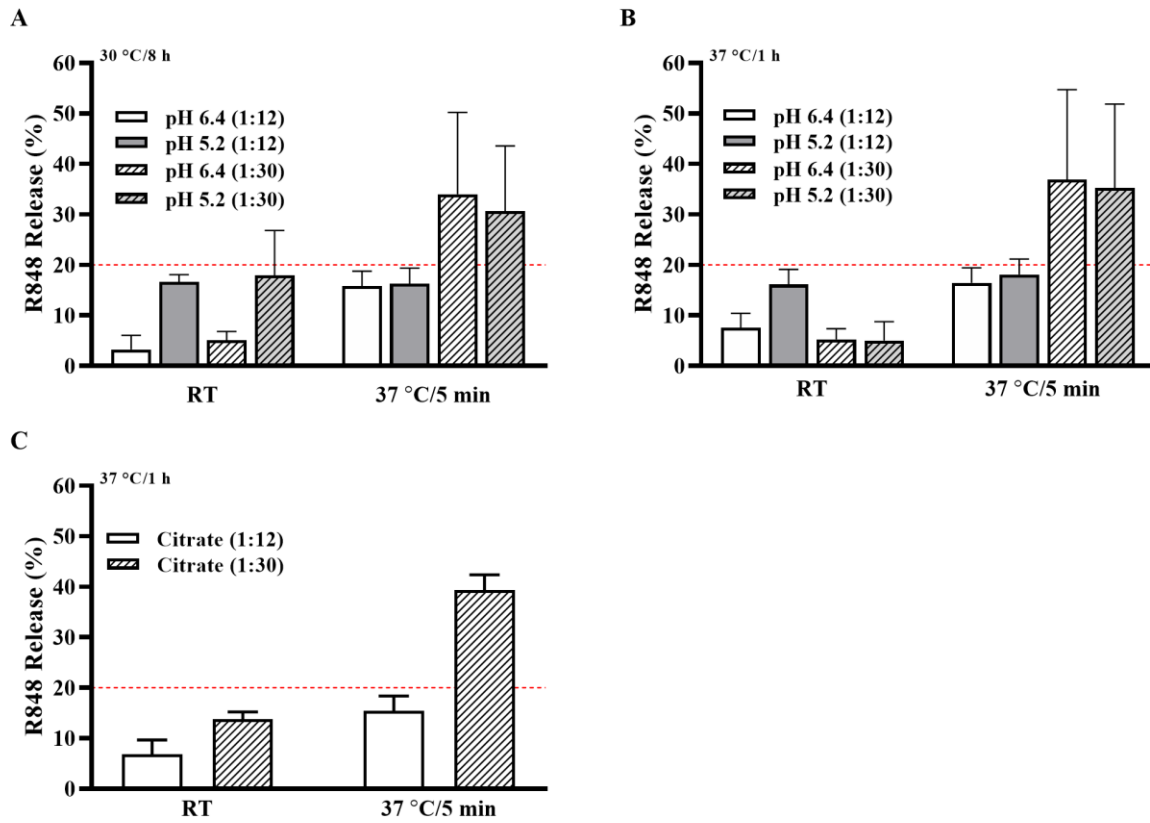
Figure 58 R848 *in vitro* leakage after dilution in FCS for different DPPG$_2$-TSL-R848.
DPPG$_2$-TSL-R848 via ammonium gradient was loaded at 30 °C/8 h (A) and 37 °C/1 h (B), whereas TSL loaded via proton gradient were loaded at 37 °C for 1 h (C). Percentages of R848 loss at RT and 37 °C/5 min were assessed calculating total content (100%, via Triton X-100) and assuming no R848 leakage as control (baseline = 0). Red dotted line in each graph highlight 20% of R848 release in the y-axis. Data are shown as mean value ± SD for three independent experimetns.

5 Discussion

5.1 Dual tumor targeting with cationic TSL

In the presented study, the potential of a novel cationic PG$_2$-based thermosensitive formulation in terms of targeted cell binding and DOX delivery efficiency was assessed. In order to evaluate advantages of DPPG$_2$ over DSPE-PEG$_{2000}$ in such context, PEG-based cationic TSL were used for comparison. The objective of the study was to investigate if dual targeting approach with cationic TSL is able to improve traditional TSL delivery. Different anionic and cationic TSL functionalized with either DPPG$_2$ or PEG were characterized after DOX-loading and extensively tested *in vitro* and *in vivo*. Superior formulations in terms of heat-triggered release function and *in vivo* targeted delivery were selected and investigated further in the second part of the thesis (refer to section 4.2).

5.1.1 *In vitro* characterization of cationic TSL

Liposome-cell interactions and fate of adsorbed liposomes (e.g., fusion, endocytosis) are mediated by different factors among which liposome charge, bilayer density, lipid components and cell morphology play an important role [160, 265]. Positively charged lipids consisting of trimethylammonium-propane (TAP) usually rearrange themselves in hexagonal structures, due to the small size of the head group in comparison to acyl chains [253]. The inclusion of PC lipids has been suggested to significantly stabilize a bilayer formed by such cationic lipids, with optimal interplay between TAP groups and zwitterionic PC observed at same molar fractions [266]. In our investigation, the TAP head group with C16 acyl chain (DPTAP) was found to have the best compatibility with a DPPC/DSPC/DPPG$_2$ bilayer, whereas the inclusion of DSTAP resulted in worst outcome in terms of particle size and PDI (Table 5 & Figure 12). The latter point might be caused by sub-optimal temperature used for liposome extrusion, suggesting DSTAP-containing liposomes require higher temperature (> 60 °C) in order to form stable vesicles. The latter point was not investigated in this study, since further increase in temperatures might result in phospholipids hydrolysis during manufacturing [259]. Similar outcome was previously suggested in a separate study where TAP-bearing lipids were screened in terms of transfection efficiency [253]. In this investigation, the inclusion of DPTAP and overall lipid composition was finely tuned in order to achieve an overall positive surface charge and efficient DOX heat triggered release (Figure 13). Both PG$_2$- and PEG-based CTSL contained the same amount of the cationic lipid DPTAP (7.5 mol %) and an anionic lipid (either 5 mol% of DSPE-PEG or DPPG$_2$) incorporated in the lipid bilayer, however the observed ζ-POT was significantly different (Table 7). PG$_2$-CTSL showed a clear and well

detectable positive surface charge, whereas PEG-CTSL ζ-POT was found positive only in non-saline containing buffer. Cationic TSL without $DPPG_2$ or $DSPE-PEG_{2000}$ displayed the highest ζ-POT in both conditions tested, so it is reasonable that anionic lipids, such as $DPPG_2$ and $DSPE-PEG_{2000}$, affect overall membrane charge by reducing it to a certain factor. However, the PEG-polymer covers the nanoparticles surface and reduces the positive charge to a larger extent than $DPPG_2$. The noteworthy PEG-shielding effect of particle surface charge was already reported in negatively-charged liposomes, confirming a significant reduction in liposomes electrophoretic mobility (5-fold loss) when compared to non-PEG containing particles [267]. However, the charge density of the liposomes has to be taken into account, as well as PEG molecular weight and conformation depending of PEG density (e.g., brush or mushrooms) [268]. Nevertheless, sterically stabilization in positively-charged particles significantly improved liposomal stability, whereas in PG- and bare-CTSL a small extra peak in size distribution became visible (Figure 15). However, during a storage stability study, a small extra peak was also visible in DOX-loaded PEG-CTSL. In accordance, a slight increase in PDI was assessed, suggesting potential aggregation happening at around 4 weeks of 2-8 °C storage (Figure 28).

Under the tested conditions, CTSL bearing cationic DPTAP tremendously increased binding and uptake in all tested cell lines, when compared to their anionic counterparts (Figure 18). In good accordance with ζ-POT measurements, PG_2-CTSL showed a 3-fold higher binding capability when compared to PEG-CTSL in both cancer cells and endothelial cells (Figure 22). The results match recent findings where the encapsulation of PEG in cationic liposomes has been described to decrease potential liposome-cell interactions and, thus, hamper delivery efficiency of encapsulated compounds [161-163, 269]. In these findings, anionic PG_2-based TSL unveiled a better cell-interaction and DOX delivery efficiency when compared to anionic PEG-TSL (Figure 23). This stands in accordance with the work of Miller et al, where the liposome-cell binding in HeLa cells significantly decreased 1.7-fold when 4.8 % of PEG was included in phosphatidylcholine liposomes [265]. Following nanoparticle injection into the blood stream, interaction with serum components takes place in relation to lipid components, charge and PEGylation. The protein corona formation unveils the biological identity of nanoparticles, which is expected to increase the complexity of the nanosystem regarding interactions with biological structures. As already proven, serum proteins might decrease targeting potential of antibody-connected liposomes [270]. Hence, an evaluation was necessary to determine whether the targeting achieved with cationic TSL, in particular with PG_2-CTSL, is retained when P-(C)TSLs are used. With the method used in this study, a reduction of targeting potential of around 60 % when using CTSL previously incubated with FCS, in comparison to non-protein CTSLs, was demonstrated (Figure 21). While the reduction was similar for PEG-CTSL and PG_2-CTSL, an overall 2-fold higher binding was retained for the latter when compared to PEG-CTSL (Figure 22).

Protein corona significantly affected surface charge of PG_2-CTSL, whereas no changes were detected in ζ-POT in case of protein adsorption on PEG-CTSL (Figure 19). In case of anionic formulations, protein adsorption also negatively affected liposome-cell interactions and no uptake was observed when PG_2-TSL[5] and PEG-TSL[70] where applied after incubation in FCS. The conservation of targeting potential for cationic particles was also reported recently for cholesterol-rich liposomes [271]. In this case, targeting of Onivyde® was compared to neutral and cationic liposomes after incubation in human serum, with the latter outperforming the other tested formulation in terms of cell binding for PANC-1 and INC-1 cancer cell lines. In another study, a similar result was observed when sterically stabilized PEGylated non-thermosensitive liposomes were incubated in human plasma and targeting in PC3 prostate cancer cell line was found reduced when compared to liposomes without proteins [159].

The higher binding assessed in cell targeting investigations was further analyzed in terms of potential higher DOX delivery efficiency with DOX-loaded nanoparticles. As already reported, a certain amount of the $DPPG_2$ is required not only to prolong circulation time but also to provide an ultra-fast drug release [106]. Indeed, in the investigation of temperature-dependent release profiles barely any release from DOX-loaded PG_2-TSL[5] was detected, whereas by increasing the $DPPG_2$ amount to 30 mol% a rapid DOX release was observed (Figure 16). The insertion of cationic DPTAP lipid in a DPPC/DSPC bilayer (CTSL) showed heat-triggered DOX release although with a significantly slower rate when compared to PG_2-TSL[30] (Figure 17). The co-presence of DPTAP and either $DSPE$-PEG_{2000} or $DPPG_2$ in PEG-CTSL and PG-CTSL respectively showed an improved DOX release profile when compare to bare CTSLs (Figure 16). T_m of DPTAP-bearing liposomes showed peculiar thermotropic behaviours with a long tow-phase solid-gel liquid-crystalline phase (Figure 14), which was already reported in simple DPTAP/DPPC liposomes in a separate study [272]. The similarity of T_m assessed for PG_2- and PEG-based CTSL was in accordance with comparable heat-triggered DOX release profiles, showing in both cases the highest release fraction at 43 °C/5 min (80% release). In a separate study, the DOX-loaded PEG-CTSL temperature-curve showed the highest fraction at 42 °C/5 min, with complete depletion assessed after 10 min in a kinetic study [254]. These data seem to be in contrast with our findings, however the CTSL tested in that study were characterized by a smaller size, thereby higher particle instability is to be expected due to increased surface tension resulting in faster release. [273].

In this investigation, the stability at 37 °C/1 h was also assessed in cell culture medium via fluorescence microscopy by imaging DOX after 1 h incubation at NT (1 h, 37 °C). At the end of the incubation time, DOX was not detectable since it was self-quenched inside liposomes being adsorbed either on cell surface or by endocytosis (Figure 24). By removal of unbound fractions and applying HT for 1 h, DOX was detectable in a punctate pattern forming red nanobursts in cytoplasmic vesicles

and to a certain extent also localized in nuclei. The distinct localization of DOX in intracellular vesicles was potentially due to a temporary entrapment in lysosome compartments, where acidic pH might induce DOX protonation, thus, slowing down further translocation into the nuclei. This is in good accordance with previous findings where HT-mediated intracellular drug release was tested in combination with PEG-CTSL in the human cancer cell line BLM [254]. Qualitative information via microscopic imaging was further confirmed by quantifying DOX by HPLC in parallel experiments. Among all formulations tested, the highest amount of recovered DOX was found in cells incubated with PG$_2$-CTSL, which is consistent with the previously described high binding rate observed during the targeting experiments (Figure 25). It has been reported that HT significantly increases chemotherapeutic efficacy in cancer cells *in vitro* or in pre-clinical settings [119, 274]. In the current investigation, HT could be witnessed as potential trigger mechanism for intracellular DOX release, but HT did neither affect DOX uptake nor cell toxicity (Figure 26). The latter point is likely due to the nature of the assay and comparable findings were reported when a similar experimental setting was used [109, 254]. The higher toxicity found for PG$_2$-CTSL is expected to be related exclusively to a higher amount of cell binding and, thus, to DOX delivery efficiency, since no cytotoxicity was observed when administrating empty liposomes at the same concentration (Table 11).

5.1.2 *In vivo* pharmacokinetic & biodistribution of (C)TSLs

As reported, positively charged nanoparticles bear the risk of a fast clearance due to opsonization and complement activation when administrated *in vivo* [275]. As demonstrated in this study, cationic TSLs had significantly different PK profiles when compared to their anionic counterparts (Figure 31). For instance, t_α of cationic PG$_2$-based TSL was drastically affected by the exposed positive charge on the lipid bilayer, with a fast drop of DOX circulation right after i.v. injection of around ~ 65 %. For PEG-CTSL, this effect was also observed but to a lesser extent, with an initial drop of only ~ 30 % ID. In both cases, a consistent reduction in AUC$_{2h}$ was assessed, equal to a 7- and 2-fold loss for PG$_2$-CTSL and PEG-CTSL, respectively, when compared to their anionic counterparts (Table 12). These findings suggest that 5 mol% DSPE-PEG$_{2000}$ did not shield 100 % of the overall surface charge, which is consistent with previous outcomes published by other groups with negatively-charged sterically stabilized liposomes [267]. Similar results in terms of particle clearance were found with cholesterol-rich cationic liposomes with or without PEG when injected in mice, in comparison to non-cationic counterparts [147, 148]. Correlation between poor PK profile and complement activation was confirmed via ELISA test. In this investigation, the lack of PEG in positive charged bilayer increased complement activation drastically, as reported in previously published studies (Figure 27) [276, 277]. Additionally, when assessing liposome-blood cell binding a higher fraction of granulocytes interacting with PG$_2$-CTSL and PEG-CTSL was observed. Similar

findings in terms of complement activation and immune-cell binding were observed in a recent investigation performed in our group (Lokerse et al, manuscript in preparation). Remarkably, in this study PG_2-based TSLs with 5 mol% of $DPPG_2$ showed significantly increased complement activation for C3a, Bb and SC5b-9 when compared to TSL with a higher $DPPG_2$ amount (10, 20 and 30 mol%). Since the amount of $DPPG_2$ in PG_2-CTSL is indeed 5 mol%, it is reasonable to assume that other factors besides positive charge are playing a crucial role in complement activation and, thus, particle safety.

In accordance to the specific PK profiles acquired, differences in the BD of DOX within the organs were assessed. In all tested formulations, whenever liposomal DOX was administrated in combination with regional HT, a significantly higher amount of DOX was recovered in heated tumors, in comparison to the non-heated ones (Figure 33). In case of PG_2-TSL, the blood stability encountered in the first hour after i.v. administration and the rapid DOX-release observed *in vitro* greatly matched the highest DOX-tumor enrichment assessed *in vivo* (14-fold, HT vs. NT tumors). For anionic PEG-TSL, a more modest improvement in tumor DOX-enrichment was observed, when compared to NT tumors (4-fold). Surprisingly, although PEG-CTSL showed a significantly lower AUC_{2h}, minimal differences in terms of tumor DOX-enrichment were detected when compared to the anionic counterpart. This can be explained by the higher DOX release rate observed *in vitro* for PEG-CTSL in comparison to PEG-TSL, which was hypothesized to compensate for the partial payload loss after i.v. injection. In case of a positive-charge well detectable on the surface as in PG_2-CTSLs, higher clearance of particles affected the outcome of the BD, including a poor DOX-tumor enrichment. These data are in good accordance with previous findings from other groups, where cationic nanoparticles were faster cleared *in vivo* than neutral or anionic particles with consistent differences in terms of tumor-drug enrichment found in tumors [148, 278]. Surprisingly, in these studies, although PK and BD showed suboptimal outcomes, a therapeutic effect was still preserved when tested in tumor-bearing mice, suggesting that a minimal binding of cationic nanoparticles may inhibit tumor angiogenesis. In this investigation, a partitioning analysis of tumor vasculature was not performed. Hence, no discrimination between the liposomal DOX-bound fraction and the released DOX could be made, which might though be an interesting parameter to be evaluated in future studies. Furthermore, BD assessment over a longer time span might be an additional point to consider. Nevertheless, several studies dealing with cationic liposomes for vascular targeting suggested that the main interactions with tumor vasculature are happening within the first 1 h after nanoparticles injection, with no further improvement over time [142, 147]. In a study reported elsewhere, PEG-based CTSL targeting was assessed after 24 h, with negligible improvements in terms of DOX accumulation and therapeutic effect when compared to TSL [279].

5.1.3 Outlook

These findings suggest that the HT-external targeting is the main mechanism for anionic and cationic TSL to induce DOX accumulation in tumors, with negligible synergistic effects due to targeting from positive charge, at least for the 1 h evaluation window as it was used in the study. Overall, PG$_2$-CTSL showed interesting and promising results *in vitro*, whereas the *in vivo* readout was sub-optimal due to complement activation and poor circulation time. While grafting PEG on cationic TSLs might improve safety and circulation properties, a decrease in liposome-cell targeting and drug delivery efficiency was assessed. Potential improvement might be achieved by increasing DOX dosage of *in vivo* application, with related higher liposomes administration and potential benefit to AUC and tumor targeting. Alternatively, different routes of administration might result in drastic benefit in exploiting advantages of PG$_2$-CTSL. For instance, intratumoral injection of cationic nanoparticles has been recently investigated in a different set-up and promising results were achieved when compared to direct APIs intratumoral administration, especially for large and/or highly hydrophilic molecules subjected to fast wash-out [280, 281]. It looks conceivable to further investigate the full potential of PG$_2$-CTSL in combination with regional HT in the latter condition and thus avoiding limitations observed after systemic administration. Remarkably, anionic DPPG$_2$-TSL significantly outperformed PEG-based TSL in terms of solid tumor targeting, although the latter showed a more stable and prolonged circulation time *in vivo*.

5.2 Immuno-cancer therapy

The current study aims to investigate the feasibility of loading of IAV (R848) in TSL intended for heat-triggered local drug delivery. Among all formulations tested in the previous section (4.1), anionic DPPG$_2$-TSL showed a superior temperature-profile with a sharp change in DOX release kinetics within 1-2 °C and optimal stability *in vitro*. Accordingly, advantages in PK and BD were observed when tested *in vivo*, whereas no synergistic effects were visible in a dual targeting approach (section 4.1). Due to their unique properties, DPPG$_2$-based TSL were chosen for this approach and tested in the next section for R848 delivery. Different loading conditions were screened in terms of encapsulation efficacy and heat-triggered release. *In vitro* activation of human PBMCs was assessed with either naked-R848 or DPPG$_2$-TSL-R848. Immune-mediated cancer cell killing was evaluated in co-culture experiments via cell viability assay and immunofluorescence. *In vivo* PK studies were performed to exhibit advantages of R848 formulated via DPPG$_2$-TSL in comparison to non-liposomal R848.

5.2.1 R848 thermosensitive liposomes

R848 is an imidazoquinoline which shows high affinity for TLR-7,8, with a 40-fold higher potency than R837 [282]. While the latter is already approved for topical treatment of actinic keratosis, BCC cancer and genital warts, R848 did not yet receive FDA-approval, despite the higher potency assessed. Potential reasons were the higher toxicity and irAEs observed in patients treated with R848, when administrated either topically or systemically. Nevertheless, different physicochemical characteristics of R848, as a slightly improved water solubility (R848 logP = 1.5; R837 logP = 2.6, at pH 7, 25 °C) and the presence of an amine group with a pKa of 6.4 would make the compound a potential candidate for liposome encapsulation [283, 284].

In a first R848 encapsulation experiment via passive loading, a DPPG$_2$-TSL lipid film was hydrated with 1 mg/ml stock solution in ammonium acetate buffer at pH 5.2. This resulted in an EE of ~15 % (Table 13), which is slightly higher as compared to other passively loaded drugs, such as CF, dexamethasone phosphate and dFdC (5-10 %) [106, 256, 285]. Due to the logP of the molecule, it is conceivable to expect fractions of R848 being entrapped in the lipid bilayer, causing a further increase in EE when compared to more hydrophilic compounds. This was also confirmed by analyzing R848 retention in FCS, unveiling amounts of drug leaking out when TSL were incubated at 37 °C (5 min) with a slight increase at 42 °C due to heat-triggered release (Figure 36). These data suggested a high affinity of R848 to the lipophilic bilayer phase, although at pH 5.2 R848 mostly exists in its protonated form. Furthermore, the R848 absolute content formulated in DPPG$_2$-TSL via passive loading was suboptimal for a further *in vivo* application.

Remote loading is one of the best approaches to achieve a high yield of API concentration per liposome particle, which is a requirement to ensure effective liposomal chemotherapy. Different amphipathic APIs (e.g., DOX, CPT-11), currently approved in the clinic also as liposomal formulation, are loaded via active loading with a stable and almost complete encapsulation [245, 286]. A rational approach for drug remote loading must take into consideration several parameters, such us type of medium (electrolytic, non-electrolytic), intra- and extra-liposomal pH, gradient ion (NH_4^+, H^+) and concentrations, temperature, time, drug/lipid ratio, and gradient magnitude [38]. When developing a new liposomal formulation, each of those factors should be steered accordingly in order to find optimal loading conditions. In case of TSL, the latter usually requires a balance between stability (both of drug & carrier) and efficiency for heat-triggered release. Remote encapsulation of R848 in cholesterol-rich liposomes was already reported in a recent published study [258]. In this investigation, vesicles formed either via electrospray or lipid film/extrusion method were actively loaded with R848 via an ammonium gradient. However, the reported method consisted of a 4-day loading time at 30 °C, assessing a maximum of 44 % EE, independently from the liposome preparation method. In this investigation, active loading of R848 in $DPPG_2$-TSL was performed in similar settings, and promoted an EE of ~60 %, assessed after 8 h of loading with an extra-liposomal pH 5.2 (Table 15). *In vitro*, these TSL not only showed a stable encapsulation of R848, but also a rapid release upon HT condition with complete depletion at 41-42 °C after 5 min (Figure 38). Nevertheless, significant amounts of lipid-degradation products were assessed in freshly loaded $DPPG_2$-TSL-R848, with a further increase over storage at 2-8 °C. This stands in correlation with the previous suggestion that the optimal pH for phospholipids storage should not be lower than pH 6.5 [259]. Lyso-lipid and fatty acid content assessed in $DPPG_2$-TSL might derive in large amount from $DPPG_2$, as the hydrolysis of the latter phospholipid was observed to occur faster than for other PCs, such as DPPC & DSPC [287]. By increasing extra-liposomal pH to 6.4 during active loading, R848 EE increased up to ~80 % (Table 15). Additionally, due to the higher pH a benefit in terms of lipid degradation was witnessed. Intra- and extra-liposomal pH differences higher than a factor of 2 have already been described to ease loading conditions [38]. Similar conditions were found beneficial also for the active loading of other weak bases, such as DOX (refer to section 4.1.1.3) and CPT-11 [256].

Temperature-dependent release profiles of R848 from $DPPG_2$-TSL were affected by loading conditions, with batches loaded at pH 6.4 showing a higher leakage at lower temperatures than TSL loaded at pH 5.2 (~15 % vs. ~5 %, respectively) (Figure 38). This was initially supposed to be caused by a different protonation rate of R848 present in the extra-liposomal phase. At pH 6.4, 50 % of R848 is in the deprotonated form, giving a larger chance to interact with the lipid membrane than in case of extra-liposomal pH 5.2. Lipophilic compounds interfere with the liposomal membrane, and their fast diffusion in the extra-liposomal phase upon dilution in FCS or HBS was already extensively

reported in a separate investigation [285]. Nevertheless, in the current study, both R848-loaded TSLs (AS-pH 5.2 & AS-pH 6.4) showed heat-triggered release profiles with a sharp change in R848 release kinetics within 1-2 °C. Recently, a different ammonium gradient with phosphate salts (AP) was established for active loading of weak bases, showing comparable EE to AS gradient in case of DOX [288]. The same gradient was tested for R848 active loading, showing a similar outcome in terms of loading efficiency and improving lipid integrity (Table 15). However, sub-optimal R848 retention was assessed at NT treatments with AP-based TSL, with higher R848 leakage when compared to AS-based $DPPG_2$-TSL (Figure 38). The latter point might be explained by poor solubility of R848 assessed at pH 7.4 (data not shown), with potential formation of intra-liposomal precipitates affecting payload retention.

The energy factor during loading procedure is another parameter which was taken into consideration while screening optimal conditions for active encapsulation. Several drugs are usually actively loaded in TSL at temperatures between 36 °C to 37 °C, whereas higher temperature are used for non-TSL vesicles [38], which are however not applicable for $DPPG_2$-TSL due to a collapse of the pH gradient [273, 289]. Loading in $DPPG_2$-TSL for 1 h at 37 °C resulted in similar EE and lipid degradation products, when compared to prolonged loading phase of 8 h at 30 °C (Table 16). Higher temperatures used during loading procedures showed a higher R848 partitioning at membrane level (Figure 43 & Figure 44). Proton gradient loading with citrate-based TSL was also tested in parallel experiments, highlighting no advantages in terms of EE and R848 heat-triggered release profile (Figure 43). Furthermore, the lower intra-liposomal pH corresponded to a higher lipid hydrolysis when compared to AS-based TSL, with a potential destabilizing effect of the liposomal system (Table 16). Payload retention in DOX-loaded PEG-TSL with different intra-liposomal excipients was investigated in a recently published study, showing higher particle instability *in vitro* for citrate-based TSL when compared to AS-TSL [104]. Due to the above findings, loading conditions via NH_4^+ gradient at 30 °C for 8 h was used for further experiments, while both extra-liposomal pH 5.2 and 6.4 were kept in the investigation to highlight potential differences driven by the R848/lipid ratio and amount of membrane fractions.

It is expected that the percentage of membrane fraction assessed during loading is related to overall drug/lipid ratio. Therefore, TSL were loaded with an initial R848/lipid ratio of 0.1 and 0.2 (mol:mol), to investigate differences in the R848 membrane-fraction. Surprisingly, all the TSLs showed similar retention at 37-39 °C (5 to 15 %, in relation to pH used for loading), with a rapid heat-triggered R848 release at 41-42 °C (Figure 41). A similar EE was assessed for all loaded TSL, independently from the used R848/lipid ratio. Nevertheless, in batches loaded with twice the amount of R848, a consequent doubling of R848 liposomal content was observed (Figure 39). These findings suggested that other mechanisms were responsible for R848 loss upon dilution in FCS, with negligible

effect driven by drug/lipid ratios, when tested at 0.1 and 0.2 (mol:mol). In temperature-and time-dependent release assays in HBS, the observed R848 leakage at NT was not detected, assuming a crucial role of serum proteins in destabilizing liposome bilayer and promoting partial content loss (Figure 45). Protein corona adsorption on liposomal bilayer has been described to affect biological identity of particles, especially in case of positive charged ones (refer to section 4.1.3.2). Serum proteins are also responsible for inducing structural defects in the liposome membrane, promoting drug diffusion at T °C > T_m condition [108]. These hypothetical mechanisms are associated to protein penetration in membranes at liquid-disordered state, proteins-induced lipid immobilization, and generation of vacancies in the membrane bilayer due to proteins dissociation [108]. Proteins and cholesterol-rich MLVs were proven to extract lipophilic drugs encapsulated in the $DPPG_2$-TSL membrane bilayer at solid-gel state (T < Tm) [285]. A similar extraction is expected to happen for the membrane-bound fraction of R848, with serum proteins acting as binding partners and promoting R848 extraction. This is supported by the observation of R848 complexation in serum proteins when recovered after filter centrifugation in presence of FCS (Figure 35B).

During a storage stability study at 2-8 °C for 4 weeks no differences in terms of size and PDI of liposomal-R848 were observed (Figure 46A, B). Nevertheless, shortcomings of the aforementioned loading procedure were represented by a consistent lipid hydrolysis assessed over time (Figure 46C). Therefore, particles were stored at frozen conditions and thawed for assessment of size, PDI, shape (e.g., cryoTEM) and content leakage. It has been reported in the literature that freezing/thawing may affect drug retention and thus induce leakage from liposomes [290]. During freezing, water crystals might harm lipid bilayer and thus promote leakage of encapsulated compounds. Furthermore, SUV liposome disruption during freezing may cause subsequent rearrangement in MLV structures, with potential effect on particle stability and heat-triggered release function [291]. The absence of electrolytes in the extra-liposomal phase and the presence of a specific concentration of disaccharides (e.g., sucrose, trehalose) have also been described to improve drug retention [292]. These compounds, usually referred to as cryoprotectants, preserve vesicles undergoing freezing due to vitrification effect [292, 293]. Therefore, in the current study, a cryo-buffer consisting of 300 mM sucrose in HEPES pH 7.4 was tested in comparison to conventional HBS in freezing/thawing of liposomes. A significantly higher leakage rate was assessed in frozen/thawed TSL when not formulated in cryo-buffer (4-fold, Figure 46D). The presence of these excipients significantly increased osmolality of TSL (Table 17) in comparison to TSL in simple HBS. However, frozen/thawed particles formulated with sucrose showed similar temperature-curves when compared to freshly formed vesicle in HBS buffer (Figure 47B), suggesting no destabilizing effect driven by osmotic stress. The storage at frozen conditions (-20 °C) was successful in avoiding further generation of lyso-lipids and fatty acids during a 30 days stability study, significantly improving

liposome integrity when compared to TSL stored at 2-8 °C (Figure 46). In the latter case, a significant lipid hydrolysis was assessed, with steady generation of lyso-lipids and fatty acids over time (Figure 46). The presence of lyso-lipids in a lipid bilayer has been extensively reported to decrease the liposomal T_m, and thus shifting the release towards lower temperatures [294]. In accordance, temperature-dependent release profiles of TSL stored at 2-8 °C for 30 days showed a higher instability in R848 retention, with release profiles shifted of 1° C to lower temperatures, when compared to freshly formed vesicles (Figure 47C). Overall, these data suggest the possibility to store DPPG$_2$-TSL-R848 liposomes at frozen condition without content loss during freezing/thawing and comparable heat-triggered R848 release profiles, with related benefit when dealing with TSL manufacturing process and stability during storage.

5.2.2 *In vitro* activation of immune-cell and killing of cancer cells

R848 has been described to induce a large variety of cytokines in different population of immune cells, such as TNF-α, IL-2, IL-6, and IFN-γ [282]. Immunogenicity of different IAVs can be tested easily *in vitro* with PBMC-based assays, which grant easy-to-use dynamics and robust results [295]. PBMCs were purified via gradient separation from full blood, resulting in a cell population mainly formed by lymphocytes (70-90 %) and monocytes (10-30 %) (Figure 51) [296]. In this investigation, monitoring of cytokines was performed via ELISA for TNF-α and IL-6, due to their relevance in modulating TME and in activating DCs subsets, respectively [297, 298]. When tested *in vitro*, R848 was able to activate PBMCs in a concentration dependent fashion (Figure 52A, B). Cytokines were monitored in cell supernatant after 24 h of incubation, assessing higher values of TNF-α when compared to IL-6 (2-fold) when stimulated either with R848 or LPS (positive control). Untreated PBMCs showed negligible amount for both cytokines (100-200 pg/ml), whereas concentrations higher than 10 µM were ineffective in increasing cytokine expression (Figure 52A, B). These findings were in accordance with previously reported studies investigating cytokine expression from stimulated PBMCs [299-301]. However, a large variability in terms of absolute cytokine content was observed when comparing data sets from different studies. This might be related to common divergences in operative procedures, such as incubation time, detection method, IAVs concentration tested, use of fresh or long-term frozen PBMCs. In HT condition (41 °C, water bath) similar cytokines were assessed with negligible differences when compared to NT, also for un-treated PBMCs (Figure 52A, B). The mechanism by which hyperthermia stimulates immune cells for cytokine production is intricate. Pre-treatment of 2 h at 39.5 °C was found effective for THP-1 cells (human monocytes) to significantly increase LPS-induced stimulation, carried out at 37 °C for 24 h [302]. On the other side, PBMCs cultured at 40 °C for 4 and 24 h showed significantly lower TNF-α amount where compared to control groups incubated at 37 °C, in case of LPS stimulation [303]. In a

separate *in vitro* study, incubation at 40 °C was tested for 90 min, showing an enhanced activation of mitogen-activated PBMCs in terms of proliferation and IFN-γ production [304]. In the same investigation, same incubation carried out at 42 °C not only nullified improvement of PBMCs activation witnessed at 40 °C, but resulted in the generation of an inhibitory effect. A proposed model for the inhibitory effect observed at either higher temperature (≥ 41 °C) or for prolonged incubation (≥ 4 h) is that long-term fever range may inhibit cytokine production by a negative feedback loop. Besides inducing cytokine expression at specific conditions, hyperthermia has been described to induce HSP expression and release, such as HSP-70 with synergistic effects in immune cell maturation and activation [305]. The latter point was not assessed in this investigation, thus further studies should be performed to detect a potential HSP-70 release when PBMCs are stimulated with R848 in combination with HT. It has been already reported the possibility to induce proliferation on PBMCs via different mitogens, such as LPS, phytohemagglutinin, or a combination of anti-CD3 & IL-2 [262, 306, 307]. Different T cell phenotypes were assessed after stimulation, suggesting that the type of stimulus strongly affects cell maturation and differentiation. In this investigation, a 2-fold increase in PBMCs proliferation was observed after 72 h of R848 stimulation, when compared to control (Figure 52C). In this case, PBMCs were incubated at the optimal working concentration assessed in the previous experiment (10 µM), whereas HT was not applied as no further improvements in PBMC activation were observed. Similar findings in terms of PBMCs cell viability were observed in separate studies, with peaks of cell proliferation assessed similarly at 72 or 96 h [308, 309]. However, effects on PBMCs viability after longer time span (> 72 h) are hardly described in the literature. Here, incubation for 120 and 168 h did not improve PBMCs proliferation, with a significant decrease in overall amount. This might be caused by potential toxicity of expressed cytokines, especially caused by TNF-α, in combination with suboptimal culturing conditions driven by cell proliferation (e.g., lack of nutrients, pH change). When R848 was tested via the DPPG$_2$-TSL delivery system, a similar pattern in PBMCs activation was observed, with 2-fold higher TNF-α when compared to IL-6 (Figure 53). As no immunogenicity for empty DPPG$_2$-TSL was assessed, the potency in PBMCs activation was expected to be related exclusively to R848. Liposomal-HT showed a higher magnitude of cytokine expression when compared to NT groups (2-fold), due to a full release of R848 in this condition (Figure 53). The cytokine levels assessed in NT groups were potentially caused by R848 leakage upon dilution in medium and also to potential liposome-cell interaction happening during incubation time. The latter was tested in parallel fluorescence microscopy experiments, indeed showing fractions of DPPG$_2$-TSL localized in endosomal compartments after 1 h of incubation at 37 °C (Figure 54). TLR-7,8 are localized in endosomes of immune cells, hence an even minimal fraction of R848-loaded liposomes being internalized can be expected to largely contribute to cytokine expression. The latter point can also explain the higher absolute cytokine values

assessed for PBMC treated with DPPG$_2$-TSL plus HT, when compared to non-liposomal R848 in similar condition (Figure 53).

R848 was not reported to have any toxicity on cancer cells in mono cell culture [310, 311]. In accordance to these previously reported findings, no differences in cancer cell viability were assessed towards rat sarcoma BN175 and human ovarian cancer SKOV-3 cells after incubation with R848 ranging from 0.1 to 100 µM (Figure 53A, B). Negligible differences were detected in case of 1 h of incubation at 41 °C, when compared to NT groups. Co-culture of target cells (e.g., cancer cells) and effector cells (e.g., PBMCs) has been reported as an easy and reliable method to evaluate immune-mediated cancer cell killing [312, 313]. In SKOV-3/PBMC (1:10) co-culture settings, R848 successfully induced cancer cell killing with significant reduction of cell viability assessed after 72 h incubation. Cancer cell-killing was related to R848 concentration, with IC50 of 0.15 µM (Figure 53C & Table 18). The maximum cell killing effect was assessed with ~1 µM, and negligible improvements were observed at higher R848 concentration (Figure 53C). Additionally, HT treatment (1 h at 41 °C) did not affect cell viability, suggesting no synergistic effects. Similar findings were reported as in the previous section assessing *in vitro* toxicity of DOX-loaded TSL (4.1.3.7), and in literature when similar experimental procedures were investigated [109, 254]. Here, the same potency in PBMCs activation and cancer cell killing was observed when R848 was formulated via DPPG$_2$-TSL (Figure 53D). Under these circumstances, HT and NT groups showed also similar outcome in cell viability, albeit significant differences in cytokine production were assessed previously. This is likely due to the nature of the assay in which cytotoxicity is measured 72 h after nanoparticle incubation and heat treatment. During the remaining 72 h also non-heat activated DPPG$_2$-TSL will release their R848 contents intracellularly due to cellular nanoparticle processing or leakage, causing cellular PBMC activation and cytotoxicity. Cancer cell killing is expected to be related to the presence of antigen specific CTL CD8$^+$ activated during incubation with R848. The capacity of R848 to induce maturation of DCs capable to prime antigen specific CD8$^+$ was already reported in recently published studies, showing effectiveness of R848 to be used for the generation of a long-lasting immune response *in vitro* and *in vivo* [224, 314]. Activated CTL promote target cancer cell killing via antigen recognition to Fc receptor which triggers release of granzymes, perforins and the death ligand/death receptor system [315]. The presence of these effectors mainly leads to the activation of caspase-dependent apoptosis in target cancer cell [316]. Here, activated caspase-3 was evaluated in a fluorescence microscopy investigation, showing large fractions of the cleaved proteins exclusively in cancer cells/PBMC groups incubated with R848 (Figure 55). The analysis was assessed at a single time point after 72 h incubation time, to match cell viability assay settings. At this time point, DNA fragmentation investigated via TUNEL assay did not show significant differences between R848 and control groups [317]. As the tumor-cell mediated cell killing via apoptosis induction and subsequent

DNA fragmentation are time-dependent events, it is of interest to further evaluate immune-mediated cell killing at different end points besides 72 h (e.g., 48 h and 96 h), or with kinetic modality via live cell imaging.

5.2.3 *In vivo* application of R848-TSL

Despite the large use in pre-clinical and clinical investigations, poor information of R848 pharmacokinetic profile is currently available for systemic administration (e.g., i.v.). In this study, a fast clearance of non-liposomal R848 was observed immediately after injection (loss of > 95 % ID at 2 min) (Table 19). After the rapid initial drop, the R848 plasma level was found overall constant in the 2 h of investigation, suggesting a long t_b potentially driven by serum protein complexes. A similar pattern was assessed monitoring the PK profile of another TLR-7,8 agonist with analogue structures [229]. DPPG$_2$-TSL significantly enhanced the circulation property of R848, when compared to naked-API (Figure 56). AUC$_{2h}$ improved 30-fold when R848 was formulated in DPPG$_2$-TSL, with R848 plasma level reaching a t_α of ~40 min. DPPG$_2$-TSL-R848 was tested with two different R848/lipid ratios, which were obtained from different loading conditions (extra-liposomal pH 5.2 and 6.4). In both cases, a similar pattern in R848 plasma levels was observed, unveiling a bi-phasic clearance and an initial loss of 20 % of total ID (Figure 56 & Table 19). The circulation time of encapsulated API may depend on several factors, such as dosage, type of loading (passive, active) & used excipients, drug/lipid ratio, type of encapsulated API, lipid components, and size of nanoparticles [318, 319]. In case of passively loaded hydrophilic APIs in DPPG$_2$-TSL, t_α ranging from ~22 to ~156 min were reported, depending on the API, formulation and dosage applied. For instance, dFdC-loaded DPPG$_2$-TSL via equilibrium method resulted in a t_α of ~156 min when tested *in vivo* in Brown Norway rats, with similar settings as performed here [109]. More recently, CF was passively loaded in DPPG$_2$-TSL promoted a t_α of ~138 min (Lokerse et al, manuscript in preparation). In a recently published pilot trial on spontaneous feline soft tissue sarcoma, DPPG$_2$-TSL-DOX administrated at low dosage (0.1 & 0.4 mg/kg) via infusion showed a t_α of ~22 and ~39 min, respectively. In case of lipophilic drugs included in the lipid bilayer, a bi-phasic clearance was observed with a rapid extraction caused by protein complexation *in vivo* [285]. Additionally, osmotic stress has been described as a destabilizer of vesicles and to potentially induce loss of encapsulated compound [320]. DPPG$_2$-TSL-R848 investigated in this study were indeed subjected to osmotic stress due to the intra-liposomal concentration of AS, which was around 2-fold higher than physiological range (Table 17). However, it was recently assessed that DPPG$_2$-TSL liposomes are less sensitive to osmotic stress when compared to other TSLs, such as LTSL and PEG-TSL [108]. The observed leakage *in vivo* was rather caused by either a suboptimal R848/lipid ratio or intrinsic physicochemical properties of the API. During an *in vitro* encapsulation stability assessment, TSL

were diluted in order to mimic potential dilution factors *in vivo* (e.g., 1:12 in FCS, v/v) and incubated at 37 °C. This induced a loss of ~20 % of overall content, which stands in good accordance with the initial ID loss observed *in vivo* (Figure 58). In case of even higher dilution (1:30 dilution, v/v), a further leakage of 30-40 % of R848 content was observed via incubation in similar condition, without differences in relation to the loading condition and R848/lipid ratio (Figure 58). The latter finding suggested that R848 is not stably encapsulated in the aqueous core of $DPPG_2$-TSL, especially when subjected to high dilution factors. Active loading with a lower drug/lipid ratio, higher gradient magnitude or different intra-liposomal pH might provide benefit for this purpose. For instance, lower intra-liposomal pH (pH < 4) in combination with lower R848/lipid ratio (e.g., < 0.1) might result in a more stable API encapsulation due to a high degree of R848 protonation. However serious concerns should be raised in relation to carrier integrity, as even further lipid hydrolysis might be expected, with consequent loss of system stability. Using higher intra-liposomal pH (pH > 7) might not be favorable since R848 is mainly present in deprotonated form and lowest solubility.

When monitoring cytokine plasma levels, detectable TNF-α was observed after R848 i.v. administration *in vivo*. Additionally, higher values were assessed when R848 was administrated via $DPPG_2$-TSL, when compared to naked-R848 (1.6 fold) (Figure 57). This can be related to unspecific activation of circulating immune cell interacting with small fraction of R848 continuous leaking out from liposomes. In these investigations, cytokine plasma levels were assessed 2 h after injection. In future studies, it is of high relevance to broadly investigate cytokine profiles by monitoring plasma levels also at other time points (e.g., 6 and 24 h), to unveil even higher differences in cytokine induction. This is supported by previously reported investigations showing highest expression peaks after 3 and 24 h, in relation to the type of cytokine [227, 321]. Nevertheless, these findings suggest that decreasing the clearance rate of IAVs by formulating them in a delivery system might induce higher cytokine plasma levels with potentially unexpected side effects. Hence, by further increasing the circulation properties of $DPPG_2$-TSL-R848, even higher cytokine plasma levels can be expected, due to prolongation of R848 in circulation. This factor should be taken into consideration when formulating IAVs in liposomal form, and a trade-off between circulation stability and potential irAEs must be specifically addressed. Nevertheless, another point to consider is that HT application will likely affect the PK profile of R848 when administered via TSL, increasing its clearance due to heat-triggered release in the heated area. Therefore, substantially different cytokine plasma levels might be expected in the latter case.

5.2.4 Outlook

In the current study, a detailed characterization of R848 active loading in $DPPG_2$-based TSL is offered. While an attempt to load cholesterol-rich liposomes with this immunoadjuvant was already

reported, there is no information in the literature describing the loading procedure in TSL, as well as the potentiality of heat-triggered release. Henceforth, this investigation provides valuable information for potential use of IAVs in combination with a TSL delivery strategy. DPPG$_2$-TSL-R848 showed promising results *in vitro* with good liposomal stability, high encapsulation efficacy, triggerable R848 release function and storage stability in frozen condition. When tested *in vivo*, liposomal-R848 significantly outperformed free-API administration, with higher potentially therapeutic response. Nevertheless, a biphasic R848 clearance was assessed which might be caused by R848 leakage upon dilution in the blood stream. This effect was also assessed *in vitro* by diluting particles in FCS at different concentration, with an increasing trend in R848 loss upon further dilution. Protein adsorption on liposomal particles was observed to not only increase the release rate at HT condition, but also to promote leakage at NT by extracting R848 membrane-bound fractions. In

Figure **59**, a schematic model is proposed to explain R848 leakage observed *in vivo* upon i.v. injection. Since the membrane bound fraction might be in equilibrium with the R848 in the aqueous core, the destabilizing effect driven by protein extraction is expected to create a driving force responsible for R848 loss. This results in a continuous translocation of R848 from the aqueous core to the membrane bilayer, and subsequent extraction during particle circulation hypothetically mediated by proteins and dilution. This is expected to happen when the encapsulated drug has a high affinity for lipophilic phases, as it was observed for R848. Additionally, electrostatic interactions between the intra-liposomal positively charged R848 towards the negatively charged DPPG$_2$-based bilayer might further increase the chance of membrane adsorption driven by lipophilicity of the drug.
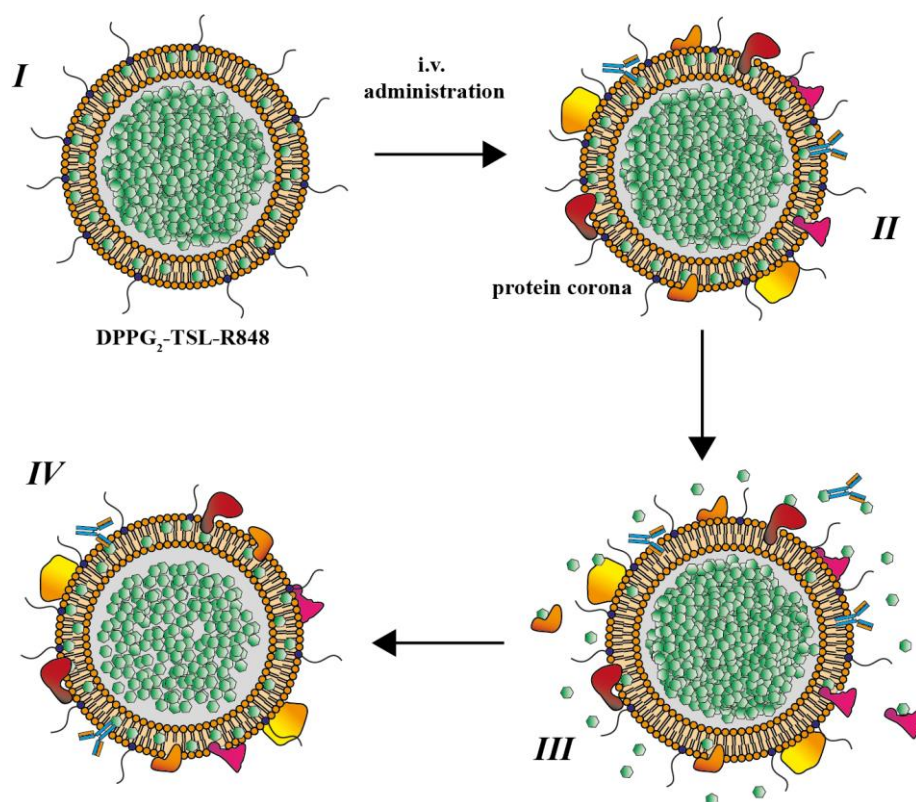
Figure 59 Schematic representation of proposed mechanism for R848 leakage upon i.v. administration.
R848-loaded DPPG$_2$-TSL with an aqueous core of R848-sulfate in equilibrium with R848 intercalated between liposomal bilayer (***I***). After i.v. administration, protein adsorption forming a corona on particle surface (***II***). Hypothetical combination of protein-induced extraction and diffusion effects of R848 membrane-fraction (***III***). Destabilizing effect on R848 in the aqueous core with translocation of R848 at liposomal bilayer establishing a new membrane fraction (***IV***).

These findings clearly confirm the noticeable improvements achievable with the DPPG$_2$-TSL delivery technology for R848, even though for *in vivo* stability is highlighted space for potential further optimization. Nevertheless, this unique behavior is mainly driven by the complexity of the system and the peculiar physicochemical characteristics of the API might result in potential advantages for a TSL targeted delivery strategy. In fact, the R848 fraction lost during *in vivo* administration has shown to provide general activation of the immune system, whereas the heat-targeted function will likely provide the targeted release in the tumor area and tumor-draining lymph nodes. Hence, while an improved stability of TSL formulations might drive a better therapeutic response for chemotherapeutics, for IAVs this might result in undesirable outcome due to irAEs caused by the cytokine-storm-effect. As explained above, it is crucial to design a formulation addressing a proper balance between stability and tolerability, to ensure an optimal therapeutic response. Further studies with the current DPPG$_2$-TSL-R848 on BD are planned in the near future, unveiling whether an effective R848-tumor enrichment is achievable at the current stage, as well as differences in cytokine-plasma levels driven by HT application.

6 Summary & Conclusion

Several nanoparticle based delivery systems are approved for clinical practice or are currently undergoing clinical trials to improve cancer therapy compared to conventional chemotherapy [322]. Although encapsulation of chemotherapeutics in stable liposome-based delivery systems greatly diminished off-target toxicity, an improved therapeutic effect is still not observed [60, 323]. This was suggested to be related to biological membranes which hamper nanoparticles passive tumor targeting, complexity of tumor biology and lack of a release mechanism [57, 323]. Hence, stimuli-responsive nanocarrier were developed to improve the biodistribution of drugs in the targeted area and thus potentially increase the therapeutic effect [14]. Among these, thermosensitive liposomes (TSL) in combination with mild-hyperthermia (41-43 °C, HT) were widely investigated with promising results in pre-clinical and clinical settings [324, 325].

The objective of this thesis was the investigation of $DPPG_2$-based thermosensitive liposomes for the transport and heat-triggered release of chemotherapeutics and immunoadjuvants (IAVs). In a first part, the heat-triggered release function of TSL was combined with the active tumor targeting approach driven by positively charged nanoparticles. Resulting $DPPG_2$-based cationic TSLs gained dual-targeting function as they were able to actively target cancer cells and release their content upon HT condition. The main aim was to identify if this dual targeting approach driven by cationic TSL could promote liposome retention in tumor vasculature and thus improve drug release upon HT, when compared to a conventional TSL delivery strategy. Polyethylene glycol (PEG) was reported to decrease potential liposome-cell interactions and, thus, hamper deliver efficiency of encapsulated compounds. Therefore, anionic and cationic TSLs functionalized either with $DPPG_2$ or PEG were tested in the investigation to assess potential advantages in using $DPPG_2$ phospholipids for solid tumor targeting. $DPPG_2$-based cationic TSL (PG$_2$-CTSL) showed a superior (2.5-fold) binding potential to endothelial and cancer cell lines when compared to PEG-CTSL, and furthermore a 1.8-fold higher intracellular DOX delivery was assessed in a parallel experiment. Higher DOX accumulation mediated by PG$_2$-CTSL was found to be connected with higher cell-killing when compared to all other TSL tested. Targeted PG$_2$-CTSL demonstrated a superior uptake by and toxicity to different tumor cell lines and endothelial cells compared to non-targeted TSL. Heat triggered intracellular DOX release in acidic cell compartments was visualized as fluorescent DOX nanobursts by live cell fluorescence microscopy. HT as trigger of endosomal escape is an intriguing concept which is worth to be investigating in future studies. Pharmacokinetic (PK) profiles showed a rapid loss of 65.5 % and 30 % ID for PG$_2$-CTSL and PEG-CTSL, respectively, and an inferior AUC_{2h} when compared to their anionic counterparts. Regional HT was successful in increasing DOX accumulation

in tumors for all TSLs tested, however no synergistic effects were observed by including cationic lipids in the formulation. In conclusion, the lack of a PEG polymer on the cationic TSL surface increased binding kinetics by promoting a better liposome-cell interaction *in vitro*. PG$_2$-CTSL showed interesting and promising results *in vitro*, whereas *in vivo* readout was sub-optimal due to complement activation and poor circulation time. Different routes of administration (e.g., i.t.) might result in a drastic benefit in exploiting advantages of targeted PG$_2$-CTSL, especially for large and/or highly hydrophilic molecules subjected to fast wash-out. Remarkably, anionic DPPG$_2$-based TSL significantly outperformed all other TSLs in terms of solid tumor targeting, showing a superior heat-triggered release profile while demonstrating an optimal stability *in vivo*. Hence, this formulation was then selected to further investigate feasibility of IAVs targeted delivery using the TSL technology.

Here, a potent toll-like receptor (TLR) 7,8 agonist, resiquimod (R848), was successfully actively loaded in DPPG$_2$-TSL and heat-triggered release was assessed in different conditions. An extensive investigation on loading conditions and excipients unveiled optimal liposomes stability when NH$_4^+$ was used as gradient force, with high loading efficiency assessed at two different R848/lipid ratio (mol:mol). This resulted in the possibility to formulate R848 in a concentration higher than 1 mg/ml in a liposomal form, easing further dosage for *in vivo* application. Obtained DPPG$_2$-TSL-R848 showed acceptable serum stability at low temperatures (e.g., 37-39 °C), with a rapid burst-like release at 41-42 °C and complete particle depletion within few minutes of application. Shortcomings of active loading conditions were observed in relation to lipid hydrolysis and generation of lyso-lipids and fatty acids over time. Formulation was successfully stored at -20 °C when specific excipients (e.g., cryoprotectants) were added to the extra-liposomal buffer, with negligible leakage assessed during freezing/thawing and no further lipid hydrolysis. Furthermore, DPPG$_2$-TSL-R848 stored at -20 °C showed comparable size & PDI to freshly formed vesicles, with same efficiency in R848 heat-triggered release. When tested *in vivo*, DPPG$_2$-TSL-R848 outperformed non-liposomal R848 in PK studies, with 30- and 35-fold higher AUC and C$_{max}$, respectively. Nevertheless, a bi-phasic elimination was observed which might suggest minor leakage of drug. Cytokine plasma level assessed after R848 injection showed detectable level of TNF-α with significantly higher values when R848 is administrated via DPPG$_2$-TSL. Overall, this data set offers valuable information about the feasibility of R848 to be encapsulated and heat-triggered release from TSL. Besides the aforementioned PK investigations, a BD study is planned in the near future to investigate R848-tumor enrichment. Additionally, therapeutic investigations in tumor bearing rats will also be investigated, either using liposomal-R848 as single treatment or in combination with DPPG$_2$-TSL-DOX. These studies will mainly focus on the generation of a strong and multifactorially generated immune response, to possibly treat not only primary tumors but also metastases and remission (refer to section 7).

7 Future work

The current study unveiled high promise of TSL as a potential system for targeted delivery of chemotherapeutics and immunoadjuvants (IAVs). These results provided support for a new grant from the Bundesministeriums für Bildung und Forschung, in cooperation with Thermosome GmbH and Helmholtz Zentrum München. In this future plan, different IAVs will be tested in combination with the DPPG$_2$-TSL technology platform, either for intravascular drug release or a dual targeting approach. In the latter case, particles will be administrated intratumorally (i.t) to avoid limitations on systemic administration and fully exploit advantages of targeting capability. Besides investigating potentially clinical relevance of different formulations for IAVs delivery, a new concept for cancer treatment will be investigated.

Current challenges in cancer therapy are raised by dissemination of metastases, high heterogeneity of tumor types and potential resistance development to conventional chemotherapy [326, 327]. In preclinical models, toll-like receptors (TLR) and stimulator of interferon genes (STING) agonists delivered i.t. showed promising antitumor activity [184, 328]. Several novel IAVs are currently undergoing clinical trials for solid tumor cancer therapy, either as single therapy or in combination with immune-check point blockade [230, 329, 330]. Nevertheless, while immunotherapy approaches showed results in some tumor types usually characterized by high tumor mutational burden (TMB), poor outcome was observed in others, usually characterized by an immune-excluded phenotype [331]. In the latter case, the lack of tumor-associated antigens, defective recruitment of dendritic cells (DC) with absence of T-cell priming require more synergistic effects to induce local inflammation and immune cell infiltration [332]. Some chemotherapeutics currently used in clinical practice have been described to cause immunogenic cell death (ICG). ICG is one of the most potent allies for a successful cancer immunotherapy, due to its capability to release a high number of tumor-associated antigens (TAAs) [333]. Anthracyclines have shown to be potent ICG-inducer, promoting caspase-dependent cell apoptosis [334, 335]. Recently, doxorubicin (DOX) treatment was found effective in increasing therapeutic response of PD-L1 blockade in patients affected by triple negative breast cancer, when compared to other chemotherapies, such as cis-platin and cyclophosphamide [336]. These findings suggest that, despite the fact DOX has been widely used in clinical practice for more than 40 years, combination with most recent approaches might rise to unique therapeutic outcome.

In the proposed future study, a model for a successful activation of tumor milieu immunity independently from tumor phenotypes (e.g., low TMB) is investigated. DOX-induced ICG is combined to IAVs (e.g., resiquimod, R848) in a treatment plan shown in Figure 60. DOX-induced TAAs are combined with specific immune-stimulatory effects driven by the selected adjuvant. In

addition, HT immune-activation is exploited as an additional factor to increase local inflammation and potentially enhance T-cell infiltration and anti-tumor-response. DOX and R848 will be administrated via the DPPG$_2$-TSL delivery technology, promoting a targeted delivery in the tumor area upon HT application. The multi-functional treatment aims to ensure a proper activation of DCs and T-cell priming in order to successfully enhance an immune response towards metastases (abscopal effect) and tumor re-challenges (long-term memory effect). This immunotherapy approach holds great promises and will potentially generate a high value system worth of clinical translation.

Besides clinically established methods as RF and microwave applicators, next-generation systems as MR-HIFU are facing clinical trials, also in combination with ThermoDOX® for different types of solid tumors [337]. MR-HIFU has shown unique advantages in combination with the immunotherapy approach, due to possibility to create localized tissue-damages via acoustic cavitation [338]. This particular technique is generally referred to as mechanical tissue fractionation or boiling histotripsy, and it has been described to induce generation of a large number of TAAs exclusively in the focused area [339]. In conclusion, it is worth to further exploit the unique features of this approach in combination with clinically established methods (e.g., RF applicator) or next-generation MR-HIFU, to ensure an additional contribution in modulating the immune system.
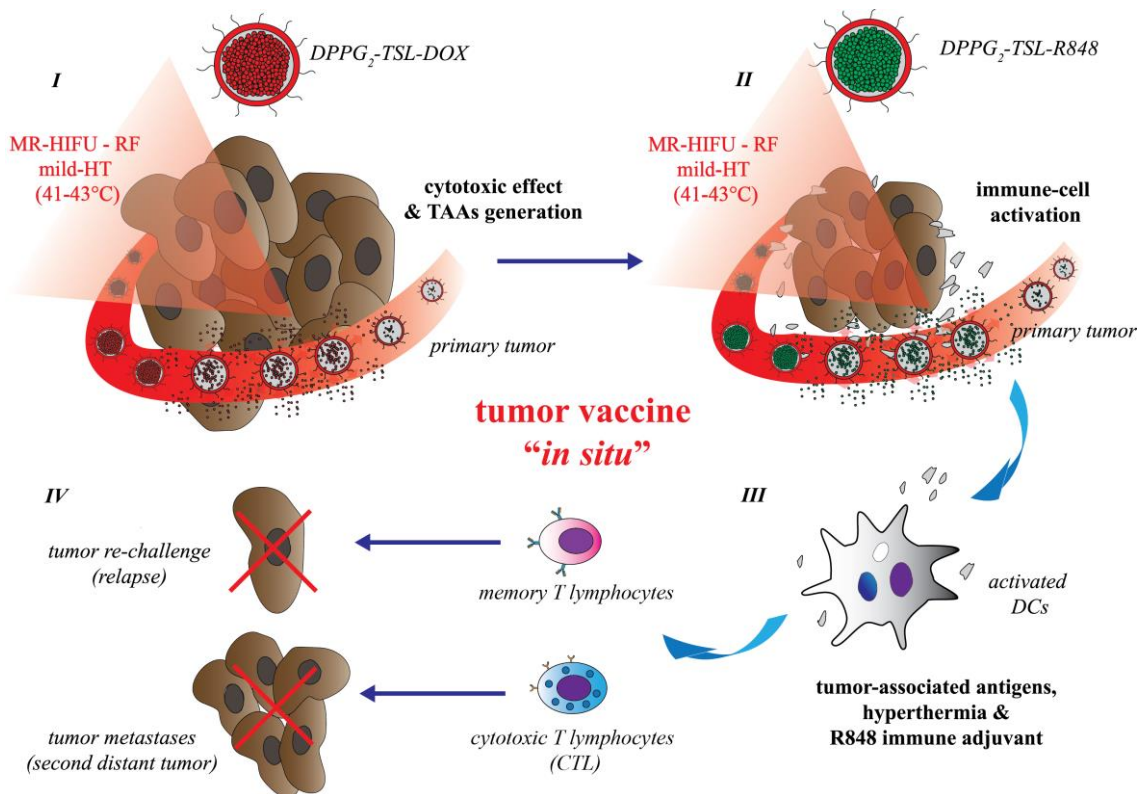
Figure 60 Schematic concept of "*in situ*" cancer vaccine for immuno-cancer therapy.
The mechanism of anti-tumor immune responses induced by DPPG$_2$-TSL-DOX and DPPG$_2$-TSL-R848 in combination with HT application. DPPG$_2$-based liposomal DOX is administrated at day 1 to induce cytotoxic effect and generation of TAAs (*I*). Liposomal R848 is administrated 2-4 days later after DOX-treatment (*II*). Co-presence of R848, HT, TAAs factors act on DCs activation and maturation (*III*). In case of successful immune activation, cytotoxic T cells and memory T cells act against metastases (long-distant tumor response) and tumor-re-challenge (long-lasting immune memory) (*IV*).

8 Appendix

8.1 References

[1]   Malvezzi M, Carioli G, Bertuccio P, Boffetta P, Levi F, La Vecchia C, et al. European cancer mortality predictions for the year 2019 with focus on breast cancer. Annals of Oncology, 30 (2019) 781-7.

[2]   World Health Organization n.d. Cancer data and statistics, accessed 29 September 2019. http://www.euro.who.int/en/health-topics/noncommunicable-diseases/cancer/data-and-statistics.

[3]   Cunningham M, Hepplestone A, Gilchrist NL, Dagg JH, Evans IL, Soukopl M. Failure of conventional chemotherapy in aggressive lymphomas. Postgraduate Medical Journal, 63 (1987) 4-11.

[4]   Alfarouk KO, Stock CM, Taylor S, Walsh M, Muddathir AK, Verduzco D, et al. Resistance to cancer chemotherapy: failure in drug response from ADME to P-gp. Cancer Cell International 15 (2015) 71-7.

[5]   Butow P, Sharpe L, Thewes B, Turner J, Gilchrist J, Beith J. Fear of Cancer Recurrence: A Practical Guide for Clinicians. Oncology, 32 (2018) 32-8.

[6]   Arruebo M, Vilaboa N, Saez-Gutierrez B, Lambea J, Tres A, Valladares M, et al. Assessment of the evolution of cancer treatment therapies. Cancers, 3(2011) 3279-330.

[7]   National Cancer Institute n.d. Types of cancer treatment, accessed 29 September 2019. https://www.cancer.gov/about-cancer/treatment/types.

[8]   Charmsaz S, Prencipe M, Kiely M, Pidgeon G, Collins D. Innovative Technologies Changing Cancer Treatment. Cancers, 10 (2018) 208-13.

[9]   Nie D, Preissner S, Dunkel M, Hoffmann MF, Preissner SC, Genov N, et al. Drug Cocktail Optimization in Chemotherapy of Cancer. PloS one, 7 (2012) 5120-6.

[10] Shi Z, Guo H-Q, Cohen PA, Yang D-H. Editorial: Novel Targets and Biomarkers in Solid Tumors. Frontiers in Pharmacology, 10 (2019)

[11] Szeto GL, Finley SD. Integrative Approaches to Cancer Immunotherapy. Trends in Cancer, 5 (2019) 400-10.

[12] Patra JK, Das G, Fraceto LF, Campos EVR, Rodriguez-Torres MdP, Acosta-Torres LS, et al. Nano based drug delivery systems: recent developments and future prospects. Journal of Nanobiotechnology, 16 (2018) 1345-53.

[13] Senapati S, Mahanta AK, Kumar S, Maiti P. Controlled drug delivery vehicles for cancer treatment and their performance. Signal Transduction and Targeted Therapy, 3 (2018) 7-13.

[14] Mura S, Nicolas J, Couvreur P. Stimuli-responsive nanocarriers for drug delivery. Nature Materials, 12 (2013) 991-1003.

[15] American Cancer Society n.d. Cancer Immunotherapy, accessed 29 September 2019. https://www.cancer.org/treatment/treatments-and-side-effects/treatment-types/immunotherapy.html. (2019)

[16] Rosenberg SA, Yang JC, Restifo NP. Cancer immunotherapy: moving beyond current vaccines. Nature Medicine, 10 (2004) 6-12.

[17] Goodman AM, Kato S, Bazhenova L, Patel SP, Frampton GM, Miller V, et al. Tumor Mutational Burden as an Independent Predictor of Response to Immunotherapy in Diverse Cancers. Molecular Cancer Therapeutics, 16 (2017) 2598-608.

[18] Alexandrov LB, Nik-Zainal S, Wedge DC, Aparicio SA, Behjati S, Biankin AV, et al. Signatures of mutational processes in human cancer. Nature, 500 (2013) 415-21.

[19] Darvin P, Toor SM, Sasidharan Nair V, Elkord E. Immune checkpoint inhibitors: recent progress and potential biomarkers. Experimental and Molecular Medicine, 50 (2018) 165-69.

[20] Hirayama AV, Gauthier J, Hay KA, Voutsinas JM, Wu Q, Pender BS, et al. High rate of durable complete remission in follicular lymphoma after CD19 CAR-T cell immunotherapy. Blood, 134 (2019) 636-40.

[21] Espinoza-Delgado I. Cancer vaccines. The oncologist, 7 (2002) 20-33.

[22] Hollingsworth RE, Jansen K. Turning the corner on therapeutic cancer vaccines. NPJ Vaccines, 4 (2019) 7-13.

[23] Shen Z. Genomic instability and cancer: an introduction. Journal of Molecular Cell Biology, 3 (2011) 1-3.

[24] Weinberg RA. How cancer arises. Scientific American, 275 (1996) 62-70.

[25] Seyfried TN, Huysentruyt LC. On the origin of cancer metastasis. Critical Reviews in Oncogenesis 18 (2013) 30-4.

[26] Quint LE. Lung cancer: assessing resectability. Cancer Imaging, 4 (2003) 15-8.

[27] Ohri N, Rapkin BD, Guha C, Kalnicki S, Garg M. Radiation Therapy Noncompliance and Clinical Outcomes in an Urban Academic Cancer Center. International Journal of Radiation Oncology, Biology, Physics, 95 (2016) 563-70.

[28] Cassinelli G. The roots of modern oncology: from discovery of new antitumor anthracyclines to their clinical use. Tumori, 2016 (2016) 226-35.

[29] Arcamone F, Franceschi G, Penco S, Selva A. Adriamycin (14-hydroxydaunomycin), a novel antitumor antibiotic. Tetrahedron letters, (1969) 1007-10.

[30] Momparler RL, Karon M, Siegel SE, Avila F. Effect of adriamycin on DNA, RNA, and protein synthesis in cell-free systems and intact cells. Cancer Research, 36 (1976) 2891-5.

[31] Chatterjee K, Zhang J, Honbo N, Karliner JS. Doxorubicin cardiomyopathy. Cardiology, 115 (2010) 155-62.

[32] Bangham AM, Standish MM, Watkins JC. Diffusion of univalent Ions across the lamellae of swollen phospholipids. Journal Molecular Biology, 13 (1965) 14-21.

[33] Gregoriadis G. Drug entrapment in liposomes. FEBS Letter, 36 (1973) 292-6.

[34] Allen TM, Cullis PR. Liposomal drug delivery systems: from concept to clinical applications. Advanced Drug Delivery Reviews, 65 (2013) 36-48.

[35] Lindner LH, Hossann M. Factors affecting drug release from liposomes. Current Opinion in Drug Discovery & Development, 13 (2010) 111-23.

[36] Riaz MK, Riaz MA, Zhang X, Lin C, Wong KH, Chen X, et al. Surface Functionalization and Targeting Strategies of Liposomes in Solid Tumor Therapy: A Review. International Journal of Molecular Sciences, 19 (2018) 235-41.

[37] Mayer LM, Cullis PR, Bally MB. The use of transmembrane ph gradient-driven drug encapsulation in the pharmacodynamic evaluation of liposomal doxorubicin. Journal of Liposomal Research, 4 (1994) 24-9.

[38] Zucker D, Marcus D, Barenholz Y, Goldblum A. Liposome drugs' loading efficiency: a working model based on loading conditions and drug's physicochemical properties. Journal of Controlled Release, 139 (2009) 73-80.

[39] Hoekstra D, Scherphof G. Effect of fetal calf serum and serum protein fractions on the uptake of liposomal phosphatidylcholine by rat hepatocytes in primary monolayer culture. Biochimica et Biophysica Acta, 551 (1979) 109-21.

[40] Scherphof GL, Dijkstra J, Spanjer HH, Derksen JT, Roerdink FH. Uptake and intracellular processing of targeted and nontargeted liposomes by rat Kupffer cells in vivo and in vitro. Annals of the New York Academy of Sciences, 446 (1985) 368-84.

[41] Senior J, Gregoriadis G. Is half-life of circulating liposomes determined by changes in their permeability? FEBS letters, 145 (1982) 109-14.

[42] Allen TM, Chonn A. Large unilamellar liposomes with low uptake into the reticuloendothelial system. FEBS Letters, 223 (1987) 42-6.

[43] Drummond DC, Meyer O, Hong K, Kirpotin DB, Papahadjopoulos D. Optimizing liposomes for delivery of chemotherapeutic agents to solid tumors. Pharmacological Reviews, 51 (1999) 691-703.

[44] Lasic DD, Martin FJ, Gabizon A, Huang SK, Papahadjopoulos D. Sterically stabilized liposomes: a hypothesis on the molecular origin of the extended circulation times. Biochimica et Biophysica Acta, 1070 (1991) 187-92.

[45] Wagner M, Wiig H. Tumor Interstitial Fluid Formation, Characterization, and Clinical Implications. Frontiers in Oncology, 5 (2015) 115.

[46] Hashizume H, Baluk P, Morikawa S, McLean JW, Thurston G, Roberge S, et al. Openings between defective endothelial cells explain tumor vessel leakiness. The American Journal of Pathology, 156 (2000) 1363-80.

[47] Langenkamp E, Molema G. Microvascular endothelial cell heterogeneity: general concepts and pharmacological consequences for anti-angiogenic therapy of cancer. Cell and Tissue Reserve, 335 (2009) 205-22.

[48] Matsumura Y, Maeda H. A new concept for macromolecular therapeutics in cancer chemotherapy: mechanism of tumoritropic accumulation of proteins and the antitumor agent smancs. Cancer Research, 46 (1986) 6387-92.

[49] Maeda H, Wu J, Sawa T, Matsumura Y, Hori K. Tumor vascular permeability and the EPR effect in macromolecular therapeutics: a review. Journal of Controlled Release 65 (2000) 271-84.

[50] Prabhakar U, Maeda H, Jain RK, Sevick-Muraca EM, Zamboni W, Farokhzad OC, et al. Challenges and key considerations of the enhanced permeability and retention effect for nanomedicine drug delivery in oncology. Cancer Research, 73 (2013) 2412-7.

[51] Food and Drug Administration n.d. FDA approved drug products, accessed 29 September 2019. https://www.accessdata.fda.gov/scripts/cder/daf/index.cfm?event=overview.process&ApplNo=050718. (1995)

[52] Barenholz Y. Doxil[(R)] - the first FDA-approved nano-drug: lessons learned. Journal Controlled Release, 160 (2012) 117-34.

[53] Petersen GH, Alzghari SK, Chee W, Sankari SS, La-Beck NM. Meta-analysis of clinical and preclinical studies comparing the anticancer efficacy of liposomal versus conventional non-liposomal doxorubicin. Journal of Controlled Release, 232 (2016) 255-64.

[54] Gabizon A, Catane R, Uziely B, Kaufman B, Safra T, Cohen R, et al. Prolonged circulation time and enhanced accumulation in malignant exudates of doxorubicin encapsulated in polyethylene-glycol coated liposomes. Cancer Research, 54 (1994) 987-92.

[55] Gabizon A, Papahadjopoulos D. Liposome formulations with prolonged circulation time in blood and enhanced uptake by tumors. Proceedings of the National Academy of Sciences of the United States of America, 85 (1988) 6949-53.

[56] Wu NZ, Da D, Rudoll TL, Needham D, Whorton AR, Dewhirst MW. Increased microvascular permeability contributes to preferential accumulation of Stealth liposomes in tumor tissue. Cancer Research, 53 (1993) 3765-70.

[57] O'Brien MER. Reduced cardiotoxicity and comparable efficacy in a phase III trial of pegylated liposomal doxorubicin HCl (CAELYX[TM]/Doxil[®]) versus conventional doxorubicin for first-line treatment of metastatic breast cancer. Annals of Oncology, 15 (2004) 440-9.

[58] Samantas E, Kalofonos H, Linardou H, Nicolaides C, Mylonakis N, Fountzilas G, et al. Phase II study of pegylated liposomal doxorubicin: inactive in recurrent small-cell lung cancer. A Hellenic Cooperative Oncology Group Study. Annals of Oncology 11 (2000) 1395-7.

[59] Silverman JA, Deitcher SR. Marqibo[®] (vincristine sulfate liposome injection) improves the pharmacokinetics and pharmacodynamics of vincristine. Cancer Chemotherapy and Pharmacology, 71 (2013) 555-64.

[60] Wang-Gillam A, Li C-P, Bodoky G, Dean A, Shan Y-S, Jameson G, et al. Nanoliposomal irinotecan with fluorouracil and folinic acid in metastatic pancreatic cancer after previous gemcitabine-based therapy (NAPOLI-1): a global, randomised, open-label, phase 3 trial. The Lancet, 387 (2016) 545-57.

[61] Hansen CB, Kao GY, Moase EH, Zalipsky S, Allen TM. Attachment of antibodies to sterically stabilized liposomes: evaluation, comparison and optimization of coupling procedures. Biochimica et Biophysica Acta, 1239 (1995) 133-44.

[62] Blume G, Cevc G, Crommelin MD, Bakker-Woudenberg IA, Kluft C, Storm G. Specific targeting with poly(ethylene glycol)-modified liposomes: coupling of homing devices to the ends of the polymeric chains combines effective target binding with long circulation times. Biochimica et Biophysica Acta, 1149 (1993) 180-4.

[63] An B, Lin YS, Brodsky B. Collagen interactions: Drug design and delivery. Advanced Drug Delivery Reviews, 97 (2016) 69-84.

[64] Yoncheva K, Momekov G. Antiangiogenic anticancer strategy based on nanoparticulate systems. Expert Opinion on Drug Delivery, 8 (2011) 1041-56.

[65] Koning GA, Schiffelers RM, Storm G. Endothelial cells at inflammatory sites as target for therapeutic intervention. Endothelium, 9 (2002) 161-71.

[66] Volkel T, Holig P, Merdan T, Muller R, Kontermann RE. Targeting of immunoliposomes to endothelial cells using a single-chain Fv fragment directed against human endoglin (CD105). Biochimica et Biophysica Acta, 1663 (2004) 158-66.

[67] Gosk S, Moos T, Gottstein C, Bendas G. VCAM-1 directed immunoliposomes selectively target tumor vasculature in vivo. Biochimica et Biophysica Acta, 1778 (2008) 854-63.

[68] Rosenblum D, Joshi N, Tao W, Karp JM, Peer D. Progress and challenges towards targeted delivery of cancer therapeutics. Nature Communications, 9 (2018) 1410-15.

[69] Garcia AA, Kempf RA, Rogers M, Muggia FM. A phase II study of Doxil (liposomal doxorubicin): lack of activity in poor prognosis soft tissue sarcomas. Annals of Oncology, 9 (1998) 1131-3.

[70] Safra T, Groshen S, Jeffers S, Tsao-Wei DD, Zhou L, Muderspach L, et al. Treatment of patients with ovarian carcinoma with pegylated liposomal doxorubicin: analysis of toxicities and predictors of outcome. Cancer, 91 (2001) 90-100.

[71] Goren D, Horowitz AT, Zalipsky S, Woodle MC, Yarden Y, Gabizon A. Targeting of stealth liposomes to erbB-2 (Her/2) receptor: in vitro and in vivo studies. British Journal of Cancer, 74 (1996) 1749-56.

[72] Danhier F. To exploit the tumor microenvironment: Since the EPR effect fails in the clinic, what is the future of nanomedicine? Journal of Controlled Release, 244 (2016) 108-21.

[73] Maeda H. Toward a full understanding of the EPR effect in primary and metastatic tumors as well as issues related to its heterogeneity. Advanced Drug Delivery Reviews, 91 (2015) 3-6.

[74] Lammers T, Kiessling F, Hennink WE, Storm G. Drug targeting to tumors: principles, pitfalls and (pre-) clinical progress. Journal of Controlled Release, 161 (2012) 175-87.

[75] Nakamura Y, Mochida A, Choyke PL, Kobayashi H. Nanodrug Delivery: Is the Enhanced Permeability and Retention Effect Sufficient for Curing Cancer? Bioconjugate Chemistry, 27 (2016) 2225-38.

[76] Harrington KJ, Mohammadtaghi S, Uster PS, Glass D, Peters AM, Vile RG, et al. Effective Targeting of Solid Tumors in Patients With Locally Advanced Cancers by Radiolabeled Pegylated Liposomes. Clinical Cancer Research, (2001)

[77] Wilhelm S, Tavares AJ, Dai Q, Ohta S, Audet J, Dvorak HF, et al. Analysis of nanoparticle delivery to tumours. Nature Reviews Materials 1(2016) 1-12.

[78] Laginha KM, Verwoert S, Charrois GJ, Allen TM. Determination of doxorubicin levels in whole tumor and tumor nuclei in murine breast cancer tumors. Clinical Cancer Reseach, 11 (2005) 6944-9.

[79] Seynhaeve AL, Dicheva BM, Hoving S, Koning GA, ten Hagen TL. Intact Doxil is taken up intracellularly and released doxorubicin sequesters in the lysosome: evaluated by in vitro/in vivo live cell imaging. Journal of Controlled Release, 172 (2013) 330-40.

[80] Tayo LL. Stimuli-responsive nanocarriers for intracellular delivery. Biophysical Reviews, 9 (2017) 931-40.

[81] van den Tempel N, Horsman MR, Kanaar R. Improving efficacy of hyperthermia in oncology by exploiting biological mechanisms. International Journal of Hyperthermia, 32 (2016) 446-54.

[82] Al-Ahmady Z, Kostarelos K. Chemical Components for the Design of Temperature-Responsive Vesicles as Cancer Therapeutics. Chemical Reviews, 116 (2016) 3883-918.

[83] Yellin N, Levin IW. Hydrocarbon trans-gauche isomerization in phospholipid bilayer gel assemblies. Biochemistry, 16 (1977) 642-7.

[84] Janiak MJ, Small DM, Shipley GG. Nature of the Thermal pretransition of synthetic phospholipids: dimyristolyl- and dipalmitoyllecithin. Biochemistry, 15 (1976) 4575-80.

[85] Kaasgaard T, Leidy C, Crowe JH, Mouritsen OG, Jorgensen K. Temperature-controlled structure and kinetics of ripple phases in one- and two-component supported lipid bilayers. Biophysical Journal, 85 (2003) 350-60.

[86] Mouritsen OG, Zuckermann MJ. Model of interfacial melting. Physical Review Letters, 58 (1987) 389-92.

[87] Melchior DL, Steim JM. Thermotropic transitions in biomembranes. Annual Review of Biophysics and Bioengineering, 5 (1976) 205-38.

[88] Papahadjopoulos D, Jacobson K, Nir S, Isac T. Phase transitions in phospholipid vesicles. Fluorescence polarization and permeability measurements concerning the effect of temperature and cholesterol. Biochimica et Biophysica Acta, 311 (1973) 330-48.

[89] Yatvin MB, Weinstein JN, Dennis WH, Blumenthal R. Design of liposomes for enhanced local release of drugs by hyperthermia. Science, 202 (1978) 1290-3.

[90] Gaber MH, Hong K, Huang SK, Papahadjopoulos D. Thermosensitive sterically stabilized liposomes: formulation and in vitro studies on mechanism of doxorubicin release by bovine serum and human plasma. Pharmaceutical Research, 12 (1995) 1407-16.

[91] Unezaki S, Maruyama K, Takahashi N, Koyama M, Yuda T, Suginaka A, et al. Enhanced delivery and antitumor activity of doxorubicin using long-circulating thermosensitive liposomes containing amphipathic polyethylene glycol in combination with local hyperthermia. Pharmaceutical Research, 11 (1994) 1180-5.

[92] Anyarambhatla GR, Needham D. Enhancement of the Phase Transition Permeability of DPPC Liposomes by Incorporation of MPPC: A New Temperature-Sensitive Liposome for use with Mild Hyperthermia. Journal of Liposome Research, 9 (2008) 491-506.

[93] Needham D, Anyarambhatla G, Kong G, Dewhirst MW. A new temperature-sensitive liposome for use with mild hyperthermia: characterization and testing in a human tumor xenograft model. Cancer Research, 60 (2000) 1197-201.

[94] Mills JK, Needham D. The materials engineering of temperature-sensitive liposomes. Methods in Enzymology, 387 (2004) 82-113.

[95] Kong G, Anyarambhatla G, Petros WP, Braun RD, Colvin OM, Needham D, et al. Efficacy of liposomes and hyperthermia in a human tumor xenograft model: importance of triggered drug release. Cancer Research, 60 (2000) 6950-7.

[96] Al-Jamal WT, Al-Ahmady ZS, Kostarelos K. Pharmacokinetics & tissue distribution of temperature-sensitive liposomal doxorubicin in tumor-bearing mice triggered with mild hyperthermia. Biomaterials, 33 (2012) 4608-17.

[97] Celsion. Study of ThermoDox with standardized radiofrequency ablation (RFA) for treatment of hepatocellular carcinoma (HCC) (OPTIMA). ClinicalTrialsgov NCT002112656, (2014)

[98] Celsion. Targeted chemotherapy using focused ultrasound for liver tumours (TARDOX). ClinicalTrialsgov NCT02181075, (2019)

[99] Zagar TM, Vujaskovic Z, Formenti S, Rugo H, Muggia F, O'Connor B, et al. Two phase I dose-escalation/pharmacokinetics studies of low temperature liposomal doxorubicin (LTLD) and mild local hyperthermia in heavily pretreated patients with local regionally recurrent breast cancer. International Journal of Hyperthermia, 30 (2014) 285-94.

[100] Celsion. Phase 3 study of ThermoDox with radiofrequency ablation (RFA) in treatment if hepatocellular carcinoma (HCC). ClinicalTrialsgov NCT00617981, (2008)

[101] Banno B, Ickenstein LM, Chiu GN, Bally MB, Thewalt J, Brief E, et al. The functional roles of poly(ethylene glycol)-lipid and lysolipid in the drug retention and release from lysolipid-containing thermosensitive liposomes in vitro and in vivo. Journal of Pharmaceutical Sciences, 99 (2010) 2295-308.

[102] Paoli EE, Kruse DE, Seo JW, Zhang H, Kheirolomoom A, Watson KD, et al. An optical and microPET assessment of thermally-sensitive liposome biodistribution in the Met-1 tumor model: Importance of formulation. Journal of Controlled Release, 143 (2010) 13-22.

[103] Li L, ten Hagen TL, Hossann M, Suss R, van Rhoon GC, Eggermont AM, et al. Mild hyperthermia triggered doxorubicin release from optimized stealth thermosensitive liposomes improves intratumoral drug delivery and efficacy. Journal of Controlled Release, 168 (2013) 142-50.

[104] Lokerse WJ, Kneepkens EC, ten Hagen TL, Eggermont AM, Grull H, Koning GA. In depth study on thermosensitive liposomes: Optimizing formulations for tumor specific therapy and in vitro to in vivo relations. Biomaterials, 82 (2016) 138-50.

[105] Tagami T, Ernsting MJ, Li SD. Optimization of a novel and improved thermosensitive liposome formulated with DPPC and a Brij surfactant using a robust in vitro system. Journal of Controlled Release 154 (2011) 290-7.

[106] Hossann M, Wiggenhorn M, Schwerdt A, Wachholz K, Teichert N, Eibl H, et al. In vitro stability and content release properties of phosphatidylglyceroglycerol containing thermosensitive liposomes. Biochimica et Biophysica Acta, 1768 (2007) 2491-9.

[107] Lindner LH, Eichhorn ME, Eibl H, Teichert N, Schmitt-Sody M, Issels RD, et al. Novel temperature-sensitive liposomes with prolonged circulation time. Clinical Cancer Research, 10 (2004) 2168-78.

[108] Hossann M, Syunyaeva Z, Schmidt R, Zengerle A, Eibl H, Issels RD, et al. Proteins and cholesterol lipid vesicles are mediators of drug release from thermosensitive liposomes. Journal of Controlled Release, 162 (2012) 400-6.

[109] Limmer S, Hahn J, Schmidt R, Wachholz K, Zengerle A, Lechner K, et al. Gemcitabine treatment of rat soft tissue sarcoma with phosphatidyldiglycerol-based thermosensitive liposomes. Pharmaceutical Research, 31 (2014) 2276-86.

[110] Schmidt R. Neuartige thermosensitive Liposomen zur zielgerichteten Therapie solider Tumoren - Charakterisierung in vitro und in vivo. Dissertation, (2011)

[111] Zimmermann K, Hossann M, Hirschberger J, Troedson K, Peller M, Schneider M, et al. A pilot trial of doxorubicin containing phosphatidyldiglycerol based thermosensitive liposomes in spontaneous feline soft tissue sarcoma. Internatioanl Journal of Hyperthermia, (2016) 1-13.

[112] Karino T, Koga S, Maeta M. Experimental studies of the effects of local hyperthermia on blood flow, oxygen pressure and pH in tumors. The Japanese Journal of Surgery, 18 (1988) 276-83.

[113] Song CW, Shakil A, Osborn JL, Iwata K. Tumour oxygenation is increased by hyperthermia at mild temperatures. International Journal of Hyperthermia, 25 (2009) 91-5.

[114] Lefor AT, Makohon S, Ackerman NB. The effects of hyperthermia on vascular permeability in experimental liver metastasis. Journal of Surgical Oncology, 28 (1985) 297-300.

[115] Schuster JM, Zalutsky MR, Noska MA, Dodge R, Friedman HS, Bigner DD, et al. Hyperthermic modulation of radiolabelled antibody uptake in a human glioma xenograft and normal tissues. International Journal of Hyperthermia, 11 (1995) 59-72.

[116] Kong G, Braun RD, Dewhirst MW. Characterization of the effect of hyperthermia on nanoparticle extravasation from tumor vasculature. Cancer Research, 61 (2001) 3027-32.

[117] Issels R, Kampmann E, Kanaar R, Lindner LH. Hallmarks of hyperthermia in driving the future of clinical hyperthermia as targeted therapy: translation into clinical application. International Journal of Hyperthermia, 32 (2016) 89-95.

[118] Toraya-Brown S, Fiering S. Local tumour hyperthermia as immunotherapy for metastatic cancer. International Journal of Hyperthermia, 30 (2014) 531-9.

[119] Overgaard J. Combined adriamycin and hyperthermia treatment of a murine mammary carcinoma in vivo. Cancer Research, 36 (1976) 3077-81.

[120] Issels RD, Lindner LH, Verweij J, Wust P, Reichardt P, Schem B-C, et al. Neo-adjuvant chemotherapy alone or with regional hyperthermia for localised high-risk soft-tissue sarcoma: a randomised phase 3 multicentre study. The Lancet Oncology, 11 (2010) 561-70.

[121] Issels RD, Lindner LH, Verweij J, Wessalowski R, Reichardt P, Wust P, et al. Effect of Neoadjuvant Chemotherapy Plus Regional Hyperthermia on Long-term Outcomes Among Patients With Localized High-Risk Soft Tissue Sarcoma: The EORTC 62961-ESHO 95 Randomized Clinical Trial. JAMA Oncology, 4 (2018) 483-92.

[122] Dewhirst MW, Secomb TW. Transport of drugs from blood vessels to tumour tissue. Nature Reviews Cancer, 17 (2017) 738-50.

[123] Manzoor AA, Lindner LH, Landon CD, Park JY, Simnick AJ, Dreher MR, et al. Overcoming limitations in nanoparticle drug delivery: triggered, intravascular release to improve drug penetration into tumors. Cancer Research, 72 (2012) 5566-75.

[124] Fatehi D, van der Zee J, de Bruijne M, Franckena M, van Rhoon GC. RF-power and temperature data analysis of 444 patients with primary cervical cancer: deep hyperthermia using the Sigma-60 applicator is reproducible. International Journal of Hyperthermia, 23 (2007) 623-43.

[125] Boreham DR, Gasmann HC, Mitchel RE. Water bath hyperthermia is a simple therapy for psoriasis and also stimulates skin tanning in response to sunlight. International Journal of Hyperthermia, 11 (1995) 745-54.

[126] Storm FK, Morton DL, Kaiser LR, Harrison WH, Elliott RS, Weisenburger TH, et al. Clinical radiofrequency hyperthermia: a review. National Cancer Institute Monograph, 61 (1982) 343-50.

[127] Stauffer PR, van Rhoon GC. Overview of bladder heating technology: matching capabilities with clinical requirements. International Journal of Hyperthermia, 32 (2016) 407-16.

[128] Hijnen N, Langereis S, Grull H. Magnetic resonance guided high-intensity focused ultrasound for image-guided temperature-induced drug delivery. Advanced Drug Delivery Reviews, 72 (2014) 65-81.

[129] Schaaf MB, Garg AD, Agostinis P. Defining the role of the tumor vasculature in antitumor immunity and immunotherapy. Cell Death & Disease, 9 (2018) 115.

[130] Klein D. The Tumor Vascular Endothelium as Decision Maker in Cancer Therapy. Frontiers in Oncology, 8 (2018) 367.

[131] Yang J, Yan J, Liu B. Targeting VEGF/VEGFR to Modulate Antitumor Immunity. Frontiers in Immunology, 9 (2018) 978.

[132] Chen F, Cai W. Tumor vasculature targeting: a generally applicable approach for functionalized nanomaterials. Small, 10 (2014) 1887-93.

[133] Denekamp J. Endothelial cell proliferation as a novel approach to targeting tumour therapy. British Journal of Cancer, 45 (1982) 136-40.

[134] Pastorino F, Brignole C, Di Paolo D, Nico B, Pezzolo A, Marimpietri D, et al. Targeting liposomal chemotherapy via both tumor cell-specific and tumor vasculature-specific ligands potentiates therapeutic efficacy. Cancer Research, 66 (2006) 10073-82.

[135] Schiffelers R. Anti-tumor efficacy of tumor vasculature-targeted liposomal doxorubicin. Journal of Controlled Release, 91 (2003) 115-22.

[136] Thorpe HE, Burrows FJ. Antibody-directed targeting of the vasculature of solid tumors. Brest Cancer Research and Treatment, 36 (1995) 237-51.

[137] Haeri A, Zalba S, Ten Hagen TL, Dadashzadeh S, Koning GA. EGFR targeted thermosensitive liposomes: A novel multifunctional platform for simultaneous tumor targeted and stimulus responsive drug delivery. Colloids and surfaces B, Biointerfaces, 146 (2016) 657-69.

[138] Kullberg M, Owens JL, Mann K. Listeriolysin O enhances cytoplasmic delivery by Her-2 targeting liposomes. Journal of Drug Targeting, 18 (2010) 313-20.

[139] Negussie AH, Miller JL, Reddy G, Drake SK, Wood BJ, Dreher MR. Synthesis and in vitro evaluation of cyclic NGR peptide targeted thermally sensitive liposome. Journal of Controlled Release, 143 (2010) 265-73.

[140] Gaber MH. Modulation of doxorubicin resistance in multidrug-resistance cells by targeted liposomes combined with hyperthermia. Journal of Biochemistry, Molecular Biology, and Biophysics, 6 (2002) 309-14.

[141] Dicheva BM, Koning GA. Targeted thermosensitive liposomes: an attractive novel approach for increased drug delivery to solid tumors. Expert Opinion on Drug Delivery, 11 (2014) 83-100.

[142] Krasnici S, Werner A, Eichhorn ME, Schmitt-Sody M, Pahernik SA, Sauer B, et al. Effect of the surface charge of liposomes on their uptake by angiogenic tumor vessels. International Journal of Cancer, 105 (2003) 561-7.

[143] Campbell RB, D. F, Brown EB, Mazzola LM, Izumi Y, Jain RK, et al. Cationic Charge Determines the Distribution of Liposomes between the Vascular and Extravascular Compartments of Tumors. Cancer research, 62 (2002) 6831-6.

[144] Augustin HA, Braun K, Telemenakis I, Modlich U, Kuhn W. Phenotypic Characterization of Endothelial Cells in a Physiological Model of Blood Vessel Growth and Regression. American Journal of Pathology, 147 (1995) 339-52.

[145] Qu H, Nagy JA, Senger DR, Dvorak HF, Dvorak AM. Ultrastructural localization of vascular permeability factor/vascular endothelial growth factor (VPF/VEGF) to the abluminal plasma membrane and vesiculovacuolar organelles of tumor microvascular endothelium. The Journal of Histochemistry and Cytochemistry, 43 (1995) 381-9.

[146] Campbell RB, Ying B, Kuesters GM, Hemphill R. Fighting cancer: from the bench to bedside using second generation cationic liposomal therapeutics. Journal of Pharmaceutical Sciences, 98 (2009) 411-29.

[147] Wu J, Lee A, Lu Y, Lee RJ. Vascular targeting of doxorubicin using cationic liposomes. International Journal of Pharmaceutics, 337 (2007) 329-35.

[148] Luo D, Geng J, Li N, Carter KA, Shao S, Atilla-Gokcumen GE, et al. Vessel-Targeted Chemophototherapy with Cationic Porphyrin-Phospholipid Liposomes. Molecular Cancer Therapeutics, 16 (2017) 2452-61.

[149] Wang W, Shao A, Zhang N, Fang J, Ruan JJ, Ruan BH. Cationic Polymethacrylate-Modified Liposomes Significantly Enhanced Doxorubicin Delivery and Antitumor Activity. Scientific Reports, 7 (2017) 43036.

[150] Strieth S, Eichhorn ME, Sauer B, Schulze B, Teifel M, Michaelis U, et al. Neovascular targeting chemotherapy: encapsulation of paclitaxel in cationic liposomes impairs functional tumor microvasculature. International Journal of Cancer, 110 (2004) 117-24.

[151] Salmaso S, Caliceti P. Stealth properties to improve therapeutic efficacy of drug nanocarriers. Journal of Drug Delivery, 2013 (2013) 374252.

[152] Klibanov AL, Maruyama K, Torchilin VP, Huang L. Amphipathic polyethyleneglycols effectively prolong the circulation time of liposomes. FEBS Letters, 268 (1990) 237-51.

[153] Maruyama K, Vuda T, Okamoto A, Kojima S, Suginaka A, lwatsuru M. Prolonged circulation time in vivo of large unilamellar liposomes composed of distearoyl phosphatidylcholine and cholesterol containing amphipathic poly(ethylene glycol). Biochimica et Biophysica Acta, 1128 (1992) 44-9.

[154] Sroda K, Rydlewski J, Langner M, Kozubek A, Grzybek M, Sikorski AF. Repeated injections of PEG-PE liposomes generate anti-PEG antibodies. Cellular & Molecular Biology Letters, 10 (2005) 37-47.

[155] Mima Y, Hashimoto Y, Shimizu T, Kiwada H, Ishida T. Anti-PEG IgM Is a Major Contributor to the Accelerated Blood Clearance of Polyethylene Glycol-Conjugated Protein. Molecular Pharmaceutics, 12 (2015) 2429-35.

[156] Yang Q, Lai SK. Anti-PEG immunity: emergence, characteristics, and unaddressed questions. Wiley interdisciplinary reviews Nanomedicine and Nanobiotechnology, 7 (2015) 655-77.

[157] Richter AW, Akerblom E. Polyethylene glycol reactive antibodies in man: titer distribution in allergic patients treated with monomethoxy polyethylene glycol modified allergens or placebo,

and in healthy blood donors. International Archives of Allergy and Applied Immunology, 74 (1984) 36-9.

[158] Mohamed M, Abu Lila AS, Shimizu T, Alaaeldin E, Hussein A, Sarhan HA, et al. PEGylated liposomes: immunological responses. Science and Technology of Advanced Materials, 20 (2019) 710-24.

[159] Pozzi D, Colapicchioni V, Caracciolo G, Piovesana S, Capriotti AL, Palchetti S, et al. Effect of polyethyleneglycol (PEG) chain length on the bio-nano-interactions between PEGylated lipid nanoparticles and biological fluids: from nanostructure to uptake in cancer cells. Nanoscale, 6 (2014) 2782-92.

[160] Dan N. Effect of liposome charge and PEG polymer layer thickness on cell–liposome electrostatic interactions. Biochimica et Biophysica Acta, 1564 (2002) 343-8.

[161] Kono Y, Jinzai H, Kotera Y, Fujita T. Influence of physicochemical properties and PEG modification of magnetic liposomes on their interaction with intestinal epithelial Caco-2 cells. Biological Pharmaceuticals Bullettin, 40 (2017) 9.

[162] Majzoub RN, Chan CL, Ewert KK, Silva BF, Liang KS, Jacovetty EL, et al. Uptake and transfection efficiency of PEGylated cationic liposome-DNA complexes with and without RGD-tagging. Biomaterials, 35 (2014) 4996-5005.

[163] Kono Y, Iwasaki A, Fujita T. Effect of surface charge, particle size, and modification by polyethylene glycol of liposomes on their association with Caco-2 cells across an unstirred water layer. Die Pharmazie, 73 (2018) 3-8.

[164] Mishra S, Webster P, Davis ME. PEGylation significantly affects cellular uptake and intracellular trafficking of non-viral gene delivery particles. European Journal of Cell Biology, 83 (2004) 97-111.

[165] Holland JW, Hui C, Cullis PR, Madden TD. Poly(ethylene glycol)--lipid conjugates regulate the calcium-induced fusion of liposomes composed of phosphatidylethanolamine and phosphatidylserine. Biochemistry, 35 (1996) 2618-24.

[166] Hatakeyama H, Akita H, Harashima H. The polyethyleneglycol dilemma: advantage and disadvantage of PEGylation of liposomes for systemic genes and nucleic acids delivery to tumors. Biological Pharmaceuticals Bullettin, 36 (2013) 8.

[167] Ashok B, Arleth L, Hjelm RP, Rubinstein I, Onyuksel H. In vitro characterization of PEGylated phospholipid micelles for improved drug solubilization: effects of PEG chain length and PC incorporation. Journal of Pharmaceutical Science, 93 (2004) 2476-87.

[168] Weiden J, Tel J, Figdor CG. Synthetic immune niches for cancer immunotherapy. Nature Reviews Immunology, (2017)

[169] Cancer.net 2019. Understanding Immunotherapy, accessed 29 September 2019. https://www.cancer.net/navigating-cancer-care/how-cancer-treated/immunotherapy-and-vaccines/understanding-immunotherapy. (2019)

[170] Jiang T, Zhou C, Ren S. Role of IL-2 in cancer immunotherapy. Oncoimmunology, 5 (2016)

[171] Miller CH, Maher SG, Young HA. Clinical Use of Interferon-gamma. Annals of the New York Academy of Sciences, 1182 (2009) 69-79.

[172] Schwartz RN, Stover L, Dutcher JP. Managing toxicities of high-dose interleukin-2. Oncology, 16 (2002) 11-20.

[173] Targeted Oncology, Harris J. 2018. Immunotherapy Pioneers Allison, Honjo Awarded Nobel Prize, accessed 29 September 2019. https://www.targetedonc.com/news/immunotherapy-pioneers-allison-honjo-awarded-nobel-prize. .

[174] Leach DR, Krummel MF, Allison JP. Enhancement of antitumor immunity by CTLA-4 blockade. Science, 271 (1996) 1734-6.

[175] Ishida Y, Agata Y, Shibahara K, Honjo T. Induced expression of PD-1, a novel member of the immunoglobulin gene superfamily, upon programmed cell death. The EMBO Journal, 11 (1992) 3887-95.

[176] Hodi FS, O'Day SJ, McDermott DF, Weber RW, Sosman JA, Haanen JB, et al. Improved survival with ipilimumab in patients with metastatic melanoma. The New England Journal of Medicine, 363 (2010) 711-23.

[177] Hamid O, Robert C, Daud A, Hodi FS, Hwu WJ, Kefford R, et al. Five-year survival outcomes for patients with advanced melanoma treated with pembrolizumab in KEYNOTE-001. Annals of Oncology, 30 (2019) 582-8.

[178] Hodi FS, Chiarion-Sileni V, Gonzalez R, Grob JJ, Rutkowski P, Cowey CL, et al. Nivolumab plus ipilimumab or nivolumab alone versus ipilimumab alone in advanced melanoma (CheckMate 067): 4-year outcomes of a multicentre, randomised, phase 3 trial. The Lancet Oncology, 19 (2018) 1480-92.

[179] Feins S, Kong W, Williams EF, Milone MC, Fraietta JA. An introduction to chimeric antigen receptor (CAR) T-cell immunotherapy for human cancer. Am J Hematol, 94 (2019) S3-S9.

[180] Seimetz D, Heller K, Richter J. Approval of First CAR-Ts: Have we Solved all Hurdles for ATMPs? Cell Medicine, 11 (2019)

[181] National Cancer Institute. CAR T Cell Receptor Immunotherapy for Patients With B-cell Lymphoma. ClinicalTrialsgov NCT00924326, (2019)

[182] Novartis. Study of Efficacy and Safety of Tisagenlecleucel in HR B-ALL EOC MRD Positive Patients (CASSIOPEIA). ClinicalTrialsgov NCT03876769, (2019)

[183] Novartis. CD19 CART Long Term Follow Up (LTFU) Study. ClinicalTrialsgov NCT02445222, (2019)

[184] Corrales L, Gajewski TF. Molecular Pathways: Targeting the Stimulator of Interferon Genes (STING) in the Immunotherapy of Cancer. Clinical Cancer Research, 21 (2015) 4774-9.

[185] Brinkman JA, Fausch SC, Weber JS, Kast WM. Peptide-based vaccines for cancer immunotherapy. Expert Opinion on Biological Therapy, 4 (2004) 181-98.

[186] Cicchelero L, Denies S, Devriendt B, de Rooster H, Sanders NN. Can dendritic cells improve whole cancer cell vaccines based on immunogenically killed cancer cells? Oncoimmunology, 4 (2015) e1048413.

[187] Kawai T, Akira S. TLR signaling. Cell Death & Differentiation, 13 (2006) 816-25.

[188] Motwani M, Pesiridis S, Fitzgerald KA. DNA sensing by the cGAS-STING pathway in health and disease. Nature Reviews Genetics, (2019)

[189] Lawrence T. The nuclear factor NF-kB pathway in inflammation. Cold Spring Harbor Perspective in Biology, 1 (2009) 651-8.

[190] Swanson KV, Deng M, Ting JP. The NLRP3 inflammasome: molecular activation and regulation to therapeutics. Nature Reviews Immunology, 19 (2019) 477-89.

[191] Jang JH, Shin HW, Lee JM, Lee HW, Kim EC, Park SH. An Overview of Pathogen Recognition Receptors for Innate Immunity in Dental Pulp. Mediators of inflammation, 2015 (2015) 794143.

[192] Li T, Chen ZJ. The cGAS-cGAMP-STING pathway connects DNA damage to inflammation, senescence, and cancer. J Exp Med, 215 (2018) 1287-99.

[193] Mogensen TH. Pathogen recognition and inflammatory signaling in innate immune defenses. Clinical microbiology reviews, 22 (2009) 240-73, Table of Contents.

[194] Chow J, Franz KM, Kagan JC. PRRs are watching you: Localization of innate sensing and signaling regulators. Virology, 479-480 (2015) 104-9.

[195] Armant MA, Fenton MJ. Toll-like receptors: a family of pattern-recognition receptors in mammals. Genome Biology, 3 (2002) 3011-15.

[196] Werling D, Jann OC, Offord V, Glass EJ, Coffey TJ. Variation matters: TLR structure and species-specific pathogen recognition. Trends in Immunology, 30 (2009) 124-30.

[197] Chattopadhyay S, Sen GC. Tyrosine phosphorylation in Toll-like receptor signaling. Cytokine Growth Factor Reviews, 25 (2014) 533-41.

[198] Ishengoma E, Agaba M. Evolution of toll-like receptors in the context of terrestrial ungulates and cetaceans diversification. BMC Evolutionary Biology, 17 (2017) 54-60.

[199] Rock FL, Hardiman G, Timans JC, Kastelein RA, Bazan JF. A family of human receptors structurally related to Drosophila Toll. PNAS, 95 (1998) 588-93.

[200] Takeda K, Akira S. Toll-like receptors in innate immunity. Int Immunol, 17 (2005) 1-14.

[201] O'Neill LA, Bowie AG. The family of five: TIR-domain-containing adaptors in Toll-like receptor signalling. Nature Reviews Immunology, 7 (2007) 353-64.

[202] Leifer CA, Medvedev AE. Molecular mechanisms of regulation of Toll-like receptor signaling. Journal of Leukocyte Biology, 100 (2016) 927-41.

[203] Basith S, Manavalan B, Yoo TH, Kim SG, Choi S. Roles of toll-like receptors in cancer: a double-edged sword for defense and offense. Archives of Pharmaceutical Research, 35 (2012) 1297-316.

[204] Dajon M, Iribarren K, Cremer I. Toll-like receptor stimulation in cancer: A pro- and anti-tumor double-edged sword. Immunobiology, 222 (2017) 89-100.

[205] Fukata M, Chen A, Vamadevan AS, Cohen J, Breglio K, Krishnareddy S, et al. Toll-like receptor-4 promotes the development of colitis-associated colorectal tumors. Gastroenterology, 133 (2007) 1869-81.

[206] Shojaei H, Oberg HH, Juricke M, Marischen L, Kunz M, Mundhenke C, et al. Toll-like receptors 3 and 7 agonists enhance tumor cell lysis by human gammadelta T cells. Cancer Research, 69 (2009) 8710-7.

[207] Smits EL, Ponsaerts P, Berneman ZN, Van Tendeloo VF. The use of TLR7 and TLR8 ligands for the enhancement of cancer immunotherapy. The Oncologist, 13 (2008) 859-75.

[208] Yu L, Wang L, Chen S. Dual character of Toll-like receptor signaling: pro-tumorigenic effects and anti-tumor functions. Biochimica et Biophysica Acta, 1835 (2013) 144-54.

[209] Engel AL, Holt GE, Lu H. The pharmacokinetics of Toll-like receptor agonists and the impact on the immune system. Expert Review of Clinical Pharmacology, 4 (2011) 275-89.

[210] Braunstein MJ, Kucharczyk J, Adams S. Targeting Toll-Like Receptors for Cancer Therapy. Target Oncology, 13 (2018) 583-98.

[211] Shi C, Xiong Z, Chittepu P, Aldrich CC, Ohlfest JR, Ferguson DM. Discovery of Imidazoquinolines with Toll-Like Receptor 7/8 Independent Cytokine Induction. ACS Medicinal Chemistry Letters, 3 (2012) 501-4.

[212] European Medicines Agency n.d. Aldara, accessed 29 September 2019. https://www.ema.europa.eu/en/medicines/human/EPAR/aldara. (2008)

[213] Geisse J, Caro I, Lindholm J, Golitz L, Stampone P, Owens M. Imiquimod 5% cream for the treatment of superficial basal cell carcinoma: results from two phase III, randomized, vehicle-controlled studies. Journal of the American Academy of Dermatology, 50 (2004) 722-33.

[214] Adams S, Kozhaya L, Martiniuk F, Meng TC, Chiriboga L, Liebes L, et al. Topical TLR7 agonist imiquimod can induce immune-mediated rejection of skin metastases in patients with breast cancer. Clinical Cancer Research, 18 (2012) 6748-57.

[215] Donin NM, Chamie K, Lenis AT, Pantuck AJ, Reddy M, Kivlin D, et al. A phase 2 study of TMX-101, intravesical imiquimod, for the treatment of carcinoma in situ bladder cancer. Urologic Oncology, 35 (2017) 39 e1- e7.

[216] Drobits B, Holcmann M, Amberg N, Swiecki M, Grundtner R, Hammer M, et al. Imiquimod clears tumors in mice independent of adaptive immunity by converting pDCs into tumor-killing effector cells. Journal of Clinical Investigation, 122 (2012) 575-85.

[217] Tomai MA, Gibson SJ, Imbertson LM, Miller RL, Myhre PE, Reiter MJ, et al. Immunomodulating and antiviral activities of the imidazoquinoline S-28463. Antiviral Research, 28 (1995) 253-64.

[218] Burns RP, Jr., Ferbel B, Tomai M, Miller R, Gaspari AA. The imidazoquinolines, imiquimod and R-848, induce functional, but not phenotypic, maturation of human epidermal Langerhans' cells. Clinical Immunology, 94 (2000) 13-23.

[219] Wagner TL, Horton VL, Carlson GL, Myhre PE, Gibson SJ, Imbertson LM, et al. Induction of cytokines in cynomolgus monkeys by the immune response modifiers, imiquimod, S-27609 and S-28463. Cytokine, 9 (1997) 837-45.

[220] Manicassamy S, Pulendran B. Modulation of adaptive immunity with Toll-like receptors. Seminars in Immunology, 21 (2009) 185-93.

[221] Singh M, Khong H, Dai Z, Huang XF, Wargo JA, Cooper ZA, et al. Effective innate and adaptive antimelanoma immunity through localized TLR7/8 activation. Journal of Immunology, 193 (2014) 4722-31.

[222] Hengge UR, Benninghoff B, Ruzicka T, Goos M. Topical immunomodulators--progress towards treating inflammation, infection, and cancer. The Lancet Infectious Diseases, 1 (2001) 189-98.

[223] Meyer T, Surber C, French LE, Stockfleth E. Resiquimod, a topical drug for viral skin lesions and skin cancer. Expert Opinion on Investigational Drugs, 22 (2013) 149-59.

[224] Michaelis KA, Norgard MA, Zhu X, Levasseur PR, Sivagnanam S, Liudahl SM, et al. The TLR7/8 agonist R848 remodels tumor and host responses to promote survival in pancreatic cancer. Nature Communications, 10 (2019) 4682.

[225] Rook AH, Gelfand JM, Wysocka M, Troxel AB, Benoit B, Surber C, et al. Topical resiquimod can induce disease regression and enhance T-cell effector functions in cutaneous T-cell lymphoma. Blood, 126 (2015) 1452-61.

[226] Gunzer M, Riemann H, Basoglu Y, Hillmer A, Weishaupt C, Balkow S, et al. Systemic administration of a TLR7 ligand leads to transient immune incompetence due to peripheral-blood leukocyte depletion. Blood, 106 (2005) 2424-32.

[227] Bourquin C, Hotz C, Noerenberg D, Voelkl A, Heidegger S, Roetzer LC, et al. Systemic cancer therapy with a small molecule agonist of toll-like receptor 7 can be improved by circumventing TLR tolerance. Cancer Research, 71 (2011) 5123-33.

[228] Dudek AZ, Yunis C, Harrison LI, Kumar S, Hawkinson R, Cooley S, et al. First in human phase I trial of 852A, a novel systemic toll-like receptor 7 agonist, to activate innate immune responses in patients with advanced cancer. Clinical Cancer Research, 13 (2007) 7119-25.

[229] Harrison LI, Astry C, Kumar S, Yunis C. Pharmacokinetics of 852A, an imidazoquinoline Toll-like receptor 7-specific agonist, following intravenous, subcutaneous, and oral administrations in humans. Journal of Clinical Pharmacology, 47 (2007) 962-9.

[230] Bristol-Myers Squibb. SD-101 and BMS-986178 in Treating Patients With Advanced or Metastatic Solid Malignancies. ClinTrialsGov NCT03831295,

[231] Medimmune LLC. A Study of MEDI9197 in Subjects With Solid Tumors or CTCL and in Combination With Durvalumab and/or Palliative Radiation in Subjects With Solid Tumors. . ClinTrialsGov NCT02556463,

[232] Peine KJ, Gupta G, Brackman DJ, Papenfuss TL, Ainslie KM, Satoskar AR, et al. Liposomal resiquimod for the treatment of Leishmania donovani infection. The Journal of Antimicrobial Chemotherapy, 69 (2014) 168-75.

[233] Widmer J, Thauvin C, Mottas I, Nguyen VN, Delie F, Allemann E, et al. Polymer-based nanoparticles loaded with a TLR7 ligand to target the lymph node for immunostimulation. International Journal of Pharmaceutics, 535 (2017) 444-51.

[234] Chen Q, Xu L, Liang C, Wang C, Peng R, Liu Z. Photothermal therapy with immune-adjuvant nanoparticles together with checkpoint blockade for effective cancer immunotherapy. Nature Communications, 7 (2016) 13193.

[235] Rodell CB, Arlauckas SP, Cuccarese MF, Garris CS, Li R, Ahmed MS, et al. TLR7/8-agonist-loaded nanoparticles promote the polarization of tumour-associated macrophages to enhance cancer immunotherapy. Nature Biomedical Engineering, 2 (2018) 11-8.

[236] Cancer Research Institute n.d. Immunotherapy, timeline of progress. Accessed 29 September 2019. https://www.cancerresearch.org/immunotherapy/timeline-of-progress. .

[237] Ngwa W, Irabor OC, Schoenfeld JD, Hesser J, Demaria S, Formenti SC. Using immunotherapy to boost the abscopal effect. Nature Reviews Cancer, 18 (2018) 313-22.

[238] Miranda Poma J, Ostios Garcia L, Villamayor Sanchez J, D'Errico G. What do we know about cancer immunotherapy? Long-term survival and immune-related adverse events. Allergologia et Immunopathologia, 47 (2019) 303-8.

[239] Chan TA, Yarchoan M, Jaffee E, Swanton C, Quezada SA, Stenzinger A, et al. Development of tumor mutation burden as an immunotherapy biomarker: utility for the oncology clinic. Annals of Oncology, 30 (2019) 44-56.

[240] Kumpers C, Jokic M, Haase O, Offermann A, Vogel W, Gratz V, et al. Immune Cell Infiltration of the Primary Tumor, Not PD-L1 Status, Is Associated With Improved Response to Checkpoint Inhibition in Metastatic Melanoma. Frontiers in Medicine, 6 (2019) 27.

[241] Galon J, Costes A, Sanchez-Cabo F, Kirilovsky A, Mlecnik B, Lagorce-Pages C, et al. Type, density, and location of immune cells within human colorectal tumors predict clinical outcome. Science, 313 (2006) 1960-4.

[242] Galon J, Bruni D. Approaches to treat immune hot, altered and cold tumours with combination immunotherapies. Nature Reviews Drug Discovery, 18 (2019) 197-218.

[243] Bonaventura P, Shekarian T, Alcazer V, Valladeau-Guilemond J, Valsesia-Wittmann S, Amigorena S, et al. Cold Tumors: A Therapeutic Challenge for Immunotherapy. Frontiers in Immunology, 10 (2019)

[244] Skitzki JJ, Repasky EA, Evans SS. Hyperthermia as an immunotherapy strategy for cancer. . Current Opinion in Investigational Drugs 10 (2009) 9.

[245] Haran G, Cohen R, Bar LK, Barenholz Y. Transmembrane ammonium sulfate gradients in liposomes produce efficient and stable entrapment of amphipathic weak bases. Biochimica et Biophysica Acta, 1151 (1993) 201-15.

[246] Eibl H, Lands WEM. A new, sensitive determination of phosphate. Analytical Biochemistry, 30 (1969) 51-7.

[247] Dittmer JC, Lester RL. A simple, specific spray for the detection of phospholipids on thin-layer chromatograms. Journal of Lipid Research, 5 (1964) 126-7.

[248] Baron CB, Coburn RF. Comparison of two copper reagents for detection of saturated and unsaturated neutral lipids by charring densitometry. Journal of Liquid Chomatography, 7(1984) 8.

[249] Holzer M, Barnert S, Momm J, Schubert R. Preparative size exclusion chromatography combined with detergent removal as a versatile tool to prepare unilamellar and spherical liposomes of highly uniform size distribution. Journal of Chromatography A, 1216 (2009) 5838-48.

[250] Palchetti S, Colapicchioni V, Digiacomo L, Caracciolo G, Pozzi D, Capriotti AL, et al. The protein corona of circulating PEGylated liposomes. Biochimica et Biophysica Acta, 1858 (2016) 189-96.

[251] Vichai V, Kirtikara K. Sulforhodamine B colorimetric assay for cytotoxicity screening. Nature Protocols, 1 (2006) 1112-6.

[252] Bonvalot S, Le Pechoux C, De Baere T, Kantor G, Buy X, Stoeckle E, et al. First-in-Human Study Testing a New Radioenhancer Using Nanoparticles (NBTXR3) Activated by Radiation Therapy in Patients with Locally Advanced Soft Tissue Sarcomas. Clinical Cancer Research, 23 (2017) 908-17.

[253] Regelin AE, Fankhaenel S, Gurtesch L, Prinz C, von Kiedrowski G, Massing U. Biophysical and lipofection studies of DOTAP analogs. Biochimica et Biophysica Acta, 1464 (2000) 151-64.

[254] Dicheva BM, ten Hagen TL, Schipper D, Seynhaeve AL, van Rhoon GC, Eggermont AM, et al. Targeted and heat-triggered doxorubicin delivery to tumors by dual targeted cationic thermosensitive liposomes. Journal of Controlled Release 195 (2014) 37-48.

[255] Caracciolo G. Liposome-protein corona in a physiological environment: challenges and opportunities for targeted delivery of nanomedicines. Nanomedicine, 11 (2015) 543-57.

[256] Kneidl B. Formulation studies, lyophilization and *in vivo* investigation of 1,2-dipalmitoyl-sn-glycero-3-phosphodiglycerol-based thermosensitive liposomes for the delivery of gemcitabine, irinotecan and SN-38. Dissertation, (2017)

[257] Laznicek M, Laznickova A. The effect of lipophilicity on the protein binding and blood cell uptake of some acidic drugs. Journal of Pharmaceutical and Biomedical Analysis, 13 (1995) 823-8.

[258] Duong AD, Collier MA, Bachelder EM, Wyslouzil BE, Ainslie KM. One Step Encapsulation of Small Molecule Drugs in Liposomes via Electrospray-Remote Loading. Molecular Pharmaceutic, 13 (2016) 92-9.

[259] Grit M, Crommelin DJ. Chemical stability of liposomes: implications for their physical stability. Chemistry and Physics of Lipids, 64 (1993) 3-18.

[260] Fransen GJ, Salemink PJM, Crommelin DJA. Critial parameters in freezing of liposomes. International Journal of Pharmaceutics, 33 (1986) 8.

[261] Wei X, Shamrakov D, Nudelman S, Peretz-Damari S, Nativ-Roth E, Regev O, et al. Cardinal Role of Intraliposome Doxorubicin-Sulfate Nanorod Crystal in Doxil Properties and Performance. ACS Omega, 3 (2018) 2508-17.

[262] Tovar Z, Dauphinee M, Talal N. Synergistic interaction between anti-CD3 and IL-2 demonstrated by proliferative response, interferon production, and non-MHC-restricted killing. Cellular Immunology, 117 (1988) 12-21.

[263] Jerome KR, Sloan DD, Aubert M. Measurement of CTL-induced cytotoxicity: the caspase 3 assay. Apoptosis, 8 (2003) 563-71.

[264] Wolf BB, Schuler M, Echeverri F, Green DR. Caspase-3 Is the Primary Activator of Apoptotic DNA Fragmentation via DNA Fragmentation Factor-45/Inhibitor of Caspase-activated DNase Inactivation. The Journal of Biological Chemistry, 274 (1999) 6.

[265] Miller CR, Bondurant B, McLean SD, McGovern KA, O'Brien DF. Liposome-cell interactions in vitro: effect of liposome surface charge on the binding and endocytosis of conventional and sterically stabilized liposomes. Biochemistry, 37 (1998) 9.

[266] Gurtovenko AA, Patra M, Karttunen M, Vattulainen I. Cationic DMPC/DMTAP lipid bilayers: molecular dynamics study. Biophysical Journal, 86 (2004) 3461-72.

[267] Webb MS, Saxon D, Wong FM, Lim HJ, Wang Z, Bally MB, et al. Comparison of different hydrophobic anchors conjugated to poly(ethylene glycol): effects on the pharmacokinetics of liposomal vincristine. Biochimica et Biophysica Acta, 1372 (1998) 272-82.

[268] Labouta HI, Gomez-Garcia MJ, Sarsons CD, Nguyen T, Kennard J, Ngo W, et al. Surface-grafted polyethylene glycol conformation impacts the transport of PEG-functionalized liposomes through a tumour extracellular matrix model. RSC Advances, 8 (2018) 7697-708.

[269] Song LY, Ahkong QF, Rong Q, Wang Z, Ansell S, Hope MJ, et al. Characterization of the inhibitory effect of PEG-lipid conjugates on the intracellular delivery of plasmid and antisense DNA mediated by cationic lipid liposomes. Biochimica et Biophysica Acta, 1558 (2002) 13.

[270] Salvati A, Pitek AS, Monopoli MP, Prapainop K, Bombelli FB, Hristov DR, et al. Transferrin-functionalized nanoparticles lose their targeting capabilities when a biomolecule corona adsorbs on the surface. Nature Nanotechnology, 8 (2013) 137-43.

[271] Palchetti S, Caputo D, Digiacomo L, Capriotti AL, Coppola R, Pozzi D, et al. Protein Corona Fingerprints of Liposomes: New Opportunities for Targeted Drug Delivery and Early Detection in Pancreatic Cancer. Pharmaceutics, 11 (2019)

[272] Troutier A, Ve´ron L, Delair T, Pichot C, Ladavie`re C. New Insights into Self-Organization of a Model Lipid Mixture and Quantification of Its Adsorption on Spherical Polymer Particles. Langmuir, 21 (2005) 10.

[273] Hossann M, Wang T, Wiggenhorn M, Schmidt R, Zengerle A, Winter G, et al. Size of thermosensitive liposomes influences content release. Journal of Controlled Release, 147 (2010) 436-43.

[274] Lindner LH, Hossann M, Vogeser M, Teichert N, Wachholz K, Eibl H, et al. Dual role of hexadecylphosphocholine (miltefosine) in thermosensitive liposomes: active ingredient and mediator of drug release. Journal of Controlled Release, 125 (2008) 112-20.

[275] Chonn A, Cullis PR, Devine DV. The role of surface charge in the activation of the classical and alternative pathways of complement by liposomes. Journal of Immunology, 146 (1991) 4234-41.

[276] Semple SC, Chonn A, Cullis PR. Interactions of liposomes and lipid-based carrier systems with blood proteins: relation to clearance behaviour in vivo. Advanced Drug Delivery Reviews, 32 (1988) 3-17.

[277] Shan X, Yuan Y, Liu C, Tao X, Sheng Y, Xu F. Influence of PEG chain on the complement activation suppression and longevity in vivo prolongation of the PCL biomedical nanoparticles. Biomedical Microdevices, 11 (2009) 1187-94.

[278] Zhao W, Zhuang S, Qi XR. Comparative study of the in vitro and in vivo characteristics of cationic and neutral liposomes. International Journal of Nanomedicine, 6 (2011) 3087-98.

[279] Dicheva BM, Seynhaeve AL, Soulie T, Eggermont AM, Ten Hagen TL, Koning GA. Pharmacokinetics, Tissue Distribution and Therapeutic Effect of Cationic Thermosensitive Liposomal Doxorubicin Upon Mild Hyperthermia. Pharmaceutical Research, 33 (2016) 627-38.

[280] Koshy ST, Cheung AS, Gu L, Graveline AR, Mooney DJ. Liposomal Delivery Enhances Immune Activation by STING Agonists for Cancer Immunotherapy. Advanced Biosystem 1(2017)

[281] Lammers T, Peschke P, Kuhnlein R, Subr V, Ulbrich K, Huber P, et al. Effect of intratumoral injection on the biodistribution and the therapeutic potential of HPMA copolymer-based drug delivery systems. Neoplasia, 8 (2006) 788-95.

[282] Tomai MA, Gibson SJ, Imbertson LM, Miller RL, Myhre PE, Reiter MJ, et al. Immunomodulating and antiviral activities of the imidazoquinoline S-28463. Antiviral Research, 28 (1995) 253-64.

[283] SciFinder v. Chemical Abstarct Service: Columbus, OH, 2007. CAS 144875-48-9, Resiquimod. Accessed 17 October 2019.

[284] SciFinder v. Chemical Abstracts Service: Columbus, OH, 2007. CAS 99011-02-6, Imiquimod. Accessed 17 October 2019.

[285] Rysin A. Investigation of lipophilic chemotherapeutics and high-molecular weight compunds for the local delivery by phosphatidyldiglycerol-based thermosensitive liposomes. Dissertation, (2019)

[286] Chou TH, Chen SC, Chu IM. Effect of composition on the stability of liposomal irinotecan prepared by a pH gradient method. Journal of Bioscience and Bioengineering, 95 (2003) 405-8.

[287] Budweiser J. Hydrolyseverhalten der synthetischen Phospholipide DPPGx (x=1,2,3) im Vergleich zu DPPC in thermosensitiven Liposomen. Dissertation (2015)

[288] Fritze A, Hens F, Kimpfler A, Schubert R, Peschka-Suss R. Remote loading of doxorubicin into liposomes driven by a transmembrane phosphate gradient. Biochimica et Biophysica Acta, 1758 (2006) 1633-40.

[289] Dos Santos N, Cox KA, McKenzie CA, van Baarda F, Gallagher RC, Karlsson G, et al. pH gradient loading of anthracyclines into cholesterol-free liposomes: enhancing drug loading rates through use of ethanol. Biochimica et Biophysica Acta, 1661 (2004) 47-60.

[290] Crommelin DJ, van Bommel EMG. Stability of liposome on storage: freeze dried, frozen or as an aqueous dispersion. Pharmaceutical Research, 1 (1984) 5.

[291] Sriwongsitanont S, Ueno M. Effect of Freeze-Thawing Process on the Size and Lamellarity of PEG-Lipid Liposomes. The Open Colloid Science Journal, 4 (2011) 6.

[292] Koster KL, Webb MS, Bryant G, Lynch DL. Interactions between soluble sugars and POPC (1-palmitoyl-2-oleoylphosphatidylcholine) during dehydration: vitrification of sugars alters the phase behavior of the phospholipid. Biochimica et Biophysica Acta, 1193 (1994) 7.

[293] Sun WQ, Leopold AC, Crowe LM, Crowe JH. Stability of Dry Liposomes in Sugar Glasses. Biophysical Journal 70 (1996) 8-15.

[294] Mills JK, Needham D. Lysolipid incorporation in dipalmitoylphosphatidylcholine bilayer membranes enhances the ion permeability and drug release rates at the membrane phase transition. Biochimica et Biophysica Acta, 1716 (2005) 77-96.

[295] Joubert MK, Deshpande M, Yang J, Reynolds H, Bryson C, Fogg M, et al. Use of In Vitro Assays to Assess Immunogenicity Risk of Antibody-Based Biotherapeutics. PloS one, 11 (2016) 159-67.

[296] Corkum CP, Ings DP, Burgess C, Karwowska S, Kroll W, Michalak TI. Immune cell subsets and their gene expression profiles from human PBMC isolated by Vacutainer Cell Preparation Tube (CPT) and standard density gradient. BMC Immunology, 16 (2015) 48-57.

[297] van Horssen R, Ten Hagen TL, Eggermont AM. TNF-alpha in cancer treatment: molecular insights, antitumor effects, and clinical utility. The Oncologist, 11 (2006) 397-408.

[298] Park SJ, Nakagawa T, Kitamura H, Atsumi T, Kamon H, Sawa S, et al. IL-6 regulates in vivo dendritic cell differentiation through STAT3 activation. Journal of Immunology, 173 (2004) 3844-54.

[299] Hamm S, Rath S, Michel S, Baumgartner R. Cancer immunotherapeutic potential of novel small molecule TLR7 and TLR8 agonists. Journal of Immunotoxicology, 6 (2009) 257-65.

[300] Thomas A, Laxton C, Rodman J, Myangar N, Horscroft N, Parkinson T. Investigating Toll-Like Receptor Agonists for Potential To Treat Hepatitis C Virus Infection. Antimicrobial Agents and Chemotherapy, 51 (2007) 2969-78.

[301] Ma Y, Poisson L, Sanchez-Schmitz G, Pawar S, Qu C, Randolph GJ, et al. Assessing the immunopotency of Toll-like receptor agonists in an in vitro tissue-engineered immunological model. Immunology, 130 (2010) 374-87.

[302] Zhao W, An H, Zhou J, Xu H, Yu Y, Cao X. Hyperthermia differentially regulates TLR4 and TLR2-mediated innate immune response. Immunology Letters, 108 (2007) 137-42.

[303] Bessler H, Djaldetti M. High Temperature Affects Cytokine Release by Human Peripheral Blood Mononuclear Cells. International Journal of Immunology and Immunotherapy, 2 (2015) 4-10.

[304] Huang YH, Haegerstrand A, Frostega JRD. Effects of in vitro hyperthermia on proliferative responses and lymphocyte activity Clinical & Experimental Immunology, 103 (1996) 67-74.

[305] Ciavarra RP, Simeone A. T lymphocyte stress response: I. Induction of heat shock protein synthesis at febrile temperatures is correlated with enhanced resistance to hyperthermic stress but not to heavy metal toxicity or dexamethasone-induced immunosuppression. Cellular Immunology, 129 (1990) 363-76.

[306] Goodier MR, Londei M. Lipopolysaccharide Stimulates the Proliferation of Human CD56$^+$CD3$^-$ NK Cells: A Regulatory Role of Monocytes and IL-10. The Journal of Immunology, 165 (2000) 139-47.

[307] Wang D, Song B, Zhong X, Sun XF, Fan Y. Phytohaemagglutinin stimulates the proliferation of peripheral blood mononuclear cells and expression of secretory cytokines. Chinese Journal of Tissue Engineering Research, 18 (2014) 3707-14.

[308] Bekeredjian-Ding IB, Wagner M, Hornung V, Giese T, Schnurr M, Endres S, et al. Plasmacytoid Dendritic Cells Control TLR7 Sensitivity of Naive B Cells via Type I IFN. The Journal of Immunology, 174 (2005) 4043-50.

[309] Biffen M, Matsui H, Edwards S, Leishman AJ, Eiho K, Holness E, et al. Biological characterization of a novel class of toll-like receptor 7 agonists designed to have reduced systemic activity. British Journal of Pharmacology, 166 (2012) 573-86.

[310] Stathopoulos A, Pretto C, Deveillers L, Pierre D, Jadus MR, Chen TC, et al. Development of immune memory to glial brain tumors after tumor regression induced by immunotherapeutic Toll-like receptor 7/8 activation. Oncoimmunology, 2 (2012) 9-15.

[311] Stary G, Bangert C, Tauber M, Strohal R, Kopp T, Stingl G. Tumoricidal activity of TLR7/8-activated inflammatory dendritic cells. Journal of Experimental Medicine, 204 (2007) 1441-51.

[312] James NE, Oliver MT, Ribeiro JR, Cantillo E, Rowswell-Turner RB, Kim K-K, et al. Human Epididymis Secretory Protein 4 (HE4) Compromises Cytotoxic Mononuclear Cells via Inducing Dual Specificity Phosphatase 6. Frontiers in Pharmacology, 10 (2019) 1456-67.

[313] Sui M, Si L, Xu T, Cui M. Establishment of specific cytotoxic T lymphocyte culture system and its inhibitory effect on ovarian cancer. Oncology Letters, 12 (2016) 4087-93.

[314] Pufnock JS, Cigal M, Rolczynski LS, Andersen-Nissen E, Wolfl M, McElrath MJ, et al. Priming CD8+ T cells with dendritic cells matured using TLR4 and TLR7/8 ligands together enhances generation of CD8+ T cells retaining CD28. Blood, 117 (2011) 6542-51.

[315] Martinez-Lostao L, Anel A, Pardo J. How Do Cytotoxic Lymphocytes Kill Cancer Cells? Clinical cancer research : an official journal of the American Association for Cancer Research, 21 (2015) 5047-56.

[316] Metkar SS, Wang B, Ebbs ML, Kim JH, Lee YJ, Raja SM, et al. Granzyme B activates procaspase-3 which signals a mitochondrial amplification loop for maximal apoptosis. Journal of Cell Biology, 160 (2003) 875-85.

[317] Metkar SS, Wang B, Ebbs ML, Kim JH, Lee YJ, Raja SM, et al. Granzyme B activates procaspase-3 which signals a mitochondrial amplification loop for maximal apoptosis. Journal of Cell Biology, 160 (2003) 875-85.

[318] Allen TM, Hansen C, Martin F, Redemann C, Yau-Young A. Liposomes containing synthetic lipid derivatives of poly(ethylene glycol) show prolonged circulation half-lives in vivo. Biochimica et Biophysica Acta, 1066 (1991) 29-36.

[319] Limmer S. Zielgerichtete Chemotherapie solider Tumoren durch thermosensitive Liposomen in Kombination mit Doxorubicin, Gemcitabin und Mitomycin C. Dissertation, (2014)

[320] Hallett FR, Marsh J, Nickel BG, Wood JM. Mechanical properties of vesicles II. A model for osmotic swelling and lysis. Biophysical Journal, 64 (1993) 7-15.

[321] Manome Y, Suzuki D, Mochizuki A, Saito E, Sasa K, Yoshimura K, et al. The inhibition of malignant melanoma cell invasion of bone by the TLR7 agonist R848 is dependent upon pro-inflammatory cytokines produced by bone marrow macrophages. Oncotarget, 9 (2018) 29934-43-50.

[322] Bulbake U, Doppalapudi S, Kommineni N, Khan W. Liposomal Formulations in Clinical Use: An Updated Review. Pharmaceutics, 9 (2017) 1345-53.

[323] Judson I, Radford JA, Harris M, Blay YI, van Hoesel Q, le Cesne A, et al. Randomized Phase II trial of pegylated liposomal doxorubicin (DOXIL®, CAELIX®) versus doxorubicin in the treatment of advanced or metastatic soft tissue sarcoma: a study by the EORTC soft tissue sarcoma group. European Journal of Cancer, 37 (2001) 7-15.

[324] Kneidl B, Peller M, Winter G, Lindner LH, Hossann M. Thermosensitive liposomal drug delivery systems: state of the art review. International Journal of Nanomedicine, 9 (2014) 4387-98-103.

[325] Nardecchia S, Sanchez-Moreno P, Vicente J, Marchal JA, Boulaiz H. Clinical Trials of Thermosensitive Nanomaterials: An Overview. Nanomaterials, 9 (2019) 451-9.

[326] Mehlen P, Puisieux A. Metastasis: a question of life or death. Nature Reviews Cancer, 6 (2006) 449-58.

[327] Turashvili G, Brogi E. Tumor Heterogeneity in Breast Cancer. Frontiers in Medicine, 4 (2017) 227-33.

[328] Mullins SR, Vasilakos JP, Deschler K, Grigsby I, Gillis P, John J, et al. Intratumoral immunotherapy with TLR7/8 agonist MEDI9197 modulates the tumor microenvironment leading to enhanced activity when combined with other immunotherapies. Journal for ImmunoTherapy of Cancer, 7 (2019) 244-50.

[329] Aduro Biotech i. Efficacy and Safety Trial of ADU-S100 and Pembrolizumab in Head and Neck Cancer. ClinTrialsGov NCT03937141,

[330] Merck Sharp & Dohme Corp. Study of MK-1454 Alone or in Combination With Pembrolizumab (MK-3475) in Participants With Advanced/Metastatic Solid Tumors or Lymphomas (MK-1454-001). ClinTrialsGov NCT03010176,

[331] Fancello L, Gandini S, Pelicci PG, Mazzarella L. Tumor mutational burden quantification from targeted gene panels: major advancements and challenges. Journal for ImmunoTherapy of Cancer, 7 (2019) 183-90.

[332] Bonaventura P, Shekarian T, Alcazer V, Valladeau-Guilemond J, Valsesia-Wittmann S, Amigorena S, et al. Cold Tumors: A Therapeutic Challenge for Immunotherapy. Frontiers in Immunology, 10 (2019) 1387-94.

[333] Serrano-del Valle A, Anel A, Naval J, Marzo I. Immunogenic Cell Death and Immunotherapy of Multiple Myeloma. Frontiers in Cell and Developmental Biology, 7 (2019) 149-56.

[334] Casares N, Pequignot MO, Tesniere A, Ghiringhelli F, Roux S, Chaput N, et al. Caspase-dependent immunogenicity of doxorubicin-induced tumor cell death. The Journal of Experimental Medicine, 202 (2005) 1691-701.

[335] Wang YJ, Fletcher R, Yu J, Zhang L. Immunogenic effects of chemotherapy-induced tumor cell death. Genes and Disease, 5 (2018) 194-203.

[336] Voorwerk L, Slagter M, Horlings HM, Sikorska K, van de Vijver KK, de Maaker M, et al. Immune induction strategies in metastatic triple-negative breast cancer to enhance the sensitivity to PD-1 blockade: the TONIC trial. Nature Medicine, 25 (2019) 920-8.

[337] Celsion. A Phase I Study of Lyso-thermosensitive Liposomal Doxorubicin and MR-HIFU for Pediatric Refractory Solid Tumors. CLinTrialsGov NCT02536183,

[338] Pahk KJ, Shin C-H, Bae IY, Yang Y, Kim S-H, Pahk K, et al. Boiling Histotripsy-induced Partial Mechanical Ablation Modulates Tumour Microenvironment by Promoting Immunogenic Cell Death of Cancers. Scientific Reports, 9 (2019) 9050-60.

[339] van den Bijgaart RJ, Eikelenboom DC, Hoogenboom M, Futterer JJ, den Brok MH, Adema GJ. Thermal and mechanical high-intensity focused ultrasound: perspectives on tumor ablation, immune effects and combination strategies. Cancer immunology, Immunotherapy, 66 (2017) 247-58.

8.2 List of abbreviations

Abs	Antibodies
ACN	Acetonitrile
AP	Ammonium phosphate
AS	Ammonium sulfate
API	Active pharmaceutical ingredient
AUC	Area-under the curve
BCC	Basal cell carcinoma
BD	Biodistribution
BSA	Bovine serum albumin
CAD	Charged-aerosol detector
CAR-T	Chimeric antigens receptors T-cells
CF	Carboxyfluorescein
CPT-11	Irinotecan
Cryo-TEM	Cryo-transmission electron microscopy
CTCL	Cutaneous T-cell lymphoma
CTL	Cytotoxic-T lymphocytes
CTSL	Cationic thermosensitive liposomes
DAD	Diode-array detector
DAMP	Damages-associated molecular pattern
DAU	Daunorubicin
DC	Dendritic cell
DC-Chol	3ß-[N-(N',N'-dimethylaminoethane)-carbamoyl]- cholesterol
DDS	Drug delivery system
dFdC	Gemcitabine
DLS	Dynamic light scattering
DMTAP	1,2-dimyristoyl-3-trimethylammonium-propane
DOX	Doxorubicin
DPPC	1,2-dipalmitoyl-sn-glycero-3-phosphocholine
DPPG$_2$	1,2-dipalmitoyl-sn-gylcero-3-phospho-di-glycerol
DPTAP	1,2-dipalmitoyl-3-trimethylammonium-propane
DSC	Dynamic scanning calorimetry
DSPC	1,2-distearoyl-sn-glycero-3-phosphocholine
DSTAP	1,2-stearoyl-3-trimethylammonium-propane
EE	Encapsulation efficacy
ELISA	Enzyme-linked immunosorbent assay

Em	Emission
EPR	Enhanced permeability and retention
Ex	Excitation
FACS	Fluorescence-activated cell sorting
FCS	Fetal calf serum
HBS	Hepes-buffered saline
HPLC	High-performance liquid chromatography
HT	Hyperthermia
HUVEC	Human umbilical veins endothelial cell
IAV	Immunoadjuvant
ID	Injected dose
IFN	Interferon
IL	Interleukin
ICG	Immunogenic cell death
irAE	Immune-related adverse effect
IRM	Immune-response modifiers
IS	Immunoscore
LPS	Lipopolysaccharides
LTSL	Low-temperature thermosensitive liposome
MHC	Major histocompatibility complex
MLV	Multi-lamellar vesicle
MPS	Macrophages phagocytic system
MR-HIFU	Magnetic resonance guided high intensity focused ultrasound
NBD	7-nitro-2-1,3 benzoxadiazol-4-yl
NP	Nanoparticles
NT	Normothermia
PAMP	Pathogen-associated molecular pattern
PBMC	Peripheral blood mononuclear cell
PBS	Phosphate-buffered saline
PC	Phosphocholine
PDI	Poly-dispersity index
PEG	Poly-ethylen glycole
PEG-CTSL	PEG-based cationic thermosensitive liposomes
PFA	Paraformaldehyde
PG_2-CTSL	$DPPG_2$-based cationic thermosensitive liposomes
PK	Pharmacokinetic

PRR	Pathogen-recognition receptor
R837	Imiquimod
R848	Resiquimod
RES	Reticuloendothelial system
Rho	Rhodamine
RFA	Radiofrequency ablation
RT	Room temperature
SD	Standard deviation
SDS	Sodium-dodecyl sulfate
SPE	Solid-phase extraction
SRB	Sulforhodamine assay
t_α	Half-life
TAA	Tumor-associated antigen
TEC	Tumor endothelial cell
TLC	Thin-layer chromatography
TLR	Toll-like receptor
TMB	Tumor mutational burden
TME	Tumor microenvironment
T_m	Phase transition temperature
TNF	Tumor-necrosis factor
TAP	Trimethyl-ammonium propane
TSL	Thermosensitive liposome
ζ -Potential	Zeta-potential

8.3 List of figures

8.4 List of tables

8.5 List of publications

Publications

1. **Liposomes for hyperthermia triggered drug release**

   W. J. M. Lokerse, B. Kneidl, A. Rysin, **M. Petrini**, L. H. Lindner

   CHAPTER 6 Liposomes for hyperthermia triggered drug release, Theranostics and Image Guided Drug Delivery, The Royal Society of Chemistry, 2018, pp. 137-163.

2. **Effects of surface charge and PEGylation on liposome-cell interactions and local drug delivery to solid tumors via thermosensitive liposomes**

   M. Petrini, W. J. M. Lokerse, A. Mach, M. Hossann, O. M. Merkel, L. H. Lindner

3. **Heat-inducible mesenchymal stem cell-mediated sodium iodide symporter (NIS) theranostic gene therapy**

   M. Tutter, C. Schug, K. A. Schmohl, S. Urnauer, N. Schwenk, **M. Petrini**, W. J. Lokerse, C. Zach, S. Ziegler, P. Bartenstein, W. Weber, L. H. Lindner, P. J. Nelson, C. Spitzweg

Manuscripts to be submitted after finalization of patentability analysis (2), or currently under submission (3).

Oral presentations

1. **Comparison of different cationic and anionic thermosensitive liposome encapsulating DOX for solid tumor targeting**

   M. Petrini, W. J. M. Lokerse, M. Hossann, O. M. Merkel, L. H. Lindner

   Oberjoch (Allgäu), 26th Mountain and Sea International Liposomes Workshop, October 2017

2. **Thermosensitive liposomes for targeted drug delivery based on focused ultrasound – Overview on consortium (BMBF-Biotransporter)**

   M. Petrini, A. Rysin, W. Lokerse, H. Gruell, J.C. Gomez, L. Sebeke, S. Ekdawi, E. Heijman, G. Shakirin, B. Wedmann, M. Hossann, P. Schweizer, L.H. Lindner

   Herrsching, 21. Wissenschaftliches Symposium der Medizinischen Klinik und Poliklinik III, July 2019

Poster Presentations

1. **Cationic and anionic thermosensitive liposomes on cancer cell targeting** *in vitro*

   M. Petrini, W. J. M. Lokerse, M. Hossann, O. M. Merkel, L. H. Lindner

   Herrsching, 18. Wissenschaftliches Symposium der Medizinischen Klinik und Poliklinik III, July 2016

2. **Feasibility and comparison of different cationic and anionic thermosensitive liposome formulations on binding efficacy**

   M. Petrini, W. J. M. Lokerse, M. Hossann, O. M. Merkel, L. H. Lindner

   Cologne, 11th European Molecular Imaging Meeting, April 2017

3. **Solid tumor angiogenesis targeting: comparative study of different cationic and anionic thermosensitive liposomes**

   M. Petrini, W. J. M. Lokerse, M. Hossann, O. M. Merkel, L. H. Lindner

   Athens, International Liposome Society and Liposome Research days combined conference, September 2017

4. **Feasibility of tumor vessel targeting: comparative study of different cationic and anionic thermosensitive liposomes**

   M. Petrini, W. J. M. Lokerse, A. Mach, M. Hossann, O. M. Merkel, L. H. Lindner

   Berlin, 32nd Annual Meeting European Society of Hyperthermic Oncology, May 2018

Acknowledgements

My deepest gratitude goes to my family, especially my parents and my sister, for all this years of support while I am abroad, and for making me feel as they were close to me the whole time. Lastly, I want to thank Teresa for being such an important person in my life, and for constantly believing in me. Thanks for your bright love and for giving me all the strength I need to proceed further, I dedicate this work to you.